Author:
Walker, Nigel Stuart

Title:
Type IV creep cavitation in low alloy ferritic steel weldments.

TYPE IV CREEP CAVITATION IN LOW ALLOY FERRITIC STEEL WELDMENTS

by

Nigel Stuart Walker

October 1997

A thesis submitted to the University of Bristol
in accordance with the requirements of
the degree of Doctor of Philosophy
in the Department of Mechanical Engineering
in the Faculty of Engineering

Engineering Materials and Structural Integrity Group,
University of Bristol, Department of Mechanical Engineering,
Bristol BS8 1TR, UK.

ABSTRACT

This thesis presents principally the results of materials testing undertaken to assess the development of creep damage in the Type IV region of ferritic steel weldments. Type IV failure which occurs in weldments operating at high is responsible for the greatest reduction in the life of high temperature components above all other failure mechanisms. The aim of the work was to establish the effects of stress, temperature and stress state on the development of creep damage specific to the Type IV region, and to thereby examine the results in terms of the time to failure.

Two casts of material have been examined, both materials were of a similar composition of ½CrMoV low alloy ferritic steel. Dead load creep rupture tests were carried out over a range of temperatures and stresses using various test specimens including cross weld specimens, plain bar specimens and circular notched bar specimens. During testing the cross weld tests specimens were interrupted to allow metallographic replicas to be taken from the polished surface for the purpose of quantifying the development of creep damage in the form of creep cavitation.

A number of methods for measuring the level of damage were investigated. However, the majority of the work was carried out using the cavity density measurements. The results of the damage measurements were finally interpreted in terms of two continuum damage models and the results compared.

ACKNOWLEDGEMENTS

I wish to express my sincere thanks to Dr. David Smith and Dr, Steve Kimmins for their support, encouragement and technical guidance throughout my studies at Bristol and during my first year of employment. I am sure that at times it appeared unlikely that this thesis would ever be completed.

I also wish to thank those members of the Engineering Materials and Structural Integrity Group for providing light relief and making the task set seem a little less daunting. In particular I would like to thank Mr. Troy Swankie and Mr Dave Ogden for all their helpful suggestions and friendship. Thanks are also due to Dr. Roger Vincent who was kind enough to assist with the more technical aspects of driving the TEM in the Physics Department.

I also wish to acknowledge the financial sponsorship of Nuclear Electric and for the use of both their expertise and their equipment. The assistance and advice of the Nuclear Electric personnel was invaluable, thanks especially to Dr. Dave Miller and Dr. Mike Colemen for their supervision of the project.

Finally, I would like to thank all my friends and my family for all their support throughout. I would also like to thank Carol for all her love and support and for putting up with me.

AUTHOR'S DECLARATION

This thesis, submitted for the degree of Doctor of Philosophy at the University of Bristol, is entirely the work of the author. No work is the result of collaboration, nor is any work of other researcher used, except where clearly referenced.

The views and opinion expressed in this thesis are solely those of the author and not the University of Bristol.

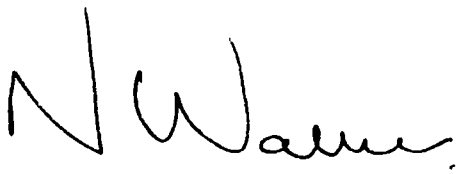

Nigel Stuart Walker

October 1997

TABLE OF CONTENTS

CHAPTER 1

CHAPTER 2

CHAPTER 3

CHAPTER 4

CHAPTER 5

CHAPTER 6

LIST OF TABLES

LIST OF FIGURES

LIST OF PLATES

NOMENCLATURE

ΔG_s	Surface related free energy
ρ	Radius of curvature of void
γ_s	Specific energy per unit area of free cavity surface
f_s	Geometric function of cavity surface where: $f_s(\varphi) = 4\pi(1-\cos\varphi)$ Fig (i)
γ_p	Specific energy per unit area of free particle surface
γ_i	Specific energy per unit area of free inclusion surface
f_b	Geometric function of grain boundary surface where: $f_b(\varphi) = \pi \sin^2\varphi$ Fig (i)
ΔG	Total free energy
σ	Tensile stress
$f_v(\varphi)$	Geometric function where: $f_v(\varphi') = \left(\frac{4\pi}{3}\right)(2-3\cos\varphi'+\cos^3\varphi'$ $: \varphi' = \frac{(\varphi+\phi-\mu)}{2}$ Fig (i)
ρ^*	Critical radius of curvature of cavity
ΔG^*	Critical free energy associated with nucleation of a cavity
N_o^*	Area density of critical clusters
c_{max}	Maximum Number. of potential nucleation sites
c	Number of potential sites occupied by supercritical cavities
k	Boltzmann constant
T	Absolute temperature (K)
J^*	Nucleation rate, the number of cavities generated per unit time/area
β^*	Rate per unit time at which single vacancies are absorbed by a critical cluster.
$\frac{dV}{dt}$	Volumetric cavity growth rate
Ω	Atomic volume

D_b	Grain boundary diffusivity
δ_b	Thickness of grain boundary diffusion layer
r	Cavity radius in line of grain boundary
λ	Centre to centre distance between cavities in grain boundary plane
$\frac{dr}{dt}$	Rate of growth of cavity radius in plane of grain boundary
D_s	Surface diffusivity
Δ	$\Delta = \frac{D_s \delta_s}{D_b \delta_b}$ where: δ_s - thickness of surface diffusion layer $\cong \Omega^{1/3}$ Db - Boundary diffusivity δb - Thickness of grain boundary diffusion layer
γ_b	Specific energy per unit area of boundary
A	Constant in power law creep
G	Elastic shear modulus
L	Material parameter used to determine the relative influence of diffusion growth and creep deformation growth.
β	Rate of production of cavities per unit area of grain boundary.
N_a	Number of cavities per unit grain boundary facet
N_m	Number of cavities per unit area of polished microsection
N_b	Number of cavities per unit length of cavitated boundary
d_i	Mean linear intercept grain size
ϕ'	fraction of boundaries cavitated
D_H	Harmonic mean of intersected cavity diameters D_i whose frequency of occurrence is f_i, equation 2.27
ϖ	Cavitated area fraction
Nf	Number of cavities per unit area of polished microsection at failure.
ω	Damage parameter
H	Strain hardening exponent
B	Constant
θ	Carbide coarsening variable

σ_e	Effective stress
$\dot{\varepsilon}_e$	Effective strain rate

Fig (i). *Schematic of angles occurring at cavities on grain boundaries and at grain boundary particles.*

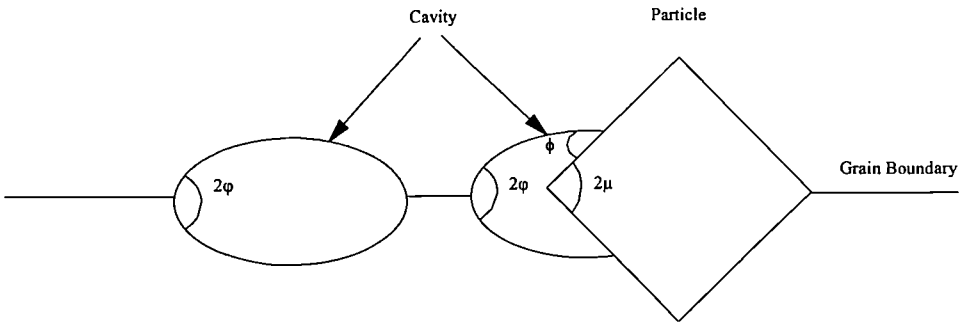

1. INTRODUCTION

1.1 FERRITIC STEEL WELDMENTS

The electricity generation industry demands a wide range of properties from the materials used to construct high temperature components. The increased desire for economy has pushed the currently available materials to the extremes of service. In order to continue safe and cost effective operation of modern power generation plants it is very important that the wide range of materials in current service is researched to investigate problems associated with both service and fabrication. This research is aimed at providing a fundamental understanding of the physical characteristics which describe the behaviour of the materials at high temperatures which will eventually lead to improving the design specifications. This information can then be related back to the operators to allow the increased demands on materials to be met within the boundaries of safe operation. To guarantee long term plant operation requires high temperature materials with adequate creep rupture strength. In addition, it is essential that the materials exhibit good weldability for the purposes of fabrication.

The average operating temperature of a power station is 540°C to 580°C with typical system stresses due to the steam pressure within the pipe of 4 to 16 MPa. This in turn relates to a mean diameter hoop stress in the region of 40 MPa. The final applied stress is

further dependent upon system stresses which are superimposed on the hoop stress as the results of poorly supported pipe work and bends, or poorly designed changes in section.

At present the construction of hot steam pipes lines is essentially limited to ferritic steels. These materials can have improved creep strength by the addition of alloy elements such as Mo Cr & or V amongst others. In general these materials have no problems during fabrication or while in service. However, the gradual transition to even bigger power station construction has given rise to difficulties in fabrication and service which has resulted in cracks and subsequently lengthy outages, where the plant is unable to run due to repair work being carried out. This proves extremely expensive, although the relative cost of repair is minimal when compared to the loss in revenue.

Low alloy ferritic steels are frequently used in the manufacture of hot steam pipelines in the power generation industry, the ferritic steels are selected for their high temperature creep resistance at an optimum cost. Due to a greater understanding of the defects affecting the welding of these steels, it has been possible to extend the service life of power station pipes and welds to times in excess of 150,000 hours. Material properties have been improved by the addition of alloying elements such as Mo, Cr, V which assist by increasing creep strength and results in steels which demonstrate good weldability. This improvement in material properties has in turn increased engineering reliability and has enabled the transition to larger more efficient power stations.

When structural members are joined by fusion welding the base metal has to be heated to its melting point and then cooled again rapidly under conditions of restraint imposed by the geometry of the joint. The result of this extreme thermal cycle is the formation of a region close to the weld metal which has altered materials properties from the original parent material. This volume of metal is referred to as the heat affected zone (HAZ). The HAZ can be sub divided into a number of zones, dependent on the material being welded. An example of a typical weld structure is presented in Fig. 1.1. Each zone refers to a different type of microstructure and more importantly each structure reflects a different mechanical property. In terms of creep strength the most susceptible region of the HAZ has been determined to be the Type IV region. It is as the result of extended service periods that the problem of Type IV damage has become more apparent, and is now one of the main causes for limiting the service life in pipe welds and joints.

The German classification described by Schuller, (**1.1**) describes the Type IV region as an intercritical region found at the transition between the heat affected zone and the unaffected parent material which is creep weak. During welding this region experiences temperatures above A_c1 resulting in a degree of tempering resulting in some recrystallisation, but not resulting in the complete dissolution of the alloy carbides. Consequently carbides tend to coagulate at the fine grained region of the heat affected zone which are intimately mixed amongst the tempered parent material. These effects of tempering and recrystallisation are promoted by the subsequent weld passes as well as the post weld heat treatments, and high service temperatures typically at 540°C. The average grain size of the type IV region is 5

to 7μm, and it is due to the grain structure that the region is often described as a microstructural notch.

At present the procedure for preventing Type IV failure is dependent upon the repeated examination of pipe work thought to be at risk, during lengthy outages when the power station is closed down. This is a time consuming business and results in high costs due to the loss of generating power. The present programme of interruption and inspection employed by Nuclear Electric has not revealed any form of Type IV cracking to date. However, there have been a number of reports of Type IV cavitation in weldments resulting in costly replacement of key components. An empirical relationship between the estimated Type IV rupture life and the cavity number density, is used to assess the effective life of the component. The weld is then either repaired or replaced completely depending on the level of cavitation. If the cavitation is less than 1000 cav/mm^2 then the weld is not repaired, but is monitored closely.

The aim of the work presented was primarily to explore in detail the combined effects of stress strain temperature and materials on the development of damage within the Type IV region of ferritic steel weldments and secondly to adopt a mechanistic approach to modelling the accumulation of this damage based upon available continuum damage mechanics. The work has demonstrated that information acquired through testing procedures can be related back to the operational conditions experienced in high temperature power plant.

During the process of this work an investigation has been carried out to determine the root causes for the susceptibility of the Type IV region to failure. It was discovered early in the test programme that one cast of parent material was resistant to Type IV failure. To investigate this phenomenon further casts of ½CrMoV steels which were known to be Type IV susceptible were supplied by Nuclear Electric to increase the number of samples analysed.

One last aspect of the research carried out was to investigate the effect of the weld metal on the Type IV susceptibility to failure. A comparison was carried out between matching ½CrMoV weld metal and 2¼CrMo weldments. In each case an assessment was made based upon failure time and accumulation of damage.

1.2 STRUCTURE OF THESIS

Following this introduction in Chapter 1 the basis of this thesis is as follows:

Chapter 2 is a review of current literature which presents a retrospective view of cavity growth and nucleation mechanisms concentrating on those mechanisms which are thought to be most relevant to Type IV failure. As a form of introduction a review of damage mechanisms which occur in welded materials has also been included.

Chapter 3 presents a full description of the test methods and damage measurement techniques adopted. The materials and welding procedures are also reviewed. In total

three types of creep test were conducted, cross weld uniaxial, plain bar uniaxial and circular notch bar tests

Chapter 4 presents the results of the characterisation of the two casts of steel used in the test programme. A full description of the creep rupture test results are also presented along side the creep cavity damage measurements

Chapter 5 is a discussion aimed at bringing together all the aspects this work. This chapter addresses the both the cavity growth mechanisms and deformation mechanisms which are dominant in the Type IV region of ferritic steel weldments. Finally, the results of this analysis are presented in terms of their applicability to service conditions.

Chapter 6 presents the main conclusions derived form this work. In addition, a section entitled future work reviews those areas of this work which could be extended to further develop the results already presented.

1.3 REFERENCES

(1.1) 1974, H.Shuller L.Hagn A.Woitscheck

Cracks In The Weld Area Of Formed Parts In Superheated Steam Lines Materials Analysis, ***Der Mashinenschaden, No1 pp 1-13.***

(1.2) 1983, Easterling, K.

Introduction to the Physical Metallurgy of Welding, ***Butterworths Monographs in Metals.***

Fig 1.1. *A schematic of the various sub-zones of the heat affected zone approximately corresponding to the alloy C_o (0.15 wt %C) indicated on the Fe-Fe_3C equilibrium diagram. (1.2)*

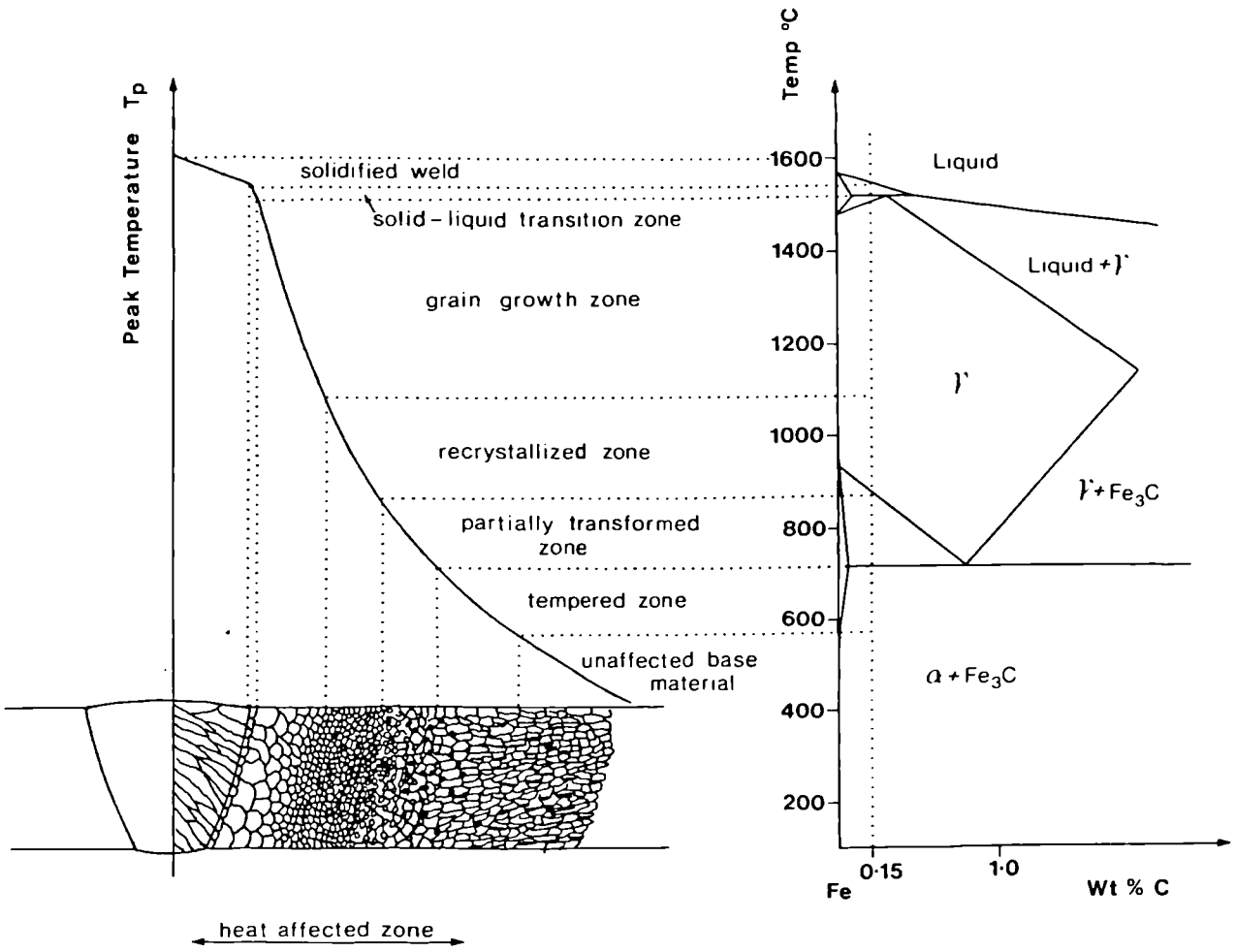

2. LITERATURE REVIEW - CREEP DAMAGE IN FERRITIC STEEL WELDS

A review of current literature is presented to introduce the various types and causes of weld failures at high temperature, previous test programmes related to Type IV failure are also presented. A number of cavity nucleation and growth mechanisms are discussed which are directly related to low alloy steels and are thought to be relevant to those mechanisms which are dominant in Type IV failures. Finally continuum damage models are discussed in terms of damage and remaining life prediction.

2.1 DEFINITIONS OF WELD DAMAGE

Evaluation of the weld cracking mechanisms discussed by (**2.1**) (**2.2**) and (**2.3**), in various case studies reveals that unlike the base material, which gives reasonable service, four distinct types of cracking are encountered in ferritic welds. The types of cracks are described using the German classification (**2.4**), Fig. 2.1.

(i). Crack Within Weld. Type I and Type II

This problem concerns the intergranular cracking which develops in weld deposit either during solidification, during subsequent stress relief of welded assembly or after extended service exposure as the result of creep damage. They can be either longitudinally or

transversely orientated. A Type I defect stops in the weld, whilst Type II grows, penetrating the Heat Affected Zone (HAZ) or even the base metal.

The characteristic damage found in each of the case studies given by Shuller et al, (**2.4**), explains how the cracks have initiated. Cracks that start in the weld, exhibiting internal oxidation, can only occur at fabrication since internal oxidation is only possible above the service temperature. This type of crack may extend by the formation of micropores as a result of creep damage so propagating and allowing growth into the base metal. It can be assumed that such cracks are initiated during stress relief annealing. Type I and II cracks can also form because of hot tearing. This occurs during solidification, as a result of residual stresses tearing the newly solidified weld apart and allowing hot liquid metal to fill the gaps, thus resulting in voids forming with in the weld.

(ii). Cracking of a Coarse Grained Region Within the HAZ. Type III

This type of cracking normally develops during post weld stress relief and is induced by alloy elements present to improve creep resistance such as V, Cr, and Mo precipitating carbides which significantly raises the creep strength of the matrix but leaves the grain boundary area relatively weak. The embrittlement of this region, by residual elements segregating to grain boundaries, is largely responsible for the reduction in the ductility. This is reflected in the final strain levels which are typically $\varepsilon_f \cong 0.1\%$ to 0.2%. In addition to carbide precipitates the segregation of impurities such as S, P, Sb, Cu, As have a similar embrittling effect. Formation of coarse grains within the HAZ during welding increases the grain boundaries susceptibility to cracking during the post weld heat treatment because

if these grain boundaries cannot accommodate the deformation, the original austenite grain boundaries break open resulting in a characteristic intercrystalline fracture with low overall deformation, observed by Gooch and Kimmins, (**2.5**). High stresses are closely related to the design and welding processes and there are additional thermal stresses that result from large temperature differences in the component walls due to over rapid heating and cooling during welding itself and as a result of subsequent annealing. Cracks form in the coarse grained region of HAZ and propagate mainly in this region running parallel to the circumferential weld.

Crack paths exhibit areas of internal oxidation along with the crack faces and crack growth is intercrystalline. Pitting at the grain boundary which can be seen using a Scanning Electron Microscope (SEM) is characteristic of ductile fracture, and indicates the large strength variations between areas near the grain boundary compared to the grain interior. Hardness measurements show an increase in hardness between the coarse and the fine grain transition indicating an embrittlement process. It is common that this type of crack existed at commissioning and may not grow while in service.

(iii). Cracking in Intercritical Region Between HAZ and Parent Metal Type IV

Type IV cracks occur only in the transition from the HAZ to the unaffected base metal. This intercritical region has been taken to temperatures above A_c1 by the welding process and causes a degree of tempering within the parent material.

In a case study conducted by Shuller et al (**2.4**), all Type IV cracks started at the outer surface of a component and followed the boundary between the HAZ and the parent metal. Type IV crack faces are generally scaled and the intercrystalline damage at the grain boundaries is characteristic of creep damage. Intercrystalline damage was noted by the authors in the transition zone between the partially transformed area of the fine grained region and the tempered area of the parent metal. The crack therefore divides the areas which have been heated to temperatures above Ac1 during welding and hence partially recrystallised (between A_c1 and A_c3) and those areas which have remained below Ac1 and have tempered but not recrystallised. The transition zone is characterised by the relatively coarse grained base metal intertwined with finer grains of the fine HAZ, known as the Type IV region

The Type IV creep damage characteristics indicate an excessive amount of creep strain occurring within a very narrow region of the welded joint. In the intercritical transition zone the applied weld heat is sufficient to cause some recrystallisation. However the temperature is not high enough to cause the complete dissolution of the alloy carbides. The majority of the Type IV zone simply undergoes a tempering effect which accelerates the degeneration of the structural components, allowing carbide growth. Consequently carbides tend to collect in the fine grained region of the HAZ and the tempered base metal boundary. This degree of degeneration is increased by subsequent post weld heat treatments and during service all of which results in a loss of creep strength. It is also possible in certain high alloy steels that this may manifest itself in lower hardness values.

2.2 SUMMARY OF WELD DAMAGE SPECIFICALLY IN ½CRMOV STEEL.

½CrMoV ferritic steel is used almost exclusively by UK Power Generators in the construction of high pressure and middle pressure main steam pipes in fossil fired steam plants due to its low cost and superior small strain creep. It is also used extensively in nuclear powered plant. Failures in main steam pipes are primarily due to the formation of cracking as a result of high temperature creep or as the result of improper post weld heat treatments. Damage may also result form material degradation due to a long operation time. Creep cracking is the most severe form of damage since it may result in a potentially fatal catastrophic failure. The main areas of risk are weldments since these are the weak points in the integrity of any steam pipe. Areas which are subjected to a higher stress concentration than the surrounding pipework such as a bend or at a change of dimension in the pipe are most susceptible to cracking. Often cracking is associated with poorly maintained hangers which do not support the pipe work adequately and result in system stresses (**2.6**).

The main reasons for the presence of these failures are listed below.

1. Stress concentrations resulting from the variation of creep properties across a weld. For example from poorly matched weld fillers
2. There are zones which exhibit low creep strength where the time to rupture is short compared with the weldment strength for a given stress, i.e. Type IV.

3. There are zones with low creep ductility, ε_f, located in the HAZ and around fusion boundary i.e. Type III.
4. Residual stresses resulting from inadequate post weld heat treatment lead to the formation of cracks in the weld and HAZ. i.e. Types I, II, III.
5. Cracks created during welding i.e. hot tearing or stress relief cracking. i.e. Types I, and II.

½CrMoV welds are generally accepted as being fairly crack resistant and cracks are more often than not the result of prolonged service of the material in the form of creep crack damage initiated from separate creep cavities forming micro cracks which link to form macro cracks, Arnswald et al (**2.7**).

2.2.1 REPORTED TYPE IV FAILURES

Failures during fabrication and while in service have been reported from USA, (**2.1**), GB, (**2.8**), Denmark, (**2.6**), Germany, (**2.4**), and occurs in various steels used in the fabrication of steam pipe work.

An investigation of a suspected Type IV failure was carried out by the Central Electricity Generating Board on a failed CrMoV weldment from a Tennessee Valley Authority power station in 1982, (**2.1**). The component had logged 75000 hours service at the time of failure operating in the creep regime above 500°C, and was reported to have failed as a result of Type IV damage. The material specified was a ½Cr½Mo¼V steam inlet pipe and a wrought bend section welded with a 2¼CrMo weld metal. It was noted that some

superimposed system stresses were present as a result of poorly maintained hangers and that the weld was in the close vicinity of a change in section

Coleman, (**2.8**), reviews a number of European cases involving Type IV failure including a number of reports from the West German Technical Insurance Company, Allianz, Shuller et al, (**2.4**). The results of uniaxial tests on ferritic steels indicate that there is a creep weak region within the partially transformed parent material at the edge of the heat affected zone. Examples of similar plant failures were found in 1Cr½Mo, 2¼CrMo, and ½Cr½Mo¼V with lives between 18,000 and 37,000 hours (**2.4**). In all cases the failures were associated with weldments between pipes and shaped components, such as header outlets or tee-pieces, which involve changes of wall thickness or diameters resulting in tapered geometry or changes in profile within the region of the weldment.

Similar observations have been made in CrMoV weldments in the Danish power industry, which are again associated with terminal or T-pieces, (**2.8**). Further examination of these cases showed that the Type IV crack had grown three quarters of its way through the wall after 45000 to 90000 hours. Examination by a replica technique (Appendix A1) revealed that the creep damage distribution had a distinct peak coincident with the partially transformed intercritical region of the HAZ and that cracking occurred in this position after a critical level of creep damage.

The first report of Type IV cracking in the United Kingdom concerned a failure at High Marnham power station, (**2.8**). This occurred in a CrMoV weldment between the main

steam line and a forged taper-piece connected to the steam chest. The investigation considered that bending stresses had been experienced across the weldment, since creep damage was confined to one side of the joint. The final conclusion suggested that the poor creep properties of the taper piece were the main reason for the failure, since the major alloying elements in the forging were at the lower end of the chemical composition specification. High levels of embrittling elements such as Antimony, Arsenic, and Tin, will reduce the creep rupture strength of a steel. Similar weld failures have been reported by the South of Scotland Electricity Board who suffered weldment cracking failures in the early 1970's in CrMoV reheat pipework at Kincardine power station.

2.3 REVIEW OF TYPE IV TESTING

This section discusses various types of steel weldments which have been tested under laboratory conditions to assess their susceptibility to Type IV failure. No transition welds were included in the review and the majority of testing was conducted in the UK, (**2.9**), (**2.10**).

2.3.1 ½CRMOV CROSS WELD TESTS.

There has been a number of Type IV laboratory test programmes using ½CrMoV steel, starting with, Gooch and Kimmins (**2.5**), who conducted a series of cross weld tests using a cast designated as M1 ½CrMoV parent material with a 2¼CrMo weld filler over a range of temperatures from 580°C to 640°C and stresses ranging from 40 MPa to 80 MPa under constant load. The specimens were 25 mm by 25 mm square section specimens with screwed ends. A reduction in area across one HAZ, was used to produce two stress regions

which in turn gave rise to different cavity number densities at different life fractions. All the specimens failed in the Type IV region.

Burke (**2.11**) carried out a series of complimentary cross weld tests based on 50 Kg laboratory melts of CrMoV which had been modified with Titanium. Titanium additions had the effect of refining the heat affected zone grain size through the pinning effect of insoluble TiN particles and promoting the formation of fully bainitic rather than predominantly ferritic parent metal microstructures. The creep strength of these fully bainitic structures was higher than the mean creep rupture properties recommended by the International Standards Organisation (ISO), (**2.12**). Because of the greater creep strength Burke showed that Type IV rupture was possible at lower temperatures and higher stresses than Gooch and Kimmins, (**2.5**). Tests were carried out on a number of cross weld specimens using several casts of parent metal, (**2.13**) (**2.14**), which resulted in Type IV failure largely independent of the addition of elements to the parent casts.

More recently Parker et al (**2.15**) published work relating to a series of cross weld tests carried out using a ½CrMoV parent cast and a 2¼CrMo weld removed from a petro-chemical steam piping system, which had experienced 130,000 hours at a temperature of 570°C. Cross weld tests were conducted using 14 mm square section screw ended specimens. It was noted that the pipe work was taken from service the two casts of parent material making up the weld were not necessarily from the same batch of castings. Parker et al (**2.15**) reported that Type IV failures were obtained in one side of the weldment but found the other cast of the weldment to be resistant to Type IV failure. It was suggested

that the main reason for the resistance of this cast was as a result of the number of inclusions within the resistant cast of steel. Tests were conducted over temperatures ranging from 565°C to 700°C, although many tests failed in the mixed coarse grained and fine grained regions of the HAZ, and not specifically the Type IV region.

2.3.2 2CRMO CROSS WELD TESTS.

The earliest work referring to low rupture creep strength in a cross weld test programme was reported by Lister (**2.16**) using a 2CrMo cast of steel. The failure location in the cross weld specimens with a 2CrMo weld metal was reported to move from the parent material to the heat affected zone with increasing time. The rupture strength was greater at 538°C than at 593°C. No metallography was reported, and it is assumed that the reduction in rupture strength was due to Type IV failure. A second set of data, showing that the rupture strength of 2CrMo parent cast weldments with matching fillers lies within the mean ISO creep rupture properties scatter band, was reported by Prager and Layda (**2.17**)

Burke (**2.11**) also reports Type IV failure in a group of Titanium modified 2CrMo cross weld specimens which show a lower dependence upon the parent cast strength. Predominantly transgranular Type IV failures in the fine grained intercritical HAZ have been reported by Laha et al, (**2.18**), these tests were conducted at 500°C and 550°C and at higher stresses than Burke, (**2.11**). A strength loss of 20 to 30% of the parent creep rupture life was observed.

2.3.3 9CRMO CROSS WELD TESTS

There is a strong variation in the cross weld strength between casts of 9CrMo steels. There is a corresponding increase in the cross weld strength with an increase in the parent cast strength (**2.19**). This underlies the importance of parent metal strength relative to the cross weld strength. It is notable, (**2.9**), that 9CrMo parent steel weldments are resistant to intergranular cavitation in most heat treatment conditions , and it is only in the Type IV zone which has been subjected to low austenitising temperatures, that intergranular cavitation readily occurs.

2.3.4 9CRMOVNB (T91) CROSS WELD TESTS

Middleton and Metcalfe (**2.20**) reviewed Type IV data generated by the Oak Ridge National Laboratory (ONRL) which indicated a strength loss of 20% in terms of stress at temperatures limited to above 600°C and that the strength loss increased to 35% at 670°C.

2.3.5 12CRMO CROSS WELD TESTS

The absence of any reported incidence of Type IV failures in 12CrMo weldments with matching and dissimilar fillers has been attributed to the low operating temperatures for this steel. Generally these temperatures are about 530°C. Cross weld tests reported by Schneider, (**2.21**), using matching and dissimilar fillers and testing at 550°C, although reporting failures for all the tests at the outside edge of the HAZ, the cross weld rupture strength was well within the parent material scatter band. There was an indication of divergence of the cross weld rupture life from the parent material rupture life at times approaching 100,000 hours for the matching filler and at 10,000 hours for the dissimilar

weld metal. The low creep rupture strength of 12CrMo boiler tubing was reported to be as a result of the low austenitising temperatures producing a low creep rupture strength with an ultra fine grained ferritic microstructure.

2.4 CAVITY NUCLEATION AND GROWTH IN ENGINEERING STEELS

2.4.1 INTRODUCTION

While the previous sections discussed the occurrence of Type IV failure, the following sections aim to review in some detail the mechanisms that may play a roll in the development of creep damage.

There are a number of types of damage which occur in engineering steels such as thermal degradation, strain softening and cavitation (**2.22**), (**2.23**). These elements of damage all contribute to the failure of steel operating in the creep regime i.e. under a constant load and above 0.4 times the melting point of the steel. However, it is only possible to quantify directly certain elements of the damage process such as creep cavitation and the degree of thermal degradation.

In this work the method of quantifying damage concentrated on the measurement of cavitation from nucleation of cavities to growth and failure. The following section reviews

the nucleation and growth mechanisms of cavities in a number of engineering steels and the development in the use of some of these mechanisms to predict remaining life.

2.4.2 CAVITY NUCLEATION

Cavity nucleation on grain boundaries in polycrystalline metals occurs due to the accumulation of strain which results from shear stresses relaxing against suitable obstacles. These areas are the most susceptible positions for cavity nucleation. At higher temperatures there is a transition from void formation within grains to cavitation at grain boundaries as a result of atomic vacancies becoming more mobile. The grain boundaries act as effective sources of vacancies and the increased mobility of the atoms leads to the possibility of grain boundary sliding. Associated with this mobility is the probability of obstacles in the vacancy path resulting in stress concentrations, which then act to enhance cavity nucleation.

There have been a number of obstacles which have been suggested, (**2.22**), (**2.24**), (**2.25**), and (**2.26**), as points of stress concentration. In pure metals, cavities are often initiated at the intersection of a slip band and a grain boundary, or at a ledge in the grain boundary, while in commercial high temperature steels cavity nucleation is often dominated by secondary particles in the vacancy path causing obstruction.

Four nucleation sites are suggested by Dyson and Taplin (**2.24**), as shown in Fig 2.2. These sites are:

i) Slip Bands
ii) Grain boundary ledges
iii) Fracture of brittle secondary particles
iv) Climb occurring about secondary particles

(I) Slip Bands

Dislocation motion during plastic deformation is concentrated in slip bands within the grains. If a slip band crosses a grain boundary the result is a stress concentration which may result in nucleating a cavity. Alternatively a slip band may initiate slip in a neighbouring grain which may lead in turn to a ledge in the grain boundary. Subsequent grain boundary sliding will result in a stress concentration at this ledge which may initiate a cavity.

(ii) Grain Boundary Ledges

In early papers by Chen and Machlin (**2.25**), and Gifkins (**2.26**), the idea of cavity nucleation at ledges was favoured as the preferred nucleation mechanism in pure metals. The ledges can be grown-in features of the grain boundary or they can result from the slip in the adjacent grains which intersects the boundary

The ledge experiences tensile or compressive stress and only the tensile ledges are expected to initiate cavities. Due to geometric reasons it is common for ledges to be compressive in nature. However, application of an external compressive load leads to ledges which will in turn experience a tensile stresses. As a result of this tensile stress at the ledge it is possible for cavities to initiate.

Davies, et al, (**2.27**), reported results which confirmed that there was a higher incidence of cavitation on inclined or sliding boundaries if the specimens were compressed before the tensile creep test was performed.

(iii/iv) Cavity Nucleation around particles

Cavity nucleation at ledges is the predominant nucleation mechanism in pure metals. In commercial materials this mechanism is much less important since these metals usually contain second phase particles on grain boundaries to prevent or minimise the amount of grain boundary sliding.

There are several reasons why grain boundary particles act as preferential nucleation sites. Firstly because they resist grain boundary sliding, and by so doing experience stress concentrations. Secondly they may be weakly bonded to the matrix. This is conceivable in the case of sulphide and oxide particles. However, in the case of carbides, it is generally accepted, (**2.24**), that the bond is strong since the carbides do not readily decohere during room temperature straining. Thirdly it may be possible that cavity nucleation at particle/matrix interfaces may be relatively easy via vacancy condensation even if the interface has a high strength

A number of investigations have shown that in low alloy steels, the cavities are often associated with carbide particles, (**2.28**), (**2.29**), (**2.30**). Needham, (**2.31**) observed that cavities nucleate preferentially on Mo_2C particles situated on grain boundaries in two low

alloy bainitic CrMo steels. It is also known that in Vanadium bearing steels Vanadium-Carbides are prone to nucleating cavities. Besides the carbides there are other inclusions at which cavities can form. Gooch (**2.32**) has reported cavity nucleation the occurrence of nucleation on sulphide and oxide inclusions in a 12 CrMo steel, and that the carbides act as secondary nucleation sites.

Another source of potential nucleation sites are Mn particles as reported by Cane, (**2.33**), Middleton (**2.34**), and Cane and Middleton, (**2.35**). Mn particles are found to precipitate along grain boundaries and are often associated with the weld heat affected zone. In the worst cases these particles may result in stress relief cracking and will certainly result in poor creep rupture properties.

2.5 KINETICS OF NUCLEATION

While the previous section reviewed the locations for nucleation here the driving force for nucleation is discussed.

2.5.1 CAVITY NUCLEATION BY VACANCY CONDENSATION

At elevated temperatures, thermally activated processes nucleate cavities at lower stress than would be required for the rupture of atomic bonds. Greenwood (**2.36**). proposed that voids could be nucleated by the condensation of atomic vacancies. This theory was successfully revived by Raj and Ashby, (**2.37**) who suggested that the driving force for vacancy diffusion was the mechanical stress, whereas in earlier work it was considered that

the supersaturation of vacancies caused by dislocation reactions was the driving force for vacancy precipitation (**2.38**). A more detailed review of Greenwoods (**2.36**) proposal is presented below followed by the theory presented by Raj and Ashby, (**2.37**).

2.5.2 FREE ENERGY OF A CAVITY

In the classical theory of cavity nucleation (**2.36**) presented by Riedel (**2.38**), the free energy of a cavity is taken to be the sum of the surface energy and the volume energy. When the cavity is formed, the energies of the surfaces which are freshly exposed must be dissipated while the energies of the grain boundary and of the particle-matrix interface are increased. Thus the surface related part of the free energy, ΔG_s, is given by

$$\Delta G_s = \rho^2 \left[\gamma_s f_s + (\gamma_p - \gamma_i) f_i - \gamma_b f_b \right]$$

equation 2.1

where f_i is the geometrical function for the newly exposed area of the inclusion and γ is the specific energy per unit area of the particle, cavity and boundary surface respectively.

The volume term of the free energy is either given by the negative work done by the applied stress during void enlargement or it can arise from a supersaturation of atomic vacancies. The stress related case will be discussed first.

A grain boundary containing atomic vacancies at the thermal equilibrium concentration is subjected to a normal stress. If a cavity grows by the acceptance of a vacancy and the equilibrium is maintained by thermal generation at sources such as jogs in grain

boundaries, then the volume of the solid increases by the atomic volume and the applied stress does the work $\sigma\Omega$ for each vacancy absorbed. Therefore the stress related part of the free energy of a cavity with a volume V is equal to $-\sigma V$. This gives the total free energy change due to the formation of a cavity as:

$$\Delta G = -\sigma\rho^3 f_v(\psi') + 3\gamma_s \rho^2 f_v(\psi')$$

equation 2.2

where ρ is the radius of curvature of the cavity and $f_v(\psi)$ is a geometric function and σ is the applied stress.

In Riedel's review (**2.38**) it was noted that elastic elongation of the material upon cavity formation also contributed to the free energy. However, since the contribution is smaller by a factor of σ/E than σV this elastic work can generally be neglected.

From the functional form of $\Delta G(\rho)$ shown in Fig. 2.3 it is clear that small voids (subcritical vacancy clusters) tend to shrink since they then gain free energy, whereas large (supercritical) cavities tend to grow to macroscopic size. The critical radius of curvature, ρ^*, is found by setting $\delta\Delta G / \delta\rho = 0$. Hence substituting equation 2.1 into 2.2 and differentiating gives:

$$\rho^* = 2\gamma_s / \sigma$$

equation 2.3

The associated critical free energy associated with the nucleation of a cavity is given by

$$\Delta G^* = 4\gamma_s^3 f_v(\psi') / \sigma^2$$

equation 2.4

2.5.3 THE NUCLEATION RATE ACCORDING TO RAJ AND ASHBY

The rate at which subcritical clusters are pushed across the nucleation barrier by thermal fluctuations to form stable cavities is proportional to the Arrhenius factor $\exp(-\Delta G^*/kT)$ using the critical free energy derived in equation 2.4. The pre-exponential frequency factor must be determined from the kinetics rather than from the (equilibrium) thermodynamics of vacancy cluster formation.

Raj and Ashby (**2.37**) argue that the maximum potential nucleation sites per grain boundary area, 'c_{max}' of which 'c' are already occupied by supercritical cavities so that c_{max}-c remain for subcritical vacancy clusters. The area density of critical clusters N_o^* is then assumed to be

$$N_o^* = (c_{\max} - c)\exp(-\Delta G^* / kT$$

equation 2.5

where T is the temperature in Kelvin and k is the Boltzman constant.

This expression would be correct if the vacancy cluster were in thermal equilibrium, i.e., if there were no drain of clusters towards supercritical cavities. The nucleation rate 'J^*' would be given by :

$$J^* = \beta^* N_o^*$$

equation 2.6

where β^* is the rate (per unit time) at which single vacancies are absorbed by a critical cluster. The absorption rate is calculated subject to the assumption that vacancies are available directly at the edge of the cavity at their equilibrium concentration, such that effective vacancy sources prevent a depletion near the void. It is also assumed that vacancies approach the void via the grain boundary

There are two apparent discrepancies between the observed nucleation rates in steels and the basic theories of cavity nucleation. First, the calculated nucleation stress is substantially higher than the observed ones. Secondly, theory predicts that nucleation occurs more or less instantaneously once the nucleation stress is applied (apart from a small incubation period), whereas nucleation actually occurs continuously throughout the creep life, and the nucleation rate is controlled by the strain rate rather than by stress.

More advanced models have been proposed by Feder et al (**2.39**) and Binder and Stauffer, (**2.40**). The conclusion of which has been that classical nucleation theory cannot predict absolute nucleation rates correctly, and that the onset of profuse nucleation as a function of the driving force for creep cavitation cannot be predicted with any reasonable accuracy.

2.6 CAVITY GROWTH MECHANISMS

Following the previous sections about nucleation this section addresses the growth of voids from nucleated cavities.

2.6.1 INTRODUCTION

The understanding of the mechanisms by which materials fracture in creep is still limited (**2.22**). The main uncertainties are associated with the identification of the processes responsible for cavity nucleation as described in the previous sections and secondly the quantification of the critical extent of cavitation necessary to promote crack propagation and growth.

2.6.2 CAVITY GROWTH

The two main models suggested for the growth of intergranular cavities during creep consider that the cavity volume increases either by the accumulation of vacancies at the cavity surfaces or by plastic void growth because of the deformation of the material surrounding the cavities.

i) Purely grain boundary diffusion growth, (unconstrained).

ii) Coupled diffusive and power law creep, (constrained).

These two basic processes can also be combined in various ways so that in some models the rate of growth by vacancy condensation is enhanced by creep deformation of the surrounding material, while in other models the vacancy type growth is constrained or limited by the rate of creep deformation. These mechanisms can be considered as the most probable for all the structural steels used in the fabrication of high temperature components, (**2.41**), (**2.44**).

Unconstrained cavity growth takes place if cavities are present at all the grain boundaries while constrained cavity growth takes place if cavities are present only on isolated grain boundaries. Conditions for purely diffusion growth in structural steels is probably less likely to occur due to the constraints arising from the steels inability to accommodate cavity growth mechanism either in terms of the associated deformation necessary for cavity formation, or due to the poor supply of vacancies. It is well known (**2.45**), (**2.47**) that diffusion controlled cavity growth can be effected by power law creep mechanisms occurring in the material surrounding the cavity. Power law creep reduces the necessary diffusion distance in grain boundaries and thus increases the rate of cavity growth; this mode of growth is commonly known as coupled diffusion and power law creep cavity growth.

As a result of these interactions any realistic prediction of the time and strain to fracture must be based on an understanding of the kinetics of cavity nucleation and on the mechanism which controls the cavity growth, (**2.22**). The laws of cavitation can be formulated on the assumption that all cavities nucleate at the same instance. The time to failure is the sum of the incubation time and the time for cavity nuclei to grow to a critical state of cavitation at which point failure occurs.

It can be expected that the final stage of specimen life is associated with the breakdown in the grain boundary integrity caused by the accumulation of cavity damage. This critical state at fracture is termed the fracture state and can be defined as the amount of damage at

which the probability of damage exceeds the critical cross sectional area. In the last few years a number of cavity growth models have been proposed. Two reviews of these models have been carried out by Riedel, (**2.38**) and Sklenicka, (**2.22**).

2.6.3 GROWTH BY UNCONSTRAINED VACANCY DIFFUSION

Balluffi and Seigle, (**2.48**), showed that it is thermodynamically possible for a void on a grain boundary, which is subject to a tensile stress across it, to grow by the migration of vacancies into the void. This occurs because of the difference in chemical potential between a vacancy located in a stressed grain boundary compared with a vacancy located at the surface of a cavity.

If the radius of curvature of the cavity is r then the critical radius of a cavity ρ^* required for cavity growth is given by:

$$\rho > \rho^* = 2\gamma_s / \sigma$$

equation 2.7

where γ_s is the surface energy and σ is the tensile stress acting across the boundary. If the chemical potential is greater in the boundary than at the cavity surface a net flux of vacancies from the cavity occurs preventing growth. This assumes that both the boundary and the cavity can act as perfect sources and sinks of vacancies.

The first detailed analysis of intergranular creep cavity growth was presented by Hull and Rimmer, (**2.49**). The model assumed a regular square array of equisized spherical cavities

lying on a plane defined by the grain boundary. The cavity volume growth rate $\frac{dV}{dt}$ is given by

$$\frac{dV}{dt} = \frac{2\pi\Omega D_b \partial_b}{kT} \frac{r}{\lambda}\left(\sigma - \frac{2\gamma_s}{r} + P\right)$$

equation 2.8

where Ω is the atomic volume, D_b is the grain boundary diffussivity, r is the cavity radius in line of grain boundary, λ is the inter cavity spacing, and δ_b is the thickness of the grain boundary diffusion layer.

Successive analyses of diffusion cavity growth have improved the boundary conditions for the solution of the basic diffusion equations.

Speight and Harris, (**2.50**), pointed out that the Hull and Rimmer, (**2.49**), formulation given in equation 2.8 predicts vanishingly small cavity growth rates at very large cavity spacing, despite the fact that a particular cavity would have available an almost unlimited expanse of grain boundary from which to collect vacancies. The subsequent analyses have led to more sophisticated expressions for the dependence of growth rate on the ratio of cavity radius to intercavity spacing r/λ than that first proposed by Hull and Rimmer.

Fig 2.4 shows the development of cavitation by steady state cavity growth from a fixed number of nuclei. The analysis of Speight and Beere, (**2.51**) and Raj et al, (**2.37**) on which Fig 2.4 was formed was based upon the following assumptions:

1. Cavities are arranged in a periodic square array with each cavity having a circular cross section in the plane of the grain boundary.
2 The cavities maintain their shape during the whole growth process by rapid material transport around their surfaces.
3. The circular grain boundary area associated with each cavity behaves as a perfect and inexhaustible source of vacancies.
4. In essence the material only deforms elastically, but the redistribution of stresses is considered to be complete so that the formation of vacancies occurs at a constant rate (β per unit area, the rate of production of cavities per unit area grain boundary) over the entire boundary surface.

(I) Non-Equilibrium Diffusive (unconstrained) Growth

In the case of simple diffusion models it is assumed that the rate of material transport around the cavities surface is much greater than along the grain boundaries, which results in an equilibrium lenticular shape, (**2.23**) and (**2.38**). However, when surface diffusion is slower than the grain boundary diffusion a cavity can change its shape during growth and so evolve into a non equilibrium crack like shape. Chung and Rice, (**2.52**), derived a relationship between the crack velocity of the cavity, the flux of matter into the boundary ahead of the cavity, and the curvature of the cavity surface adjacent to the crack tip of the cavity.

Goods and Nix, (**2.53**), used the results of Chung and Rice, (**2.52**), to formulate a general expression for the growth rate of an array of thin lenticular cavities lying on a boundary between two rigid grains giving the growth rate, $\frac{dr}{dt}$, as:

$$\frac{dr}{dt} = \left(\frac{3}{4}\right)^3 \left[(1+2\Sigma_1)^{1/2} - 1\right] D_s \gamma_s \Omega^{4/3} \frac{1}{\Delta^3} \frac{1}{(\lambda/3 - r)^3}$$

equation 2.9

where :

$$\Sigma_1 = \frac{2}{3\sqrt{2}} \Delta \frac{\lambda\sigma}{\gamma_s (1 - \gamma_b / 2\gamma_s)^{1/2}}$$

equation 2.10

and Δ is related to the boundary diffusivity.

Goods and Nix, (**2.53**), present two solutions to these equations:

i) In the limits $\Delta >> 1$ the growth is controlled by grain boundary sliding.

ii) In the limits $\Delta << 1$ the growth is controlled by surface diffusion.

The growth rate equations, derived from these limits, are as follows:

1. Grain boundary diffusion control

$$\frac{dr}{dt} = \frac{3\sqrt{3}}{8(2)^{3/4}} \frac{D_b \delta_b^{3/2} \Omega^{5/4}}{kT\gamma_s^2 (1 - \gamma_b / 2\gamma_s)^{3/4} D_s^{1/2} \lambda^{1/2}} \frac{1}{(1/2 - r/\lambda)^3}$$

equation 2.11

2. Surface diffusion control

$$\frac{dr}{dt} = \frac{\sqrt{2}}{16} \frac{D_s \Omega^{4/3}}{kT\gamma_s^2 (1-\gamma_b/2\gamma_s)^{3/2}} \frac{1}{(½ - r/\lambda)^3} (\sigma^3)$$

equation 2.12

(ii) Strain Enhanced Diffusive (unconstrained) Growth

In vacancy diffusion the simplification is made that the grains do not deform plastically. i.e. they behave as elastic blocks and that the diffusion flux of material away from the cavities is deposited evenly over the entire area of uncavitated grain boundary, (**2.23**). In practice the grains usually deform by dislocation creep and it can be expected that the vacancies are predominantly created near to the cavity rather than uniformly over the grain boundary surface. The two principle models for coupled diffusive/strain controlled cavity growth are those of Speight and Beere, (**2.51**) and of Chen and Argon, (**2.46**). Both of these models make use of the Hull and Rimmer, (**2.49**), type of diffusive growth of creep cavities. (**2.54**)

Beere and Speight, (**2.51**) have summarised the situation in Fig 2.5. Vacancies generated uniformly in the boundary of region I are considered to diffuse towards the cavity. The counter flux of atoms plating out in region I wedges the boundary apart. No vacancies are created in region II but the displacements are matched by dislocation creep. This results in a stress distribution along the grain boundary of the type shown above. The distances described by Beere et al, (**2.51**), suggests therefore that the diffusion distance in the

presence of creep is much smaller than the cavity half spacing, λ/2, and that creep enhances diffusive cavity growth substantially.

The transition from diffusive cavity growth to hole growth by creep flow occurs when the diffusion distance becomes smaller than the cavity radius. For higher stress growth occurs predominantly by creep flow while at lower stresses diffusion will dominate. In creep resistant materials as a result of the relatively small ratio of $\dot{\varepsilon}/\sigma$, the diffusion length is usually so large that diffusive growth predominates over the entire range of conditions generally applied in creep testing.

The Speight and Beere, (**2.51**), model relies on the variation of the vacancy chemical potential and is solved for region I using the following boundary conditions

$$\sigma = 2\gamma_s / r \qquad \text{at R=r}$$

$$\frac{d\sigma}{dr} = 0 \qquad \text{at R=b}$$

Leading to:

$$2\pi \int R\sigma dR = \sigma_I \pi b^2 - 2\pi r\gamma_s$$

equation 2.13

where σ_I is the average stress acting over both region I and the cavity. This leads to an expression for the variation of the tensile stress across the boundary in region I, given by:

$$\sigma = \frac{2\gamma_s}{r} + \frac{(\sigma_I - 2\gamma_s / r)\left[2b^2 Ln(R/r) + r^2 - R^2\right]}{\left[2b^2 Ln(b/r) - r^4/2b^2 + 2r^2 - 3b^2/2\right.}$$

equation 2.14

The tensile stress acting in region II is the maximum stress in region I and can be obtained by putting R=b.

The growth rate $\frac{dV}{dt}$ can be expressed as

$$\frac{dV}{dt} = \pi b^2 \beta\Omega$$

equation 2.15

where $\beta\Omega$ is the jacking velocity due to atom plating on the boundary. Evaluating β leads to

$$\frac{dV}{dt} = \left[\frac{2\pi D_b \partial\Omega}{kT}\right]\cdot\left[\frac{\sigma_I - 2\gamma_s / r}{Ln(b/r) - r^4/4b^4 + r^2/b^2 - 3\,4}\right]$$

equation 2.16

Assuming a power law creep relation of strain rate $\dot{\varepsilon}$ to stress σ:

$$\dot{\varepsilon} = A\left(\frac{\sigma}{G}\right)^n$$

equation 2.17

where A is the power law constant n is the stress exponent and G is the elastic shear modulus.

If it is also assumed that the shear relaxes the boundary stress profile at a distance b from the boundary then the displacement rates in region I and region II can be matched.

$$\beta\Omega = 2bA\left(\frac{\sigma_{II}}{G}\right)^n$$

equation 2.18

Substituting β and σ_{II} into equation 2.14 gives:

$$A\left(\frac{\sigma_{II}}{G}\right)^{n} = \frac{D_b \partial_b \Omega}{kT}\left[\frac{(\sigma_I - 2\gamma_s / r)b}{b^4 Ln(b/r) - r^4/4 + r^2 b^2 - 3b^4/4}\right]$$

equation 2.19

Equating the forces acting on the boundary with the applied stress gives

$$\sigma_I b^2 + \sigma_{II}\left(\frac{\lambda^2}{4} - b^2\right) = \sigma\frac{\lambda^2}{4}$$

equation 2.20

The three unknowns σ_I, σ_{II} and b can be determined by simultaneous solutions to equations 2.14, 2.19 and 2.20.

From equations 2.15 and 2.18 the cavity growth rate, $\frac{dV}{dt}$, can be expressed as

$$\frac{dV}{dt} = 2\pi b^3 A\left(\sigma_{II}/G\right)^{n}$$

equation 2.21

At high strain rates region I becomes very small as b approaches r. From equations 2.14 and 2.20 the stress in region II becomes

$$\sigma_{II} = \frac{\sigma\lambda^2}{(\lambda^2 - 4r)}$$

equation 2.22

Therefore in the limit $b \rightarrow r$ and $\sigma >> 2\gamma_s/r$ the growth rate can be expressed in terms of the cavity radius as

$$\frac{dr}{dt} = \frac{r}{2}\dot{\varepsilon}\left[\frac{\lambda^2}{\lambda^2 - 4r^2}\right]^n$$

equation 2.23

The model of Chen and Argon, (**2.46**) is much simpler since the diffusion length is taken to be independent of the cavity radius and half spacing and is given by $b = r + L$ where L is the diffusion length and is given by

$$L = \left(\frac{D_b \partial_b \Omega \sigma_\infty}{kT\dot{\varepsilon}_\infty}\right)^{1/3}$$

equation 2.24

However, despite impressive agreement with the results of Needlemen and Rice, (**2.55**), Schneibel and Martinez, (**2.56**) and Lu and Delph (**2.54**), pointed out that the continuity of the vacancy chemical potential is not maintained in the model by Chen and Argon, (**2.46**), and is therefore flawed.

2.6.4 CONSTRAINED DIFFUSIVE GROWTH.

Dyson, (**2.42**) and (**2.43**), has considered a number of situations where the rate of diffusive growth may be constrained by either the rate of deformation of the surrounding material or by the rate of the supply of vacancies at the adjacent boundary.

Three possible situations leading to constrained growth have been derived, (i) geometric constraint, (ii) vacancy source control and (iii) particle inhibition.

(i) Geometric constraint

In creeping polycrystals the cavities are usually fairly homogeneously distributed on each individual grain facet which is transverse to the applied stress, but the density of cavities may vary markedly from facet to facet. In fact many grain facets may be totally free of all cavitation while neighbouring facets are highly cavitated, Fig. 2.6. If the predicted strain rate due to cavity growth at the boundary between grains I and II is greater than the strain rate of the surrounding material then the actual cavity growth rate will be determined by the overall creep rate and not by the diffusive growth laws.

(ii) Vacancy source control

The diffusive growth models presented previously assume that grain boundaries can behave as perfect sources of vacancies. Likely sources of vacancies are climbing grain boundary dislocations, but it is feasible that the density and rate of climb of such dislocations are insufficient to provide the vacancies needed by the diffusive growth laws. It has been suggested from as early as 1967 by Ishida and McClean, (**2.57**), that dislocations arriving at the grain boundaries from the grain interiors provide the necessary vacancy sources via their subsequent glide/climb motion in the grain boundary plane. The proportionality often observed between grain strain and strain resulting from grain boundary sliding does suggest that the grain boundary dislocations formed by the decomposition of matrix dislocations are the major contributors to grain boundary sliding. Thus it may be expected that these dislocations which glide and climb in the boundary plane are also the prime source of vacancies for cavity growth. It therefore follows then

that the rate of cavity growth is directly linked to the rate of grain boundary sliding which will be proportional to the overall strain rate.

(iii) Particle Inhibition

It has been shown by experiments involving diffusive creep that intergranular precipitate particles reduce the creep rate and provide a threshold stress for creep deformation, (**2.23**). It is generally accepted that this is due to the particle/matrix interfaces acting as poor sources and sinks of vacancies. Harris, (**2.58**), has suggested that a similar situation arises with cavity growth by diffusion. Dyson, (**2.43**), analyses this model further to show an approximate proportionality with strain rate.

2.6.5 MODEL FOR CONSTRAINED DIFFUSIVE CAVITY GROWTH

By assuming power law creep behaviour using equation 2.17, Dyson, (**2.43**), has shown that all three models of constrained growth lead to a growth rate equation of the following form:

$$\frac{dV}{dt} = KA\lambda^2\left(\frac{\sigma}{G}\right)^n$$

equation 2.25

where K is a factor which varies for the different types of constraint.

For geometric constraint $K = d$

where d is the grain diameter

For vacancy source control $K = \frac{fl\,d}{L}$

where f is the fraction of emitted vacancies captured by the cavities and L is the glide distance of dislocations before meeting the boundary and l' is the average climb distance of the grain boundary dislocations

$$K = 1 - y$$

where y is the fraction of grain boundary area occupied by particles.

In conclusion constrained cavity growth may be rate controlling at lower stresses but other mechanisms are likely to dominate at higher stresses.

2.6.6 SUMMARY

In order to summarise the two cavity growth mechanisms in terms of cavity growth rate and stress, a schematic of a cavity growth mechanism map is presented by Riedel (**2.38**) has been reproduced. Fig 2.7 indicates the two cavity growth mechanisms which are considered to dominate cavity growth in the Type IV region over the range of test stresses as well as service conditions. The slope of the line is related to the stress exponent 'n' expressed in terms of power law creep. It can clearly be seen that at lower stresses constrained cavity growth dominates while at higher stresses the cavity growth rate is unconstrained.

2.7 QUANTIFICATION OF NUCLEATION KINETICS

In order to gain an understanding of the mechanisms controlling the nucleation of cavitation it is necessary to determine an accurate method for measuring the rate of cavity nucleation. Accurate measurement of the rate of development of cavitation associated with

cavity nucleation has been devised using both electronic and optical methods. However, the results are inherently sensitive to the accuracy of the measuring method. Artefacts such as carbides, precipitates, and debris on the surface of samples can readily be confused for cavities and reduce the reliability of the techniques employed to measure the microscopic nucleating cavities.

One example of an electronic technique is the use of a high voltage electron microscopy which has been used to measure the location size and shape of very small cavities in studies conducted by Fleck et al (**2.59**) and Svennsson and Dunlop, (**2.23**)

The two most widely used methods for the quantification of cavity nucleation are the counting of the number of cavities per unit grain boundary area following the brittle fracture of specimens at various fractions of the creep life, (**2.60**). The second method which is now well established in the power generation industry is the quantification of the number of visible cavities per polished area section at various fractions of the components lifetime using either optical electron or transmission microscopy, (**2.61**) to (**2.64**).

2.7.1 CAVITY DENSITY PER UNIT GRAIN BOUNDARY

Cane and Greenwood, (**2.60**), investigated the nucleation kinetics in pure iron. Due to the brittle fracture properties of pure iron it was possible to obtain a surface consisting almost entirely of grain boundary faces with only small areas of cleavage fracture. This allowed the measurement of the size and population of cavities per unit grain boundary area N_a

based upon the quantitative fractographic technique. The results indicated that apart from a few cavities which formed instantaneously on inclusions that cavity nucleation was dependent of both the strain and the stress level. The approximate constant value of $\dot{\varepsilon}_m t_f$ (where $\dot{\varepsilon}_m$ is the minimum creep rate and t_f is the time to failure), which is commonly observed was also found to hold true. Cane and Greenwood, (**2.60**) concluded that cavity nucleation growth were uniquely controlled by deformation processes, but that growth was time dependent. It was also suggested by this work that for material of constant grain size and composition at a given temperature, fracture will occur after a given fraction of the grain boundary area is occupied by cavities.

2.7.2 CAVITY DENSITY PER UNIT POLISHED SURFACE

The most widely employed, (**2.61**) to (**2.64**), method of quantifying the nucleation kinetics is the measurement of the number of cavities per unit area of polished microsection N_m, since this method does not require an inherently brittle material. Measurements of nucleation kinetics have been carried out using a number of engineering alloys by Dyson and Mclean, (**2.61**), Tipler and Hopkins, (**2.62**), Lonsdale and Flewitt, (**2.63**), and Needham, and Gladman, (**2.64**)

Dyson and Mclean, (**2.61**), showed that following a number of creep tests conducted using Nimonic 80 that quantification of the number of cavities/mm^2 visible under an optical microscope, increases linearly with strain up to three quarters of the creep lifetime and was therefore a good indication of the remnant life of the material under test.

Chen and Argon, (**2.65**), chose a further parameter to describe the nucleation of cavities by including the length of the cavitated boundaries to give N_b the cavities per unit length of cavitated boundary

The three parameters N_a, N_m, and N_b can be related using standard stereological relationships

$$N_a = \frac{d_i}{\pi D_H} N_M$$
$$N_M = \frac{2\phi}{d_i} N_b$$

equation 2.26

where d_i is the mean linear intercept grain size, ϕ is the fraction of boundaries cavitated and D_h is the harmonic mean of intersected cavity diameters D_i whose frequency of occurrence is f_i

$$Dh = \frac{1}{\Sigma f_i (1/D_i)}$$

equation 2.27

Chen and Argon **(2.65)** reported that the cavities were not all nucleated immediately upon the application of the creep load or even after an incubation period as assumed in modelling studies but that the number of cavities did increase progressively during the test. Therefore, nucleation was either continuous until fracture intervened, (**2.61**) to (**2.64**), or the number reached an approximate saturation value before fracture (**2.66**) (**2.67**).

Dyson, (**2.68**), has suggested that since the cavity counts are usually made based upon a cavity size of between 0.5μm to 1μm and cavity nuclei are much smaller than this size, normally no greater than 20μm, the apparent nucleation kinetics may be distorted by cavity growth. However, since small cavities tend to grow rapidly, the use of cavities which are 0.5μm in size reflects the kinetics of cavity nucleation sufficiently accurately.

Dyson, (**2.68**), further noted that a common result of many experimental studies is that the number of cavities N per unit grain boundary area increases approximately in proportion to the creep strain with a factor of proportionality, which is independent of stress.

$$N = \alpha' \varepsilon$$
$$J^* = \alpha' \dot{\varepsilon}$$

equation 2.28

where J^* is the cavity nucleation rate per unit grain boundary area and α is an empirical factor in the proportionality having physical dimensions (m^{-2}) and $\dot{\varepsilon}$ is the strain rate.

Dyson concluded that nucleation was a continuous process rather than spontaneous and that nucleation of cavities was a characteristic feature of a number of engineering alloys. Further to this the strain rate was found to be the important parameter controlling nucleation rate and that the number produced per unit strain was strongly material dependent. Finally it was noted that the applied stress state and the level of impurities such as 'Mn' both affected the rate of cavity nucleation.

2.8 CAVITATION STUDIES

A number of damage measurement techniques such as cavity number density, the 'A' parameter and the cavity area fraction have been developed by Needham and Cane (**2.69**) and Shammas (**2.70**). Further methods of damage quantification incorporated in this present work have included cavity area, and void fraction. A short summary of the most widely used methods of creep cavity damage quantification are presented below. In addition, where available, the relationship between these measures of damage and the remaining life is included.

2.8.1 CAVITY DAMAGE CLASSIFICATION

This is the most basic assessment of cavity damage and is purely qualitative. The method has been frequently used in continental Europe, (**2.4**), (**2.71**) to determine safe operating periods. Routine replication is carried out on critical areas and each replica is examined and placed into one of the following categories suggested by Neubauer (**2.72**)

Damage Rating	**Description**
Undamaged	No creep damage observed.
Isolated	Cavities are seen isolated on grain boundaries without obvious orientation to the distribution of cavitated boundaries.
Oriented	The cavities are distributed so that an alignment of damaged boundaries normal to the maximum principle stress axis can be seen.
Microcracked	Coalescence of cavities causes the separation of some of the grain boundaries.
Macrocracked	Long cracks have formed on many boundaries by the interlinkage of cracked boundaries.

This is a relatively fast classification to perform but is based upon the interpretation of schematic figures, such as those shown in Fig 2.8, rather than formal rules and does not give a quantitative assessment of the damage although Fig 2.9 shows an empirical relationship between the various grades of damage and the time to failure, (**2.73**).

2.8.2 CAVITY NUMBER DENSITY

This measurement is made using the procedures described previously, and is the main research tool of this project, to give a quantitative value of the cavitation in cavities per unit area. An empirical relationship has been suggested for materials such as 1Cr½Mo parent steel using a matching weld by Bollerup et al (**2.74**).

$$N_A = Kt^m$$

equation 2.29

where t is the time to cavitate N_A the number of cavities per unit area, and K and m are constants. By defining a critical value for N_A a life prediction can be made. One problem with the cavity number density is that during the later stages of creep it is common for the cavities to coalesce, joining to form larger cavities and so reducing the number density. This gives an inaccurate estimate of the cavity number density at failure.

A cavitation model proposed by Brett, (**2.75**), which may be applicable to the Type IV region, assumes that cavitation occurs in waves which decreases the space, c, between the cavities as new cavities form and grow at each nucleation step. It is assumed that the cavities grow to a limiting size after each burst of nucleation, and in this derivation a model for unconstrained diffusive cavity growth is used.

By using the assumptions described above the rupture life from the onset of cavitation becomes:

$$t_r = \frac{B}{\sigma} \sum_{j=1,2,3,\ldots} \ln\left(\frac{z^j d}{3.6} - 0.5\right)$$

equation 2.30

where B is a temperature dependent constant, and z and j are constants selected to incorporate the observed cavity spacing. If $c=1/\sqrt{N_a} = z^j d$, then j is the number of nucleation steps that resulted in the observed cavity spacing, 'c'. 'z' is a constant describing the factor by which c changes at each step. Therefore, an initial cavity spacing could have a starting value of 40μm decreasing in three steps (j=3) to a limiting value of 10 μm, halving at each step the cavity spacing c (z=2).

2.8.3 CAVITY SIZE DISTRIBUTIONS FOR CONTINUOUS NUCLEATION

Following Riedel **(2.38)**, the cavity size distribution links experimental data, cavity nucleation and growth theory, denoted by $N(R,t)$, where NdR is the number of cavities per unit grain boundary area having a radii between R and $R+dR$. The cavity density only applies to those grain boundaries which are under a tensile load allowing cavity growth. Cavities can only pass from R to $R+dR$ by cavity growth. At times near to when cavities coalesce the cavity number density is effectively decreased hence this data is not incorporated into the distribution. Finally the distribution must obey the continuity of size and space such that the rate of cavity nucleation, $\dot{N}$:

$$\dot{N} + \partial(N\dot{R})/\partial R = 0$$

equation 2.31

where $\dot{N}$ is the time derivative of the cavity size distribution and $R(R,t)$ is the growth rate of the cavities having a radius R at time t. The growth rate will be dependant upon the cavity growth mechanism. The time dependency is derived from the cavity spacing which decreases continuously as more cavities are nucleated.

2.8.4 THE CAVITATED AREA FRACTION

The cavitated area fraction, $\overline{\varpi}$, of the grain boundaries having orientations between 60° and 90° to the tensile axis is obtained by integrating the areas πR^2, occupied by the individual cavities multiplied by their number density, NdR:

$$\overline{\varpi} = \int \pi R^2 N(R,t) \partial R$$

equation 2.32

Rupture is assumed to occur when the area voidage attains a critical value denoted ϖ_f.

The volume fraction of cavities 'f' can be used to determine the strain accumulated, where the strain has been related to the area or volume fraction of cavities by Auerkari et al, (**2.77**), as follows:

$$\varepsilon = \varepsilon_r \left(\frac{f}{f_{crit}}\right)^{1/q}$$

equation 2.33

where q is a material constant ($1<q<2$) and f_{crit} is the critical cavity volume fraction value of the f the cavity volume fraction at failure.

2.9 CONTINUUM DAMAGE MODELS FOR CREEP LIFE PREDICTION

The concept of continuum damage mechanics originated with Kachanov's realisation (**2.78**) and (**2.79**) that simple flow models (**2.80**) could not explain creep rupture under certain load conditions, such as a simple bar under torsion. In response to this Kachanov developed the concept of a damage parameter which evolved in a manner similar to that of creep strain accumulation over time. Various models have been developed relating the differing interactions between the damage rate of evolution and the strain rate. Whilst Kachanov's original work left the damage parameter as a hidden variable, his later work (**2.81**) and that of other workers such as Rabotnov, (**2.82**), and Dyson and Ashby, (**2.83**) have related the parameter to a variety of physical degradation processes. The parallelism between the continuum damage mechanics formulation and the mechanism of constrained cavity growth, (**2.42**) and (**2.69**) has been used extensively in developing methods of metallographic condition assessment and life prediction for low alloy creep resistant steels such as ½CrMoV steel.

Each model is characterised by a coupled pair of differential equations describing strain and damage rates as functions of applied conditions, stress, σ, and temperature, T, materials state and the current strain, ε, and damage levels, ω.

$$\left.\begin{aligned}\dot{\varepsilon} &= \dot{\varepsilon}\left(\sigma, T, \varepsilon, \omega\right)\\ \dot{\omega} &= \dot{\omega}\left(\sigma, T, \varepsilon, \omega\right)\end{aligned}\right\}$$

equation 2.34

In general, the models developed have been restricted to secondary-tertiary creep.

(I) The 'A' Parameter

The 'A' Parameter was investigated by Cane and Shammas, (**2.76**), using 2¼CrMo steels and later in more detail by Shammas, (**2.70**), using ½CrMoV. The 'A' parameter is defined as the number fraction of grain boundaries that are damaged by cavitation or cracking (measured along a transverse line parallel to the direction of maximum principal stress). Equation 2.35 directly equates the damage parameter, ω, to the degree of creep cavitation quantified by the 'A' parameter

$$(1-\frac{1}{t_r}) = (1-A)^{\lambda-1}^{n\lambda}$$

equation 2.35

Life prediction using the 'A' parameter requires only a limited amount of materials data, including a knowledge of the Norton's stress exponent n (**2.38**), and the materials parameter $\lambda \cong \varepsilon_r/\varepsilon_s$ where ε_r is the strain to rupture and ε_s is the secondary strain.

Shammas (**2.70**) found that equation 2.35 for the prediction of time to failure using measurements of the 'A' parameter proved too conservative to be realistic for the Type IV region. The main problem with 'A' parameter in relation to Type IV damage, is that it is

basically a line scanning method and is sensitive to grain orientation. Therefore its application to the Type IV region is particularly limited since it is often difficult to identify the grain structure.

An original Kachanov model proposed by Cane and Needham, (**2.69**), which was later developed by Cane and Shammas, (**2.76**), to form the 'A' parameter model originally developed a direct relationship between the cavity number and the damage parameter, ω. The model has been further developed to equate the cavity number density to the time to failure by the following relationship:

$$LF = \left[1 - \left(1 - \frac{N^A}{N_f}\right)^{\lambda}\right]^{\mu}$$

equation 2.36

where LF is the life fraction.

The above approach requires values of λ and μ. These are specific to the steel and the temperature and stress and do not require detailed plant history in the application of life prediction.

(ii) Hyperbolic Sine Damage Model

Dyson and Osgerby (**2.84**) have recently proposed that climb and glide mechanisms occur in parallel to each other rather than as a sequential process. This parallel process leads to a creep strain which has a hyperbolic sine dependence on the applied stress, instead of a conventional power law dependence. Based upon this proposed mechanism an equation

relating the effective creep strain to specific material variables may be derived as follows, (**2.85**):

$$\dot{\varepsilon}_e = A\sinh\left[\frac{B\sigma_e(1-H)}{(1-\vartheta)(1-\omega)}\right]$$

equation 2.37

where A and B are material parameters, H is the strain hardening exponent, θ is the carbide coarsening variable with the last variable, ω, related to damage. The hyperbolic sine dependence of the creep strain rate on the stress inherently predicts an increase in the Norton creep exponent with increasing stress and therefore allows the creep behaviour to be described over a wide range of stress. The influence of the hyperbolic sine term on the material properties leads to accurate descriptions of the damage evolution and the strain for materials whose failure is predominantly by tertiary creep.

2.10 SUMMARY

The purpose of the literature review was to present a review of Type IV experience both from service conditions to testing conditions. A review of those mechanisms which are of relevance to creep cavitation development has been carried out detailing potential nucleation mechanisms as well as cavity growth mechanisms which occur in structural steels. To complete the review of cavity growth and nucleation studies a review of practical methods of determining the accumulation of damage has been included.

Finally the cavity growth and nucleation mechanisms have been discussed in terms of remaining life. A description of continuum damage models has been presented to illustrate

the relationships between damage and remaining life which have been developed based upon cavity growth mechanisms and damage accumulation. The mechanisms which have been highlighted in this review will form the basis of the analysis and discussion of the results of this work.

2.11 REFERENCES.

(2.1) 1982, F.Ellis S.Hilton J.Henry J.Bynum
Influence Of Service Exposure On Base And Weld Metal ½CrMoV High Pressure Inlet Piping, ***Int Journal Pressure Vessels And Piping, Vol. 104, p102***

(2.2) 1990, R.Townsend
Historical Perspective :A Review Of Service Problems, ***Rupture Of Creep Resistant Steels, York, UK.***

(2.3) 1985, C.Lundin J.Henning R.Menon K.Khan
Transformation Metallurgical Response And Behaviour Of The Weld Fusion Zone And HAZ In Cr-Mo Steels For Fossil Energy Application, ***Final Tech Report Ornl/Sub/81-07685/02&77, University Tennessee, Knoxville, USA.***

(2.4) 1974, H.Shuller L.Hagn A.Woitscheck
Cracks In The Weld Area Of Formed Parts In Superheated Steam Lines Materials Analysis, ***Der Mashinenschaden, No1 pp 1-13.***

(2.5) 1988,.D.Gooch S.Kimmins
A Study Of Type IV Cracking In ½CrMoV Steel Weldments, ***CEGB Research Report, RD\L\3383\R88.***

(2.6) 1987, S.Hertzman R.Sandstrom J.Wale
Creep Damage In Welded Joints Of 0.5CrMoV Steel, ***High Temperature Technology, Vol. 5 No1.***

(2.7) 1985, Arswald, W. Kaes, H.
Verwendend Des Stahles 14MoV63 Fur Rohrleitungen, ***Vgb Konferenz Werkstoffe Und Schweisstechnik Im Kraftwerk.***

(2.8) 1981, M.Coleman
Type IV Cracking In Ferritic Steel Weldments, ***CEGB Research Report Rd\M\R309.***

(2.9) 1991, Soo. J
A Review Of Laboratory Data For Type IV Cracking In ½CrMoV And Other Ferritic Steel Welds, ***National Power, TEC/L/0185/M91.***

(2.10) 1986, Brett, S.J.
Type IV Cracking In Steam Line Components, ***CEGB, Research Report SWR/SSD/0727/N/86*** .

(2.11) 1989, Burke P
Improved Performance Of Welded High Temperature Steels, ***British Steel Report BS Ref: FR S201-7892.***

(2.12) 1984, Barraclough, D.R., Hamm, C.D. Plastow, B.
Creep Rupture Equations Of Steels For Use In Life Assessment Calculations Based On ISO (1978) Data, ***CEGB Report NWR/SSD/84/006/R***

(2.13) Buchmayr, B. Cerjak, H. Witmer, M. Maile, K. Theofel, H. Eckert, W.
Steel Research Verlag Stahleisen MBH, Dussledorf, Issue No 6/90, pp268-273.

(2.14) 1985, Brett,S,J.
Inconel 182 Cold Weld Repair, Cross Weld Creep Rupture Tests In Cr Mo V Cast Parents, ***CEGB Report SWR/SSD/0580/N/85.***

(2.15) 1995, Parker, J.D., Parsons, A.W.J.
High temperature deformation and fracture process in 2¼Cr1Mo-½CrMoV weldments. ***Int.J. Pres. Ves and Piping Vol. 63 pp45-44***

(2.16) 1981, Lister, E.
Comparison Of Rupture Data On 2 CrMo Pipe And Butt Welded Joints, ***Iron And Steel, Vol. 34, pp 666-667.***

(2.17) 1988, Prager, M, Leydaw.E.
Effects Of Heat Treatment Variables On The Creep And Rupture Behaviour Of 2¼Cr1Mo Steel, ***ASME Pressure Vessel And Piping Conference, Pittsburgh.***

(2.18) 1990, Laha,K., Bhanu Sankara Rao,K., And Mannan,S.L.
Creep Behaviour Of Post-Weld Heat Treated 2.25 Cr-1Mo Ferritic Steel Base, Weld Metal And Weldments, ***Metal Science And Engineering, A129, pp 183-195.***

(2.19) 1989, Soo, J.
The Uniaxial Creep And Rupture Properties Of The Heysham 2/Torness 9CrMo - Alloy 600 Boiler Tube Transition Weld, ***CEGB Report RD/L/3379/R88.***

(2.20) 1990, Middleton,C.J., Metcalfe,E.
A Review Of Laboratory Type IV Cracking Data In High Chromium Ferritic Steels, ***Proceedings Of The Institute Of Mechanical Engineers, International Conference, Steam Plant For The 1990's, IMECHE.***

(2.21) 1990, Schneider, H.J.
Qualification Of Dissimilar Weldments For Operation In The Creep Regime, ***Life Of Welds At High Temperature, I Mech E Conference.***

(2.22) 1995, Sklenicka, V.
Development Of Intergranular Damage Under High Temperature Loading Conditions, ***Mechanical Behaviour Of Materials At High Temperature, Portugal***.

(2.23) 1981, L.Svensson G.Dunlop.
Growth Of Intergranular Creep Cavities, ***International Metals Reviews, No. 2 p109.***

(2.24) 1976, Dyson, B.F., Taplin,D.M.R.
Creep Damage Accumulation, ***Grain Boundaries Spring Residential Conference Series 3 No 5, Institute Of Metallurgists.***

(2.25) 1956, Chen, C.W., Machlin, E.S.
Acta Metall, Vol. 4, pp655-656.

(2.26) 1956. Gifkins, R.D.
Acta Metall, Vol. 4, pp98-99

(2.27) 1968. Davies, P.W., Williams, K.R., Whilshire, B.
Phil Mag., Vol. 18, pp 197-200.

(2.28) 1976. Cane, B.J.
Metal Sci. And Eng., Vol. 10.

(2.29) 1978, Miller, D.A., Pilkington, R.
Metal Trans., Vol. 9a, pp 1221-1227.

(2.30) 1979, Lonsdale, D., Flewitt, P.E.J.
Mat. Sci. Eng., Vol. 39, p217.

(2.31) 1983, Needham, N.G.
Report Of British Steel Corporation To The Commission Of European Communities, Contract No 7210.MA/802.

(2.32) 1982, Gooch, D.J.
Metal Sci., Vol. 16, pp 79-89.

(2.33) 1981, Cane, B.J.
Metal Sci., Vol. 15, p 302.

(2.34) 1981, Middleton, C.J.
Metal Sci., Vol. 15, p 154.

(2.35) 1981, Cane, B.J. Middleton, C.J.
Metal Sci., Vol. 15, p 295.

(2.36) 1952, Greenwood, J.N.
J. Iron Steel Inst., Vol. 171, p 380.

(2.37) 1975, Raj, R., Ashby, M.F.
Acta Metall., Vol. 23, pp 653-666.

(2.38) 1978, Riedel,H.
Fracture At High Temperatures, *Materials Research And Engineering, Edited By B.Ilschner, And N.J.Grant, Springer-Verlag.*

(2.39) 1966, Feder, J. Russel, K.C. Lothe, J. Pound, G.M.
Adv. Physics, Vol. 15, pp 111-179.

(2.40) 1976, Binder, K. Stauffer, D.
Advances In Physics, Vol. 25, pp 343-396.

(2.41) 1982, Sklenicka, V. Saxl, I. Cadek, J.
Res Mechanica, Vol. 4, p 225.

(2.42) 1976, Dyson, B.F.
Metal Sci, Vol. 10, p 349.

(2.43) 1979, Dyson, B.F.
Canadian Met Q, Vol. 18, p31.

(2.44) 1981, Raj, R. Ghosh, A.K.
Metall Trans., Vol. 12 A, p1291.

(2.45) 1978, Beere, W. Speight, M.V.
Metal Sci., Vol. 12, p 172.

(2.46) 1981, Chen, L.W. Argon, A.S.
Acta Metall., Vol. 29., p 1759.

(2.47) 1983, Wang, J.S. Martinez, W.D. Nix, W.D.
Acta Metall, Vol. 31, p 873.

(2.48) 1955, Ballufi, R.W. Seigle, L.L.
Acta Metall., Vol. 3, p 107.

(2.49) 1959, D.Hull D.Rimmer,
The Growth Of Grain Boundary Voids Under Stress,
Phil Mag, Vol. 4, pp 673-687.

(2.50) 1967, M.Speight J.Harris
The Kinetics Of Stress Induced Growth Of Grain Boundary Voids,
Metal Science Journal, Vol. 1, p83.

(2.51) 1975, Speight, M.V. Beere, W.
Met Sci., Vol. 9, p190.

(2.52) 1973, Chuang, T.J. Rice, J.R.
Acta Metall, Vol. 21, p1625.

(2.53) 1978, Goods, S.H. Nix, W.D.
Acta Metall., Vol. 26, p 739.

(2.54) 1993, Lu, H.M. Delph, T.J.
Models For Coupled Diffusive/Strain Controlled Growth Of Creep Cavities,
Scripta Meta Et Materialia, Vol. 29, pp 281-285.

(2.55) 1980, Needlman, A Rice, J.R.
Acta Met., Vol. 28, p1315.

(2.56) 1987, Schneibel, J.H. Martinez, L.
Scripta Met., Vol. 21, p495.

(2.57) 1967, Ishida, Y. Mclean,D.
Met Sci. J., Vol. 1, p 171.

(2.58) 1976, Harris, J.E.
J. Nuclear Materials, Vol. 59, p 303.

(2.59) 1975, Fleck, R.G., Taplin, D.M.R., Beevers, C.J.
An Investigation Of The Nucleation Of Creep Cavities By 1mV Electron Microscopy, ***Acta Met, Vol. 23, pp 415-424.***

(2.60) 1975, B.Cane G.Greenwood.
The Nucleation And Growth Of Cavities In Iron During Deformation At Elevated Temperatures, ***Metal Science, Vol. 9.***

(2.61) 1972, Dyson,B.F. Mclean,D.
Met. Science, Vol. 6, p 220.

(2.62) 1976, Tipler,H.R. Hopkins,B.E.
Met. Science, Vol. 10, p 47.

(2.63) 1979, Lonsdale, D. Flewitt, P.E.J.
Mat. Sci. And Engng., Vol. 39, p 217.

(2.64) 1980, Needham, N. Gladman, T.
Met. Science, Vol. 14, p 64.

(2.65) 1981, Chen , I.W. Argon, A.S.
Creep And Fracture Of Eng Materials And Structures, ***Ed. Whilshire, B. Owen, D.R.J, Pineridge Press.***

(2.66) 1977, Dyson, B.F. Mclean,D.
Met. Science, Vol. 11, p 37.

(2.67) 1979, Cane, B.J.
Met. Science, Vol. 13, p287.

(2.68) 1983, Dyson, B.F.
Scripta Metall., Vol. 17, pp 31-37.

(2.69) 1983, Needham, N.G. Cane, B.J.
Creep Strain And Rupture Properties By Cavitation Assessment In 2¼Cr 1Mo Steel Weldments, ***ASME International Conf. On Advanced Life Prediction Methods, Materials Conf Albany New York.***

(2.70) 1987, M.Shammas.
Remanent Life Assessment Of Ferritic Weld HAZ By A Metallographic Measurement Of Cavitation Damage - The A Parameter, ***CEGB, Research Report TPRD/L/3200/R87.***

(2.71) 1996, Auerkari, P. Salonen, J. Borggreen, K.
Towards Unified Evaluation Of Replica Inspection For Power Plant Applications, ***Sixth International Conference On Creep And Fatigue, I Mech E Conference Transactions, pp 501 510.***

(2.72) Neubauer, B.
Recent Advances In Creep And Fracture Of Engineering Materials And Structures, ***Ed Whilshire, B. Owen,D.R.J, Pineridge Press, Swansea, pp 617-619.***

(2.73) 1994, EPRI Guidelines,
Guidelines For The Evaluation Of Seam Welded High Energy Piping, ***2nd Edition.***

(2.74) Bollerup,J., Hertzman,S., Ludvigsen,P.B., Sandstrom,R.,Von Walden,E
Cavitation In New And Service Exposed 1Cr½Mo Steel, ***High Temp. Techn., Vol. 4, pp3-11.***

(2.75) 1987, Brett,S.J.
A Model For The Development Of Type IV Cavitation In CrMoV Components, ***CEGB Research Report OED/STM/87/10115/N.***

(2.76) 1984, Cane,B.J., Shammas,M.
A Method Of Remanent Life Estimation By Quantitative Assessment Of Creep On Plant, ***CERL Research Report No TPRD/L/2645/N84.***

(2.77) 1987, Auerkari,P., Vierros,P.
Relation Between Creep Damage, Strain And Residual Life In Power Plant Steam Plants, ***Proc 3rd Int. Conf. On Creep Fracture Of Eng. Materials And Structures, Swansea (UK) Ed. B.Whilshire R.W.Evens Inst. Of Metals, pp 905-914.***

(2.78) 1958, Kachanov, L.M.
Time To Rupture Under Creep Conditions, ***Izv Akad Nauk, USSR, otd. Tekd. Nauk, Vol. 8.***

(2.79) 1960, Kachanov, L.M.
The Theory Of Creep, ***Translated Bishop, E., National Lending Library For Science And Technology Boston Spa, England 1967.***

(2.80) 1953, Hoff, N.
The Necking And Rupture Of Rods Subjected To Constant Tensile Loads, ***J. Applied Mechanics, Vol. 20, p 1.***

(2.81) 1990, Kachanov, L.M.
Introduction To Continuum Damage Mechanics, ***Kluwer Academic Publishing Dordrecht, Nederlands, 2nd Edition.***

(2.82) 1969, Rabotnov, Y.N.
Creep Problems In Structural Members, ***North Holland Publishing Co. Amsterdam, Nederlands.***

(2.83) 1984, Ashby, M.F. Dyson, B.F.
Creep Damage Mechanics And Mechanisms, ***Adv. Fracture Research, Vol. 1, pp 3-30.***

(2.84) 1993, Dyson,B.F. Osgerby,S.
Modeling And Analysis Of Creep Deformation And Fracture In A 1Cr½Mo Ferritic Steel, ***NPL Research Report DMM(A)116.***

(2.85) 1995, Perrin,I.J., Hayhurst,D.R
Creep Constitutive Equations For A 0.5Cr 0.5Mo 0.25V Ferritic Steel In The Temperature Range 600°C To 675°C, ***Department Of Mechanical Engineering, UMIST, Research Report No DMM.95.3.***

Fig 2.1. *Definition of weld crack damage in ferritic steel weldments, (2.4)*

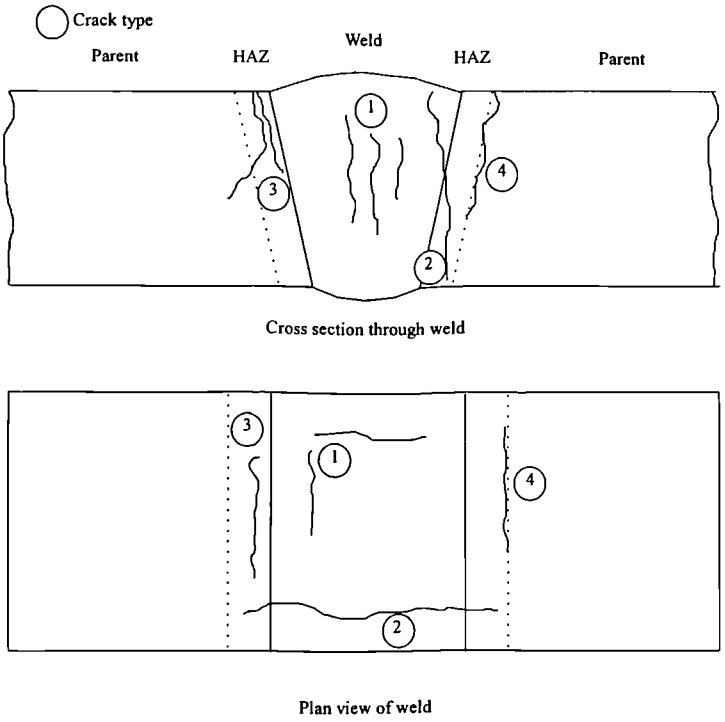

Fig 2.2. *Schematic diagram of four cavity nucleation mechanisms.*

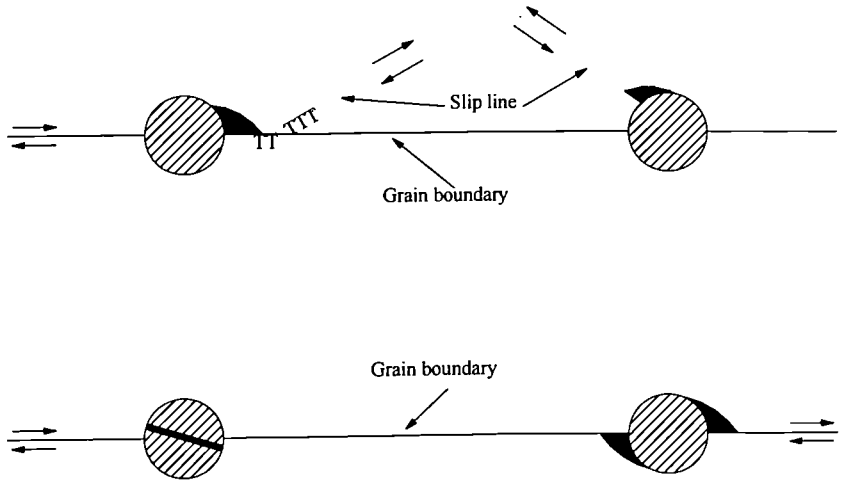

Fig 2.3. *Matrix creep is assumed to produce a distribution of particle/matrix decohesions of effective spherical radii r. Only those with $r > 2\gamma/\sigma_1$ will continue to grow by vacancy absorption to form cavities.*

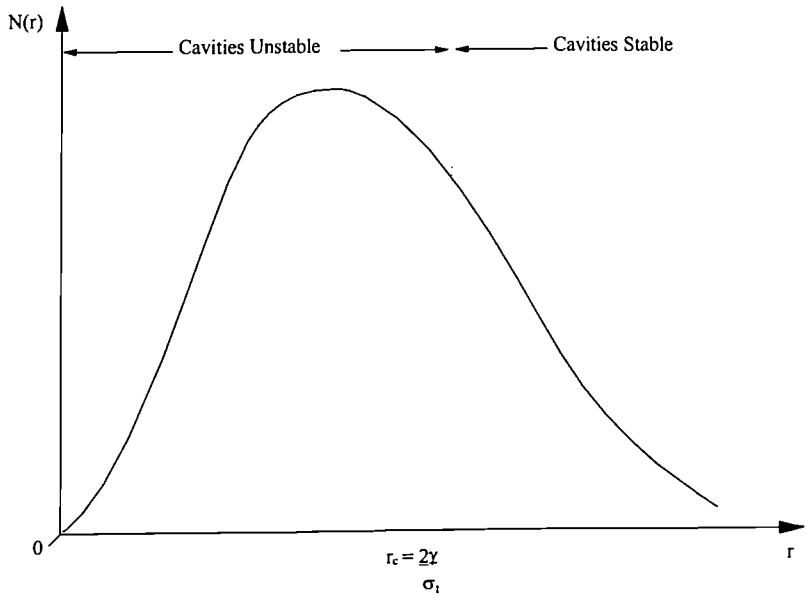

Fig 2.4. *Model for steady-state diffusion growth of intergranular cavities controlled by rate of grain-boundary diffusion.*

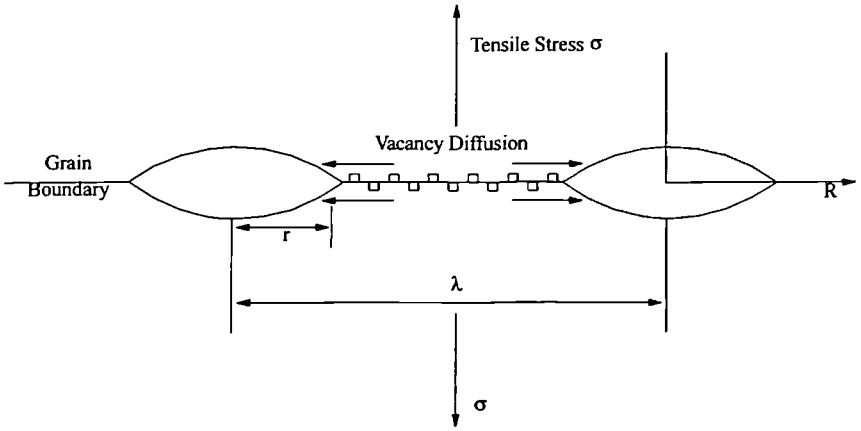

Fig 2.5. *Model for strain-enhanced diffusive growth: A cavity of radius r is associated with circular grain-boundary area of radius c; vacancies which are created in region I (radius b) diffuse to cavity; b schematic distribution of normal stresses acting across grain-boundary*

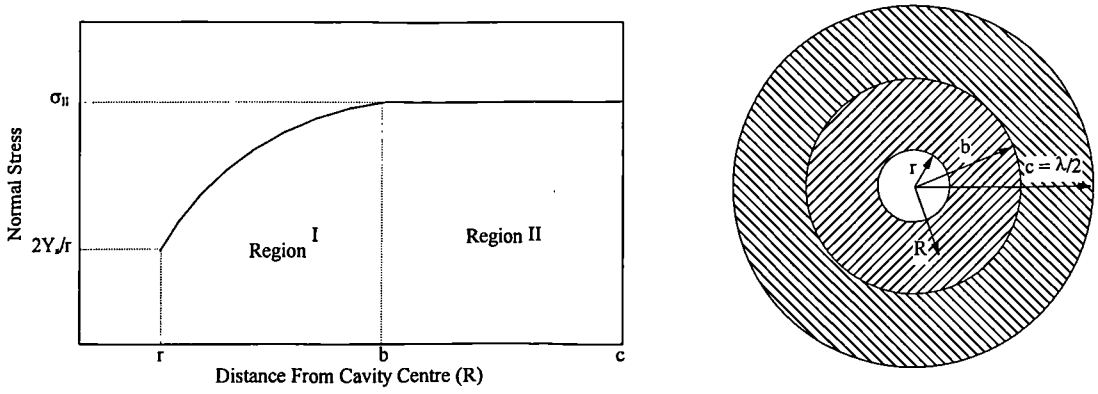

Fig 2.6. *Geometrical constraint of cavity growth; growth rate is constrained if predicted creep rate due to plating out of material at boundary I/II is greater than creep rate of surrounding grains.*

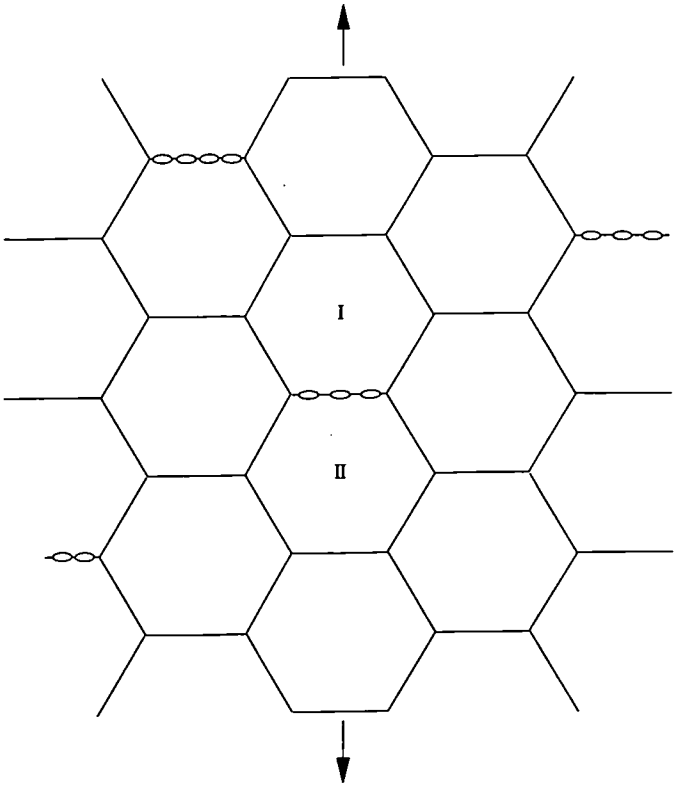

Fig 2.7. *Schematic of cavity growth mechanism map showing calculated cavity growth rates for constrained and unconstrained diffusive cavity growth.*

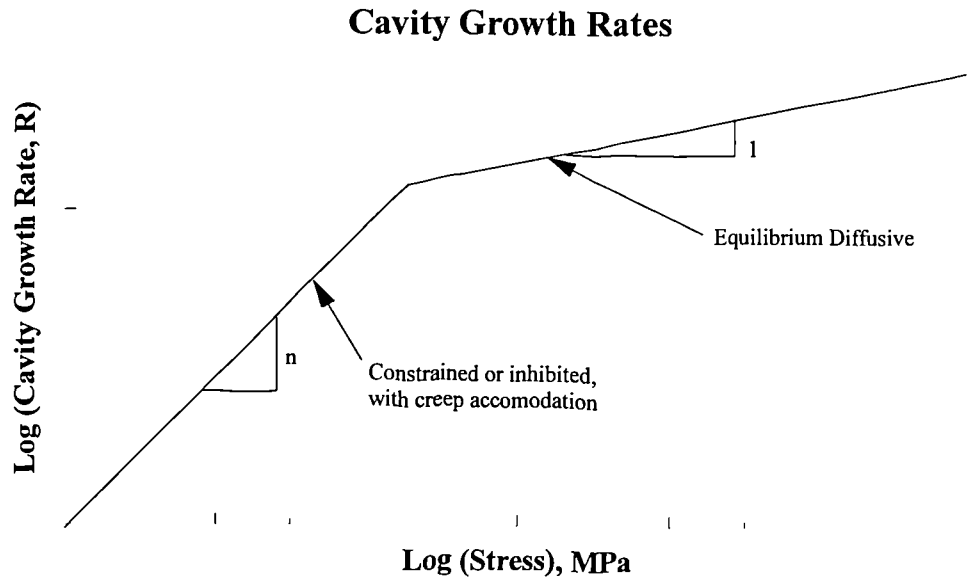

Fig 2.8. *Neubauer damage classification.*

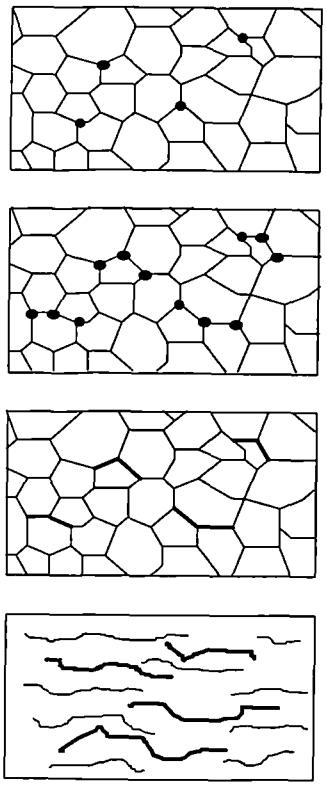

Fig 2.9. *EPRI relationship between damage classification and remaining life*

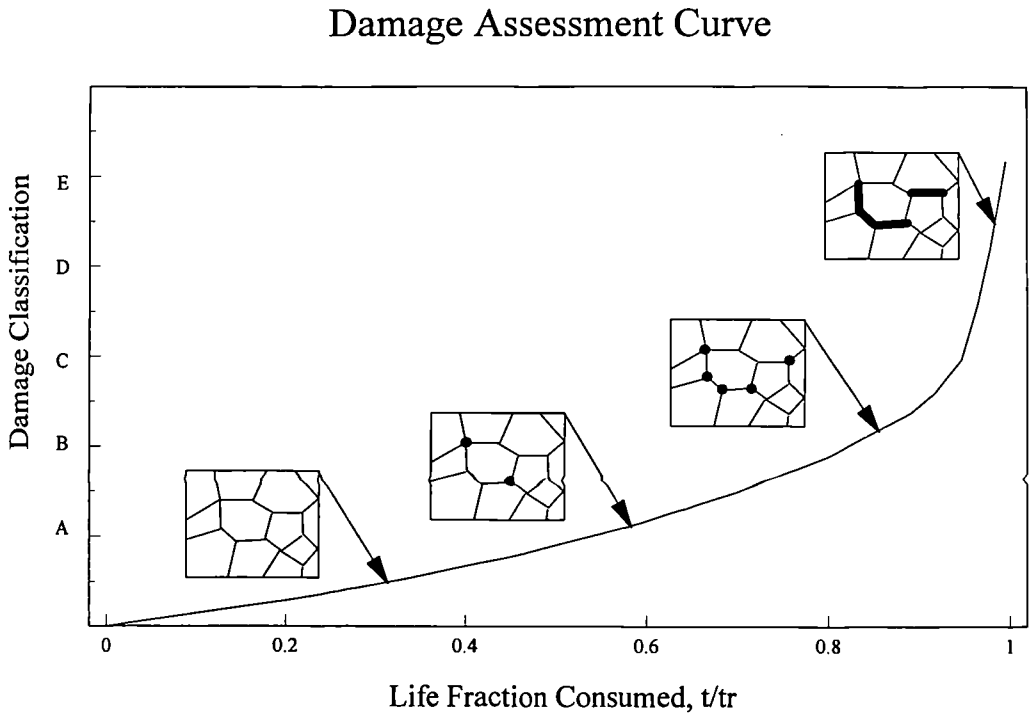

Appendix A1.

A1.1. 'SITE PREPARATION' LARGE SECTION METALLOGRAPHIC PROCEDURE

The steps described below are in accordance with recommendations made by Gooch and Shammas, (**A1.1**) Bates, (**A1.2**) Parker, (**A1.3**).

A1.1.1 GRINDING

i.) Pre-Grinding

Assuming that the specimen site is unprepared oxidised and decarburised layers should be removed by grinding. Excessive and heavy grinding should be avoided, in order to maintain the specimen or component dimensions and to prevent distortion of the true microstructure.

ii.) Grinding

Rough grinding should be performed using a suitable angle grinder or hand held polisher or 'Transpol'. A sequence of coarse through fine SiC grit papers will be used. The final rough ground finish should be that from a 120 grit disc. No lubricant should be used during the grinding stages. Where, decarburisation exists or other such layer, these layers should be removed providing that the shape of the specimens or the integrity of the component is not affected.

iii.) Intermediate Grinding

Intermediate grinding should be performed using a 220 grit paper.

iv.) Final Grinding

Final grinding should be carried out using increasingly finer grades of paper from 400 grit paper to 800 grit paper. Intermediate and final grinding stages should be carried out dry.

v.) Cleaning

All grinding debris should be removed from the sample or prepared area at every stage by washing or swabbing with Acetone or Methanol. Wherever possible the direction of grinding should be change through 90° between each stage of preparation. The grinding time should be twice that required to completely remove all traces of the previous grinding lines.

A1.1.2 POLISHING

Polishing shall be performed following the final stage of grinding. A commercially available diamond polishing compound should be used in conjunction with an appropriate non-water based lubricant. The following schedule should be adopted:

6μm Diamond	DUR/MOL polishing cloth (Struers)
3μm Diamond	MOL polishing cloth (Struers)
1μm Diamond	NAP polishing cloth (Struers)

The polishing speed should be lowered between each diamond grade until the final stage is a gentle buffing action. Hard pressure should never be used in case the surface is accidentally worked. The surface should be swabbed between each polishing stage with copious amounts of Acetone.

A1.1.3 POLISH/ETCH PROCEDURE

The initial 1μm diamond polish should be followed by etching in 2% Nital to develop the microstructure within the grains to a stage suitable for optical metallography. The surface should then be repolished using a 1μm diamond to a depth sufficient to remove all evidence of etching. This polish/etch procedure should be repeated to give a total of three etching procedures with a final etch to produce a structure suitable for replication and optical microscopy.

A1.2. LABORATORY PREPARATION

A1.2.1 GRINDING

i.) Pre-grinding

Pre-grinding is not generally necessary for laboratory specimens. This procedure assumes the starting surface to have a machined or abrasive wheel cut surface or equivalent. Where saw cut or flame cut surfaces are involved suitable precautions must be taken to ensure that cold or heat affected material is removed.

ii.) Grinding

It is assumed that the samples have been mounted using a suitable edge retentive resin and may be prepared using grinding discs fitted with silicon Carbide papers and using water as a lubricant. If samples are too large for this procedure the site preparation should be used. Specimens should be ground using wet papers starting with 80 or 120 grit and finishing with 600 or 1200 grit. A typical sequence would be

80(120)/220/320/400/600/1200. The grinding direction should be changed by 90° between each paper and the grinding time should be double that required to remove the grinding lines from the previous grade.

A1.2.2 POLISHING

The following schedule should be followed after the grinding stages.

6μm Diamond	DUR/MOL polishing cloth (Struers)
3μm Diamond	MOL polishing cloth (Struers)
1μm Diamond	NAP polishing cloth (Struers)

Each stage of polishing should be performed for double the time required to remove the previous stage.

A1.2.3 POLISH/ETCH PROCEDURE

The same procedure should be carried out as described in the site preparation section A.1.3.

A1.3. REPLICATION

The replication of surface topography is achieved by the application of a cellulose acetate sheet, which has resolution characteristics such that it can provide replicated detail suitable for subsequent examination by optical or scanning electron microscopy.

The replica material is available in a range of thickness' from 35μm to 250μm. Generally the thinnest material is used in preference to thicker grades.

The following procedure should be carried out:

i.) Clean the replica site using Acetone.

ii.) Swab the replica site with Acetone which is the recommended solvent for cellulose acetate sheet. Immediately lay the acetate sheet down in one movement displacing the excess Acetone.

iii.) Leave the sheet to harden. As a guide approximately 5 to 10 minutes is required at room temperature for a 35μm sheet.

iv.) Label the replica while still attached to the sample so that the surfaces can be identified.

v.) Remove the replica from the site by carefully peeling. The replica can now be stored in a clean replica sample bag flattened in a hard bound note book this prevents the replica from curling.

vi.) The replica can now be mounted for examination. Carefully remove the replica and apply the labelled surface to a glass slide backed with double sided sticky tape. The replica side which was in contact with the sample surface should now be facing upwards. Firmly apply pressure to the replica using the backing paper from the adhesive tape do not scratch the replica or damage it by moving across the surface.

vii.) For laboratory examination the replica should be gold coated in order to improve the contrast.

A1.4. OBJECTIVE

The objective of a replica procedure should be to produce a replica exhibiting the same detail as that seen by direct observation of a laboratory prepared metallographic section. Use of this procedure should enable that objective to be achieved on a routine basis.

A1.5. REFERENCES

(A1.1) 1987, Gooch, D.J., Shammas, M.S.

A procedure for surface preparation and replication for creep cavity detection in low alloy ferritic steels, ***CEGB Report TPRD/L/3225/R87***

(A1.2) 1989, Bates, P.B.

Metallographic replication of steels on-site and in the laboratory, ***CEGB Report STM/WI/348.***

(A1.3) 1982, Parker, P.D.

The application of a surface replica technique to weldments, ***CEGB Report TPRD/M/1268/N82***

3. MATERIALS AND TEST METHODS.

The following section describes the methodology and testing procedures adopted during the experimental section of this work. The structure of the chapter addresses the materials tested and each different type of test carried out. The final section is devoted to the methods used in quantifying creep cavitation damage.

3.1 INTRODUCTION.

The selection of materials for the research programme was made jointly with Nuclear Electric who supplied a section of pipe taken from a batch of ½CrMoV ferritic steel cast (to be called AB cast), originally intended for use in the construction of the Aberthaw power station. Following initial tests which will be described in more detail later in this chapter, the AB cast was found to be resistant to Type IV damage and it was decided to test a batch of ½CrMoV used for an earlier research programme by Nuclear Electric. This cast is designated M1 and was known to experience Type IV damage as shown by Gooch and Kimmins, (**3.1**). The following section compares the welding procedures and various metallographic features found in the Type IV resistant cast (AB) and the cast (M1) susceptible to Type IV failure.

3.1.1 MATERIALS

The ½CrMoV cast designated AB was originally fabricated for the construction of the Aberthaw power station. The Aberthaw Power Station was historically well known for Type IV damage associated with steam pipework (**3.2**),. Therefore, the cast AB was expected to be susceptible to this form of creep damage. The M1 ½CrMoV experimental cast has been widely used in a number of internal Nuclear Electric test programmes and its rupture properties are well documented, by Gooch and Kimmins, (**3.1**), as well as Nuclear Electric, (**3.3**). The composition of the parent material casts AB and M1 were determined using spark spectroscopy and the results are listed in Table 3.1. These two materials are of similar composition and do not contain any unusually high concentrations of other residual elements.

The weld metals used in the fabrication of the welds were supplied by Nuclear Electric and are in accordance with BS standards 2901 and 2493 respectively. 2¼CrMo weld metal is widely used in the fabrication of steam line weldments. Initial tests using this weld metal suggested that the rupture strength of this material was not sufficient to create the conditions required for Type IV failure to occur in the intercritical region of the AB cast weldment. As a consequence of this it was decided to use a matching ½CrMoV weld metal with a greater rupture strength. However, it was found that the AB cast remained resistant to Type IV damage. Subsequent tests carried out using the M1 cast of material concentrated on the matching ½CrMoV weld metal. Finally in order to look at the effect of

weld strength on the Type IV susceptibility of the M1 parent cast a number of tests were carried out using the 2¼CrMo weld metal.

3.1.2 WELDING PROCEDURE.

The AB cast material was fabricated as a pipe and in common with plant procedure and in accordance with BS 2633 the pipe was welded using a full circumferential butt weld. The pipe wall thickness was 62 mm and the welded lengths , prior to welding , were approximately 250 mm. The angle of the weld was machined to 15 degrees and the weld was constructed using a manual metal arc process (MMA). There were two welds made, one using a 2¼CrMo weld consumable and the other using a ½CrMoV weld consumable.

The M1 cast came in the form of a 104 mm diameter bar. This was then subdivided into five bars each approximately 250 mm long into which, a groove was cut, 70 mm deep in a V shape with sides at an angle of 15 degrees. The MMA process was then used to fill the grooves to make two welds using 2¼CrMo consumable and three welds using ½CrMoV consumable. The welds were all inspected using magnetic particle inspection (MPI) and ultrasonic methods of non destructive examination (NDE) to identify any cracks or defects within the weld and within the heat affected zone. The majority of the welds were defect free. However, one bar did give an indication of a fabrication defect and care was taken not to incorporate this damage in any of the creep test specimens used in the test programme.

The welding procedure for both parent casts M1 and AB included a pre-weld heat treatment of 100°C and a post weld heat treatment at 700°C carried out using electrical resistance heaters. The post weld heat treatment was carried out for 180 minutes and the welds were then cooled at a rate of 50°C per hour until 350°C and thereafter cooled in air. Appendix A2 details the welding procedure for both casts.

3.1.3 TYPE IV SIMULATION PROCEDURE.

In order to produce a uniform homogeneous structure similar in grain size and properties to the Type IV region in a weld, a number of heat treatments were carried out on the as received parent AB cast. The simulation of the Type IV structure had previously been carried out by Gooch and Kimmins (**3.1**) using a number of heat treatments and rupture tests carried out on the M1 cast, the basis of this procedure was repeated using the AB cast by the author.

The heat treatments were carried out at 800°C, 850°C 900°C and 950°C and were kept at temperature for 10 minutes, the specimens used 25 mm cubes and the temperature monitored by using a chrome-alumel thermocouple placed in to a hole drilled to the centre of the specimen. Following the initial heat treatment the specimens were quenched in oil at room temperature, this process was then repeated in order to further refine the grain size. Gooch and Kimmins (**3.1,**) reported that subsequent cycles did little to improve the amount of refinement. Finally the samples were tempered at 700°C for three hours to simulate the post weld heat treatment.

Comparisons were made between the AB Type IV structure in a cross weld specimen and the structure produced by the heat treatment of the parent AB cast. Using optical microscopy it was observed that the simulation heat treatments were very different, with varying degrees of thermal degradation evident in the microstructure. The most microstructurally similar simulation was provided by the 850°C simulation. This was therefore selected as being representative of the Type IV structure found in the AB cast weldments. The microstructures are shown in Plates 3.1 to 3.4.

Vickers hardness measurements were made on the AB simulated samples and the AB cross weld in the Type IV region. The average hardness results of ten measurements are shown in Table 3.2. The results show that the 850°C heat treatment resulted in a similar hardness to the Type IV region; agreeing with the initial observations of grain structure and degradation. These results agree closely with the findings of Gooch and Kimmins (**3.1**) who reported similar results using the 850°C heat treatment from the M1 cast and further showed that this heat treatment produced the lowest creep rupture strength.

3.1.4 TEST PROCEDURES

In order to investigate the effect of stress state tests were conducted using cross weld large section uniaxial specimens, plain bar uniaxial specimens and notched bar specimens. Cross weld specimens were all tested using three 50 kN. dead load creep machines under constant load conditions over a range of temperatures from 600°C to 700°C. Applied stresses ranged from 20 MPa to 80 MPa. The uniaxial constitutive tests and multiaxial notch bar specimens were tested on 5 ton dead load creep rigs. The use of constant load

tests is justified by the fact that design codes are based on constant load creep tests, and for the purposes of comparisons with previous rupture data taken from other projects using the M1 cast and data from the International Standards Organisation. The load is applied through a self levelling beam which is attached to a load train (manufactured from Nimonic 80), via a universal joint. A motorised capstan at the base allowed the beam to be raised or lowered in response to the micro-switches on the beam.

In order to further limit the amount of bending which may occur in the weld metal of the cross weld specimens as a result of the 'V' shape, the loading of the specimen was constrained by fixing the universal joint at the base of the loading train it should be noted that the top universal joint was still retained. With the lower universal joint removed the specimen was constrained from creeping in a non-uniform manner in the weld and so limiting any bending. Uniaxial test and multiaxial notch tests were all carried out in an unconstrained manner, by using a universal joint at the top of the load train and at the base allowing free movement of the specimen. The load calibration of the creep rigs was carried out using a calibrated load cell.

Thermal monitoring of each test specimens was carried out using three Chrom-Alumel thermocouples distributed along the length of the specimen located at the top and bottom HAZ on three of the four faces of the specimen. In addition to these thermocouples two further Platinum-Platinum Rhodium thermocouples were used to control the furnace and to act as a guard controller to prevent over heating these thermocouples were located on the

wall of the furnace or attached to the specimen depending on the furnace set-up. These thermocouples were monitored using a data logger with alarms set for ±2°C of the required temperature.

Strain measurements were made based upon measurements made of the specimens before and after testing. In addition continuous strain measurements were made using extensometry and linear displacement transducers. The data logger provided a print out of the transducer voltage readings at regular intervals along with any alarm readings. In the case of the cross weld specimens it was not possible to measure any strain accumulation in the Type IV region, due to the very small displacements. It is possible to use capacitance strain gauges, although even these gauges are unable to be located exactly across the Type IV region and the results are still subject to some interpretation. As a result measurements were made as a global indicator to the failure mode, with large displacements measured for weld failures and little displacement indicated in the Type IV failures. Continuous strain measurements were made on both the uniaxial plain bar specimens and the uniaxial specimens using extensometry. In addition reduction in area measurements were made.

3.2 CROSS WELD UNIAXIAL CREEP TESTS

3.2.1 SPECIMEN EXTRACTION AND DESIGN.

AB Cross weld test specimens were taken from the welded bar perpendicular to the weld and axial to the pipe, so that they were in line with the direction of the fabrication of the

original pipe as shown in Fig 3.1. Four specimens were taken from each quarter of the pipe and their relative positions noted. In total there were twelve specimens cut from the 2¼CrMo weld and a further four specimens cut from the ½CrMoV weld. The number of samples extracted are summarised in Table 3.3

The M1 cross weld specimens were extracted in a similar way, with specimens taken perpendicular to the welds so that the specimens would lie axially within the bar as shown in Fig. 3.2. In total three specimens were taken from each bar. This meant that there was not enough material to form all of the threaded ends and therefore it was necessary to have flat sides to the threaded ends. This did not seem to have any adverse effect on the loading of the specimen and that there was still sufficient material to prevent any possibility of failure in the threads. From the three ½CrMoV welded M1 bars six cross weld specimens were cut and a further two cross weld specimens were extracted from the 2¼CrMo weld.

The specimen design used during the cross weld test programme were based on a 25 mm x 25 mm threaded square section cross weld samples. The specimen were designed so that the two sides of the welds heat affected zone were split by a change in section which resulted in two distinctly different stress levels which differed by a factor of 1.2, and thus provided cavity data for the low stress HAZ at approximately 50% of the estimated Type IV life at the lower stress. The geometry of the specimen was such that the effects of oxidation which act to reduce the load bearing section were largely negligible, especially since the tests were all interrupted and as a result the applied load was adjusted to maintain

a constant stress. To prevent bending in the weld, the weld has been geometrically constrained to force the weld deformation to occur at the same rate as the parent material. To constrain the weld the height (diameter in a pipe) of the weld metal portion must be at least as great as the length of the weld in the gauge length or width of the weld. Fig. 3.3 shows a schematic of the cross weld specimen.

3.2.2 CREEP TESTS

Cross weld test specimens were taken from both the AB and M1 casts using both combinations of the 2¼CrMo weld and the ½CrMoV weld. The results and the test conditions are detailed below. For the M1 cast cross weld specimens and some of the AB cast cross weld specimens, a number of interruptions were made during the progress of the test in order to conduct detailed metallographic examinations.

The procedure for interruptions based on BS 3500 was aimed at limiting the amount of primary creep experienced when the test is reinstated after each stoppage. Test specimens were not unloaded until after the temperature of the specimen had decreased by at least 300°C when cooling in air. The effect of this was to prevent the dislocations from moving and not allowing stress relaxation while the specimen was still at temperature. Reloading followed the same procedure as that used for initiating a new test, allowing the temperature gradually to increase until it settled at the correct test temperature while at the same time ensuring that there was no load on the specimen and that the maximum temperature was not exceeded. The specimen was then loaded using the auto leveller, and the test temperature was maintained within ±2°C of the set temperature.

Displacement measurements were carried out on all the cross weld tests using a single transducer located remotely on the load train to measure the global strain. This measurement gave a continuous measure of strain accumulation in the cross weld specimen and gave a clear indication of the failure mode. However, it was noted that the measurement was not able to detect the strain accumulation in the Type IV region due to the narrow region over which the strain was occurring. One method of measuring strain is the use of pop marks applied to the surface of the specimen and measured during interruptions. Due to the small displacements and the small gauge length required for measuring strain in the Type IV region it was found that this method was not practical in this situation, hence there is little detailed knowledge of strain accumulation in the Type IV region of the cross weld specimens.

3.3 PLAIN BAR UNIAXIAL CREEP TESTS

In addition to the cross weld tests a series of tests were carried out on the main elements of the weld, including the parent material, the weld metal and a simulation of the Type IV structure formed by the heat treatment of the parent material as described earlier. Tests were carried out on both casts AB and M1. No tests were carried out on the parent form of the cast M1, this was because there is already a large database of results from test programmes conducted by Nuclear Electric, (**3.3**), using the M1 cast of material.

The constitutive testing concentrated on comparing the rupture properties found in the Type IV simulated structure taken from the M1 and AB casts. All the tests were carried

out at 640°C at stresses equal to those tests being conducted in the cross weld test programme. Displacements were measured using transducers attached to extensometers located on the shoulders of the round bar, Fig. 3.4. In addition accurate measurements were taken of the gauge length and diameter of the specimen. These measurements were repeated after the tests had failed in order to calculate the strain accumulated at failure.

3.3.1 SPECIMEN EXTRACTION AND DESIGN

Specimens were extracted from both the AB and the M1 casts of material. All the samples were extracted such that they were oriented parallel to the major axis of the respective bar or pipe.

Two types of specimen design were used a round 9 mm diameter and a 15 mm x 15 mm square section, Fig. 3.5. The round bar tests were initially used as purely rupture specimens to test the constitutive elements of the weldment. The larger square section specimens were developed in order to allow the detailed measurement of the cavity number density both at failure and during the life of the specimen.

3.3.2 CREEP TESTS

The square section bar specimens were tested at 640°C and were all performed using the M1 cast of material, heat treated to give a simulated Type IV structure. The stresses for the tests were between 45 MPa and 160 MPa and the selection was based upon the cross weld test conditions. An additional test was conducted at 700°C and 20 MPa. For all tests

measurements were made of the time to failure, the strain to failure and the cavity number density at failure, as well as the accumulated strain.

A further set of tests were conducted at 640°C and 60 MPa using the M1 cast heat treated to give a simulated Type IV structures. These tests were terminated at various life fractions for destructive metallography and cavity measurements. These were compared to the cross weld test cavity density measurements and similar tests conducted using notch bar specimens described in the next section. The timing of the test interruptions were based upon the cross weld tests. In addition to the cavity measurements, measurements were also taken of the change in gauge length and cross-sectional area.

3.4 NOTCHED BAR CREEP TESTS

Notch bar creep tests were conducted using a round notched bar specimen. The specimens were all extracted from the M1 cast of material heat treated to give a simulated Type IV structure. No notched bar tests were conducted using the AB cast.

3.4.1 SPECIMEN EXTRACTION AND DESIGN

The notch bar specimens were all extracted from the M1 cast and orientated parallel to the axial direction of the parent bar. All the specimens were heat treated to simulate the Type IV microstructure. In addition two specimens were extracted from the ½CrMoV M1 weld bar. These specimens were orientated such that the Type IV region was perpendicular to

the axial line of the specimen, with one end incorporating the weld metal with the other side comprising of the parent material .

3.4.2 NOTCHED BAR SPECIMEN DESIGN

The specimens contained Bridgman notches. The main bar diameter was 17 mm with a notch radius of 3.4 mm, this gave an r/a ratio of 1.5. The stress state within the notched region under creep conditions is given by Hayhurst and Webster (**3.4**). The specimen dimensions are illustrated in Fig 3.6 and 3.7. For the cross weld notched bar specimen the rough machined specimen was macro-etched prior to machining the circular notch so as to assist the correct positioning of the Type IV region within the notch.

3.4.3 CREEP TESTS

Tests were carried out at 640°C and 6.3 kN. The first test was tested to rupture, while subsequent tests were carried out in order to measure the development of damage. These measurements were directly compared these results with measurements which were carried out on the uniaxial cross weld specimens and those interrupted tests which were conducted using the plain bar specimens.

3.5 METHODS OF MEASURING CAVITATION

3.5.1 METHODS OF SPECIMEN PREPARATION.

There are two methods presented in Appendix A1 for specimen preparation that can be used to obtain cavitation measurements, dependant upon the size and shape of specimen.

Firstly there is the traditional method of grinding and polishing a small specimen on a grinding wheel or diamond cloth. A second method is to use a Transpol designed for much larger samples which can not be cut down or do not have a flat side for polishing. The Transpol is a hand held motorised polisher which is able to polish irregular shaped or large objects.

The specimen Transpol preparation technique followed Nuclear Electric guidelines, (**3.3**). These guidelines were developed for the detection of cavitation creep damage by using grinding papers and diamond polishing cloths and paste. Investigations by Shammas et al (**3.6**) showed that a polish etch sequence using 2% Nital and a 1μm diamond paste was the best way to remove any material which has smeared over the surface of any cavitation. The optimum number of polish and etch sequences is three, followed by a last polish and etch to reveal the final microstructure. The more traditional method of sample preparation followed the same guide lines, but uses a larger number of grinding papers in the initial preparation starting at 80 grit and finishing at 1200 grit. The Transpol method of preparation was only employed in the preparation of interrupted cross weld specimens while the more traditional method of specimen preparation was used for the preparation of bulk specimens.

3.5.2 REPLICATION TECHNIQUES

Replication of a polished and etched surface was achieved by the application of a suitable mouldable plastic sheet. This sheet can provide replicated details for subsequent examination by optical or scanning electron microscopy. The Nuclear Electric guidelines

(**3.5**), suggest the use of cellulose acetate of thickness 35 μm to 250 μm. The thickness of the sheet did not appear to effect the results obtained. The procedure detailed by Shammas (**3.6**), is presented in Chapter 2, Appendix A1.

3.5.3 CAVITY COUNTING

The cavity damage in the Type IV region was very localised, and will be discussed in more detail later. A Nuclear Electric procedure (**3.5**) Appendix A3 was followed in order to identify the region and to quantify the amount of maximum cavitation at any one point on the weld. An initial low magnification pass was made of each sample to locate the fusion boundary and HAZ. The replica or specimen was then oriented such that the fusion boundary lay parallel to one of the microscopes traversing directions. Once the fine grained intercritical region had been located the magnification was increased to 200 and a scan was made to identify any regions of high cavity density. If obvious cavitation was not detected then the magnification was increased to 400 and a systematic examination of the Type IV region was made. If any cavitation was found then the region of maximum damage was measured. For the interrupted cross weld specimens this routine was carried out at three locations at the top of the weld the middle and the bottom, as shown in Fig. 3.8.

In order to measure the area of cavitation a reference grid was inserted into the field of view of the microscope. This area was 0.25 mm x 0.25 mm in size and the magnification was X400. The next step was to count the number of cavities inside the reference grid and record the results on a printed sheet with a copy of the grid printed on it. Cavities lying on the edge of a grid were included or excluded systematically from that box, to ensure that

multiple counting of cavities did not occur. Finally the number of cavities divided by the reference area, taking account of the magnification, gave a cavity number density in cavities per mm^2. Plate 3.5 shows a typical region of cavitation in the Type IV region taken from test 103 tested at 640°C and 60 MPa.

3.5.4 DIFFERENTIATION BETWEEN CAVITIES AND OTHER FEATURES

There were a number of observations which allowed us to distinguish between cavities and other microstructural features such as carbides or polishing damage. First, Type IV cavities were always found on grain boundaries, no cavitation was found to occur within the grains. Secondly, focusing and defocusing brought the cavity into focus at different positions relative to the matrix and other features such as precipitates and inclusions. Finally, the cavity on a replica often appeared to sparkle during focusing and defocusing due to the presence of replicating acetate within the void. Plate 3.6 shows a micrograph of a replica showing cavitation in the Type IV region, it was noted that the results obtained from the replica were of equal quality to those obtained from direct observation of the surface.

There were a number of possible sources of error in the measurement of cavitation. In order to assess these errors fully it was important to consider all aspects of the preparation and counting process. The use of a hand held polishing device required a degree of skill to produce the same results especially during the polish etch sequence. In order to give a higher confidence on repeatability the amount of time spent polishing was kept as constant as possible and the amount of time etching was also the same for each step. It was noted

that the method of replication, although giving a true image of the grain structure, was prone to contamination from polishing debris. Although this was reduced by careful cleaning of the specimen, it could in some cases obscure some regions of the Type IV region. However, since the debris artefacts were much larger than the cavity size they do not affect the valuation of the cavity number density.

In order to increase repeatability of measurements and reduce errors in replication and cavity counting, interrupted cross weld specimens were prepared and replicated twice for each interruption, comparisons of the quality of replica were made, and the final measurement was carried out on the cleanest replica. Since the preparation and measurements were carried out by one operator variations are limited, and agree well with spot checks carried out by Nuclear Electric personnel, and was found to be consistent with Nuclear Electric's own cross weld test data will be shown later in Fig. 4.32. Cavity counts were taken from three areas and from these measurements the average number of cavities was calculated, the standard deviation of these measurements was then taken as an error band for the distribution of cavitation across the Type IV region. The magnification at which the cavity measurements did not reveal any real affect on the cavity number density, since it was still possible to identify cavities whether they were viewed at 400 or 3000 using electron microscopy.

3.5.5 FINAL PROCEDURE FOR CAVITY MEASUREMENTS.

Following interruptions 0.5 mm of surface material was removed from the unprofiled sides of the specimen in order to give a representative value of the bulk cavity number density at

the surface, the reason for this removal of material is explained in more detail in chapter 4. Fig. 3.9 shows a schematic of a specimen with the areas marked for removal. Following the rough preparation of the surfaces one side of the specimen was prepared metallographically using the procedures discussed in Appendix A1. Surface replicas were then taken and these were subsequently coated with gold to improve the contrast of the replica. Three replicas were taken on average from the first preparation, and a subsequent two more replicas were taken after the specimen was prepared.

After selecting the best replica, based upon cleanliness and appearance of the etched surface, the cavity number density was measured from three positions located at the top, middle and the bottom of the weld. The measurements were then repeated on the low stress side of the weld using the same replica. This maintained a consistency of preparation on the cavity number density. The results plotted and presented in Chapter 4 as an average of these three measurements and the standard deviation based on the three values.

3.6 REFERENCES

(3.1) 1988,..D.Gooch S.Kimmins
A Study Of Type IV Cracking In ½CrMoV Steel Weldments, ***CEGB Research Report, RD\L\3383\R88.***

(3.2) 1982, Davies, P
ERA Report No 82-0587
Private and Confidential Communication

(3.3) 1995 Nuclear Electric
Private Communication, D Miller.

(3.4) 1986, Hayhurst, D.R., Webster, G.A.
Techniques for multiaxial creep testing, ***Gooch, D.J., How, I.M., Eds. pp137-176***

(3.5) 1995 Nuclear Electric
Guidelines for Cavity Counting
Private Communication, D Miller

(3.6) 1987, Gooch, D.J. Shammas, M.S.
Approach for surface preparation and replication for creep cavity detection in low alloy ferritic steels, ***CEGB Report TPRD/L/3225/R87.***

Table 3.1 *Parent cast and weld composition.*

Aberthaw ½CrMoV Parent Cast Composition								
Element	**C**	**Si**	**Mn**	**P**	**S**	**Cr**	**Mo**	**Ni**
%	0.11	0.17	0.52	0.03	0.03	0.41	0.53	0.11
Element	**Cu**	**Nb**	**Ti**	**V**	**Sn**	**Al**	**As**	**Sb**
%	0.12	<0.01	<0.01	0.25	0.012	<0.001	0.02	0.009

M1 ½CrMoV Parent Cast Composition								
Element	**C**	**Si**	**Mn**	**P**	**S**	**Cr**	**Mo**	**Ni**
%	0.14	0.26	0.59	0.009	0.018	0.32	0.61	0.19
Element	**Cu**	**Nb**	**Ti**	**V**	**Sn**	**Al**	**As**	**Sb**
%	0.16	<0.01	<0.01	0.29	0.01	<0.01	0.02	<0.01

2¼CrMo Weld metal Composition								
Element	**C**	**Si**	**Mn**	**P**	**S**	**Cr**	**Mo**	**Ni**
%	0.05	0.35	0.96	0.014	0.009	2.18	0.91	0.05
Element	**Cu**	**Nb**	**Ti**	**V**	**Sn**	**Al**	**As**	**Sb**
%	0.03	<0.01	0.01	0.03	0.004	0.004	0.01	0.008

Table 3.2 *AB Type IV simulation heat treatment hardness measurements*

AB Type IV Simulation and *AB Cross Weld Hardness Measurements*	
Specimen	Average Vickers Hardness, Kg/mm^2
AB Simulation 800°C	196
AB Simulation 850°C	220
AB Simulation 900°C	249
AB Simulation 950°C	254
AB Type IV Cross Weld	210

Table 3.3 *Specimen extraction*

Parent Cast	Weld	Form	No Samples
AB	2¼CrMo	pipe	12
AB	½CrMoV	pipe	4
M1	2¼CrMo	bar	2
M1	½CrMoV	bar	6

Fig 3.1 *Cutting diagram AB pipe.*

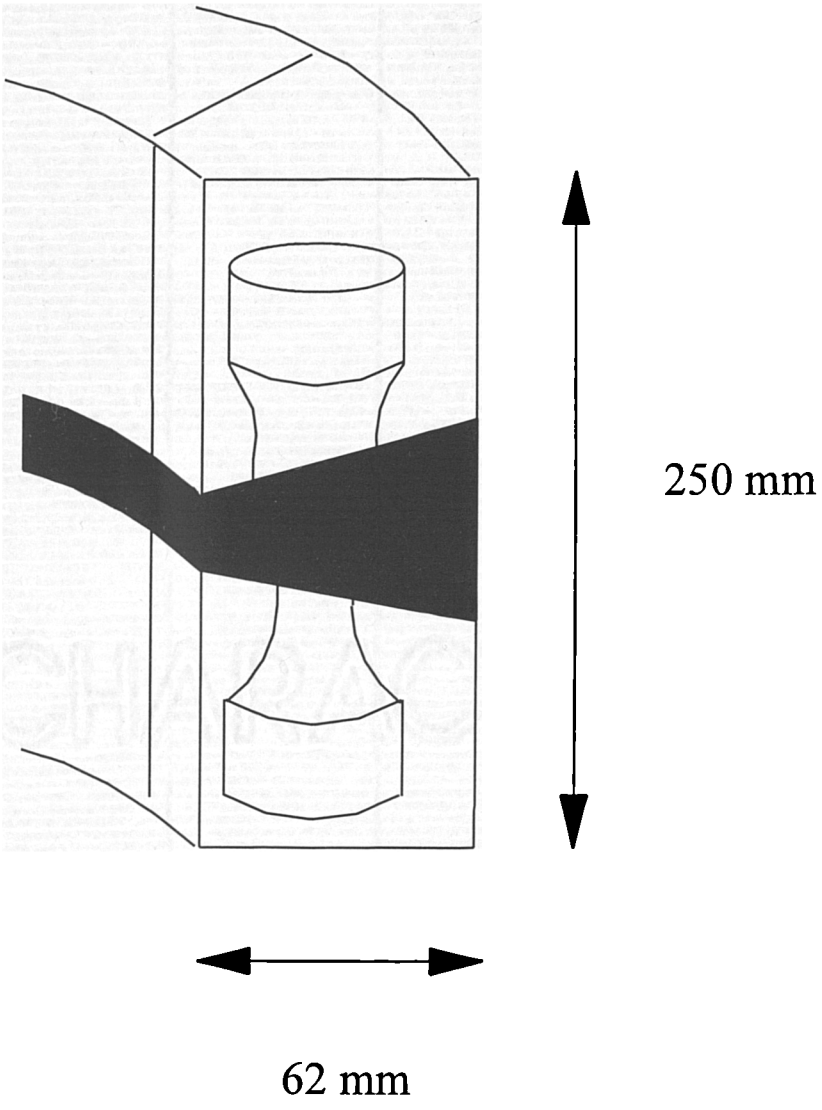

Fig 3.2 *Cutting diagram M1 bar.*

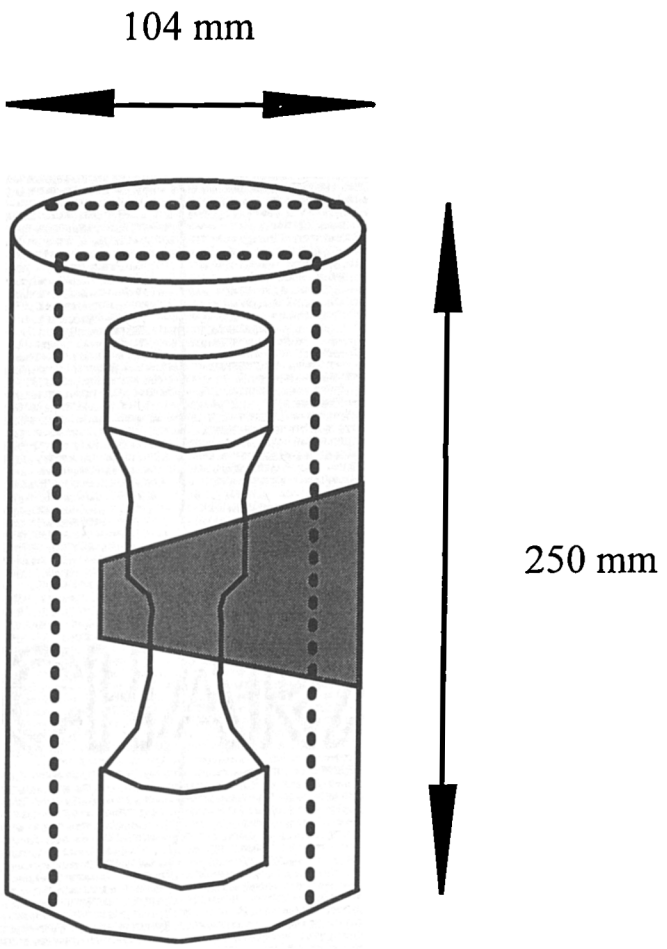

Fig 3.3 *Cross weld specimen design.*

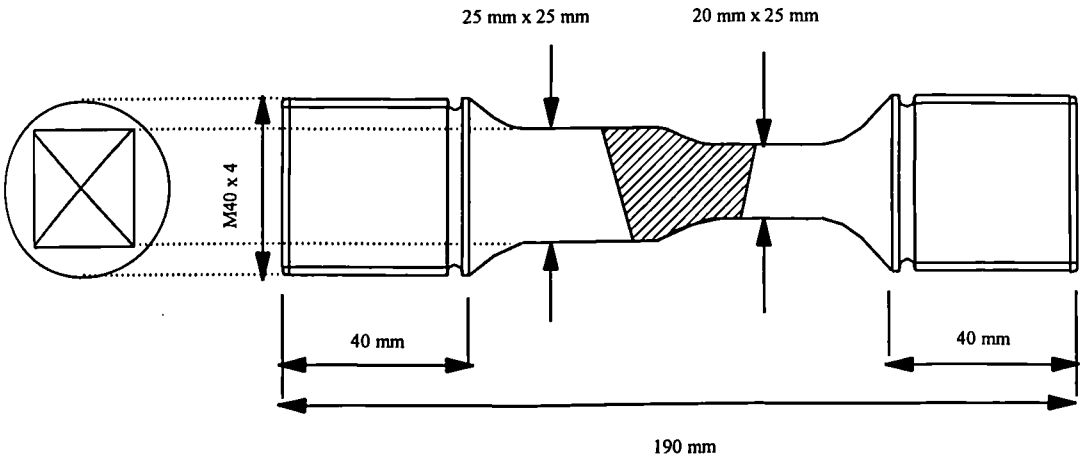

Fig 3.4 *Uniaxial plain round bar specimen design.*

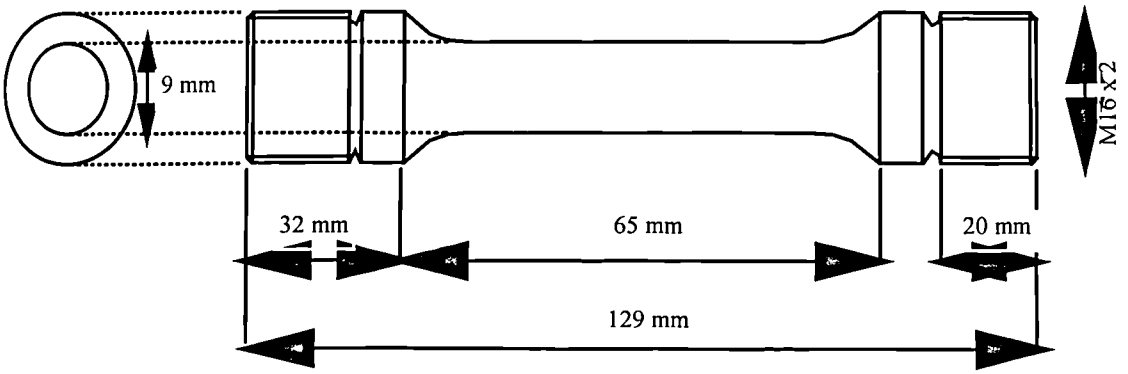

Fig 3.5 *Uniaxial plain bar square section specimen design.*

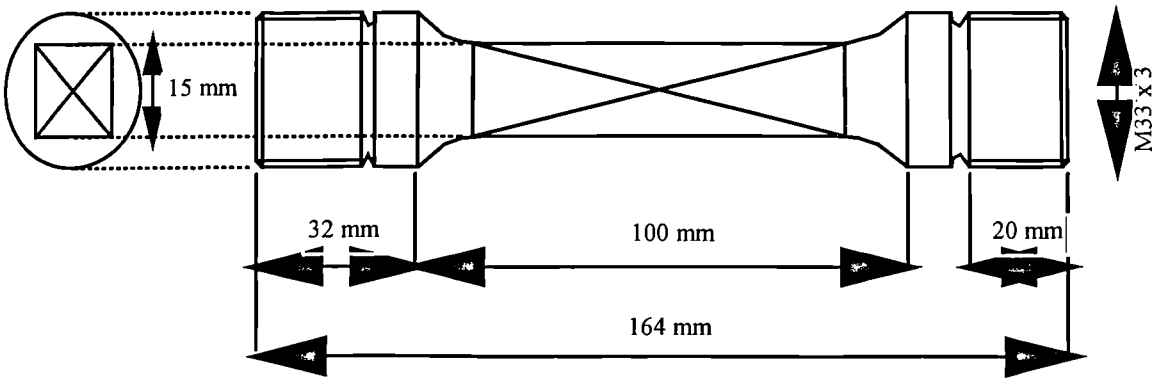

Fig 3.6 *Notch bar specimen design.*

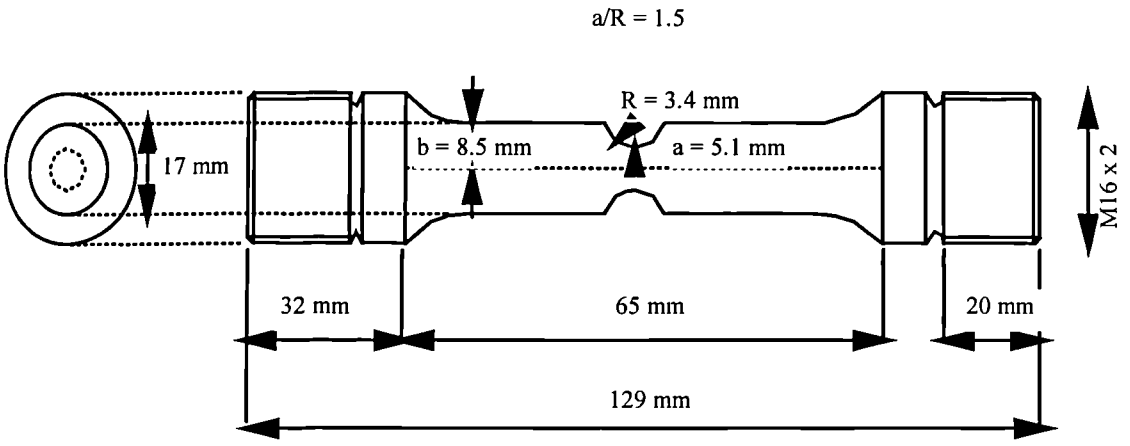

Fig 3.7 *Notch bar cross weld specimen design.*

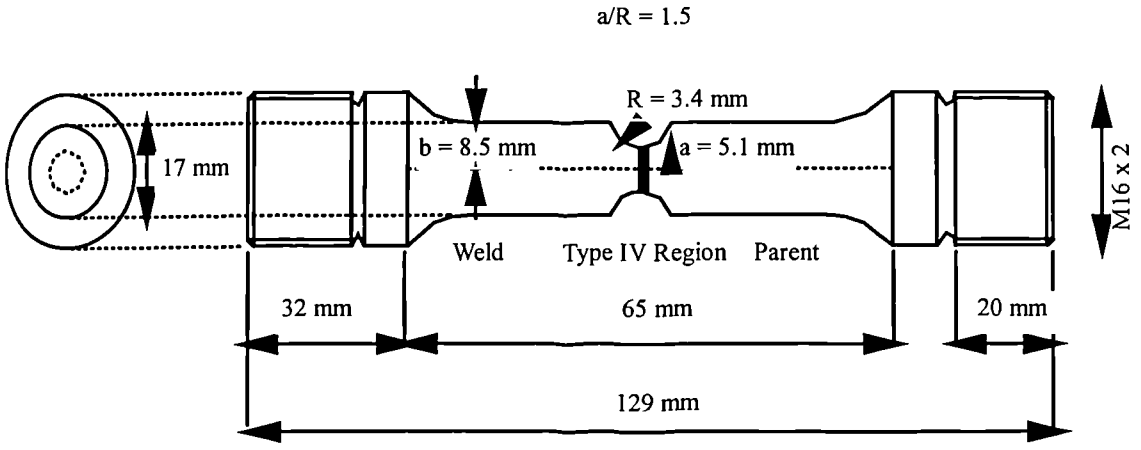

Fig 3.8 *Schematic of weld specimen indicating cavity density measurement locations.*

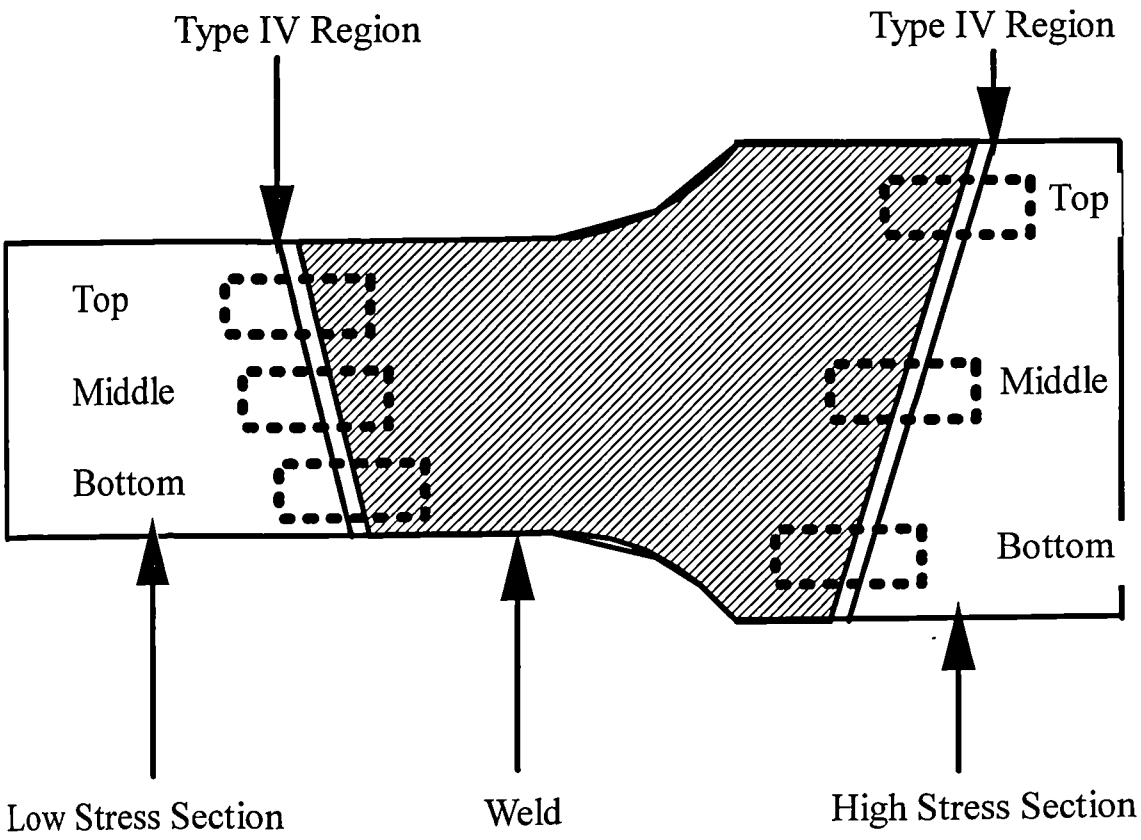

Fig 3.9 *Specimen preparation prior to replication and cavity damage assessment.*

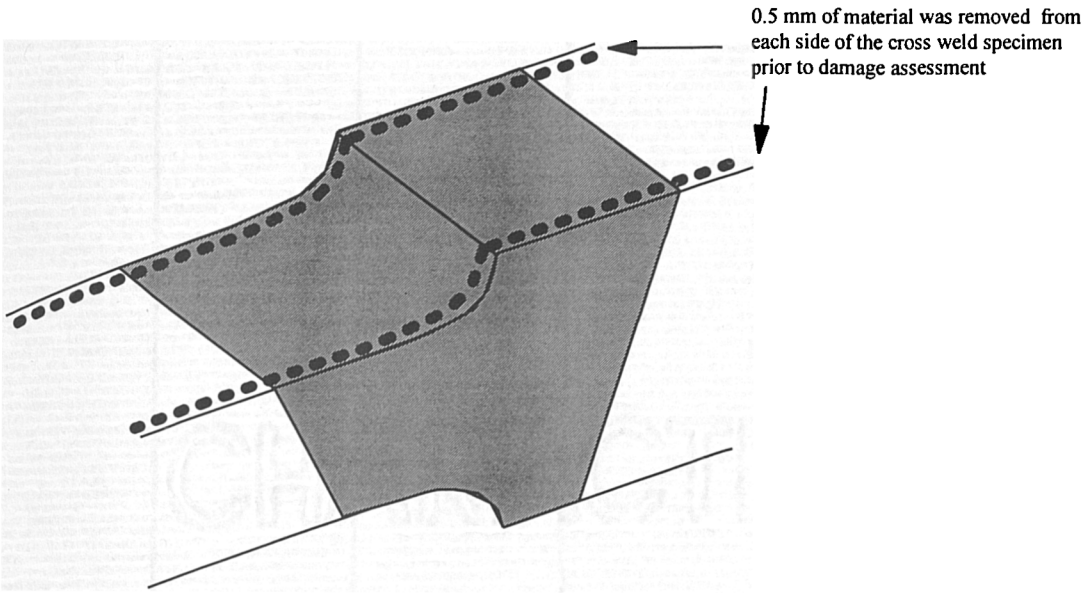

Plate 3.1. *AB Type IV simulation heat treatment 800°C, Magnification x320.*

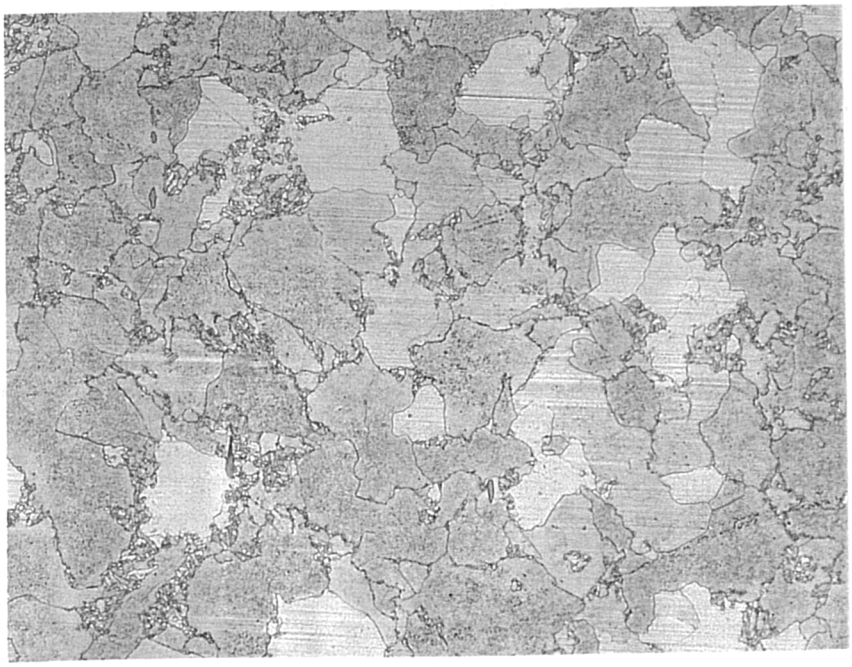

Plate 3.2. *AB Type IV simulation heat treatment 850°C, Magnification x320.*

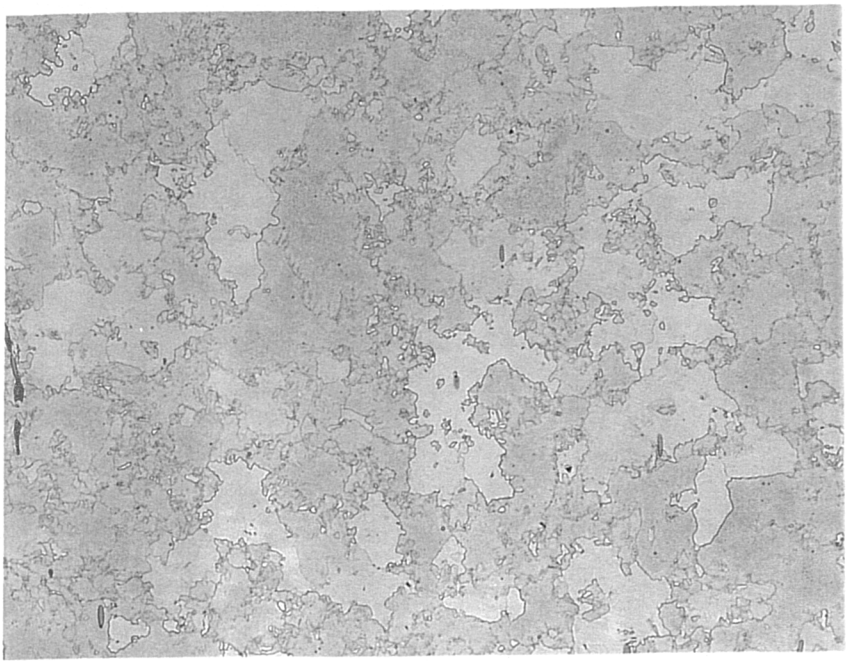

Plate 3.3.*AB Type IV simulation heat treatment 900°C, Magnification x320.*

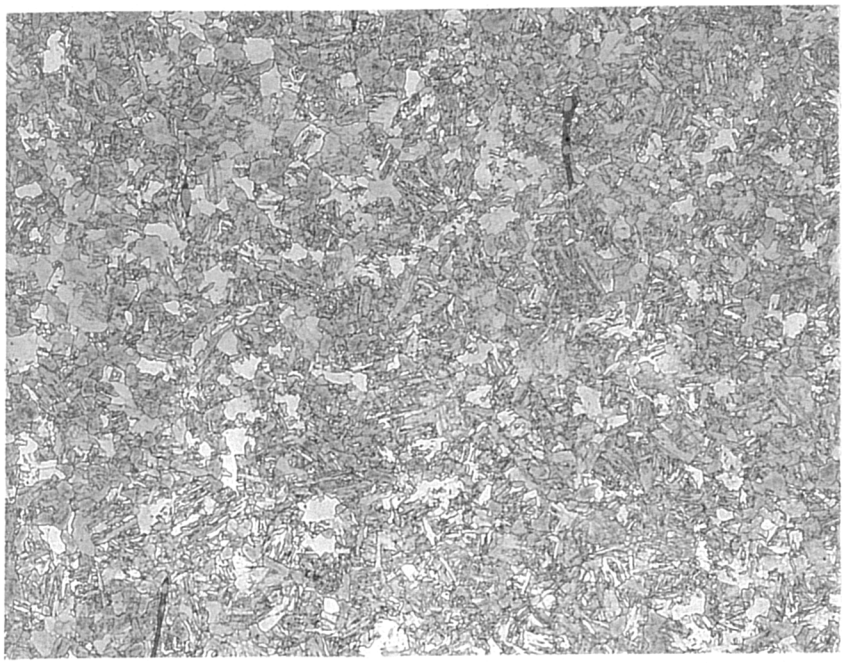

Plate 3.4.*AB Type IV simulation heat treatment 950°C, Magnification x320.*

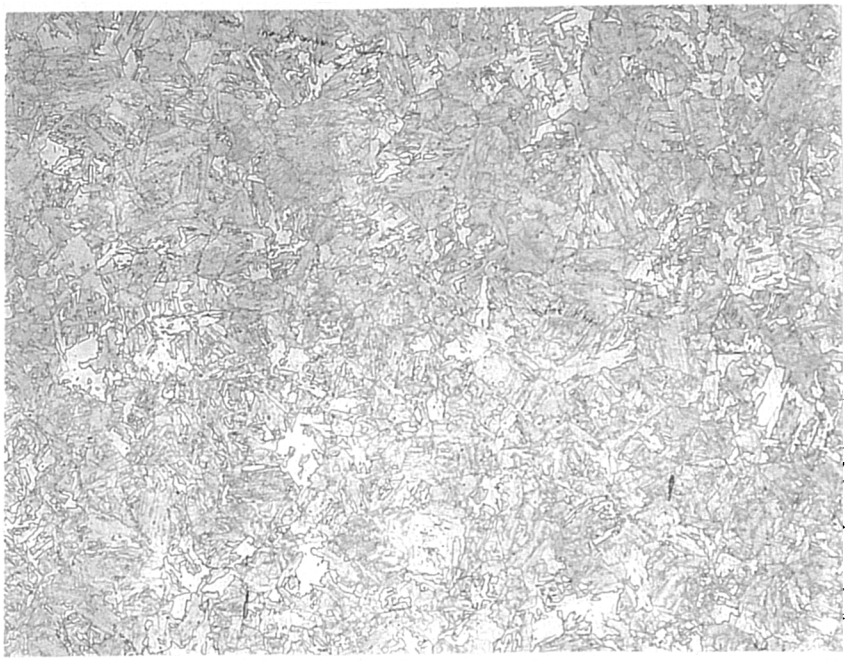

Plate 3.5. *Typical Type IV region Test 103 tested at 640°C and 60 MPa, failed 1064 hours, bulk specimen. Magnification X200.*

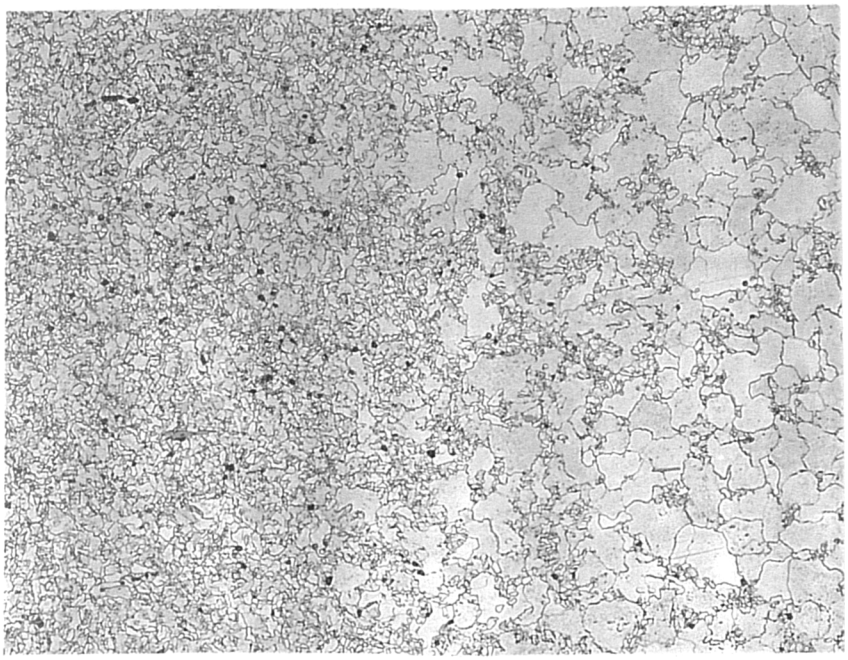

Plate 3.6. *Typical Type IV region Test 103 tested at 640°C and 60 MPa, failed 1064 hours, Replica specimen. Magnification X200.*

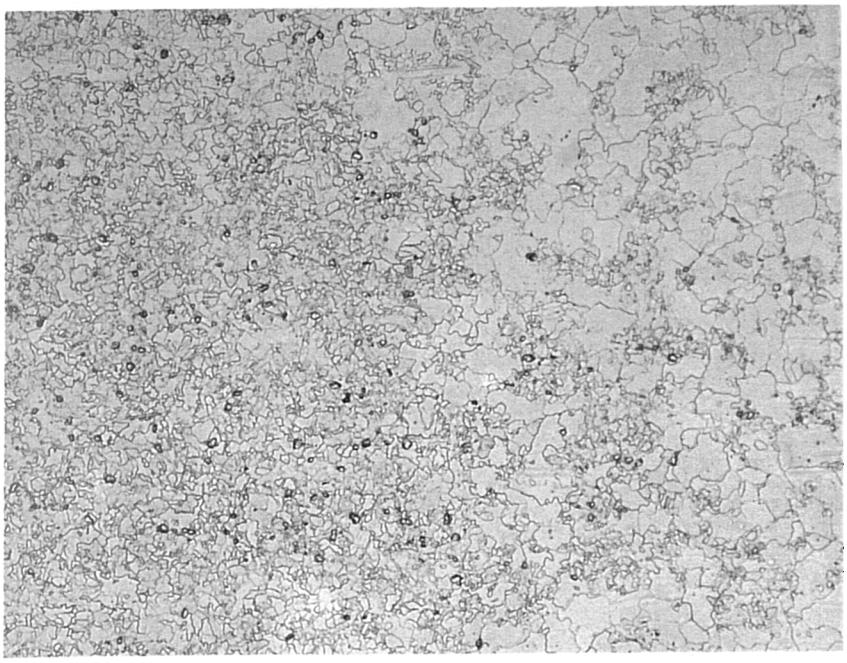

Appendix A2.

A2.1. WELDING PROCEDURE.

South Western Region

SCIENTIFIC SERVICES DEPT

WELD PROCEDURE | A | 05-05 | cc | 01 | TM |

NUMBER BASED ON GOM 104 1980

MATERIAL	1Cr ½Mo – ¼% V Steel 660			
WELD TYPE	Pipe Butt		POSITION	All
SIZE RANGE	Greater than 88.9mm Wall thickness over 12.5mm		JOINT PREPARATION SEE OVER FOR DRAWING	FIG.No 1 or 2 according to thickness
PREHEAT	ROOT 100°C		FILL AND CAP 250°C	
	METHOD Electrical Res.Heaters		MEASUREMENT Thermocouple	
CONSUMABLES	ROOT BS 2901 Pt 1. A33			
	FILL BS 2493 2Cr Mo B			
	SHIELDING GAS Argon 99.95% Pure			
CONSUMABLE DRYING	Electrodes to be baked at 250°C for 2 hours then store in heated quiver.			

		PROCESS	POLARITY	SIZE	OTHER REQUIREMENTS
WELDING PROCEDURE	ROOT	T.I.G.	DC -ve	1.6-2.4mm	Electrode 2% Thiorated Tungsten 2.4mm Shielding Gas Flow 3.7-4.8 lit/m
	FILL	M.M.A.	DC +ve	2.4- 4mm	Welding Current in accordance with Manufacturers Recommendatio
					Weave to be restricted to 3x core wire diameter

POST WELD HEAT TREATMENT SEE OVERLEAF FOR THERMOCOUPLE ARRANGEMENT.	METHOD	Electric Resistance Heaters
	HEATING RATE.	100°C
	SOAKING TEMP.	690°C - 720°C
	SOAKING TIME	25 min/mm thickness Minimum Time 180 minutes
	COOLING RATE	50°C/hr down to 350°C then in still air
	OTHER REQUIREMENTS	Weld Profile to be hot ground before post weld heat treatment and polished afterwards.
WELD SURFACE FINISH	As specified for ultrasonic testing	
FINAL INSPECTION	Magnetic and Ultrasonic examination	
ACCEPTANCE STANDARD	BS 2633	

Appendix A3.

A3.1. CAVITY COUNTING

A3.1.1 QUANTIFICATION OF CAVITATION

Once an area of cavitation has been selected for quantification the following steps should be taken:

i.) Locate the area to be measured centrally in the field of view at a magnification of approximately X200.

ii.) Increase the magnification to approximately X400 and fractional move the specimen in the X and Y directions to maximise the number of cavities in the field of view.

iii.) Insert a boundary box or reference grid into the optical system to superimpose a fixed area on the region to be measured. This area should be typically 0.25 mm x 0.25 mm in size. Again, fractionally move the specimen to maximise the number of cavities within the grid.

iv.) Count and record the total number of cavities in each square of the reference grid or in the total fixed area. It is important that multiple counting of cavities does not occur. If using a reference grid, this can be achieved by counting and recording cavities in individual squares of the grid as shown in Fig. A3.1.

v.) Where cavities touch a boundary box or grid line they should be included or excluded from the reference area in a systematic manner as, for example in Fig. A3.2.

vi.) Total the number of cavities counted and divide by the reference area, taking account of the magnification, to produce a cavity density in cavities per mm^2.

A3.1.2 DIFFERENTIATION BETWEEN CAVITIES AND OTHER FEATURES

There are a number of observations that can assist the examiner to distinguish between cavities and other artefacts. These are listed below, for guidance:

i.) Cavities are always located on grain boundaries.

ii.) Focusing and defocusing brings the cavities in and out of focus at a different position to the matrix and other features such as precipitates and inclusions.

iii.) In replicas, during focusing and defocusing, the cavities often appear to sparkle due to the presence of replicating acetate within the void.

A3.1.3 VERIFICATION

The engineer conducting the assessment should at appropriate stages ensure that the areas assessed are verified the level of verification is entirely dependent on the importance of the activity. Reporting assessment requires the highest level of verification. Verification should be recorded by the verifier countersigning the assessment engineers cavity count sheet as shown in Fig. A3.1.

Cavity Counting

	A	B	C	D	E	F	G	H	I	J	
1											
2											
3											
4											
5											
6											
7											
8											
9											
10											Total

Cavities /mm^2 = Total / 0.0625 for examination carried out at X400

Cavities/mm^2 = / 0.0625

Cavity Density = _____ Cavities /mm^2

Signed: _____ Assessment Engineer

Verified: _____ Date : _____

Fig A3.1. *A typical record sheet for recording cavity counts systematically using a graticule*

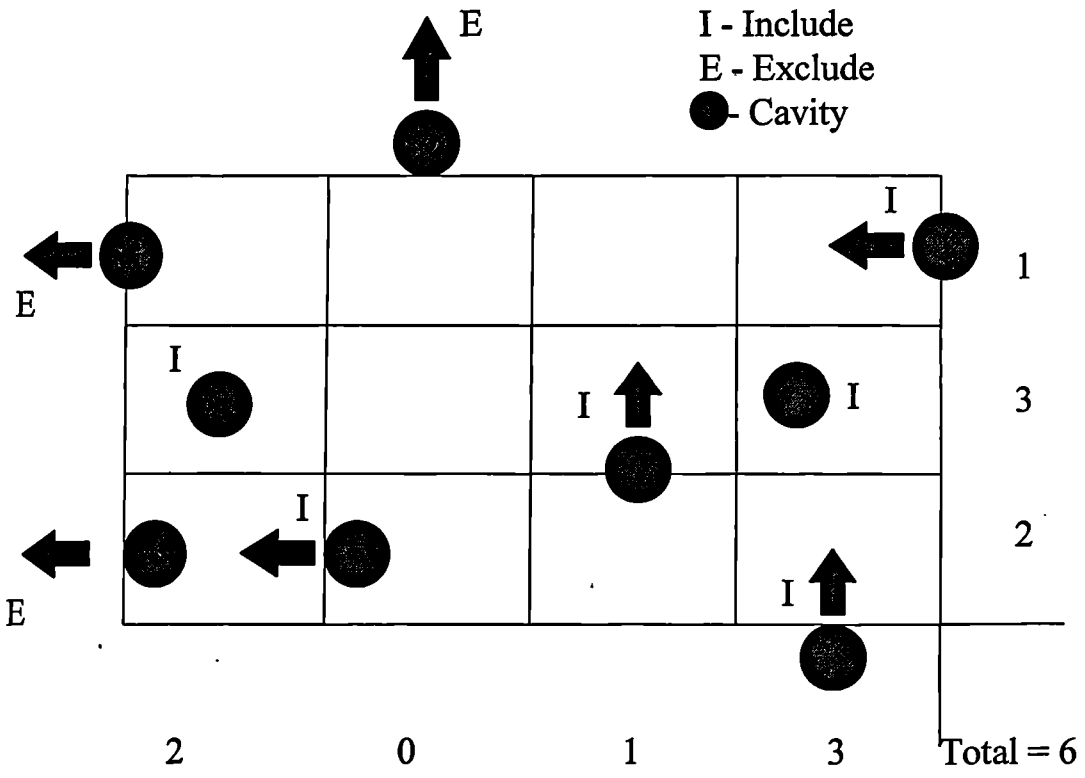

Fig A3.2. *The systematic counting of cavities touching a boundary box or grid lines.*

4. EXPERIMENTAL RESULTS

This chapter present the results of all the metallographic work carried out to characterise the two casts of materials used in this work and the results of all the stress rupture creep tests conducted. In addition, cavity quantification measurements are presented and the results analysed.

4.1 CHARACTERISATION OF THE HAZ

An extensive examination of the all the welds was carried out to compare the welds being used by Bristol University with those which had previously been tested by Nuclear Electric and to identify any distinguishing differences between those casts which were resistant to Type IV creep damage and those which were not.

An initial basic spectroscopic examination of the two casts of steel did not reveal any unusual differences in the major alloying elements. However, there was significant variation in the level of Aluminium between the two casts M1 and AB with a much lower level in the AB cast of material. Aluminium is known to have effects on the grain size and general materials properties such as hardness and creep resistance.

4.1.1 PARENT GRAIN SIZES.

Using a line intercept technique the grain sizes of the parent casts supplied by Nuclear Electric and the Bristol University casts were measured. Examples of all of the grain sizes

are shown in Plates 4.1 to 4.5. Two further parent ½CrMoV casts supplied by Nuclear Electric, and designated MF and US, have both high and low creep rupture strength respectively. The parent material grain size measurements are shown in Table 4.1. Both MF and US casts exhibited susceptibility to Type IV cracking and it was noted that the grain size of the M1 cast was of the same order as both the MF and US casts. However, the AB cast had a grain size which was approximately twice the size of the other casts investigated.

4.1.2 GRAIN SIZE ACROSS THE TYPE IV REGION

The grain size for each weld were measured from the fusion boundary and then into the parent material. The grain size measurements as a function of distance are shown in Fig. 4.1 to 4.5. It was clear, when comparing the parent material casts, that the MMA welding process did not produce the same weld from any one cast and that there were distinct differences which may have arisen as a result of the heat input and time for weld pass and number of weld passes. It was observed that the width of the heat affected zone and the amount of grain refinement in the weld metals varied from weld to weld. The observations also revealed significant variations in grain size across the heat affected zones of the welds.

In spite of these variations, measurements of the grain size in the heat affected zone revealed that the average size of the fine grained regions of the heat affected zone were fairly uniform in size for any given weld, with limited areas of coarse grain structure within the HAZ. Table 4.2 summarises the HAZ average grain size measurements. Plates 4.6 to 4.10 show montages of the weld structure for each of the weldments examined. The

average Type IV grain size appeared strongly dependent upon the parent grain size. This was reflected in the characteristic grouping of fine grains within the AB material surrounded by the much larger parent size grains, while the M1 material and the other Nuclear Electric materials MF and US, was characterised by the degree of blending between the parent grains and those in the fine grained Type IV region. As a result of this blending between the various elements comprising the Type IV region it is difficult to positively define the region in microstructural terms, but instead it is defined as a creep weak region at the intercritical region of the HAZ. Fig. 4.1 to 4.5 illustrates that there is a microstructural transition which is associated with the region where Type IV failure is commonly observed to occur. Figs 4.1 to 4.5 denote this region as the point at which the average grain size is greater than the maximum grain size measured in the HAZ.

4.1.3 HEAT TREATMENTS

Since it was found that the cast AB welds did not provide Type IV failure it was decided to examine the relative thermal degradation of casts M1 and AB. A series of heat treatment tests, carried out for a range of temperatures for various times were conducted. The results of the heat treatments were then compared using Vickers hardness measurements and metallographically using both optical and Scanning Electron Microscopy (SEM).

Heat treatments were carried out at 750°C, 850°C and 900°C and at each temperature for times of 10, 20, and 30 minutes. Since all the specimens were taken from parent casts used in the fabrication of the welds they had already received a heat treatment of 700°C for 180 minutes (i.e. PWHT) prior to these heat treatments. This post weld heat treatment (PWHT)

was then repeated on the heat treated samples in order to simulate the welding process. The time taken for each heat treatment was accurately determined using thermocouples attached to the specimens. Both M1 and AB casts received identical heat treatments followed by oil quenching at close to room temperature. Following the heat treatment the specimens were sectioned and polished and a series of five hardness measurements per sample were made using a Vickers diamond pyramid indentor with a 30 Kg load, on the sectioned surface away from any decarburisation effects. In addition to these specimens a set of specimens in the as received form were measured as a control. The results for each duration of heat treatment are shown in Figs 4.6 and 4.7 for casts M1 and AB respectively. The results are also presented in Table 4.3. The relative trends between the AB and M1 were similar irrespective of the heat treatment time.

Despite the M1 cast being approximately 10% harder than the AB cast there was very little to distinguish between the tempering behaviour of these two casts. However it must be noted that the hardness value does not reflect the creep rupture strength of the material. Examination of the heat treatment microstructures shown in Plates 4.11 to 4.24 was carried out both optically and with the scanning electron microscope (SEM). Plates 4.11 to 4.19 show the M1 and AB microstructure following tempering at 850°C. Plates 4.20 to 4.24 show the M1 and AB casts tempered at 900°C. It was observed that in the heat treated M1 cast the grains were much more refined, and that the levels of martensite which remained in the heat treated AB cast was much greater than that observed in the M1 heat treatments.

4.1.4 MICRO HARDNESS MEASUREMENTS ACROSS THE TYPE IV REGION.

Micro hardness measurements were carried out on both the welded AB and M1 casts for each of the 2¼CrMo and the ½CrMoV welds. This was done for two reasons; first to examine whether there was a distinct difference between the microhardness values of the Type IV regions and second to see if there was any strain softening in the Type IV region for specimens subjected to creep conditions of constant load and temperature.

The micro hardnesses of the weld and HAZ of the unaged AB and M1 cross weld specimens welds are shown in Figs 4.8 and 4.9 respectively for both the 2¼CrMo and ½CrMoV. It was apparent from the M1 unaged hardness distribution, Fig. 4.8, that there was a region of lower hardness located at the transition from the fine HAZ to the parent material. This effect was not evident in the AB cast welds, Fig. 4.9. Fig. 4.10 and 4.11 shows a direct comparison between the M1 and AB unaged 2¼CrMo and ½CrMoV welds, and indicates that the parent materials are of a similar hardness before any thermal effects. However, it was evident that the Type IV region in the M1 material exhibited a lower hardness than in the AB material.

Fig. 4.12 shows the hardness distribution of a strained and thermally aged M1 ½CrMoV weld. The specimen was tested at 620°C and 60 MPa for 2800 hours, which is equivalent to a Manson-Hafferd value of 22.9. A direct comparison with the unstrained unaged M1 weld showed little difference between the hardness values. Fig. 4.13 shows the hardness distribution for an unstrained aged M1 2¼CrMo weld. The specimen was tested at 640°C and 60 MPa for 990 hours this gives an equivalent Manson-Haferd value of 22.9. It is

again clear that there is little thermal softening in either the weld or the parent material. It was noted that there was a region of lower hardness located around the Type IV zone. However, this region did not decrease in hardness compared to the surrounding parent and weld metal following testing as would be expected if there were any strain softening effect as reported by Laha et al, (**4.1.**)

Fig. 4.14 and 4.15 show a comparison between the strained and aged and the unstrained and unaged AB welds. The aged and strained 2¼CrMo and ½CrMoV welds were tested for 720 hours at 60 MPa and 640°C and 780 hours at 60 MPa and 640°C respectively. Thermal degradation was found to be much more apparent in the AB cast welds than in the M1 cast. Although a similar batch of welding consumable was used in both casts of material weldments the hardness values indicate a higher level of degradation throughout the weldment. The discrepancy between the weld metals used in the AB and M1 casts may be linked to the mechanism of failure in the AB weldments which was predominantly in the weld metal. Advanced creep damage within the weldment could have resulted in a lower hardness value.

4.1.5 MICROSTRUCTURE AND CARBIDE MORPHOLOGY

The scanning electron microscope was used to compare both the morphological and microstructural differences between the M1 and AB welds and their Type IV regions.

The main difference between the M1 Type IV region and the AB Type IV region was that the AB cast had a characteristic wide dispersion of fine grains contained in the intercritical

zone roughly mixed with a matrix of large coarse parent grains. The M1 Type IV region was found to be a more refined structure with the fine grains of the HAZ blending into the parent grains in a uniform manner. This resulted in a structure which was intimately mixed with the relatively fine grained parent material independent of the weld. These aspects can be seen in micrographs of the Type IV regions. Plates 4.25 to 4.30

A detailed examination of the distribution of carbides within the Type IV region and the heat affected zone revealed some distinct differences between the M1 and AB welds. It was observed that there was little to distinguish, by visual inspection using the SEM, between the relative amounts of intergranular and transgranular carbides in the HAZ and the parent material. There did appear, however, to be a greater concentration of carbides within the fine grained region of the heat affected zone in the M1 cast than in the AB cast, Plates 4.29 and 4.30. Further investigation was carried out using carbide replicas to determine the composition and morphology of these carbides.

The method consisted of coating a polished and etched specimen with a thin layer of amorphous carbon, removing carbon from the surface of the material in a electro-chemical etch. The thin carbon coat and extracted carbides were then mounted and viewed using a transmission electron microscope (TEM). An X-ray analysis technique called EDAX, together with the examination of diffraction patterns observed using the TEM, allowed the identification of the main carbides present in the two casts M1 and AB. In total four samples were analysed. Due to the dispersed nature of the Type IV region, which was narrow and difficult to isolate, simulated Type IV samples were used, thus providing a

homogenous structure. The samples of each parent cast were prepared in both an aged condition at 640°C for 1000 hours for the M1 cast and 1200 hours for the AB cast, and in the as received Type IV simulated condition. All the samples were unstrained.

The main carbides, identified by diffraction pattern, were cementite Fe_3C, Vanadium and Molybdenum VC and Mo_2C carbides respectively. The extraction technique used did not produce a high density of carbide particles. However, there were areas of sufficiently high density to allow qualitative estimates of the relative numbers of particles to be made. The main problem, which limited the number of particles observed, was due to corrosion on the surface of the specimen after etching. This meant that the amount of time which the sample could be etched was limited and as a result the number of carbides exposed at the surface was reduced.

The aged M1 Type IV simulated specimens revealed 'H' particles, Plate 4.31, which consisted of a single cubic VC which had two lathe like Mo_2C particles forming the uprights of the 'H'. Investigation of the formation of these 'H' particles by determining the diffraction patterns, has suggested that the particles form as the result of Mo particles nucleating on pre-existing VC carbides, there were no equivalent structures observed in the AB aged cast, Plate 4.32. These particles were shown, by EDAX examination, to have a higher concentration of Mo than those particles which have already formed 'H' particles. The concentration of these Mo rich Vanadium particles was much greater in the M1 unaged condition than the AB unaged cast as shown in Plates 4.33 and 4.34 respectively. It is suggested by the author that the VC carbides were preferential sites for nucleation of

the Mo_2C carbides. It was observed that the occurrence of these particles was as great as 50% in the M1 aged material, while in the AB material the frequency was as low as one in fifty.

It was also observed that the amount of cementite in the AB simulated Type IV aged material was much greater than that observed in the M1 simulated Type IV aged material. The majority of the remaining surrounding particles were very fine Mo_2C particles, the concentrations of which were much greater in the aged AB material than in the aged M1 material. It was also noted that the general size of the carbide particles was greater in the aged M1 material compared to the aged AB material.

The unaged Type IV simulated samples showed a similar distribution and composition of carbides to the aged condition, although the occurrence of cementite was much greater in both casts which reflects the degree of carbide coarsening resulting from thermal ageing of the samples. However, the AB aged simulated Type IV material still contained a much higher concentration of cementite than the M1 aged Type IV simulated material, Plate 4.31 and 4.32. Element analysis, using the EDAX technique, confirmed that VC carbides in the M1 unaged Type IV simulated condition contained a far higher concentration of Mo in solution than the aged condition. This suggests that the ageing mechanism has resulted in the Mo coming out of solution and then nucleating the Mo_2C on the VC carbides, while the VC carbide coarsened. It was observed that the relative sizes of the AB and M1 aged carbides surrounding the cementite particles were much finer in the AB aged Type IV simulated material than in the M1 aged Type IV simulated material. These observations

suggest that the simulation heat treatment is more thermally degrading in the M1 cast than in the AB cast. Alloy elements such as Mo and V contained within the AB cast remain in solution for longer. This provides a greater strengthening effect for longer at high temperatures. The fine carbides observed in the AB Type IV simulation samples in both the aged and unaged condition help to maintain the strength of the material. M1 cast, which was observed to contain a greater number of coarsened carbides, will have a reduced creep strength. The effect of thermal degradation will be greatest during a welding cycle, resulting in the creep weak region of the intercritical zone.

4.2 STRESS RUPTURE

The following sections summarise each type of creep test conducted, the method and the type of specimen design.

4.2.1 CROSS WELD TESTS

The results of all the cross weld testing are presented in Table 4.4. As well as the temperature stress and failure times, a Manson- Haferd time-temperature parameter has been calculated in order to combine the test results in one plot. The time temperature parameter is given by:

$$\Delta = \frac{-1000((\log time) - 20.01)}{(T + 104)}$$

equation 4.1

where

Δ = Manson Haferd Time Temperature parameter

T = Temperature in °C

The rupture results illustrate the reduction in the Type IV creep rupture strength compared to that of the ½CrMoV parent material. The Type IV strength is approximately one sixth that of the mean ½CrMoV strength based upon a parametric equation derived from a combination of ISO data, (**4.2,**) and M1 stress rupture data obtained from stress rupture tests carried out using M1 cast material by Nuclear Electric, (**4.3**)and (**4.4.**)

The constants for the parametric fit to this data are presented below

a	= 17.609311594
b	= 2.1323072785
c	= -0.1218696545
d	= -0.05093140765
e	= 0.15530906738

A further parametric fit for predicting the Type IV rupture life is presented based upon the Phillips equation, (**4.4**)where t is the time and $P(\sigma)$ is a function of stress and stress σ is in MPa, T temperature is in °C

$$P(\sigma) = \frac{\log(t) - 20.01}{T + 104}$$

equation 4.2

where:

$$P(\sigma) = -2.0818171x10^{-2} - 3.82507799x10^{-5}(\sigma) + 6.78012145x10^{-8}(\sigma^2$$

equation 4.3

All failures in the M1 cast weldments occurred within the Type IV region, resulting in a characteristic almost brittle style fracture surface, following each cusp of the weldment and HAZ with little evidence of deformation. In addition to tests carried out on the ½CrMoV welds, two tests were carried out using the M1 2¼CrMo cross weld specimens. These tests also failed within the Type IV region. It was noted that there was a small degree of deformation at the fracture surface, although the failure still maintained the same characteristic form of a brittle fracture surface.

Fig 4.16 shows all the M1 cross weld rupture data. It is apparent that at higher stresses (σ>60 MPa) there is a trend towards the mean ISO/M1 ½CrMoV parent rupture times. Meanwhile the variance between the parent properties and the Type IV properties clearly increases as the stress decreases (σ<60 MPa). Nuclear Electric testing has shown that M1 parent material strength is equivalent to ISO mean strength (**4.2**), (**4.3**), and (**4.5**).

All the tests allowed to continue to failure using the AB 2¼CrMo weld resulted in weld metal failures, with no evidence of cavitation or cracking within the parent material or within the Type IV region. Subsequent cross weld tests using the matching ½CrMoV weld metal, which was found to be much stronger during cross weld testing than the 2¼CrMo weld metal also resulted in weld metal failure.

Figure 4.17 shows the results obtained from the AB cast cross weld tests. The result of a single uniaxial creep test conducted using the AB parents casts was also included in Fig.

4.17. Comparison with the ISO/M1 parametric fit indicates that the strength of the AB cast of material was greater than the mean ISO/M1 materials strength for ½CrMoV steels

4.2.2 UNIAXIAL TESTS

All the results of the uniaxial tests are presented in Table 4.5. Uniaxial tests were carried out using both M1 cast materials and the AB cast in the simulated Type IV structure. Sighter tests were conducted to compare the creep strength of the simulated structure with that of the cross weld specimens. The results were consistent with the cross weld failure times for the M1 cast. The results of the AB tests were significantly longer and were almost equal to the ISO/M1 mean strength. Fig 4.18 shows the AB simulated results as well as the AB parent test and the 2¼CrMo weld test. Fig 4.19 shows the M1 Uniaxial tests carried out using the M1 Type IV simulated material. The plot shows that the M1 cast of material closely agrees with the Phillips parametric fit for ½CrMoV cross weld Type IV failure times.

Although different specimen sizes and designs were used in the 'Sighter' tests conducted there was no apparent effect on the failure mechanism or the failure time, although there was a small decrease in the ductility measured.

4.2.3 NOTCHED BAR TESTS

The stress rupture results from the notch bar tests are presented in Table 4.6. The notched bar specimen has a non-uniform stress distribution. This was confirmed by comparison with work carried out by Hayhurst and Webster (**4.6,**) (see also Appendix A4). The

average maximum principal stress over the specimen cross section is the net section stress. The average equivalent stress may be obtained by dividing the average maximum principal stress by a factor of 1.34.

A second set of multiaxial tests were conducted using a pin loaded specimen oriented in a manner so as to test the entire Type IV region under shear stress conditions. The multiaxial state of the tests may be represented by two stresses; σ_{vm}, the Von Mises equivalent stress, and σ_1, the maximum principal stress. The result of the unique shear pin tests was to impose a different principal stress, to that obtained by the notched bar tests, while maintaining the same equivalent Von Mises stress.

Fig 4.20 shows that although the maximum principal stress of the notched bar tests is effectively reversed in the shear pin tests, the ratio of the maximum principal stress to the Von Mises equivalent stress is the same. Indicating that the ratio of maximum principal stress to equivalent stress has a fixed effect on the mechanism of failure within the Type IV region. The results show that the mechanism is mainly dominated by the Von Mises equivalent stress.

4.3 CAVITY NUMBER DENSITY MEASUREMENTS

This section presents the results of the cavity measurements obtained from the cross weld, uniaxial and notched bar tests. Before presenting in detail the cavity measurement results are presented for the effect of magnification.

4.3.1 EFFECT OF MAGNIFICATION ON CAVITY DENSITY MEASUREMENTS

Measurements were carried out over a range of magnifications, on the unfailed low stress section of a M1 ½CrMoV cross weld, test 103, see Table 4.7. All measurements resulted in similar cavity number densities, over a constant area. A comparison was also made over an area of 0.0625 mm^2 between the measurements carried out using the scanning electron microscope, as shown in Plate 4.35 at a magnification of 400 and the optical measurement carried out at the same magnification, Plate 4.36. The scanning electron microscope gave a cavity number density of 1513 cavities/mm^2 compared with an average cavity number density measured optically of 1478 cav/mm^2.

4.3.2 CROSS WELD CAVITY NUMBER DENSITY MEASUREMENTS

Initially the distribution of cavities in a specimen were examined in a M1 parent ½CrMoV cross weld specimen, test 103, which had not been interrupted. The results were compared to another M1 ½CrMoV cross weld specimen, test 304. This specimen had been interrupted using the procedure described in Chapter 3. and included the removal of 0.5 mm from its surface prior to replication and examination. Both the specimens were tested at 640°C and 60 MPa and both failed in the Type IV region. Test 103 failed after 1064 hours and test 304 failed after 1223 hours. A metallurgical examination was carried out on the unfailed low stress side of both the cross weld specimens to quantify the cavity damage and to assess the relative distribution of creep cavitation damage.

The distribution of cavities were examined to assess the effect of cavity measurements taken at the surface compared with those measurements taken from the bulk of the

specimen, Table 4.8. Measurements were taken along the HAZ designated **'L'** at a position half way through the weld from top to bottom, through the weld designated **'W'** located at a position a quarter way across the weld, and across the HAZ designated **'T'**, as shown in Fig 4.21. In the case of test 304 the distance **'T'** was the width of the specimen minus 0.5 mm multiplied by the number of interruptions.

The results presented in Fig 4.22 show that the accumulation of damage is lower at the surface and that cavitation increases towards a bulk material cavity damage level. The aim of removing the material from the surface was to remove the surface effects which was shown to limit the level of cavitation. Test 304 was interrupted four times prior to failure and approximately 2 mm of material had been removed from the surface of the specimen. It can be seen that the increase in cavities is continuous from the results of the uninterrupted test 103 despite the removal of the surface. It was also noted that the results of the interrupted specimens were more representative of the bulk material cavity density following removal of material from the surface. Since the specimen is 25 mm x 25 mm it was not possible to remove a large amount of material at each interruption, and therefore a simple procedure was limited to the removal of 0.5 mm from the surface to provide a more realistic estimate of the materials bulk cavity number density.

Measurements across the HAZ show that the damage was very localised in the Type IV region with very little damage within the parent material, increasing gradually from the fusion boundary and dropping rapidly on the parent side of the Type IV region. It was noted that the distribution of cavity number density across the Type IV failure is much

more localised at the Type IV region, as shown in Fig 4.23. This effect is even more apparent at failure as shown in Fig 4.24. It was also noted that both welds gave a similar distribution of damage through the weld, Fig 4.25. This was mainly due to the constraint placed upon the loading of the specimen which reduced the amount of bending to a negligible level, resulting in consistent cavity readings at any point through the weld.

The results of the cavity number density measurements have been presented from the average of three measurements in Tables 4.9 to 4.17 with the time of interruption and test conditions. The results for the M1 cast cross weld tests, which failed in the Type IV region and the AB cast cross weld tests which failed in the weld metal, are presented. Since the load applied was calculated from the high stress side of the cross weld specimen there were some variations in the stress applied to the low stress section. This was mainly attributed to variations in the amount of material removed during preparation for polishing prior to replication.

Fig. 4.26 shows a plot of the average cavity number density for a stress of approximately 48 MPa. These measurements were all taken from the low stress side of cross weld specimens, at temperatures of 600°C, 620°C, and 640°C. Fig. 4.27 shows the results of the cavity density measurements taken from the same test specimens at the higher stress HAZ at approximately 60 MPa. It is shown in Fig 4.28 that for test 205 the M1 2¼CrMo cross weld test carried out at 640°C and test 304 the M1 ½CrMoV cross weld test that there is no influence of weld metal at the higher stress of 60 MPa.

Fig. 4.29 shows a plot of three tests carried out at 600°C at three different stresses of 48 MPa 60 MPa and 80 MPa. It can be seen that as the stress decreases the cavity number density increases indicating that the development of cavitation in the Type IV region is influenced by stress at a constant temperature of 600°C. Figure 4.29b shows the same data normalised with respect to the time to failure.

In order to compare the tests carried out at different temperatures the time was normalised with respect to the time to failure. Fig. 4.30 shows that for similar stresses of approximately 48 MPa, at various temperatures of 600°C, 620°C and 640°C, there was no distinct trend of temperature, and that there was no influence as a result of difference in weld metal.

Fig. 4.31 is based upon normalised times to failure for tests carried out at 60 MPa over a temperature range of 600°C, 620°C and 640°C. It is again shown that there is no influence of temperature or of weld metal. Finally, Fig. 4.32 cavity number density measurements obtained from a Nuclear Electric specimen designated CW14 tested at 620°C and 50 MPa. For comparison cavity density measurements from an M1 cross weld specimen tested at 620°C and 60 MPa have been included The results indicate that the Nuclear Electric cavity density measurements are slightly higher than those obtained at the same temperature, but a higher stress, this was consistent with the main findings of this work.

4.3.3 PLAIN BAR UNIAXIAL SIMULATED TYPE IV CAVITY DENSITY MEASUREMENTS.

In order to investigate the dependence of stress on the development of cavitation damage within the Type IV region further creep testing was carried out on plain bar uniaxial creep specimens, using the M1 cast heat treated to give a microstructure similar to that found in the Type IV region, were tested over a range of stresses at a constant temperature. One aspect of the heat treatment simulation was that the grain size was between 10 and 15 μm almost twice as large as the fine grained regions found in the Type IV region of the weld HAZ. Initial tests were carried out at 60 MPa at a temperature of 640°C and were terminated at various life fractions to allow metallographic examination of the bulk cavity number density. The results are given in Table 4.18, and show the strain accumulated, the reduction in area, the time to interruption and the average cavity number density.

Fig. 4.33 shows a comparison between cavity number density in a cross weld specimen and a M1 Type IV simulated uniaxial specimen, tested at 640°C and 60 MPa. The results of this comparison show that there is some similarity between the cavity number density in the simulated Type IV structure and the cross weld Type IV structure although it is clear that the cavity number density in the simulated Type IV specimen is lower. The only true variation between the specimens was the grain size, which was judged to be twice the size of the fine grained regions observed in the Type IV region of the cross weld specimens. This was demonstrated by a test carried out at 700°C and 20 MPa which in a high level of grain growth because of the high test temperature. It was significant that the cavity density

measurement was unexpectedly low, and the result indicated a relationship between the cavity number density and the grain size.

Further tests were carried out at higher and lower stresses and the results of the cavity density at failure are given in Table 4.19. Fig. 4.34 show the results of the cavity number density as a function of time. It was noted that for the test presented that the rate of damage accumulation was much greater as the specimen approached failure and that up to 50% life the development of damage was limited.

Fig. 4.35, shows that for the tests carried out at 60 MPa and 640°C the cavity number density was proportional to the measured creep strain. The results shown in Fig. 4.35 illustrate over a wider range of stresses than the cross weld tests that the cavity growth mechanism was strongly dependent upon stress. Fig. 4.36 shows this stress dependence and reveals a transition in the development of cavity creep damage from high stress where the failure mechanism was ductile to low stresses where the failure mechanism was dominated by cavity growth mechanisms. This increase in ductility as a function of stress is shown in Fig. 4.37. Figure 4.38 shows a similar plot of the reduction in area plotted as a function of stress, all the tests were conducted at 640°C.

The effect of the increased ductility on the cavity number density and cavity shape can be seen more clearly in Plates 4.37 to 4.40. Plate 4.37 shows cavitation in a simulated structure tested at 640°C and 60 MPa although the cavitation is more lenticular in shape than those cavities observed in the cross weld Type IV region, they are still of equal size to

the surrounding grains. Plate 4.38 shows much larger cavitation in a specimen tested at the same temperature, but at a higher stress of 80 MPa. Plates 4.39 and 4.40 show that as the stress increases the cavitation is extremely distorted and the number density is reduced, this is associated with an increase in ductility.

4.3.4 BRIDGMAN NOTCH CAVITY NUMBER DENSITY MEASUREMENTS.

The results of the stress rupture tests indicated that the multiaxial failure times were controlled by a mixture of principal and equivalent stress it appears however, that the failure mechanism is dependent more upon the equivalent stress than the principal stress. However, the cavity number density obtained was significantly lower at failure in the multiaxial tests than those values obtained from the uniaxial tests, indicating that cavity growth is not dominated by the equivalent stress, but instead by the principal stress. The results are shown in Table 4.20 for the M1 simulated Type IV notch bar tests and Table 4.21 for the cross weld notch bar specimens. Fig. 4.39 shows the cavity number density measurements plotted as a function of time, included in the plot is the uniaxial data taken from the simulated plain bar specimens carried out at 60 MPa at 640°C.

Since there were no strain measurements taken from the multiaxial tests direct comparisons with the uniaxial tests was carried out by plotting the cavity number density as a function of the reduction in area as shown in Fig. 4.40. It is clear that there is some difference between the cross weld and simulated notched bar cavity number density results.

Fig. 4.41 shows the number of cavities at failure divided by the reduction in area at failure plotted against the equivalent stress and the principal stress. The results are compared with the uniaxial cavity density test data and suggests that cavity growth was influenced more by the principal stress than the equivalent stress. If, the cavity growth was dominated by the equivalent stress the cavity density at failure in the notch bar specimens would have been higher than the uniaxial measurements not lower.

Metallographic examination of the Bridgman notch simulated materials shows that there was little variation in cavity number density across the notched region, Fig 4.42. However, when this distribution was compared optically with the cross weld specimen there was a distinct region of shear occurring at the centre of the specimen at failure, moving into the HAZ away from the Type IV region. FE analysis, Appendix A4 has shown that the principal stress is highest at the centre and it is suggested that as a result the cavity density is reduced so altering the mode of failure in the Type IV region.

4.4 CAVITY SIZE DISTRIBUTION MEASUREMENTS

4.4.1 CROSS WELD CAVITY SIZE DISTRIBUTION MEASUREMENTS

Measurements were made using the SEM to assess the cavity size distribution over a range of life fractions using specimens taken from uniaxial tests and Notched bar tests carried out using the M1 Type IV simulated structure in addition limited measurements were made using the M1 cast cross weld uniaxial and notched bar specimens. The simulated Type IV specimens used were tested at an equivalent stress of 60 MPa at 640°C and interrupted at

various life fractions. The cross weld tests were limited to two life fractions of 50% and 100 % using the same test conditions. Measurements for all the test specimens were made using a constant population of 100 cavities. The smallest cavity which could be measured using the grid was 0.427 μm giving an area of $0.1825\mu m^2$.

Measurements taken from the M1 cross weld uniaxial specimens included the area of the cavity and the length of the cavity perpendicular to the principal stress as well as the width of the cavity. In addition an aspect ratio was measured using the overall dimensions of the cavity shape, length divided by breadth.

Fig 4.43 shows the cross weld measurements made on the uniaxial and notch bar specimens. It can be seen from the plots that the area of the cavities increases from 50 to 100%. Comparison between the notch bar specimens and uniaxial cross weld specimens indicates a similar distribution of measurements. Although there is a definite increase in the size of the cavities towards failure, it is clear that the cavitation at failure did not coalesce significantly. Fig 4.44 shows a schematic of how the aspect ratio was calculated from the maximum length divided by the minimum breadth Fig 4.45 shows this aspect ratio plotted as a function of frequency. It is shown that the shape of the cavitation is maintained right up to failure with the majority of cavities circular in shape, with an aspect ratio close to one.

4.4.2 PLAIN BAR UNIAXIAL CAVITY SIZE DISTRIBUTION MEASUREMENTS

Measurements were made using the square section plain bar uniaxial specimens terminated at fixed fractions of the failure time. The cavity sizes are plotted in terms of the area and the aspect ratio as a function of the frequency. The results of the area measurements presented in Fig 4.46 indicate that there was a range of cavity populations at each life fraction suggesting a staggered or burst mechanism of nucleation occurring continuously through the life of the specimen. It is suggested that cavities nucleate in bursts and then grow to a maximum size as time increases it appears that new cavities nucleate. From the results presented it can be seen that nucleation is continuous through out the life of the specimen. However, it would seem that the nucleation rate is not continuous. This results in groups of cavities all of a similar size and growing at the same rate but all groups having different nucleation times.

Fig 4.47 shows a plot of the aspect ratio which relates to the shape of the cavity. It is shown that the aspect ratio of the cavities in the simulated Type IV uniaxial specimens are lenticular in shape, compared with the circular shaped cavities observed in the cross weld. This would indicate that the cavity growth is influenced by an increase in the amount of diffusion allowing the cavity to grow. It further suggests that the cavity growth in the cross weld specimens is highly constrained.

4.4.3 NOTCHED BAR MULTIAXIAL CAVITY SIZE DISTRIBUTION MEASUREMENTS

Measurements were made of the cavity size distribution across the narrow section ligament using the Type IV simulated round bar notched specimens terminated at fixed fractions of the failure time. The location of the cavities was maintained within a narrow region along the line of the centre of the notch. The results of the area and aspect ratio measurements are plotted as a function of frequency, Fig 4.48 and Fig 4.49 respectively. In addition to the simulated specimens two cross weld notch bar specimens were examined. The two specimens were terminated at failure and at 50% of the failure time, to be consistent with the uniaxial cross weld specimens. This would indicate that cavity growth is slightly more constrained in the multiaxial specimens than in the uniaxial specimens.

4.5 SUMMARY

The two casts of material have been characterised based on grain size, hardness thermal response and carbide morphology. It is clear that there are differences between the characteristics of the AB cast which is resistant to Type IV failure and the M1 cast which is susceptible. One major difference between the two steels was the Aluminium content of the two steels which is known to have detrimental effects on materials properties.

The results of the creep tests have been presented, along with the results of the damage quantification. It has been demonstrated that the Type IV region exhibits the lowest creep strength both in the cross weld and in the Type IV simulated microstructure.

The results of the analysis of the cavity measurements have provided a number of conclusions firstly that there is strong evidence to suggest that cavity nucleation is continuous in the M1 cast. Secondly, the effects of temperature and stress have been addressed, it has been shown that over the range of temperatures tested that the accumulation of creep cavitation damage in the Type IV region is independent of temperature for a given life fraction. It has further been demonstrated that cavity creep damage is dependent on the stress. Thirdly, there is some indication that the stress state although not directly altering the time to failure of specimens does have an effect on the development of creep cavitation damage in the Type IV region. Therefore, it has been suggested from the results that creep cavitation damage is dominated by the principal stress

4.6 REFERENCES

(4.1) 1990, Laha,K., Bhanu Sankara Rao,K., And Mannan,S.L.
Creep Behavior Of Post-Weld Heat Treated 2.25Cr-1Mo Ferritic Steel Base, Weld Metal And Weldments, ***Metal Science And Engineering, A129, pp 183-195.***

(4.2) 1984, Baraclough, D.R., Hamm, C.D., Plastow, B.
Creep rupture equations of steels for use in life assessment calculations based on ISO (1978) data., ***CEGB Report NWR/SSD/84/006/R***

(4.3) 1995, Nuclear Electric, ***Private Communication***

(4.4) 1990, Sanham, E.J., Phillips, J.L.
Derivation of a parametric equation to describe Type IV creep rupture lives in ½CrMoV/2¼CrMo steel weldments, ***Nuclear Electric Report TD/SIP/MEM/1239/90***

(4.5) 1982, Hamm, C.D., Gates, R.S.
ISO creep rupture coefficients for use in boiler plant life assessments, ***CEGB Report SSD/SW/82/N91.***

(4.6) 1986, Hayhurst, D.R. Webster, G.A.
Techniques for multiaxial creep testing. Eds. Gooch, D.J. How, I.M., Elsevier, London, pp137-176.

Table 4.1. *Parent cast grain sizes.*

Parent Grain Size Measurements	
Parent Cast	Grain Size (μm)
AB 2¼CrMo	30
AB ½CrMoV	36
NE Specimen M1	16
NE Specimen MF	16
NE Specimen US	19

Table 4.2. *HAZ and type IV grain size measurements*

Average Grain Size of HAZ	
Parent Cast	Average Grain Size (μm)
AB 2¼CrMo	5.8
AB ½CrMoV	6.8
NE Specimen M1	5.1
NE Specimen MF	5.2
NE Specimen US	4.8

Table 4.3. *Heat treatment hardness measurements*

Hardness Measurements Heat Treated Samples					
Heat Treatment Time/min	Cast	Control	750°C	850°C	900°C
0	AB	158			
10	AB		177	169	246
20	AB		171	173	249
30	AB		170	233	247
0	M1	173			
10	M1		185	190	272
20	M1		179	212	268
30	M1		174	217	272

Table 4.4. *Cross Weld Rupture Results*

a) Aberthaw Cross Weld Rupture Tests								
Test No	Weld Type	Temp (°C)	Load (kN)	Initial Cross Sectional Area (mm^2)	Stress (MPa)	Time to Failure (h)	Time Temp parameter, (Λ)	Overall Displacement at Failure (mm)
T 101	2¼CrMo	640	31	516.7	60	720 *Weld Failure.*	23.1	4.3
T 102	2¼CrMo	640	20.3	507.5	40	3354 *Weld Failure.*	22.2	5.4
T 201	2¼CrMo	640	20.3	506.3	40	2035 *Stopped.*	22.5	0.611
T 301	2¼CrMo	640	20.3	507.5	40	3692 *Weld Failure.*	22.1	2.2
T 202	½CrMoV	640	39.9	498.9	80	788 *Weld Failure.*	23	3.1
T 302	½CrMoV	640	39.8	497.3	80	667 *Weld Failure.*	23.1	4.3
T 303	½CrMoV	600	30.0	499.3	60	3620 *Stopped.*	23.4	1.4
T 203	½CrMoV	580	49.9	498.9	100	4977 *Stopped.*	23.8	0.8
T 311	½CrMoV	700	15.0	500.0	30	633 *Weld Failure.*	21.4	8.6

Table 4.4. *Continued*

b) M1 Cross Weld Rupture Tests								
Test No	Weld Type	Temp (°C)	Load (kN)	Initial Cross Sectional Area (mm^2)	Stress (MPa)	Time to Failure (h)	Time Temp parameter, (Λ)	Overall Displacement at Failure (mm)
T 205	2¼CrMo	640	29.8	497.3	60	996 *Type IV*	22.9	2.7
T 440	2¼CrMo	700	9.9	497.8	20	1601 *Type IV*	20.9	1.5
T 103	½CrMoV	640	29.9	498.9	60	1064 *Type IV*	22.8	2.0
T 104	½CrMoV	600	29.9	498.5	60	8886 *Type IV*	22.8	1.4
T 204	½CrMoV	620	30.0	499.7	60	2885 *Type IV*	22.9	1.6
T 304	½CrMoV	640	29.9	498.5	60	1223 *Type IV*	22.7	1.3
T 305	½CrMoV	600	39.9	498.9	80	4100 *Type IV*	23.3	1.0
T 306	½CrMoV	640	22.3	495.3	45	1784 *Type IV*	22.5	3.1

Table 4.5 *Uniaxial Rupture Results*

Uniaxial Creep Tests										
Test No	Cast	Form	Temp (°C)	Initial Cross Sectional Area (mm^2)	Load (kN)	Stress (MPa)	Time to Failure (h)	Time Temp parameter, (Λ)	Strain to Failure (ε_f%)	Reduction in Area
T 401	AB	Parent 9 mm	640	63.1	5.1	80	2614	22.3	28.1	-
T402	AB	IV Sim 9 mm	640	62.5	5.0	80	1449	22.6	31.5	-
T 403	M1	IV Sim (untemp) 9 mm	640	61.5	4.9	80	728	23.0	4.8	-
T 501	AB	2¼CrMo Weld 9 mm	640	62.9	3.1	50	1441	22.7	33.5	-
T 504	M1	IV Sim 9 mm	640	62.9	5.0	80	603	23.2	15.9	37
T 505	AB	IV Sim 9 mm	640	62.8	3.8	60	2580	22.3	12.8	-
T 601	M1	IV Sim 9 mm	640	62.3	3.7	60	1263	22.7	29.1	-
T 410	M1	IV Sim 15 mm	640	220.5	13.2	60	1310	22.7	14.6	31
T 430	M1	IV Sim 15 mm	640	216.8	26.0	120	83	24.3	32	68
T 431	M1	IV Sim 15 mm	640	136.4	21.8	160	13	25.4	36.7	83
T 631	M1	IV Sim 15 mm	700	223.5	4.5	20	1459	21.0	15.7	-

Table 4.6. *Notch bar rupture results*

Notch bar Creep Tests										
Test No	Cast	Form	Temp (°C)	Initial Cross Sectional Area (mm^2)	Load (kN)	Stress (MPa)	Time to Failure (h)	Time Temp parameter, (Λ)	Strain to Failure (ε_f%)	Reduction in Area
T 521	M1	Xwld Notch Bar	640	80.4	6.3	60	854	23	-	14.9
T520	M1	IV Sim Notch Bar	640	80.9	6.3	60	829	23	-	20.4

Table 4.7. *Cavity number as a function of magnification, test 304 low stress HAZ*

Cavity Number At Various Magnifications	
Magnification	Number of cavities Measured
400	15
650	14
800	14
1000	15
1200	15
1600	14

Table 4.8 *Cavity number density measurements indicating the cavity distribution in the type IV region.*

Cavity Number Density Across Weld (T at W/2)		
Position (mm) **T**	Test 103 (T)	Test 304 (T-2 mm)
0.25	176	1808
0.5		1328
0.75	480	1744
1		2304
1.25	848	2112
1.5		2352
1.75	1056	2384
2		1904

Cavity Number Density Through Weld		
Position (mm) **W**	Test 103 (W at T/4)	Test 304 (W at (T-2 mm)/4)
0	688	1824
5	1136	1936
10	1312	2608
15	1024	2224
20	1952	1936

Cavity Number Density Across HAZ (L at W/2)		
Position (mm)	Test 103	Test 304
0.25	112	288
0.5		400
0.56	272	
0.75		528
0.84	320	
1		864
1.3	576	
1.25		1168
1.38	1024	
1.5		1536
1.7	1200	
1.75		1632
2	1249	496
2.3	800	
2.63	336	
3	48	

Table 4.9 *Cavity number density measurements for interrupted AB cross weld tests*

Low Stress Cavity Number Density Measurements						
Test No.	Temp (°C)	Load (kN.)	Cross Sectional Area (mm^2)	Stress (MPa)	Time (h)	Average Cavity Density (mm^{-2})
T 101 AB 2¼CrMo Weld	640	31	643.1	48.2	720 Weld Failure	No Measurable Cavitation
T 102 AB 2¼CrMo Weld	640	20.3	624.6	32.5	3354 Weld Failure	No Measurable Cavitation
T 201 AB 2¼CrMo Weld	640	20.3	642.4	31.6	2035 Terminated	No Measurable Cavitation
T 3.01 AB 2¼CrMo Weld	640	20.3	630.4	32.2	3692 Weld Failure	No Measurable Cavitation
T 202 AB ½CrMoV Weld	640	39.9	622.5	64.1	788 Weld Failure	No Measurable Cavitation
T 3.02 AB ½CrMoV Weld	Heat-treated 700°C Tested 640°C	39.8	615.1	64.7	667 Weld Failure	No Measurable Cavitation
T 303 AB ½CrMoV Weld	600	30.0	619.8	48.4	3620 Terminated	No Measurable Cavitation
T 2.03 AB ½CrMoV Weld	580	49.9	624.5	79.7	4977 Terminated	No Measurable Cavitation
T 3.11 AB ½CrMoV Weld	700	15	625	24	633 Weld Failure	No Measurable Cavitation

Table 4.9 *Continued.*

High Stress Cavity Number Density Measurements						
Test No.	Temp (°C)	Load (kN.)	Cross Sectional Area (mm^2)	Stress (MPa)	Time (h)	Average Cavity Density (mm^{-2})
T 101 AB 2¼CrMo Weld	640	31	516.7	60	720 Weld Failure	Nominal 100
T 102 AB 2¼CrMo Weld	640	20.3	507.5	40	3354 Weld Failure	Nominal 100
T 201 AB 2¼CrMo Weld	640	20.3	507.5	40	2035 Terminated	Nominal 100
T 3.01 AB 2¼CrMo Weld	640	20.3	507.5	40	3692 Weld Failure	Nominal 100
T 202 AB ½CrMoV Weld	640	39.9	498.8	80	788 Weld Failure	160
T 3.02 AB ½CrMoV Weld	Heat-treated 700°C Tested 640	39.8	497.5	80	667 Weld Failure	Nominal 100
T 303 AB ½CrMoV Weld	600	30.0	500	60	3620 Terminated	No Data
T 2.03 AB ½CrMoV Weld	580	49. 9	499	100	4977 Terminated	No Data
T 3.11 AB ½CrMoV Weld	700	15	500	30	633 Weld Failure	264

Table 4.10` *Cavity number density measurements for interrupted M1 cross weld tests.*

Low Stress Cavity Number Density Measurements							
Test No.	Temp (°C)	Load (kN.)	Cross Sectional Area (mm^2)	Stress (MPa)	Time (h)	Average Cavity Density (mm^{-2})	Standard Deviation (mm^{-2})
T 103 ½CrMoV Weld	640	29.9	625.5	47.8	1064	1457	494.3

High Stress Cavity Number Density Measurements							
Test No.	Temp (°C)	Load (kn.)	Cross Sectional Area (mm^2)	Stress (MPa)	Time (h)	Average Cavity Density (mm^{-2})	Standard Deviation (mm^{-2})
T 103 ½CrMoV Weld	640	29.9	498.3	60	1064	2160	

Table 4.11 *Cavity number density measurements for interrupted M1 cross weld tests.*

Low Stress Cavity Number Density Measurements							
Test No.	Temp (°C)	Load (kN.)	Cross Sectional Area (mm^2)	Stress (MPa)	Time (h)	Average Cavity Density (mm^{-2})	Standard Deviation (mm^{-2})
T 104 M1	600	29.9	622.9	48.4	4049	240	72.7
Weld		28.6	595.8	48.6	5678	1032	1264
½CrMoV		27.2	566.7	48.4	6599	1424	239.1
		25.8	537.5	48.0	7287	1253	229.8
		24.6	512.5	48.0	8289	1104	125
		23.3	485.4	48.0	8886	1787	433.6

High Stress Cavity Number Density Measurements							
Test No.	Temp (°C)	Load (kN.)	Cross Sectional Area (mm^2)	Stress (MPa)	Time (h)	Average Cavity Density (mm^{-2})	Standard Deviation (mm^{-2})
T 104 M1	600	29.9	498.3	60	4049	1092	277.6
Weld		28.6	476.7	60	5678	1388	160.7
½CrMoV		27.2	453.3	60	6599	1744	141.9
		25.8	430.0	60	7287	1642	282.8
		24.6	410.0	60	8289	1802	269.8
Failed		23.3	388.3	60	8886	3061	275.4

Table 4.12 *Cavity number density measurements for interrupted M1 cross weld tests.*

Low Stress Cavity Number Density Measurements							
Test No.	Temp (°C)	Load (kN.)	Cross Sectional Area (mm^2)	Stress (MPa)	Time (h)	Average Cavity Density (mm^{-2})	Standard Deviation (mm^{-2})
T 204 M1	620	30.0	625	48.0	1410	228	149.2
Weld		28.4	588	48.3	1960	1360	228.5
½CrMoV		27.0	559	48.3	2246	1492	251.8
		25.7	534.3	48.1	2552	1716	355.2
		23.9	506.3	47.2	2912	1301	

High Stress Cavity Number Density Measurements							
Test No.	Temp (°C)	Load (kN.)	Cross Sectional Area (mm^2)	Stress (MPa)	Time (h)	Average Cavity Density (mm^{-2})	Standard Deviation (mm^{-2})
T 204 M1	620	30.0	500	60	1410	1040	246.5
Weld		28.4	473.3	60	1960	1596	418.5
½CrMoV		27.0	450	60	2246	1396	113.4
		25.7	428.3	60	2552	2072	645.6
Failed		23.9	398.3	60	2912	2885	80.5

Table 4.13 *Cavity number density measurements for interrupted M1 cross weld tests.*

Low Stress Cavity Number Density Measurements							
Test No.	Temp (°C)	Load (kN.)	Cross Sectional Area (mm^2)	Stress (MPa)	Time (h)	Average Cavity Density (mm^{-2})	Standard Deviation (mm^{-2})
T 304 M1	640	29.9	622.9	48	545	184	131
Weld		28.5	586.4	48.6	710	360	145.8
½CrMoV		25.7	572.4	44.9	804	720	124.6
		23.8	540.9	44.0	904	1088	267.1
		23.1	519.1	44.5	1223	1776	251

High Stress Cavity Number Density Measurements							
Test No.	Temp (°C)	Load (kN.)	Cross Sectional Area (mm^2)	Stress (MPa)	Time (h)	Average Cavity Density (mm^{-2})	Standard Deviation (mm^{-2})
T 304 M1	640	29.9	498.3	60	545	828	288.4
Weld		28.5	475	60	710	1144	244.6
½CrMoV		25.7	428.3	60	804	1460	146.3
		23.8	396.7	60	904	2300	90.9
Failed		23.1	385	60	1223	4261	598.7

Table 4.14 *Cavity number density measurements for interrupted M1 cross weld tests.*

Low Stress Cavity Number Density Measurements							
Test No.	Temp (°C)	Load (kN.)	Cross Sectional Area (mm^2)	Stress (MPa)	Time (h)	Average Cavity Density (mm^{-2})	Standard Deviation (mm^{-2})
T 305 M1	600	39.9	623.4	64	1674	392	220.4
Weld		38.2	597.8	63.9	2244	596	165.4
½CrMoV		36.3	568.1	63.9	2574	748	103.2
		34.7	542.2	64.0	2880	984	313.9
		32.9	518.1	63.5	3376	1296	250.3
		31.3	490.6	63.8	4100	1104	115.4

High Stress Cavity Number Density Measurements							
Test No.	Temp (°C)	Load (kN.)	Cross Sectional Area (mm^2)	Stress (MPa)	Time (h)	Average Cavity Density (mm^{-2})	Standard Deviation (mm^{-2})
T 305 M1	600	39.9	498.8	80	1674	684	197.0
Weld		38.2	477.5	80	2244	788	94.5
½CrMoV		36.3	453.8	80	2574	1444	414.4
		34.7	433.8	80	2880	1432	198.3
		32.9	411.3	80	3376	1488	244.1
Failed		31.3	391.3	80	4100	2181	389.5

Table 4.15 *Cavity number density measurements for interrupted M1 cross weld tests.*

Low Stress Cavity Number Density Measurements							
Test No.	Temp (°C)	Load (kN.)	Cross Sectional Area (mm^2)	Stress (MPa)	Time (h)	Average Cavity Density (mm^{-2})	Standard Deviation (mm^{-2})
T 306 M1	640	22.3	619.4	36.0	1127	752	256
Weld		21	588.2	35.7	1536	1034.666	96.4
½CrMoV		20.4	566.7	36.0	1813	922.67	227
		19.1	532	35.9	2001	1126	299
		18.3	515.5	35.5	2784	1301	280

High Stress Cavity Number Density Measurements							
Test No.	Temp (°C)	Load (kN.)	Cross Sectional Area (mm^2)	Stress (MPa)	Time (h)	Average Cavity Density (mm^{-2})	Standard Deviation (mm^{-2})
T 306 M1	640	22.3	495.8	45	1127	880	104.9
Weld		21	466.7	45	1536	1285.3	88.1
½CrMoV		20.4	453.3	45	1813	1829	300
		19.1	424.4	45	2001	1262	138
Failed		18.3	406.7	45	2784	2576	69.7

Table 4.16 *Cavity number density measurements for interrupted M1 cross weld tests.*

Low Stress Cavity Number Density Measurements							
Test No.	Temp (°C)	Load (kN.)	Cross Sectional Area (mm^2)	Stress (MPa)	Time (h)	Average Cavity Density (mm^{-2})	Standard Deviation (mm^{-2})
T 205 M1	640	29.8	624.7	47.7	499	693	80.5
Weld		28.2	591.2	47.7	732	970	184.1
2¼CrMo		27.2	569.0	47.8	835	1290	324.9
		25.7	538.8	47.7	924	1738	227
		24.3	507.3	47.9	996	1456	461

High Stress Cavity Number Density Measurements							
Test No.	Temp (°C)	Load (kN.)	Cross Sectional Area (mm^2)	Stress (MPa)	Time (h)	Average Cavity Density (mm^{-2})	Standard Deviation (mm^{-2})
T 205 M1	640	29.8	496.7	60	499	656	83.1
Weld		28.2	470.0	60	732	1493	104.1
2¼CrMo		27.2	453.3	60	835	1915	201.3
		25.7	428.3	60	924	2245	291
Failed		24.3	405.0	60	996	2832	481

Table 4.17 *Cavity number density measurements for interrupted M1 cross weld tests.*

Low Stress Cavity Number Density Measurements							
Test No.	Temp (°C)	Load (kN.)	Cross Sectional Area (mm^2)	Stress (MPa)	Time (h)	Average Cavity Density (mm^{-2})	Standard Deviation (mm^{-2})
T 440 M1	700	10.0	628.9	15.9	624	1109.3	122.2
2¼CrMo Weld		9.0	548.8	16.4	963	1024	136
		8.0	512.8	15.6	1601	1333	506

High Stress Cavity Number Density Measurements							
Test No.	Temp (°C)	Load (kN.)	Cross Sectional Area (mm^2)	Stress (MPa)	Time (h)	Average Cavity Density (mm^{-2})	Standard Deviation (mm^{-2})
T 440 M1	700	10.0	500	20	624	1696	372.8
2¼CrMo Weld		9.0	450	20	963	928	57.6
Failed		8.0	400	20	1601	2538	545

Table 4.18 *Cavity number density measurements for uniaxial M1 Type IV simulated tests.*

Uniaxial M1 Simulated Type IV Structure Cavity Number Density Measurements									
Test No	Temp (°C)	Load (kN)	Cross Sectional Area (mm^2)	Stress (MPa)	Time (h)	Strain ε (%)	R of A (%)	Ave. Cav No (mm^{-2})	STD (mm^{-2})
Uni 410	640	13.2	220.4	60	1300	14.6	31	4160	
Uni 411	640	13.3	222.2	60	1170	6.8	16.8	2725	177.1
Uni 413	640	13.4	222.8	60	1007	5.1	13.3	880	97.3
Uni 414	640	13.2	220.3	60	907	3.3	9	629.3	144.3

Table 4.19 *Cavity number density measurements for uniaxial M1 Type IV simulated tests.*

Uniaxial M1 Simulated Type IV Structure Cavity Number Density Measurements									
Test No	Temp (°C)	Load (kN)	Cross Sectional Area (mm^2)	Stress (MPa)	Time (h)	Strain ε (%)	R of A (%)	Ave. Cav No (mm^{-2})	STD (mm^{-2})
Uni 631	700	5	249.7	20	1459	15.7	48.5	1130	106
Uni 504	640	5	62.4	80	603	15.9	37.4	1626	242.3
Uni 430	640	26	216.4	120	83	32	68.0	1264	536.2
Uni 431	640	22	137.3	160	13	36.7	83.1	1061	535.8

Table 4.20 *Cavity number density measurements for notch bar M1 Type IV simulated tests.*

Notch Bar M1 Simulated Type IV Structure Cavity Number Density Measurements								
Test No.	Temp (°C)	Load (kN)	Cross Sectional Area (mm^2)	Equi. Stress (MPa)	Time (h)	R of A (%)	Ave. Cav No (mm^{-2})	STD (mm^{-2})
BN 610	640	6.0	80.9	60	829	20.4	1509	281.9
BN 611	640	6.0	80.6	60	719	6.5	1072	69.7
BN 612	640	6.0	80.0	60	626	6.7	773	148.7
BN 613	640	6.0	78.5	60	575	6.2	804	163.1
BN 530	640	6.0	81.1	60	406	3.0	443	51.4

Table 4.21 *Cavity number density measurements for Notch Bar M1 cross weld tests.*

Notch Bar M1 ½CrMoV Cross Weld Cavity Number Density Measurements								
Test No.	Temp (°C)	Load (kN)	Cross Sectional Area (mm^2)	Equi. Stress (MPa)	Time (h)	R of A (%)	Ave. Cav No (mm^{-2})	STD (mm^{-2})
BNX 520	640	6.0	80.4	60	854	14.9	2213	160.3
BNX 521	640	6.0	81.9	60	427	2.3	1258.7	106.3

Fig 4.1 *Grain size across HAZ AB 2¼CrMo cross weld specimen*

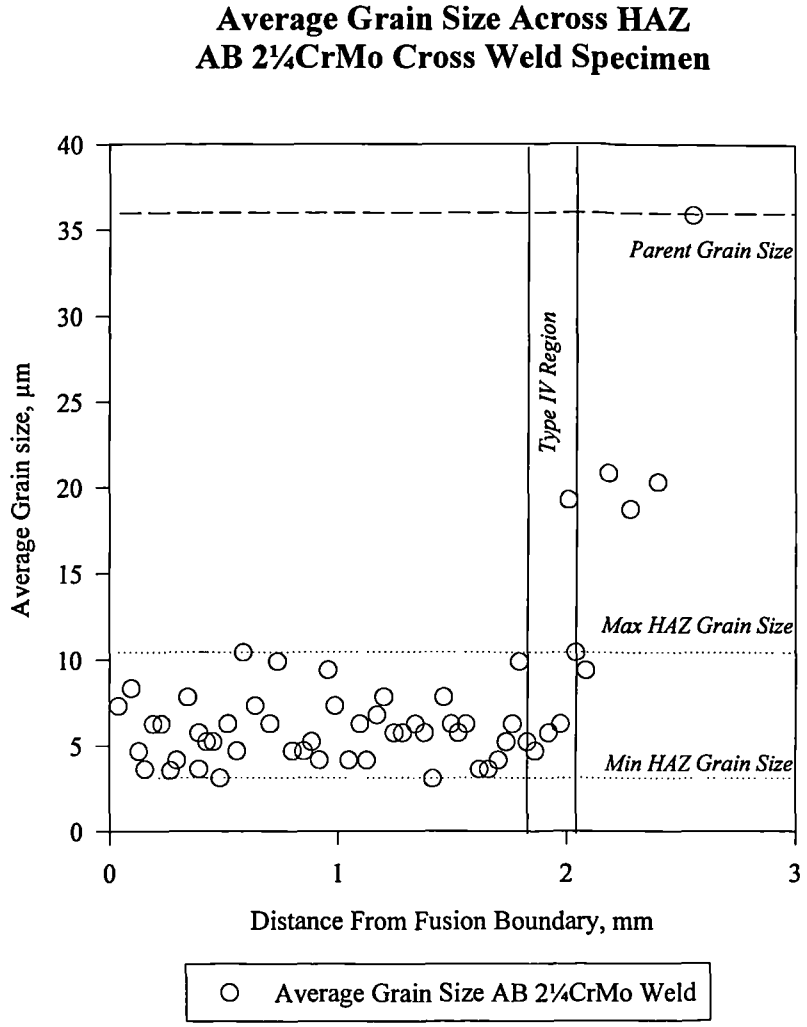

Fig 4.2 *Grain size across HAZ AB ½CrMoV cross weld specimen*

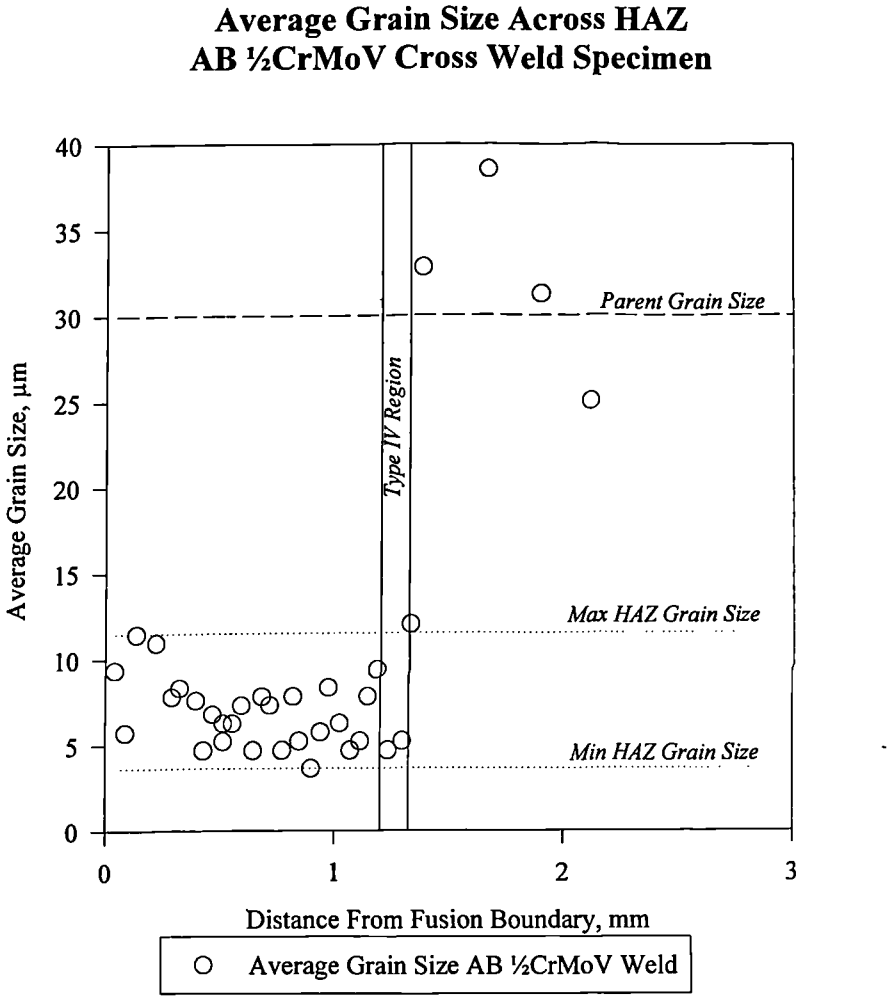

Fig 4.3 *Grain size across HAZ M1 2¼CrMo cross weld specimen*

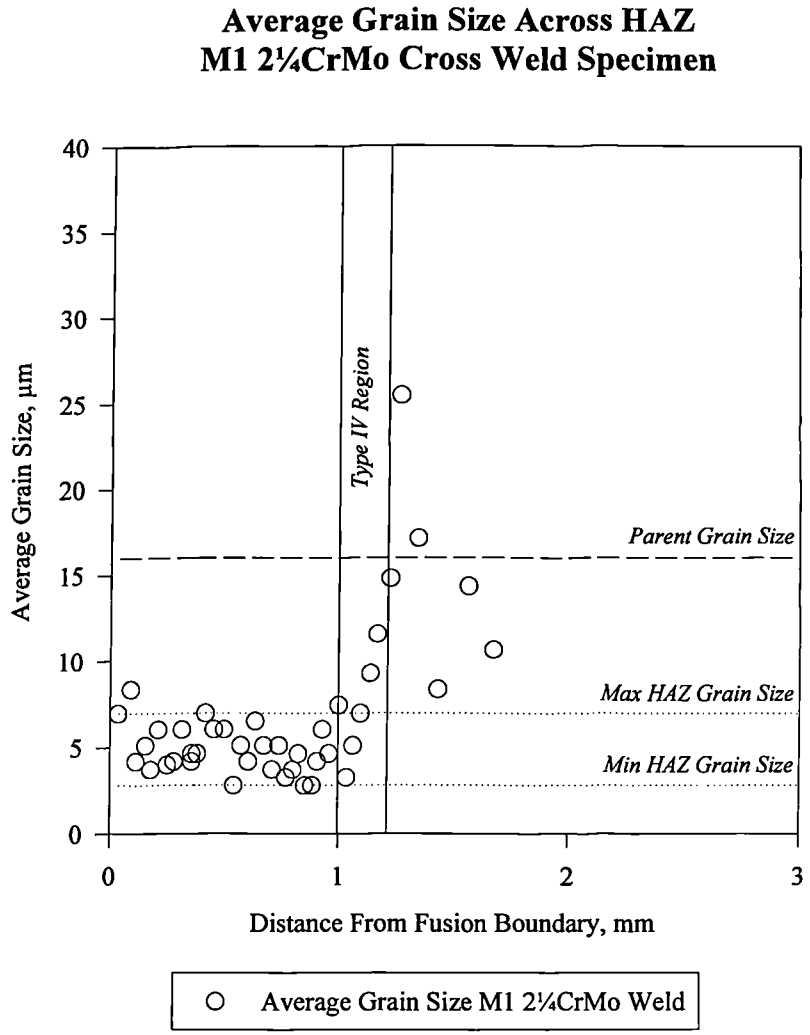

Fig 4.4 *Grain size across HAZ US 2¼CrMo cross weld specimen*

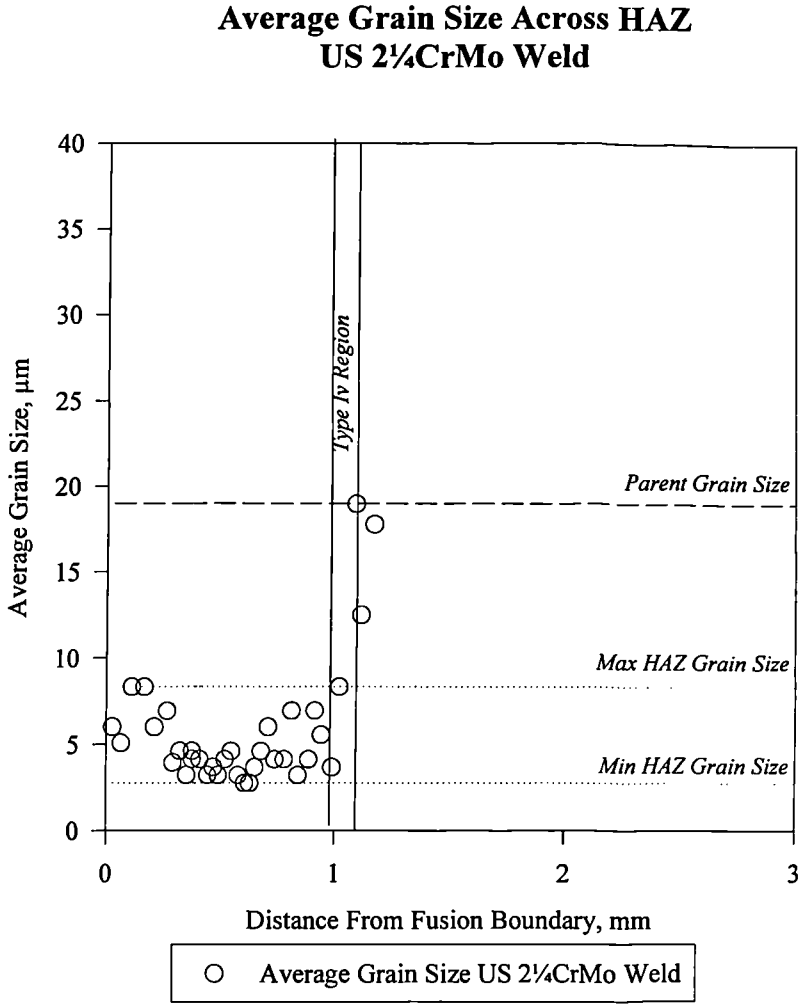

Fig 4.5 *Grain size across HAZ MF 2¼CrMo cross weld specimen*

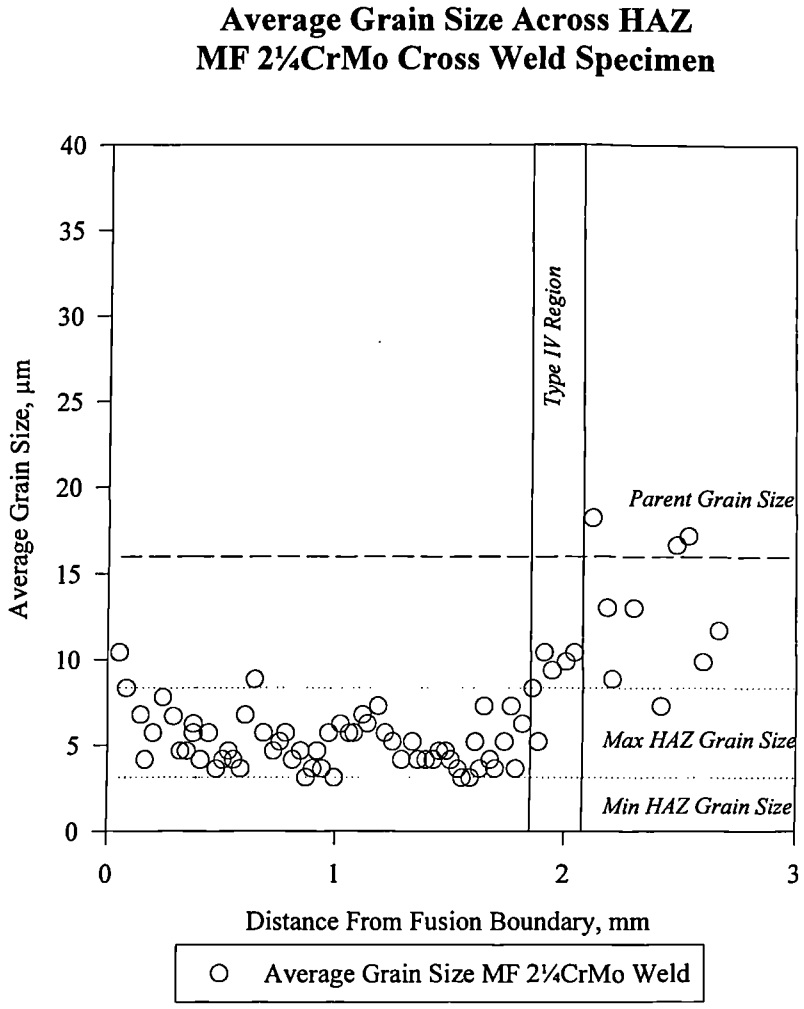

Fig 4.6 *Heat treatment of AB parent cast, tempered 700°C 3 hours.*

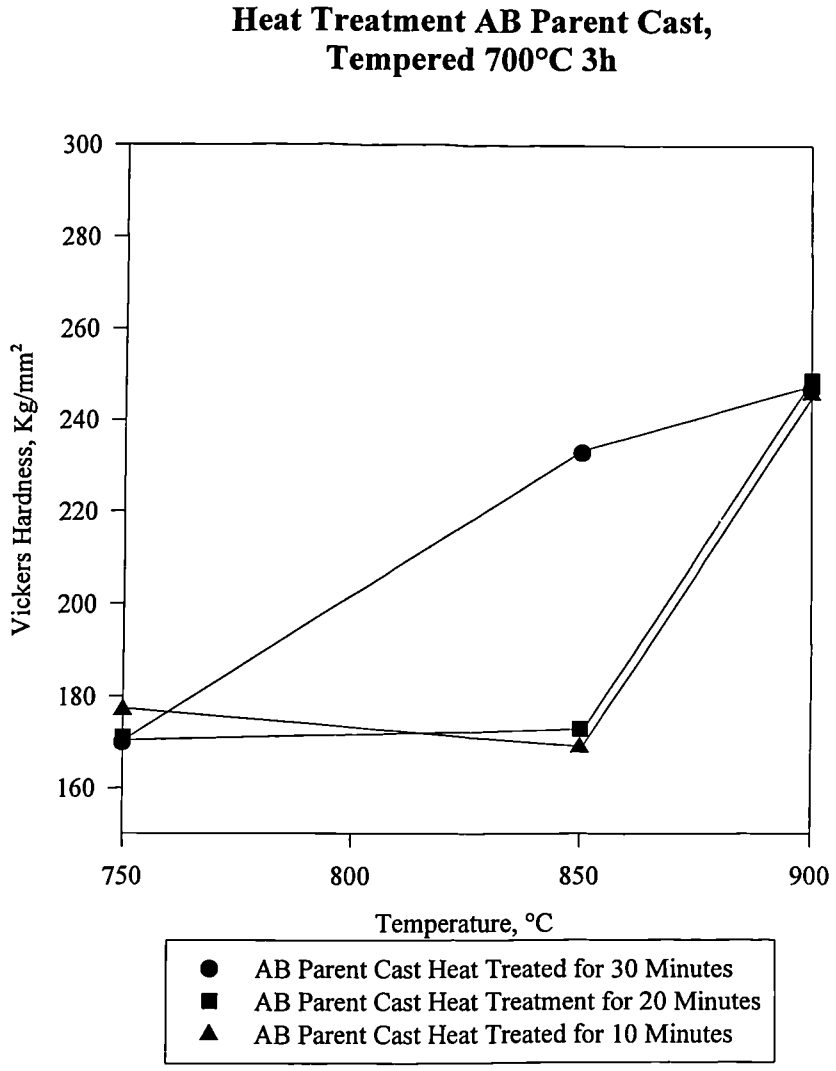

Fig 4.7 *Heat treatment of M1 parent cast, tempered 700°C 3 hours*

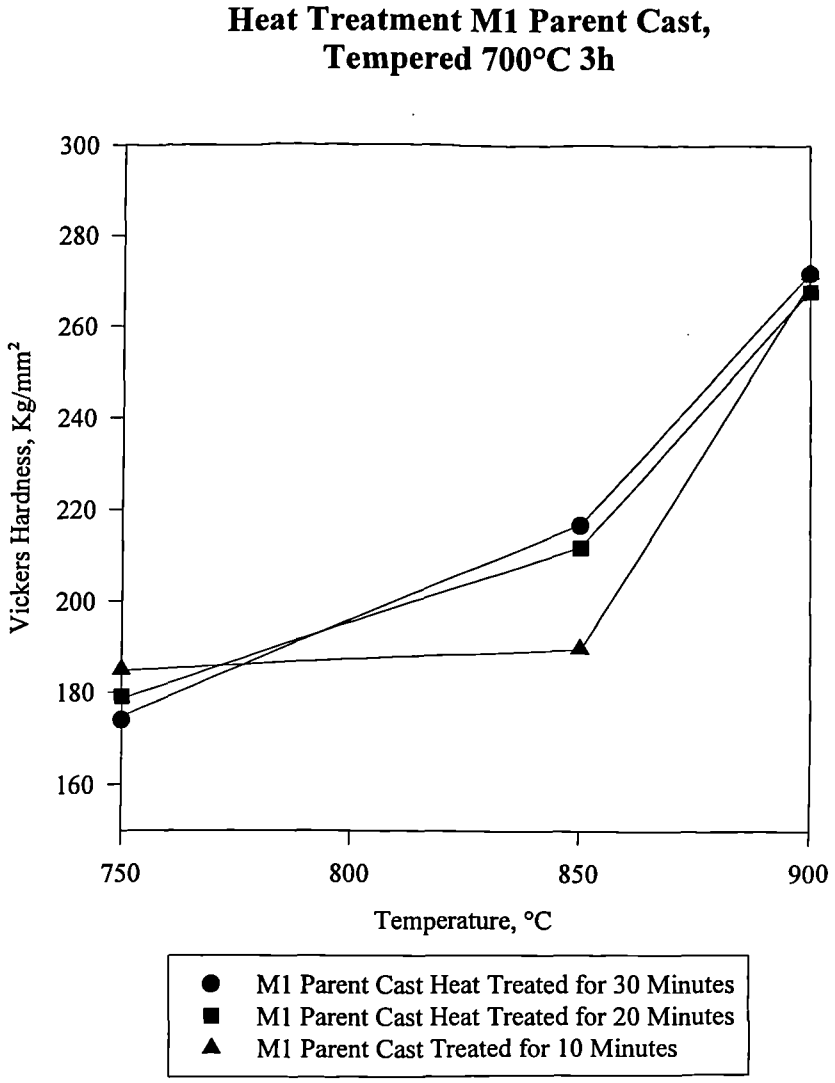

Fig 4.8 *Comparison of micro-hardness measurements M1 ½CrMoV and 2¼CrMo unaged weldments.*

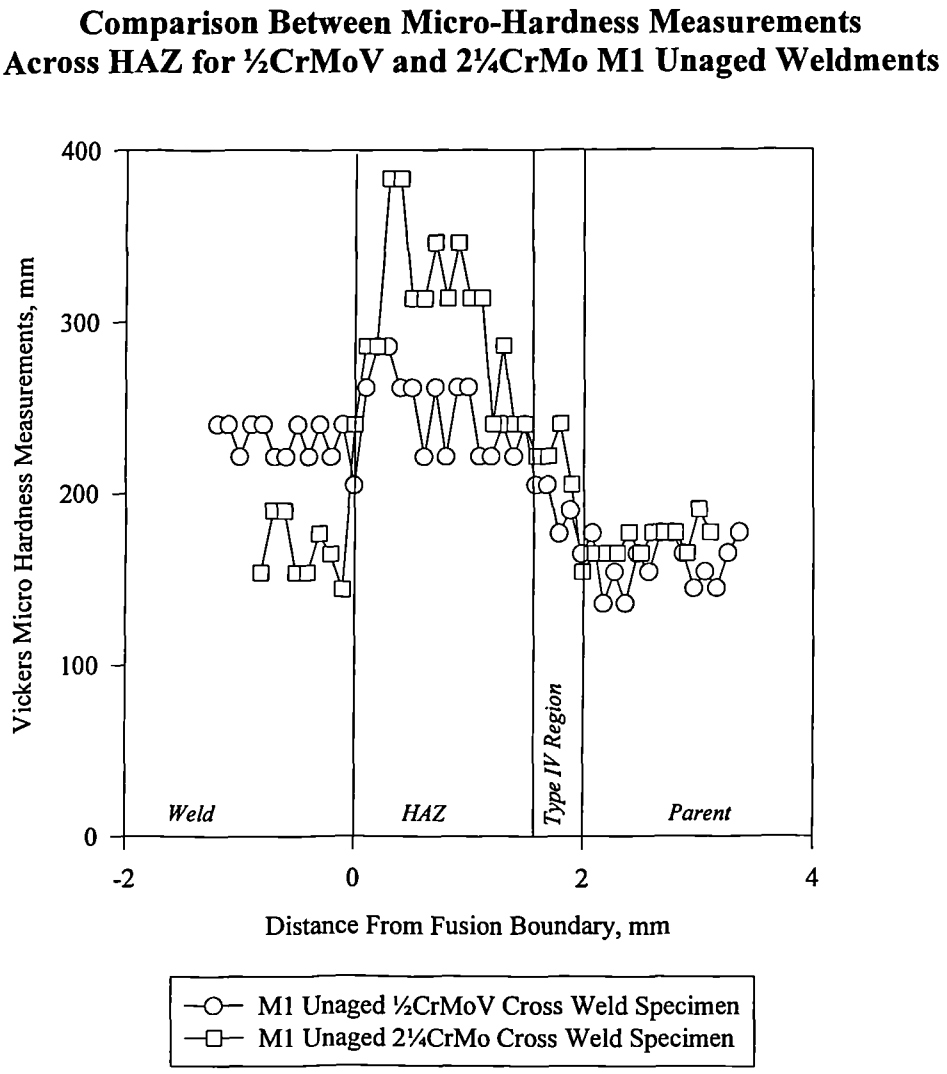

Fig 4.9 *Comparison of micro-hardness measurements AB ½CrMoV and 2¼CrMo unaged weldments*

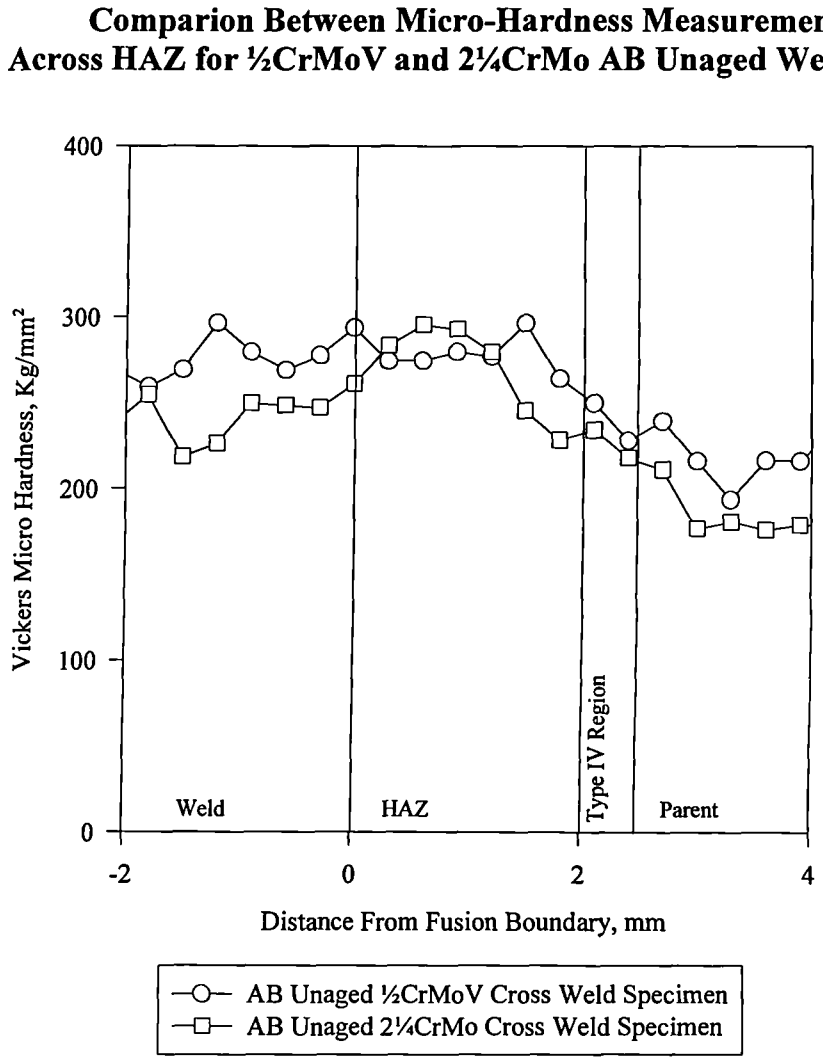

Fig 4.10 *Comparison of micro-hardness measurements M1 and AB 2¼CrMo unaged weldments*

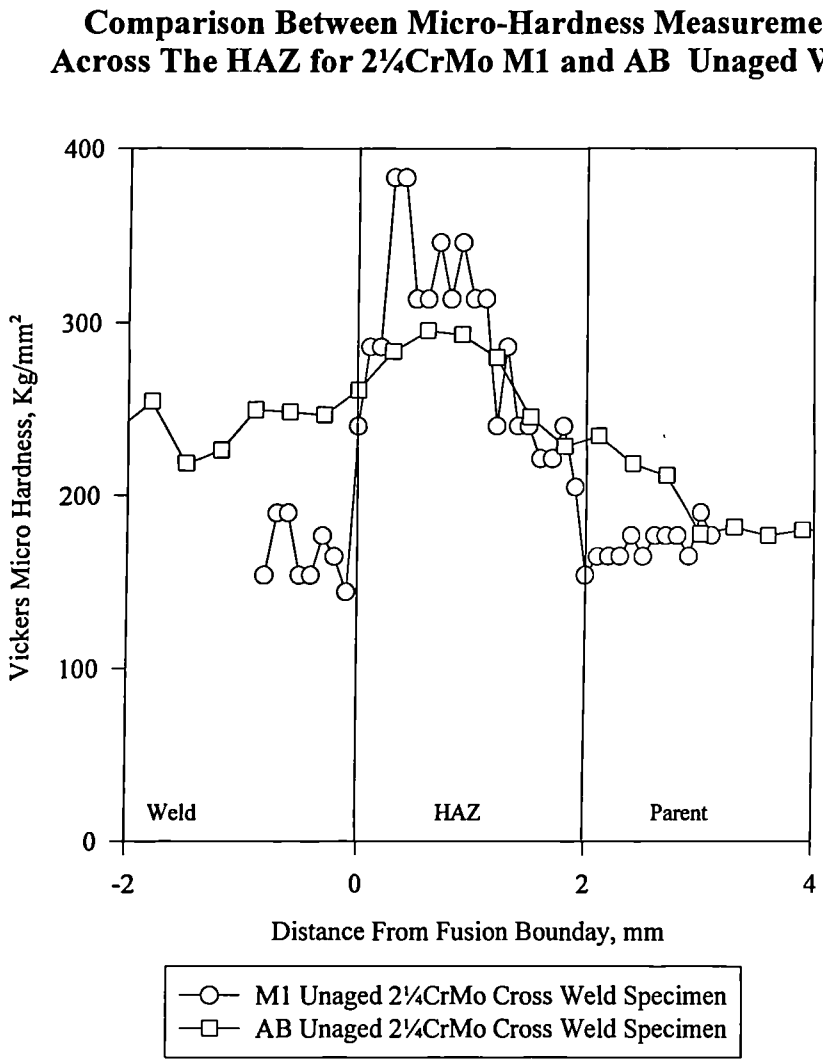

Fig 4.11 *Comparison of micro-hardness measurements M1 and AB ½CrMoV unaged weldments*

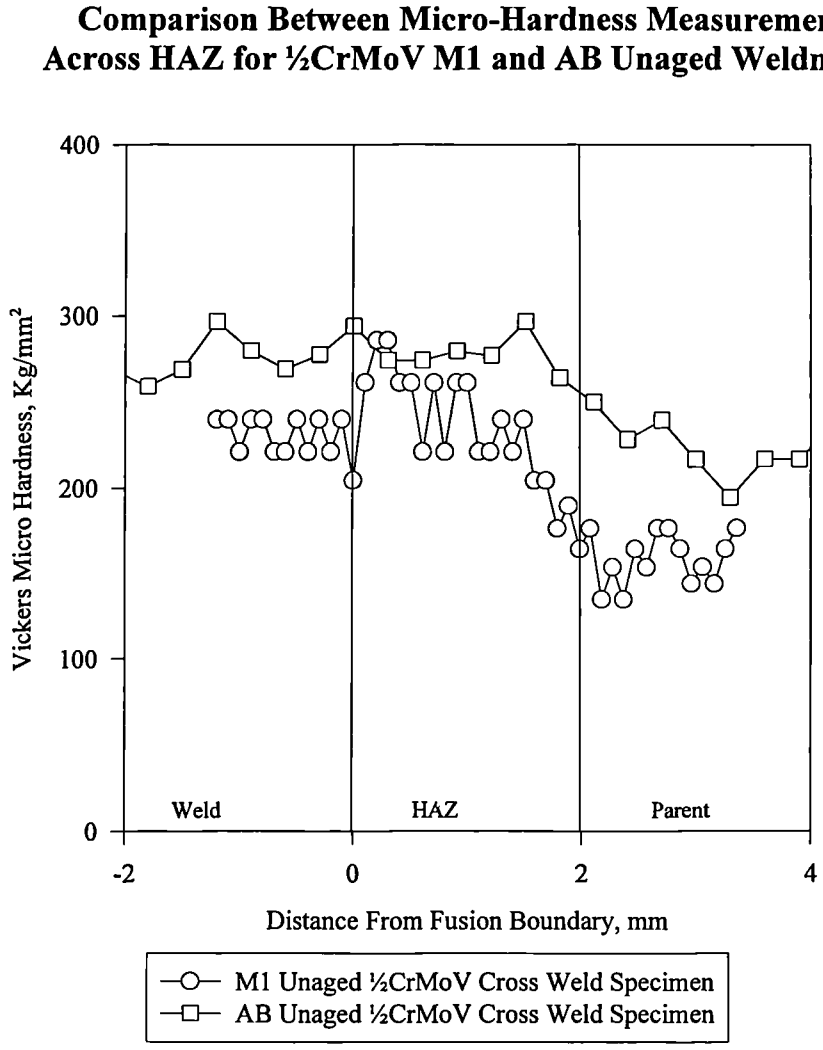

Fig 4.12 *Comparison of micro-hardness measurements M1 ½CrMoV aged and unaged weldments*

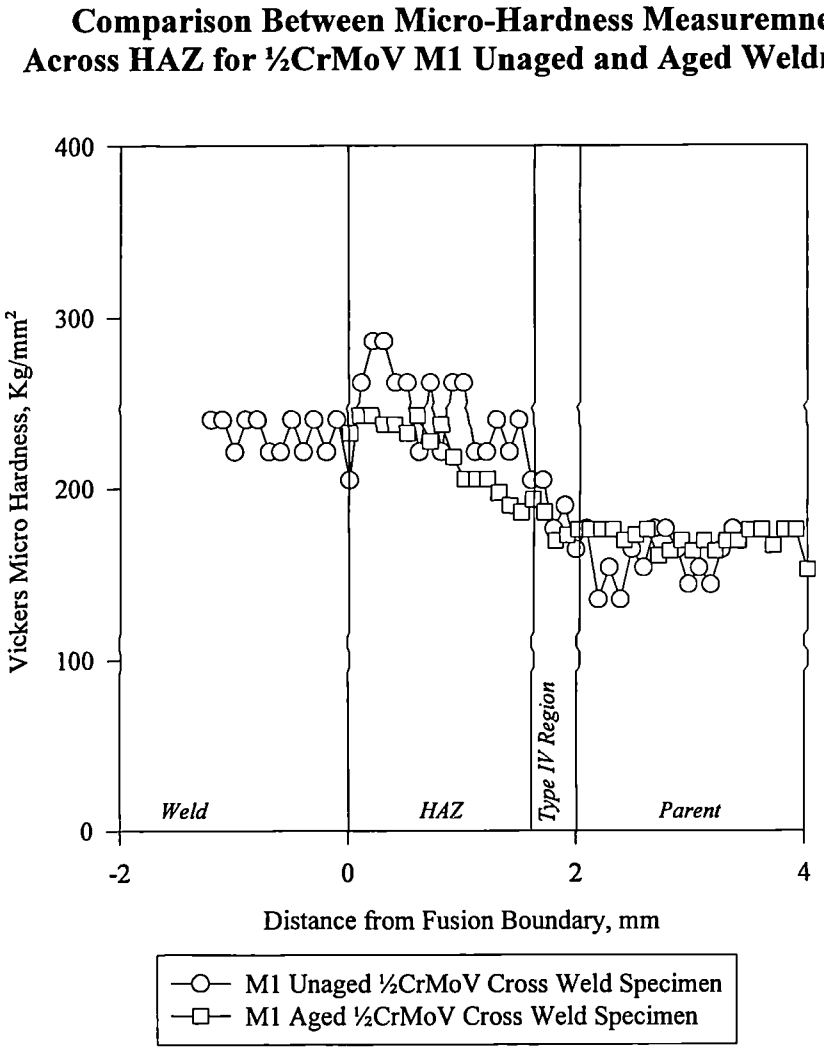

Fig 4.13 *Comparison of micro-hardness measurements M1 2¼CrMo aged and unaged weldments*

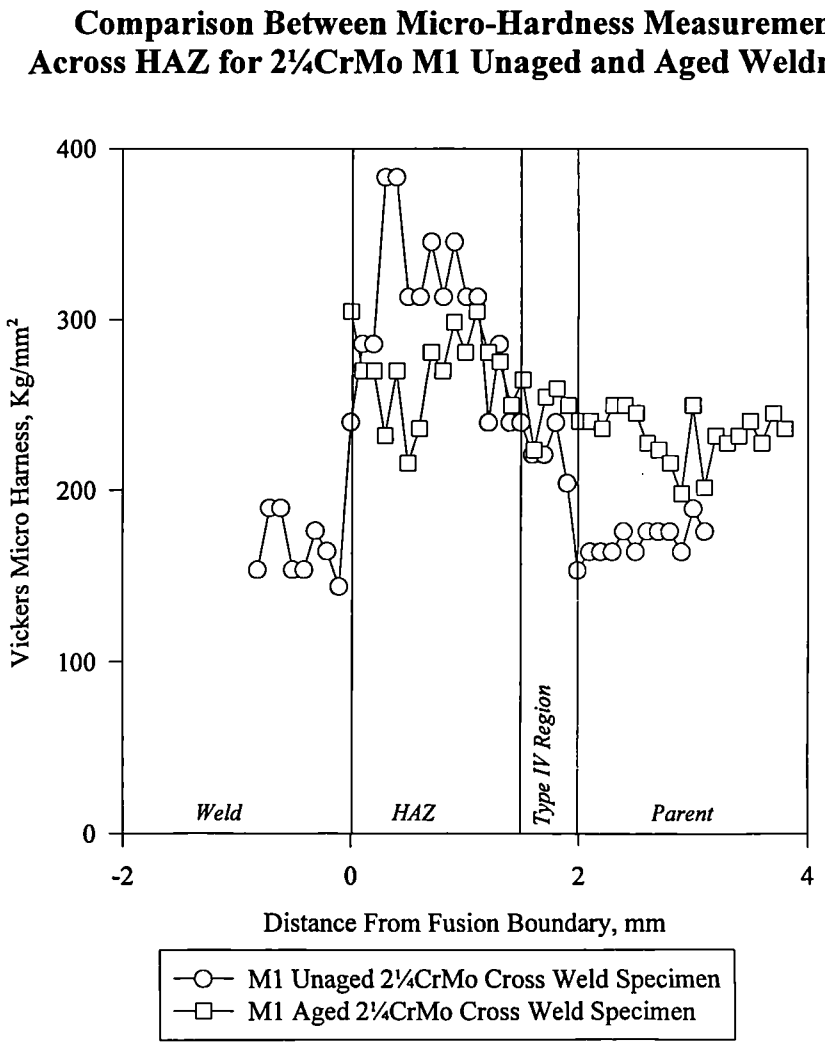

Fig 4.14 *Comparison of micro-hardness measurements AB 2¼CrMo aged and unaged weldments*

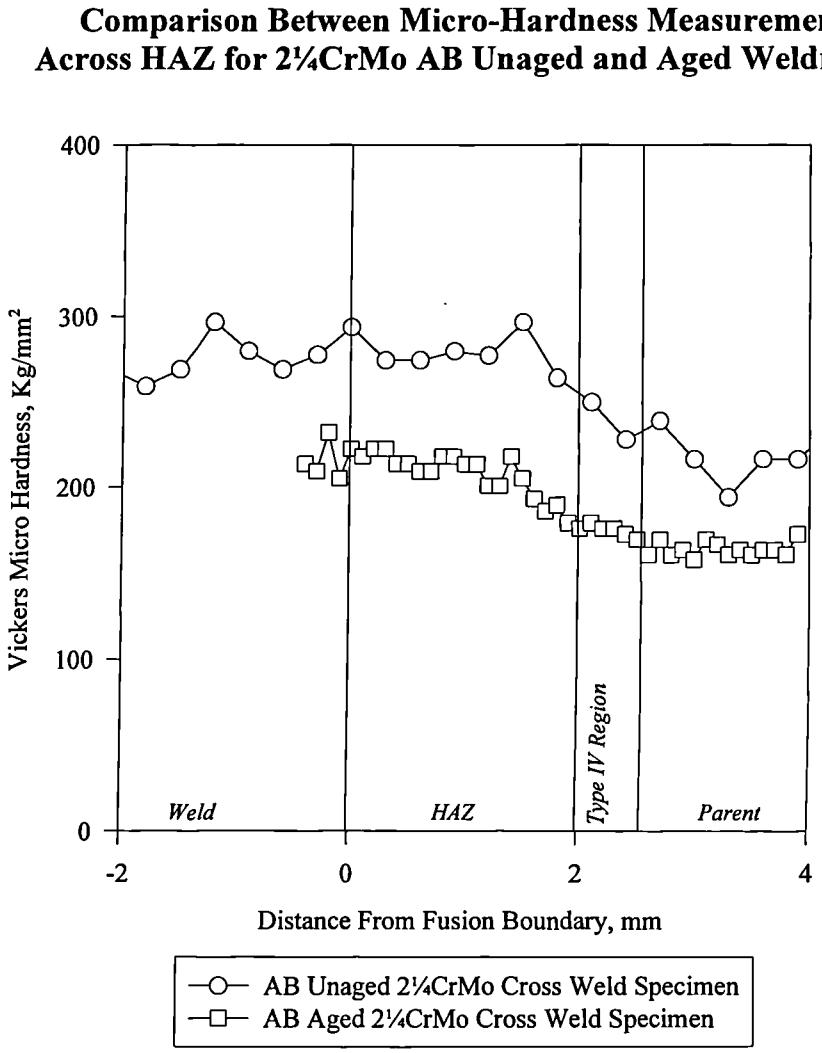

Fig 4.15 *Comparison of micro-hardness measurements AB ½CrMoV aged and unaged weldments*

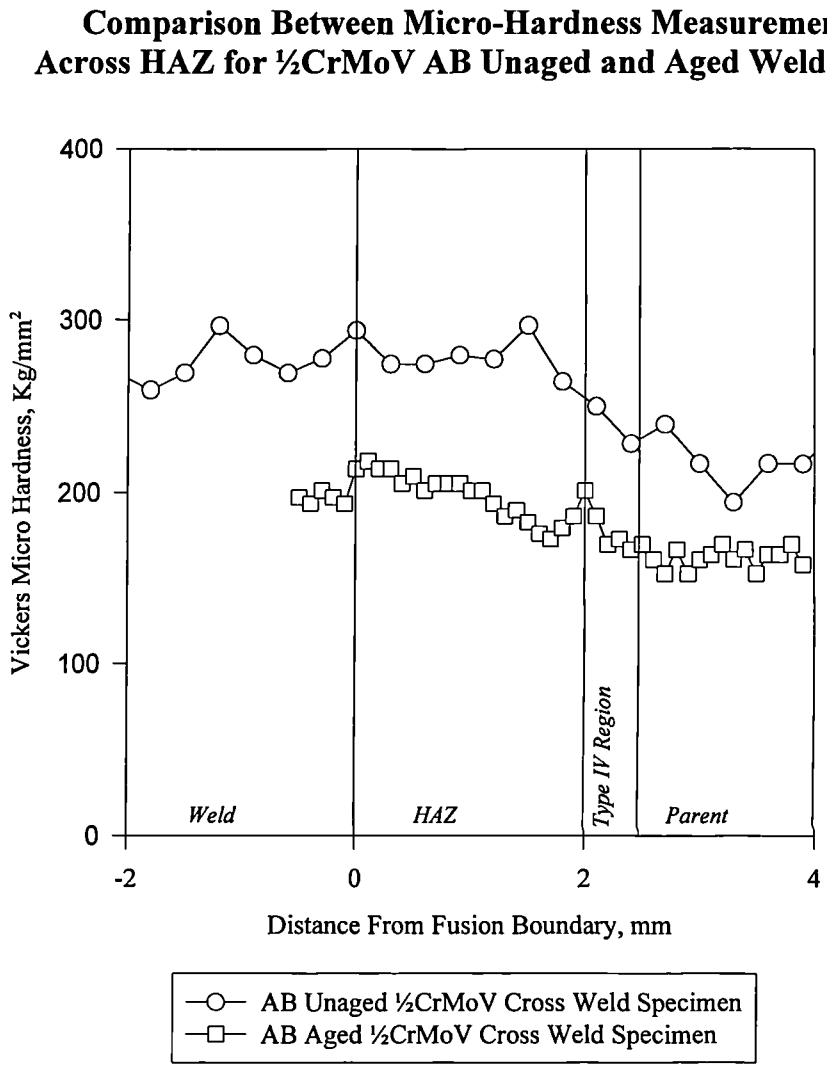

Fig 4.16 *Stress rupture plot showing M1 ½CrMoV and 2¼CrMo Type IV rupture data.*

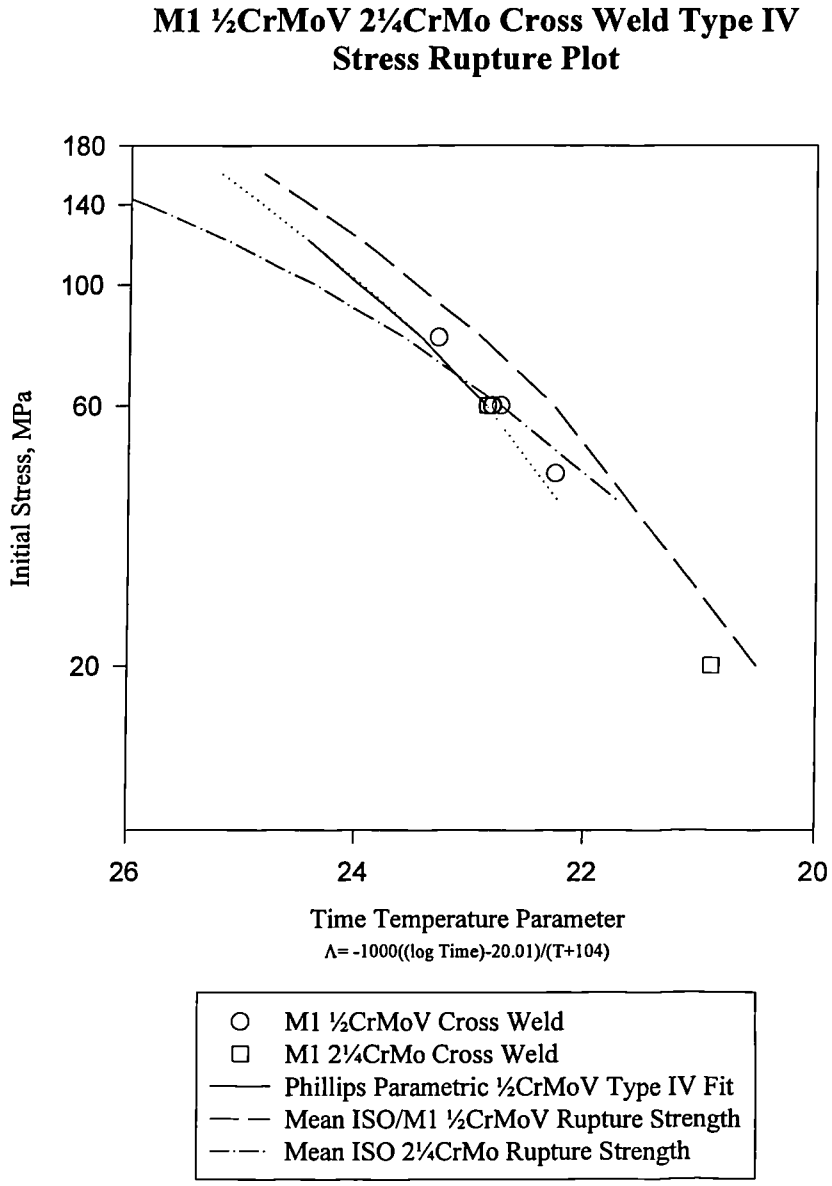

Fig 4.17 *Stress rupture plot showing AB ½CrMoV and 2¼CrMo cross weld rupture data including AB ½CrMoV parent cast rupture point.*

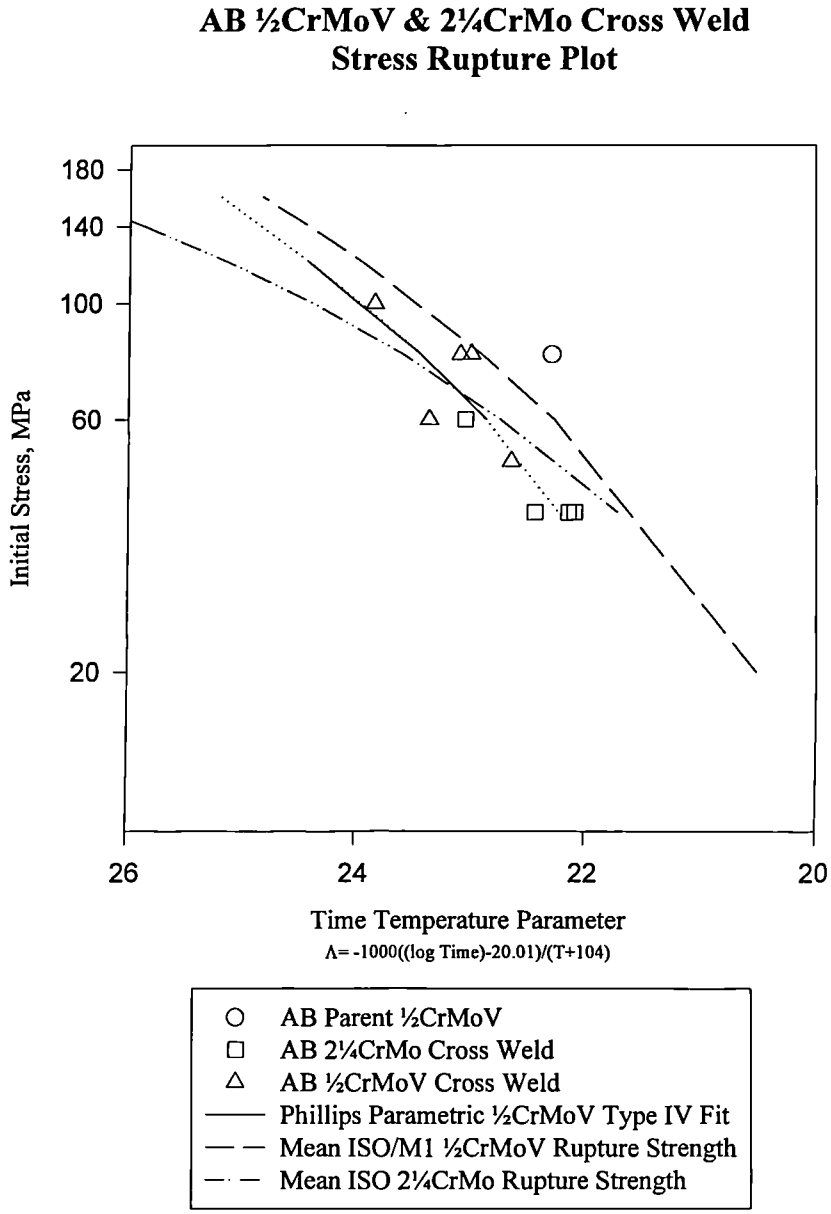

Fig 4.18 *Stress rupture plot showing AB cast uniaxial plain bar Type IV simulated rupture data.*

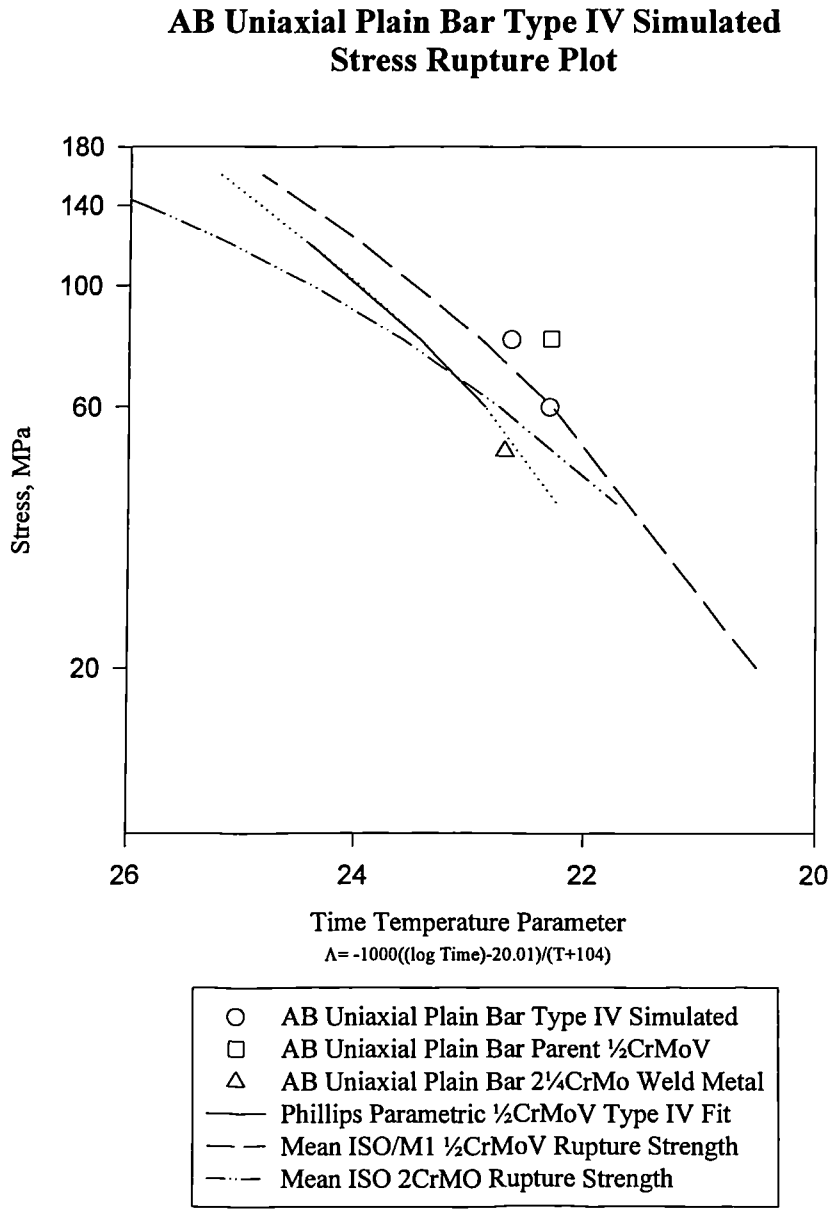

Fig 4.19 *Stress rupture plot showing M1 cast uniaxial plain bar Type IV simulated rupture data*

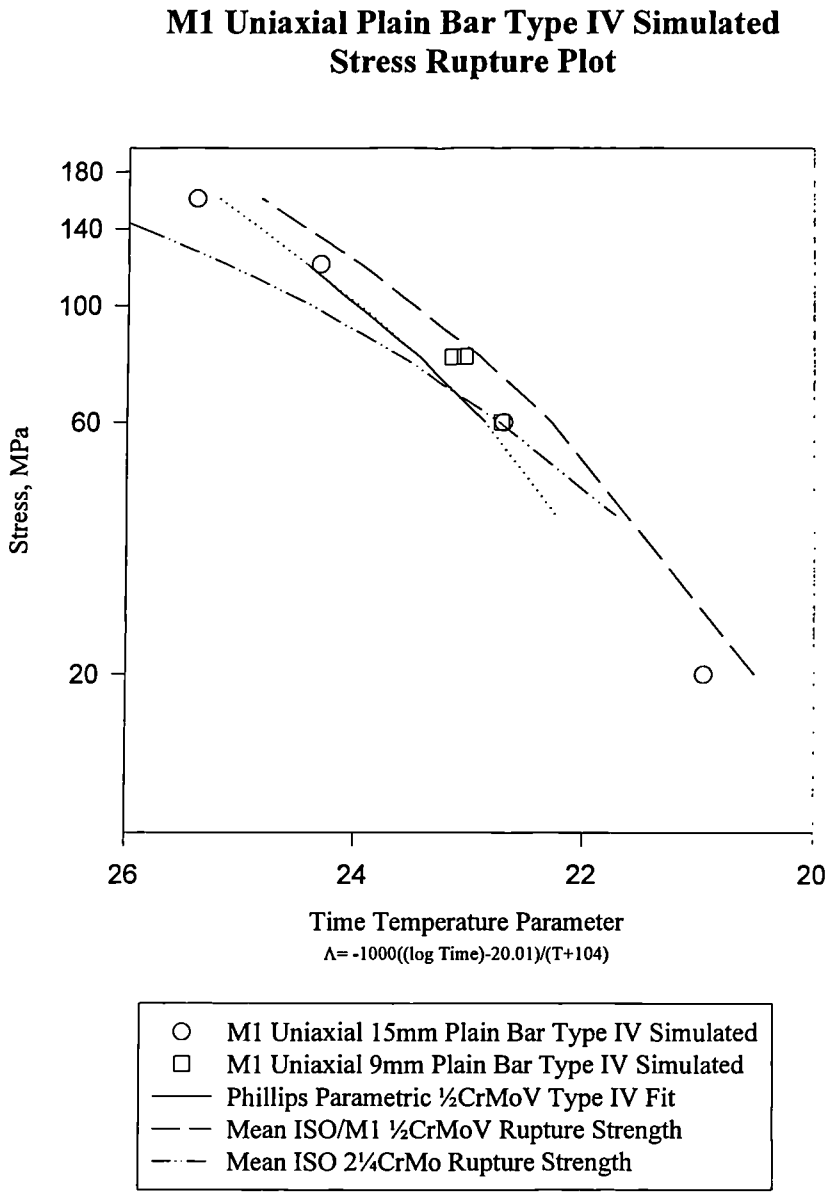

Fig 4.20 *Stress rupture plot showing M1 cast multiaxial shear pin and notch bar Type IV simulated and cross weld rupture data*

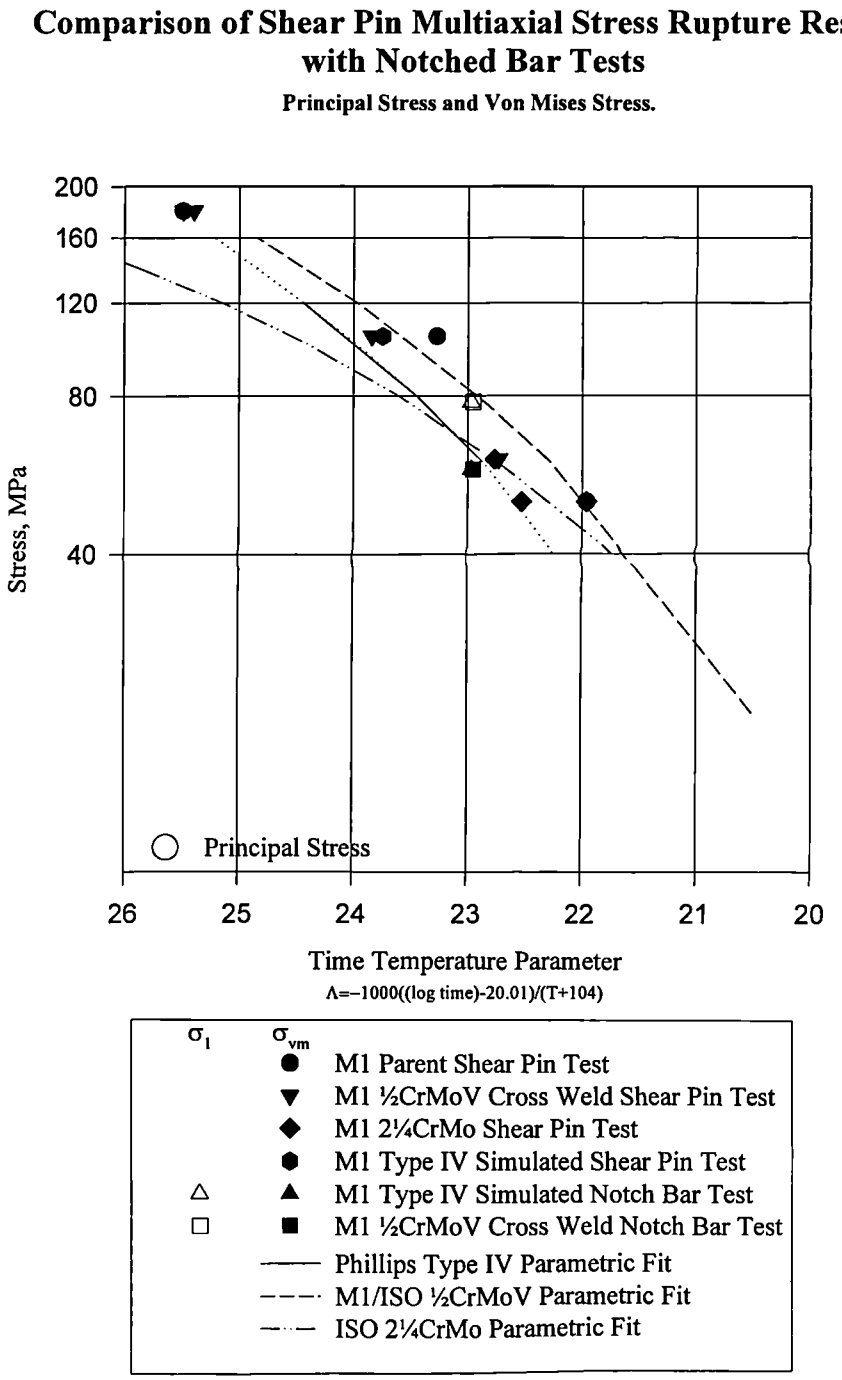

Fig 4.21 *Schematic showing the direction of the cross weld specimen prior to damage assessment.*

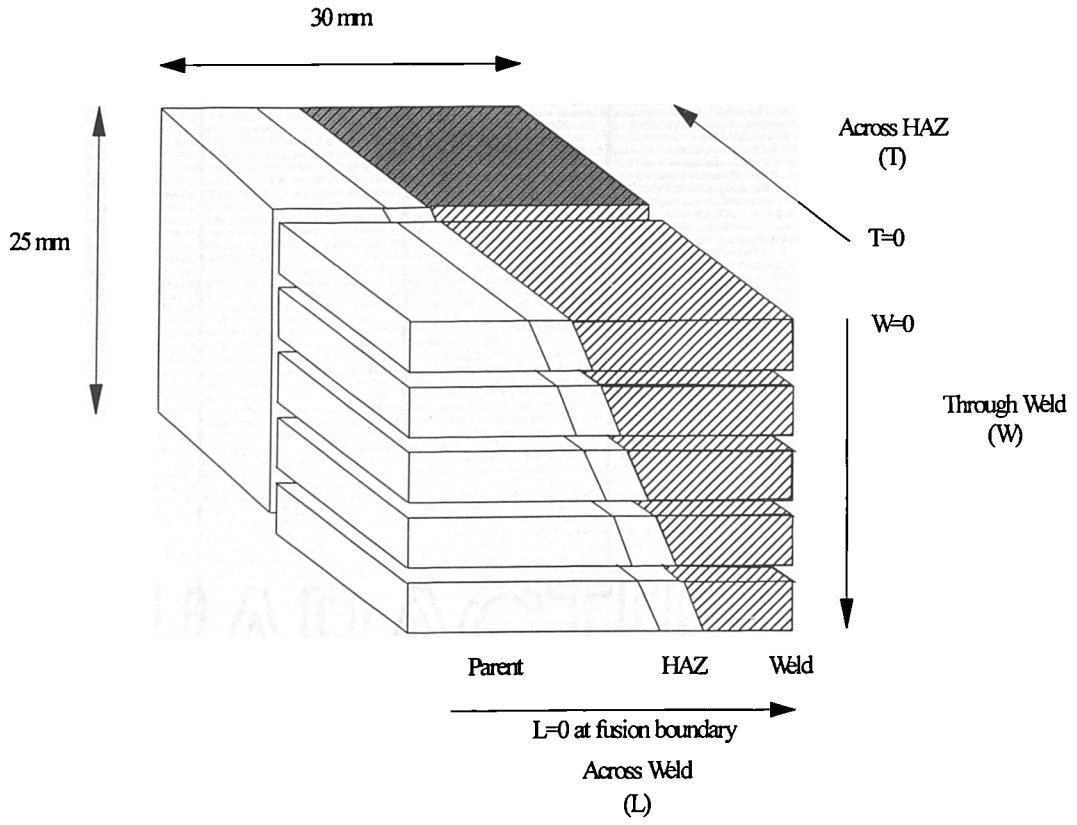

Fig 4.22 *Measurement of cavity number density across weld*

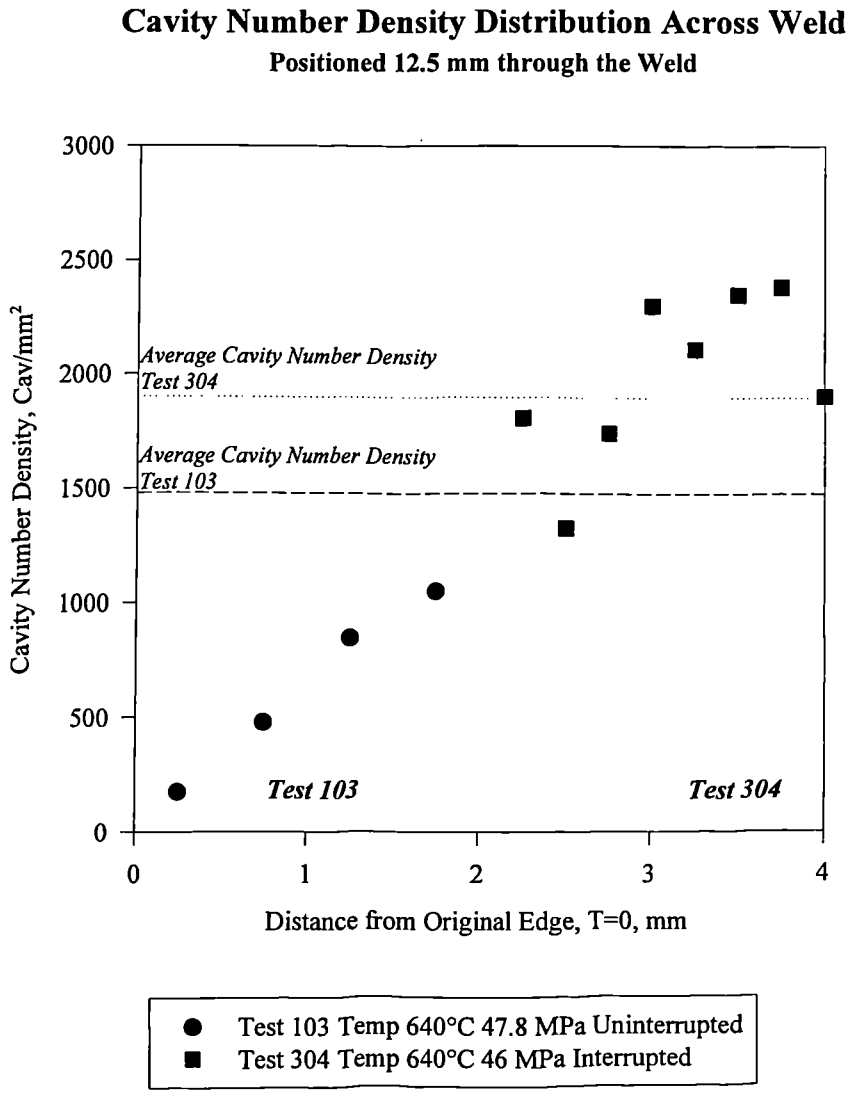

Fig 4.23 *Measurement of cavity number density across HAZ*

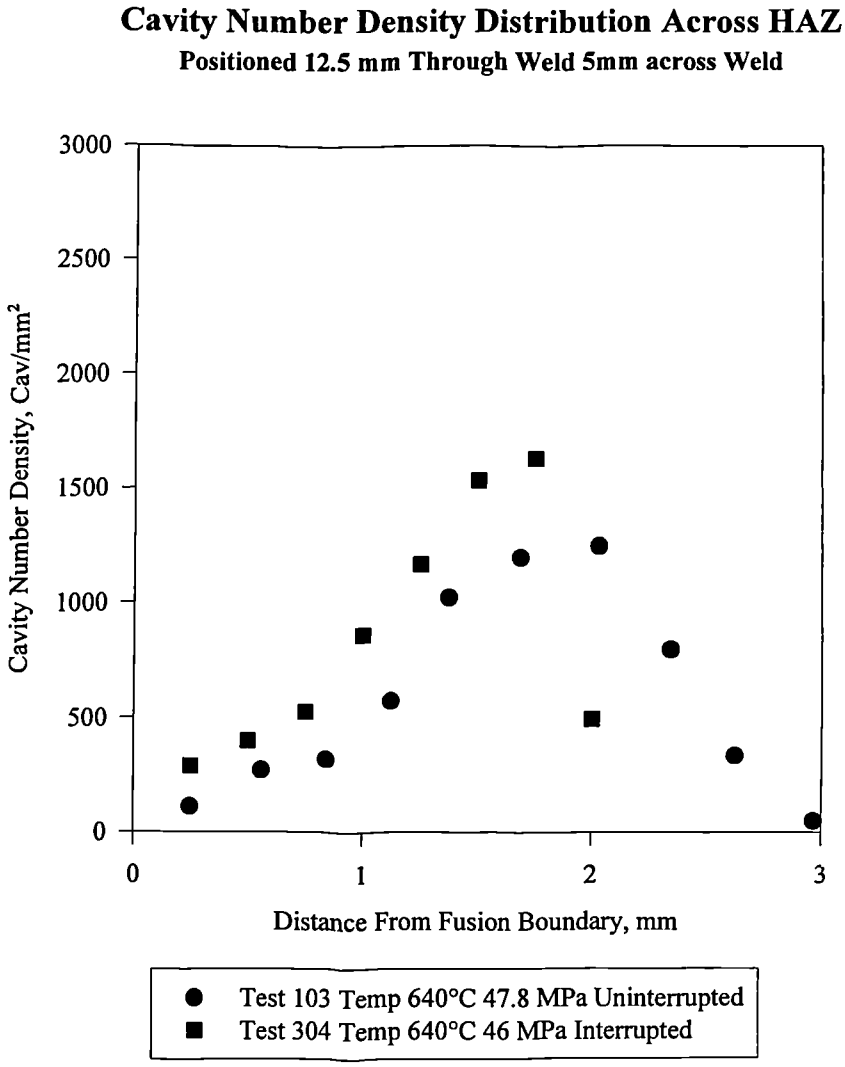

Fig 4.24 *Measurement of cavity number density across Fracture*

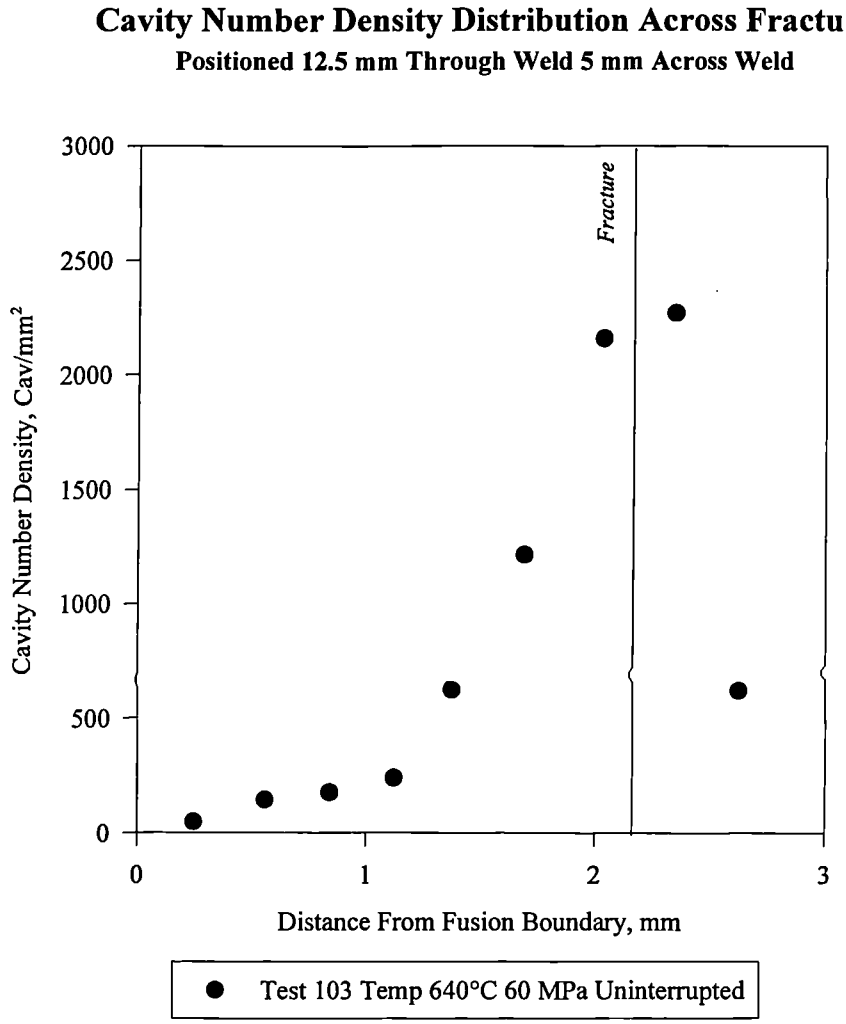

Fig 4.25 *Measurement of cavity number density through weld*

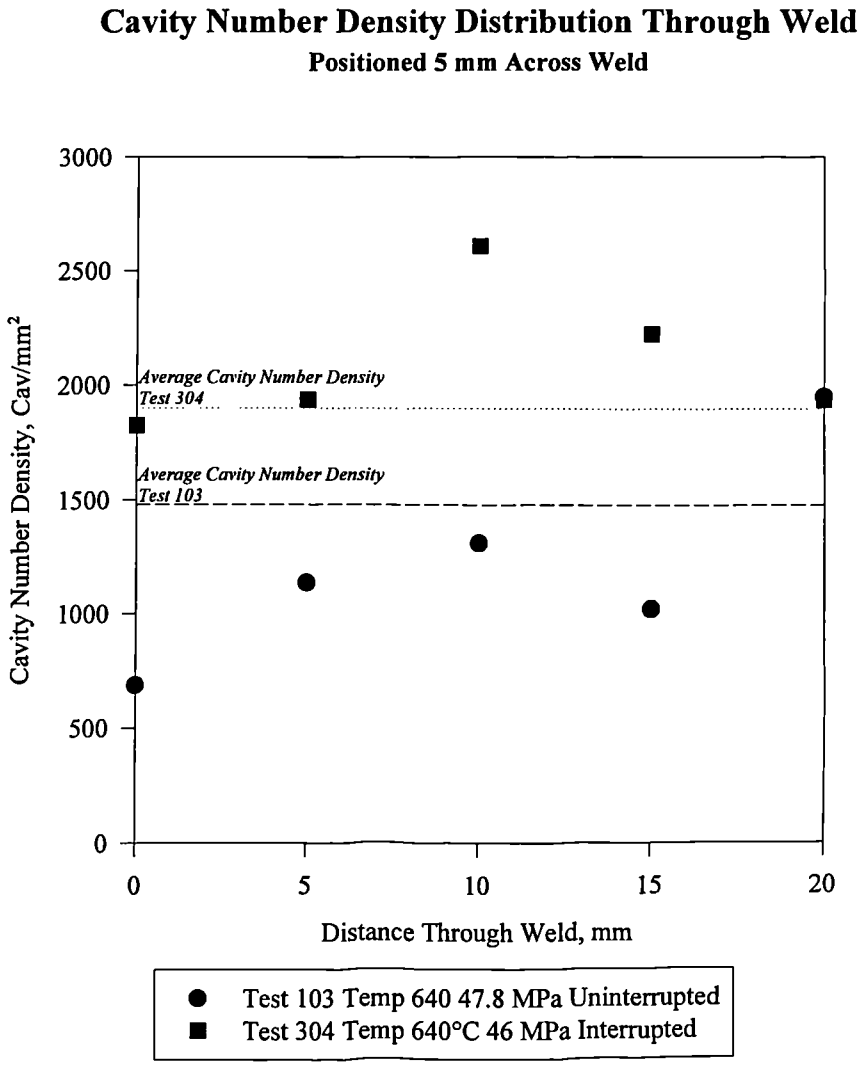

Fig 4.26 *Measurement of cavity number density M1 cross weld tests at approximately 48 MPa*

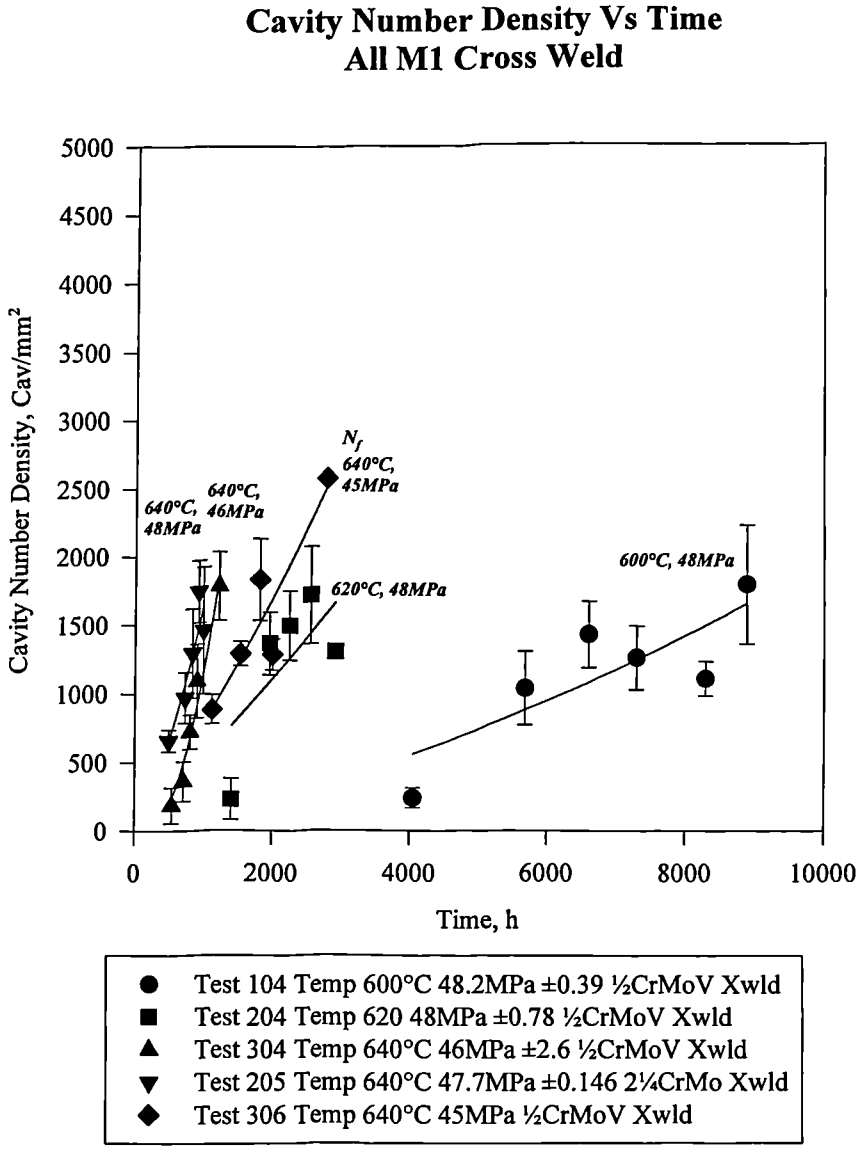

Fig 4.27 *Measurement of cavity number density M1 cross weld tests at approximately 60 MPa.*

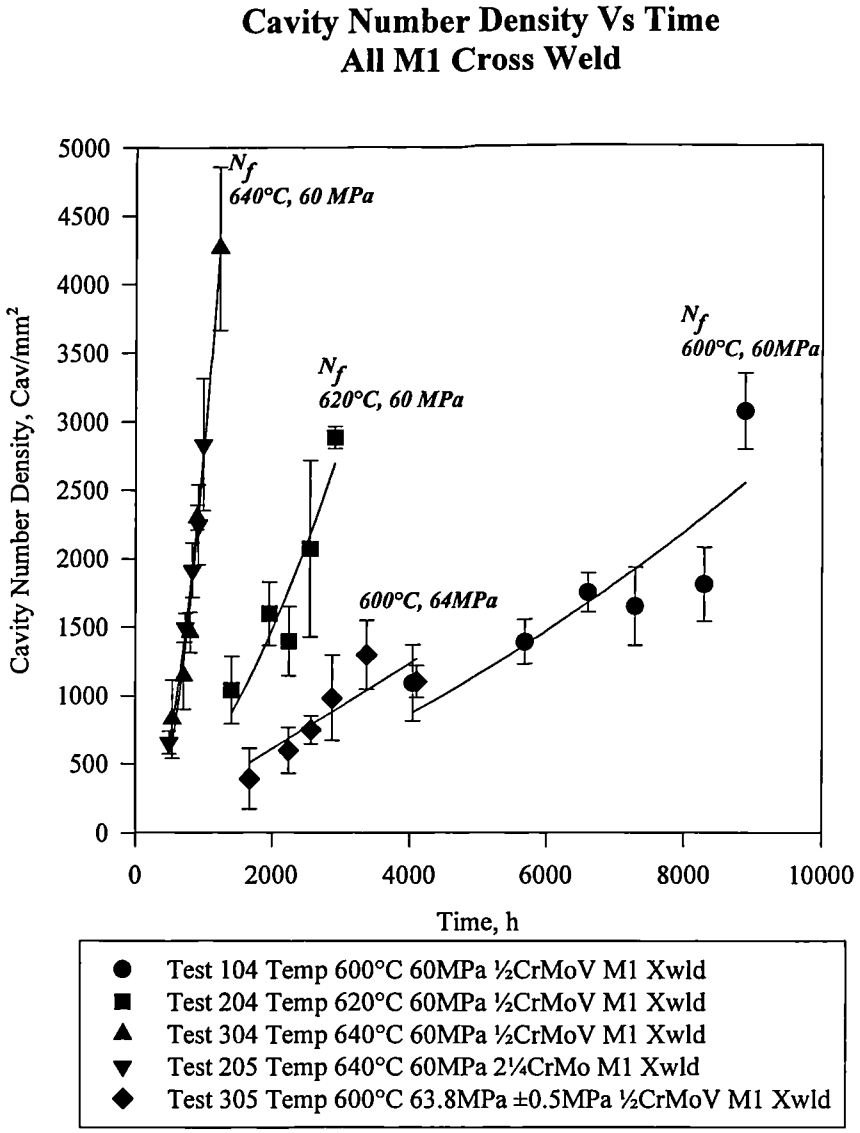

Fig 4.28 *Comparison of cavity number density measurements in M1 2¼CrMo and ½CrMoV cross weld test specimens at 60 MPa and 640°C*

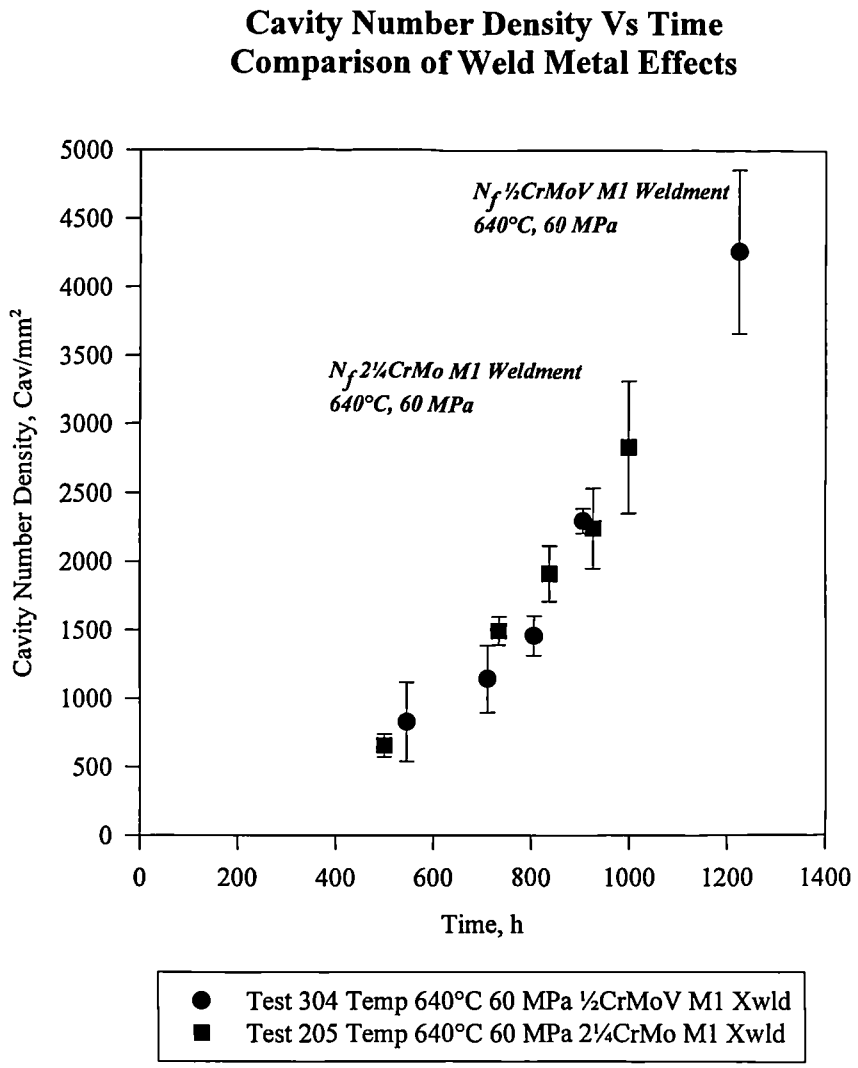

Fig 4.29 *Comparison of cavity number density measurements taken from M1 cross weld tests carried out at 600°C*

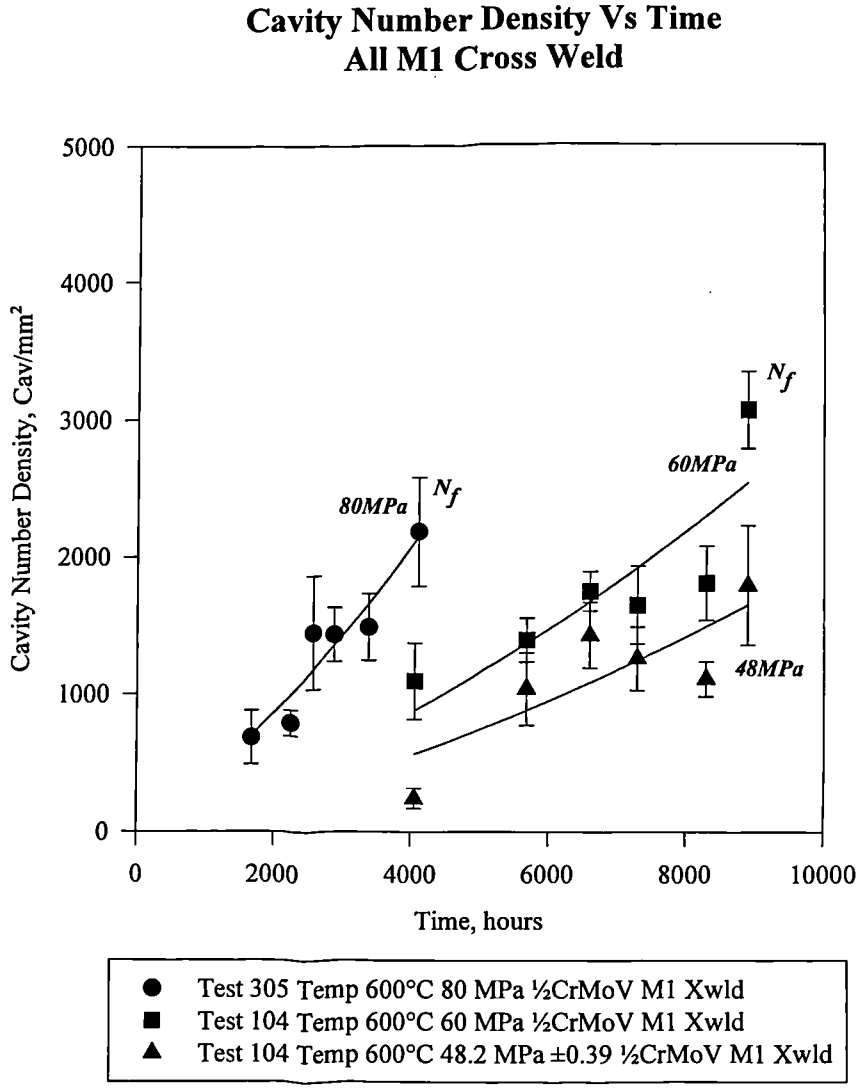

Fig 4.29b *Comparison of cavity number density measurements taken from M1 cross weld tests carried out at 600°C.*

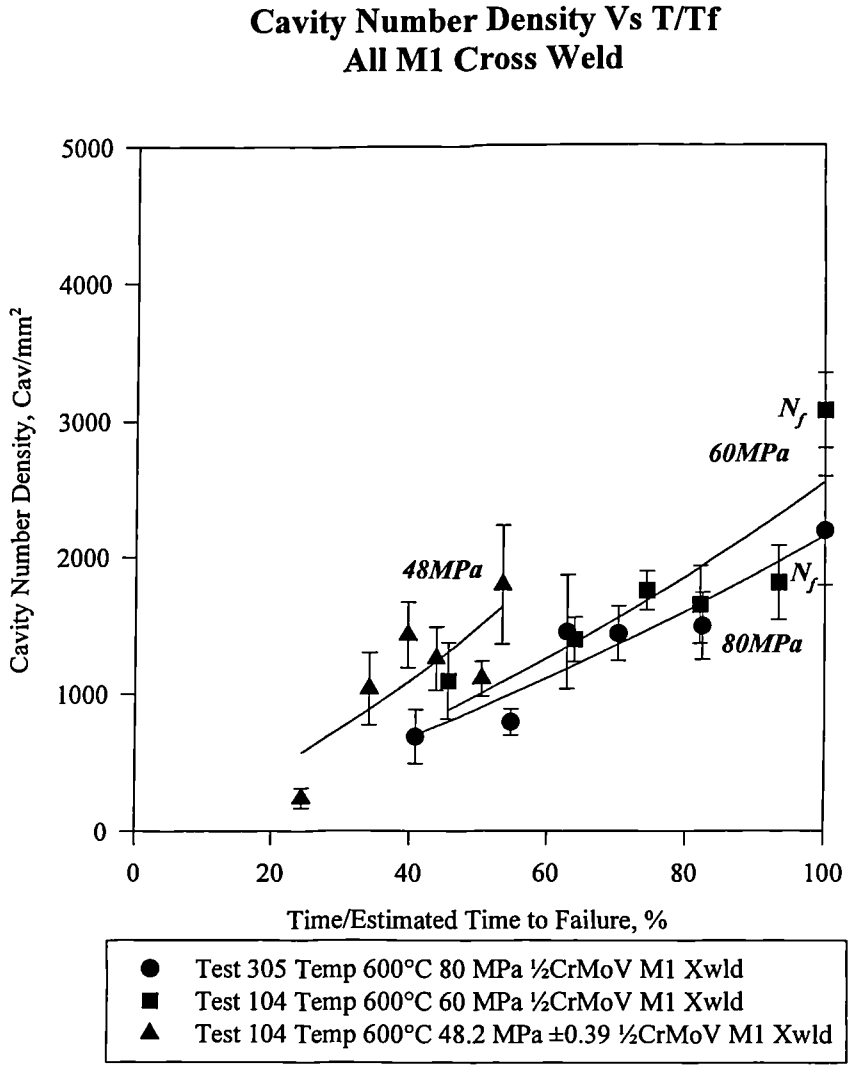

Fig 4.30 *Comparison of cavity number density measurements taken from M1 cross weld tests carried out at approximately 48 MPa and 600°C 620°C and 640°C*

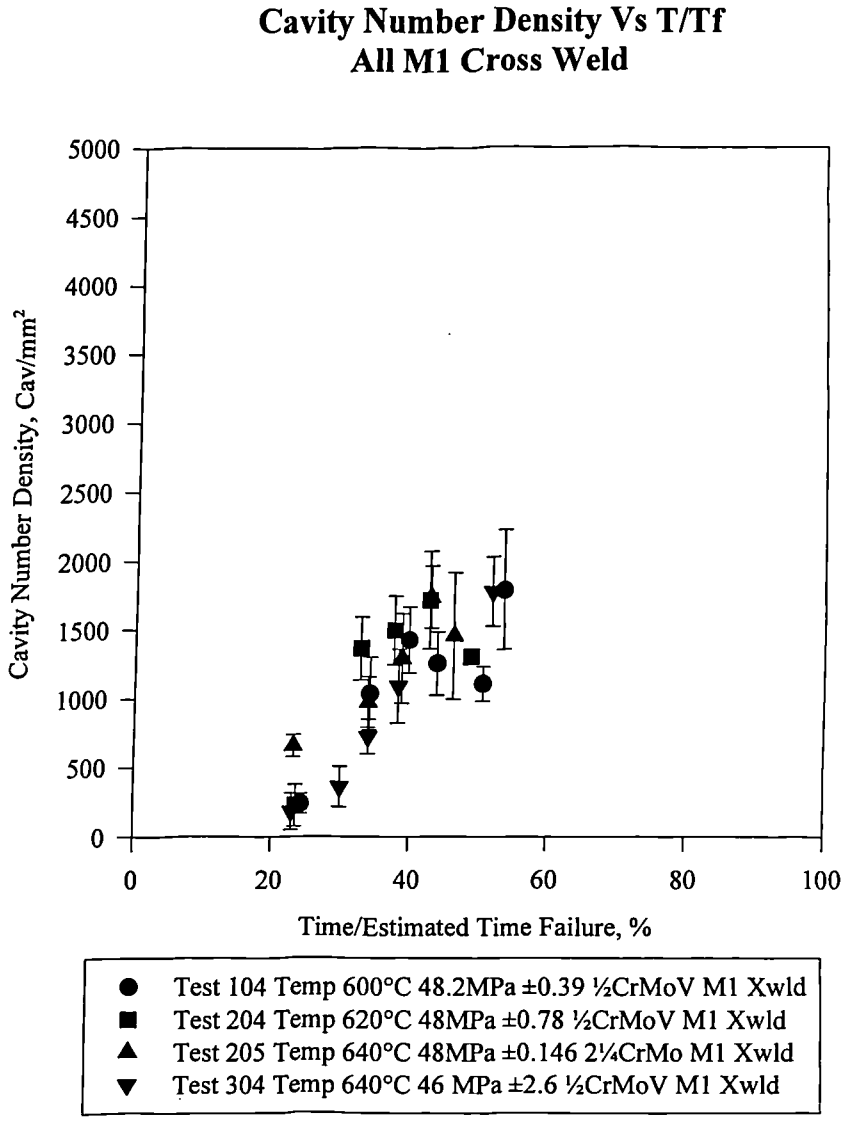

Fig 4.31 *Comparison of cavity number density measurements taken from M1 cross weld tests carried out at 60 MPa and 600°C 620°C and 640°C*

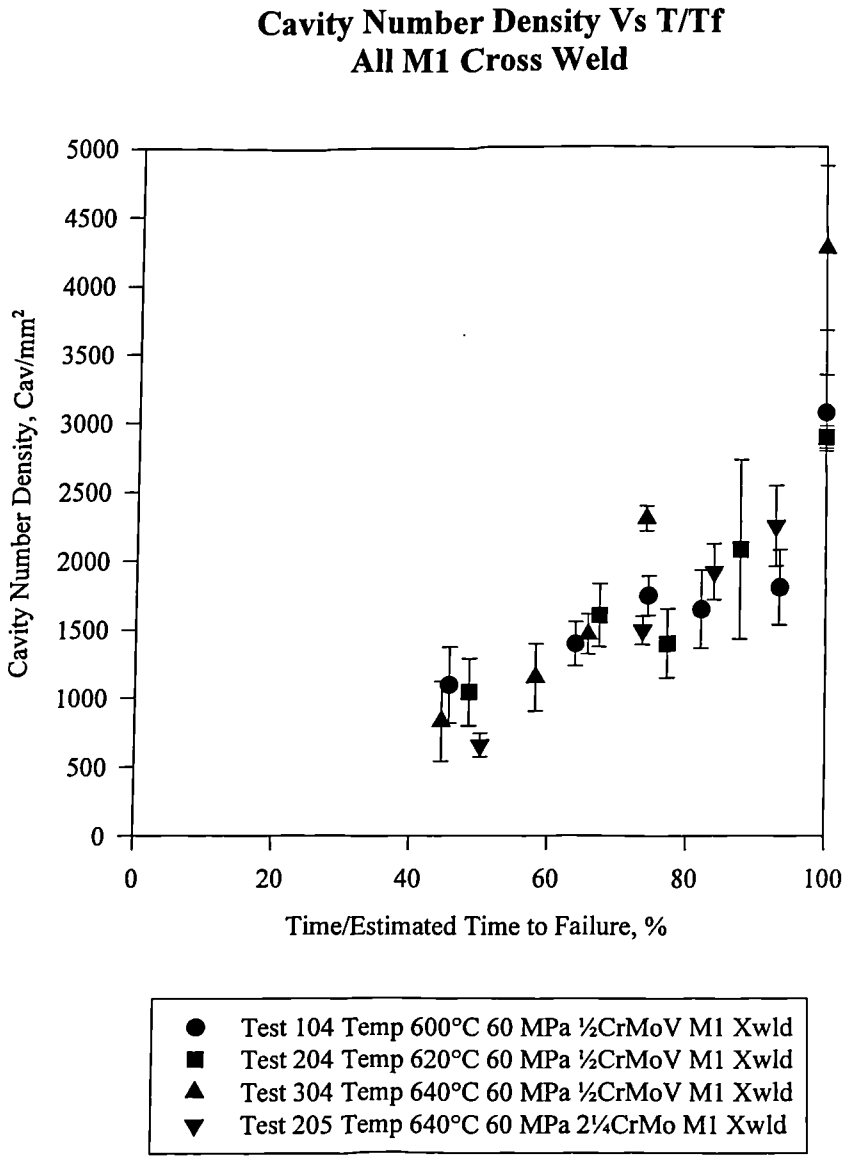

Fig 4.32 *Comparison of Nuclear Electric cavity number density measurements with Bristol University Data.*

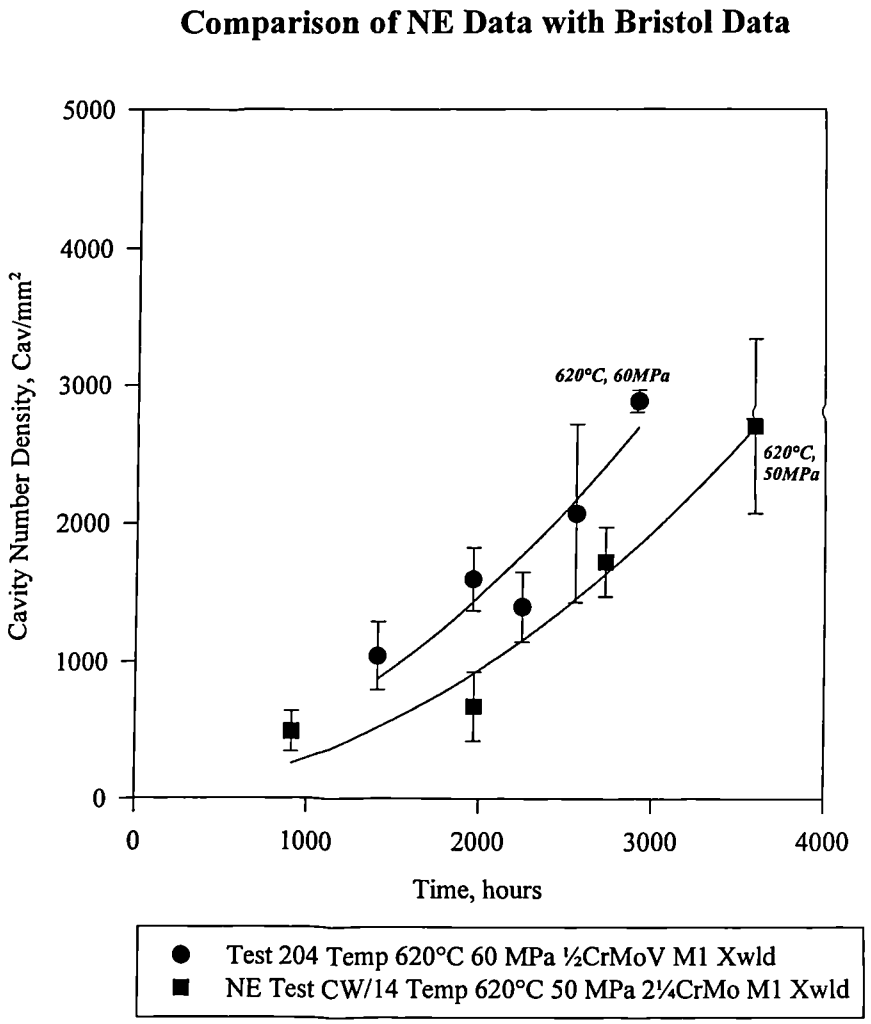

Fig 4.33 *Comparison of M1 cross weld and uniaxial Type IV simulated specimen cavity number density measurements.*

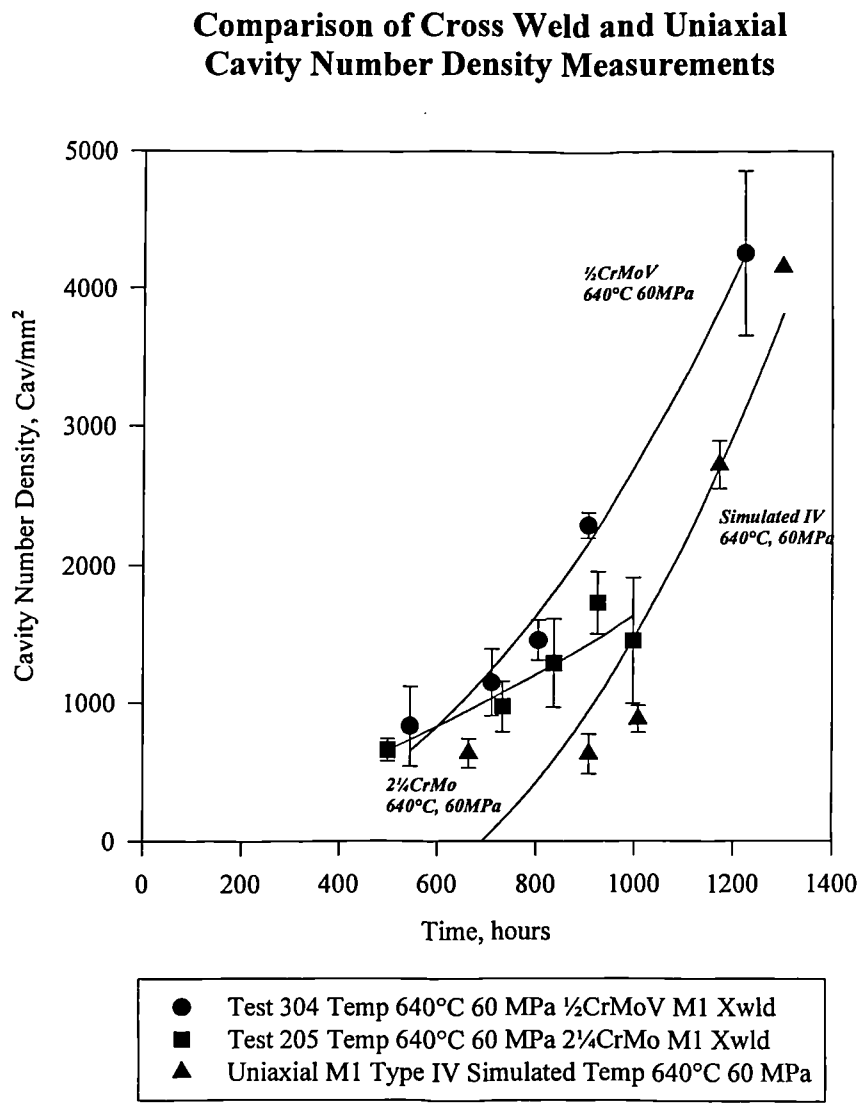

Fig 4.34 *Measurement of cavity number density M1 uniaxial Type IV simulated specimens at 640°C*

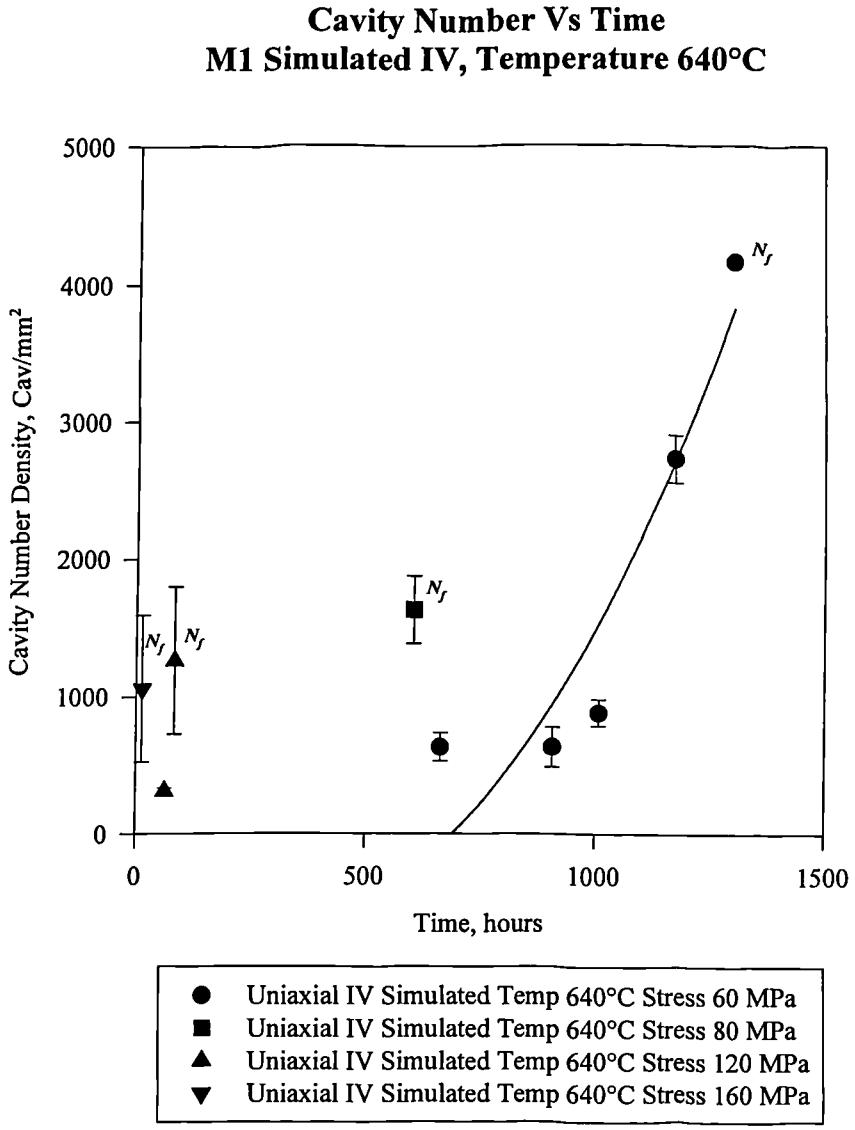

Fig 4.35 *Plot of M1 uniaxial Type IV simulated cavity number density measurements against strain.*

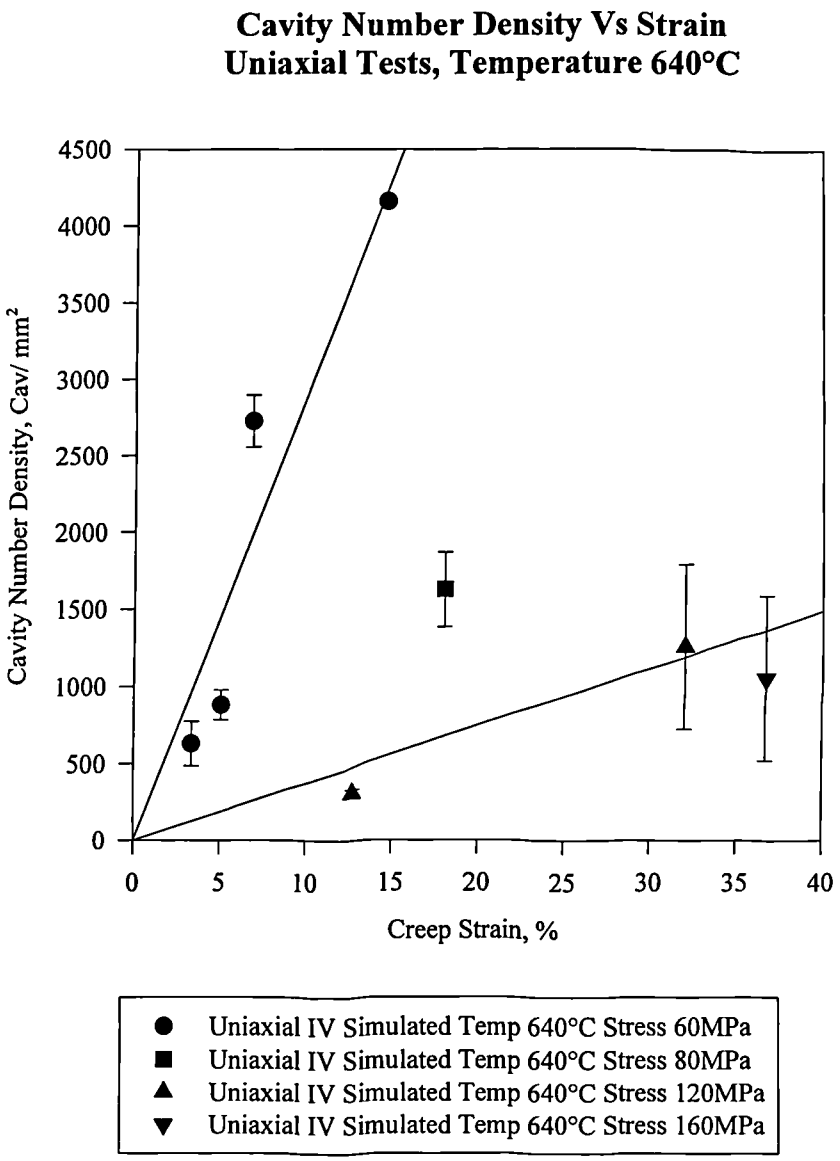

Fig 4.36 *Plot of M1 Type IV simulated cavity number density/strain against stress at 640°C.*

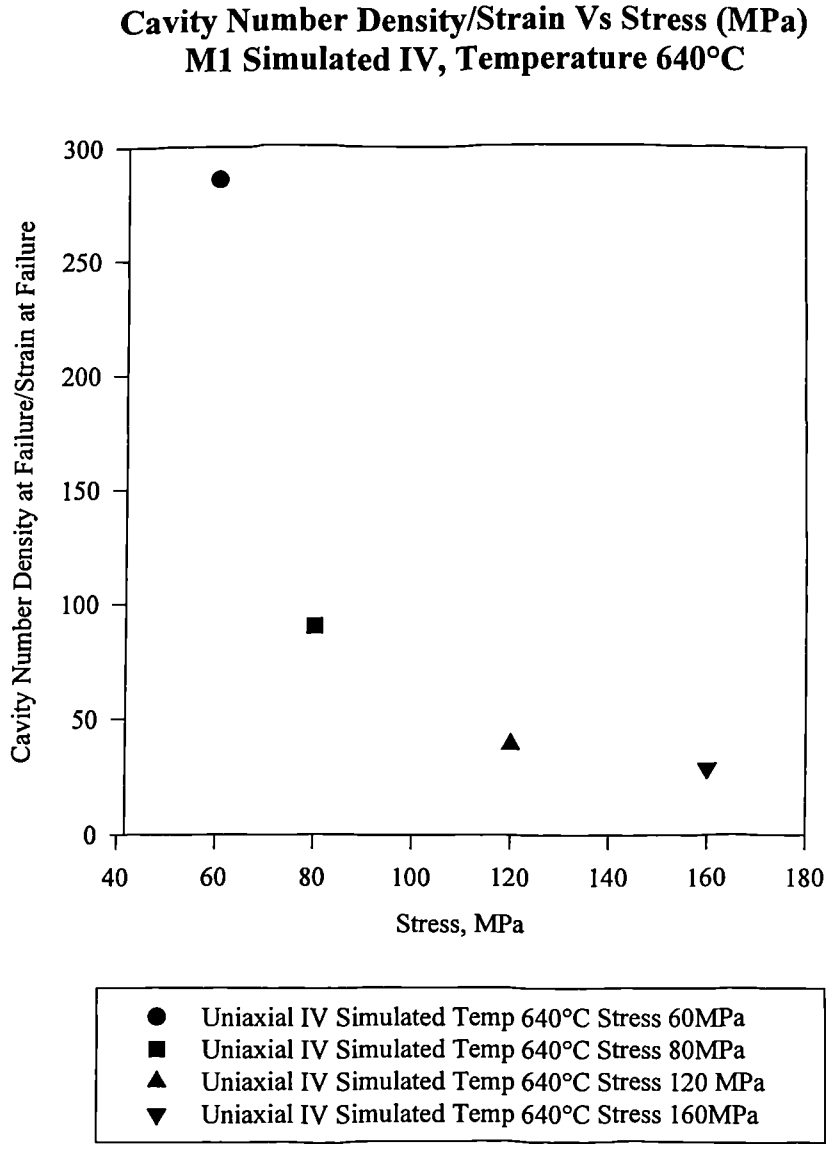

Fig 4.37 *Plot of Stress against strain to failure for uniaxial Type IV simulated specimens.*

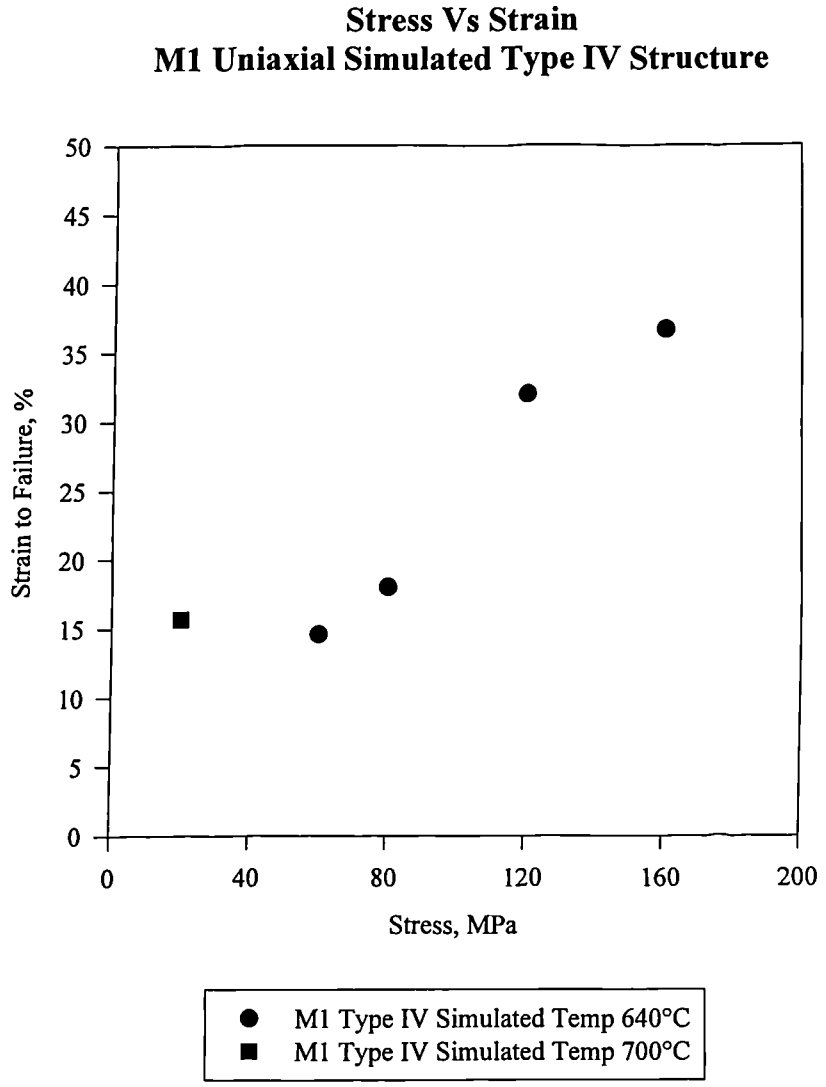

Fig 4.38 *Plot of reduction in area against strain to failure for uniaxial Type IV simulated specimens*

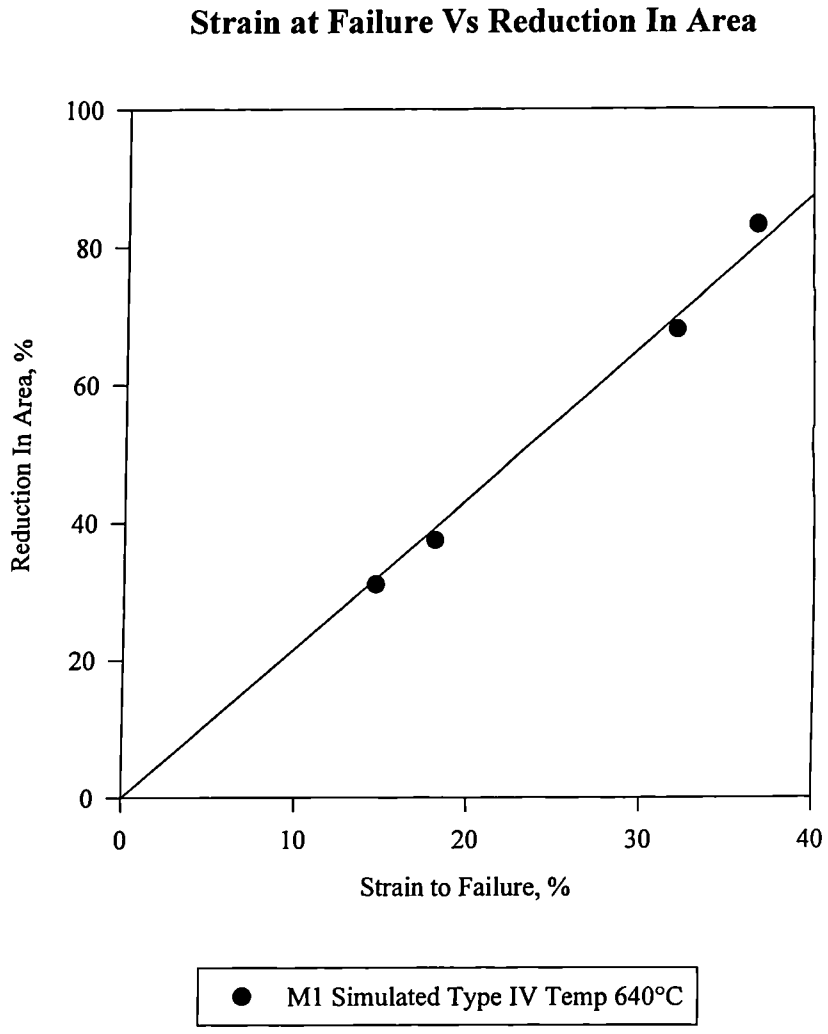

Fig 4.39 *Measurement of cavity number density M1 notch bar Type IV simulated and cross weld specimens at 640°C*

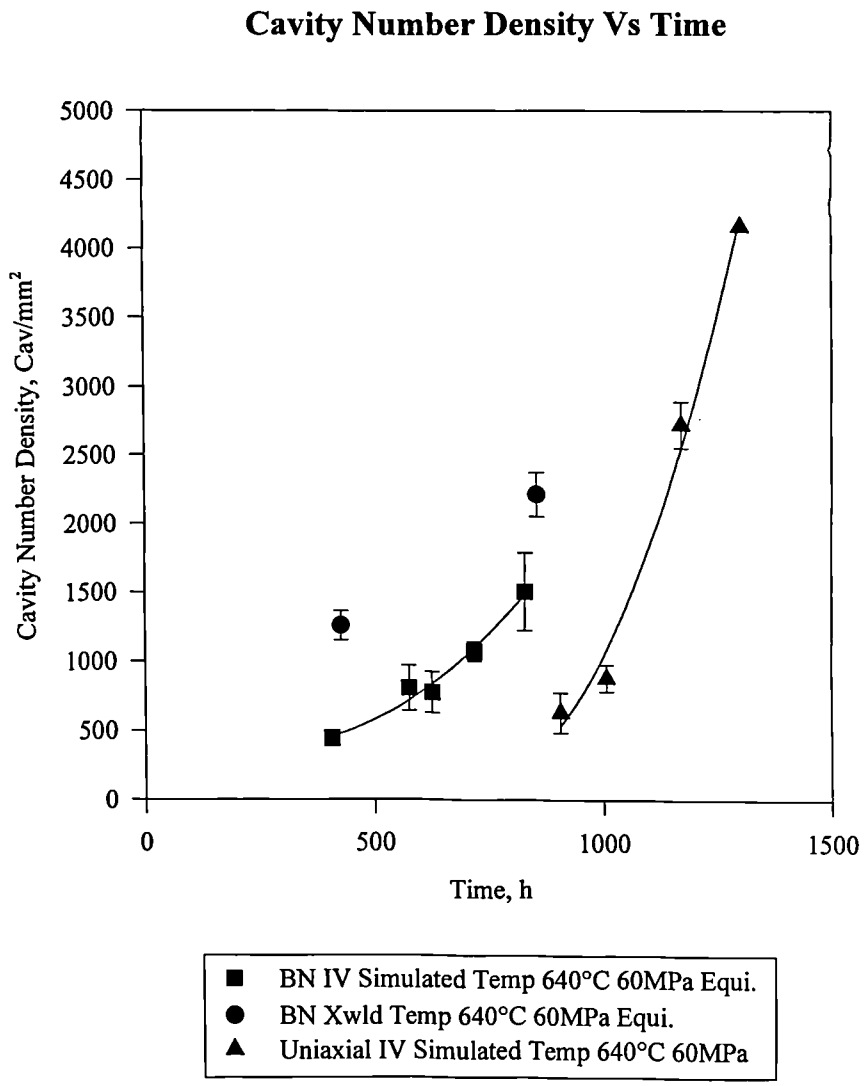

Fig 4.40 *Plot of cavity number density against reduction in area for M1 notch bar Type IV simulated and cross weld specimens*

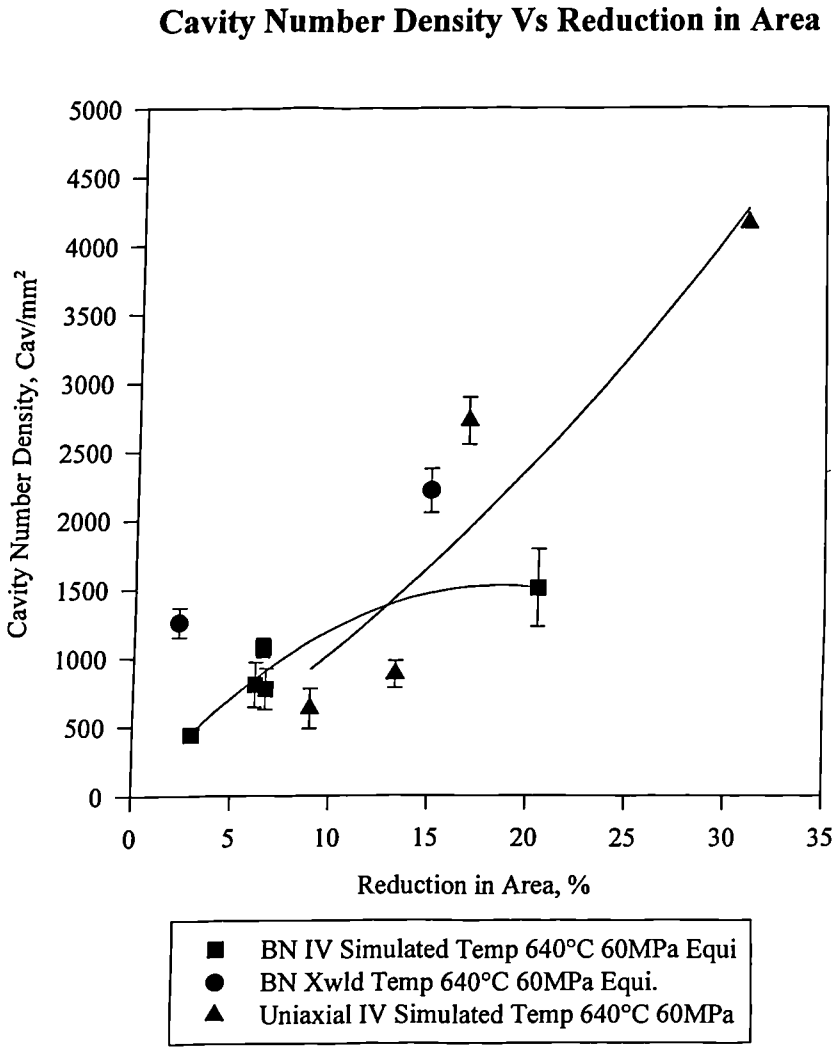

Fig 4.41 *Plot of cavity number density/reduction in area against stress for both uniaxial and notch bar specimens at 640°C*

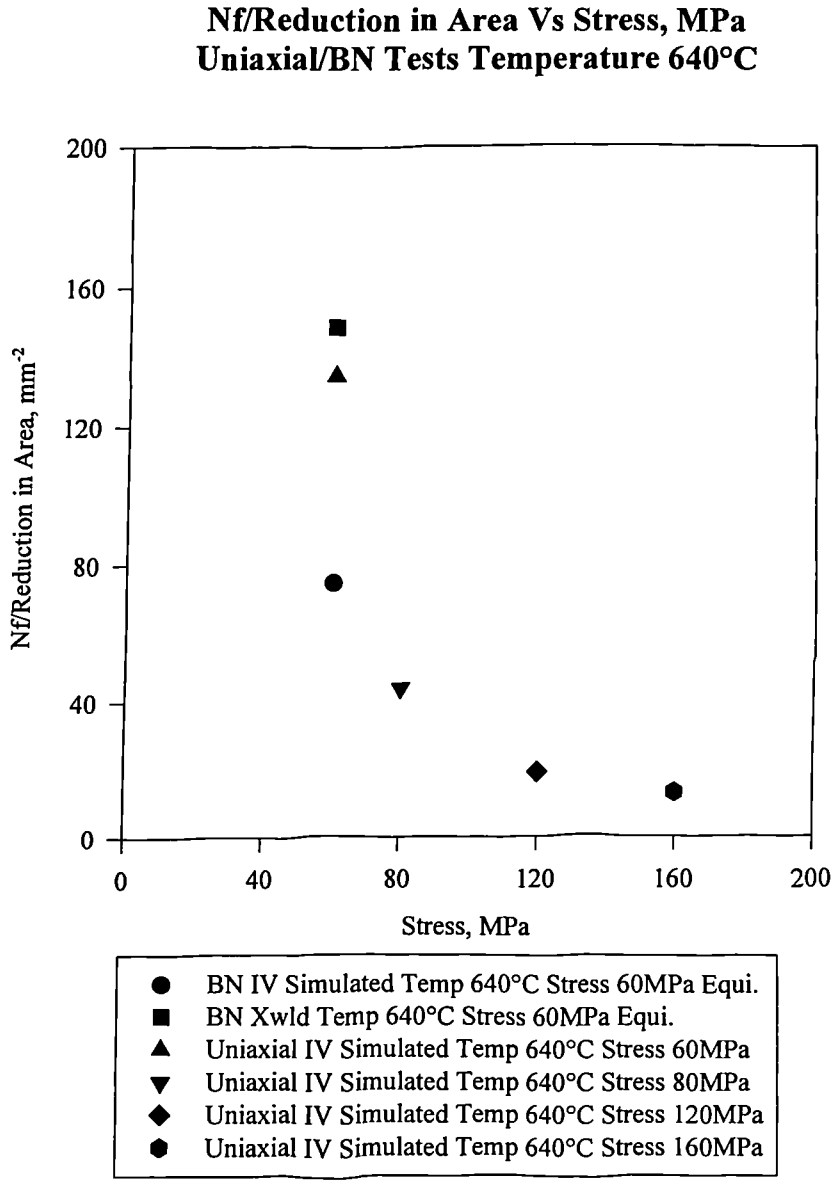

Fig 4.42 *Measurement of cavity number density across Type IV simulated notch bar* region

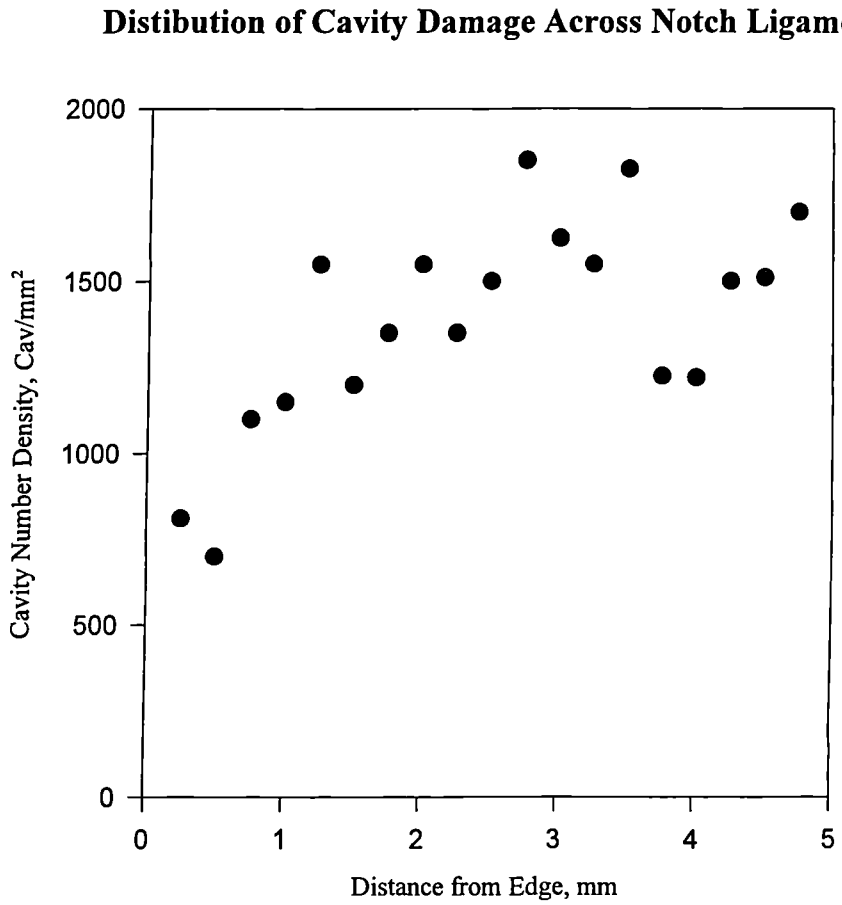

Fig 4.43 *M1 cross weld cavity area measurements uniaxial and notch bar specimens*

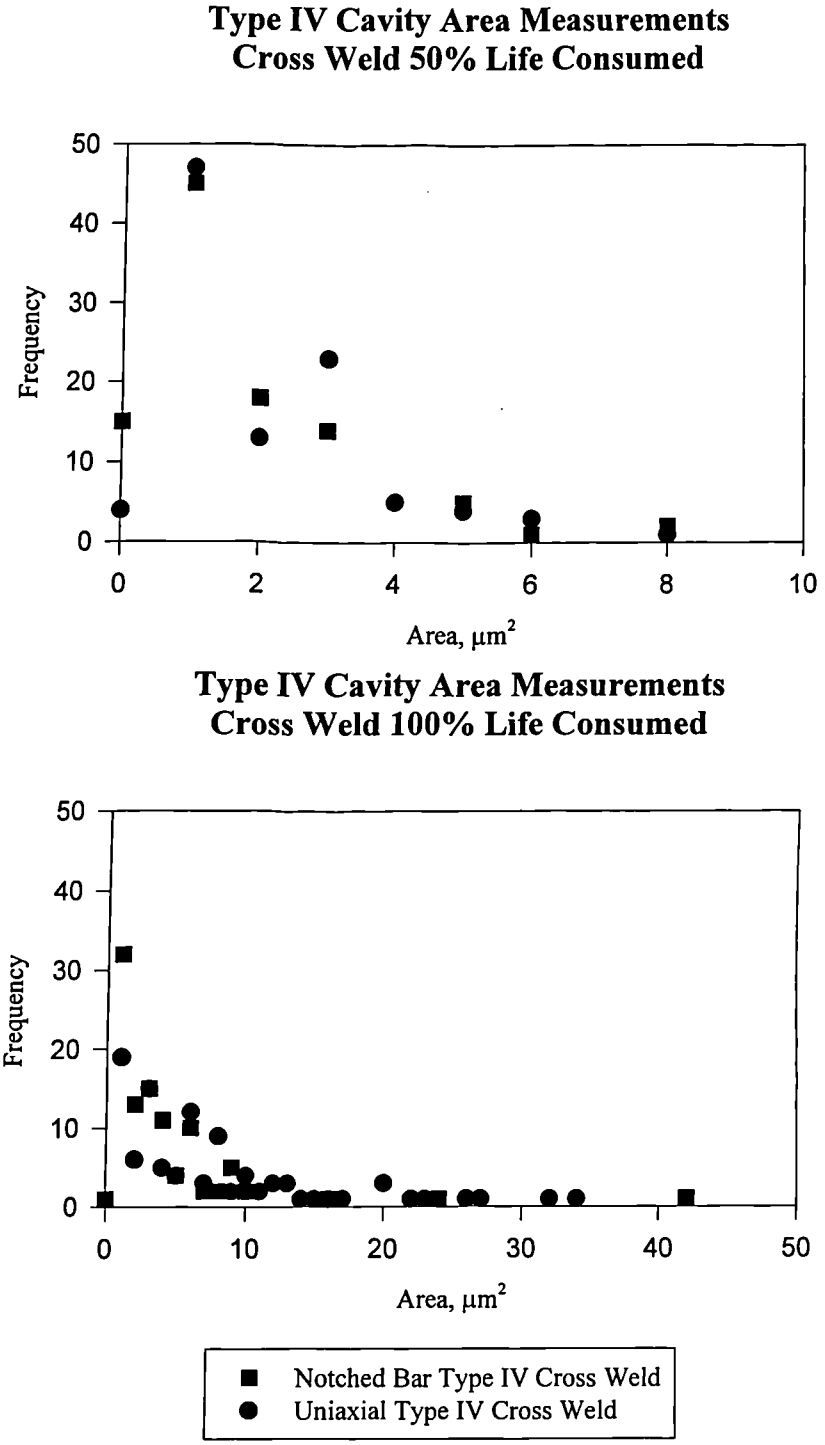

Fig 4.44 *Schematic of cavity illustrating aspect ratio measurement*

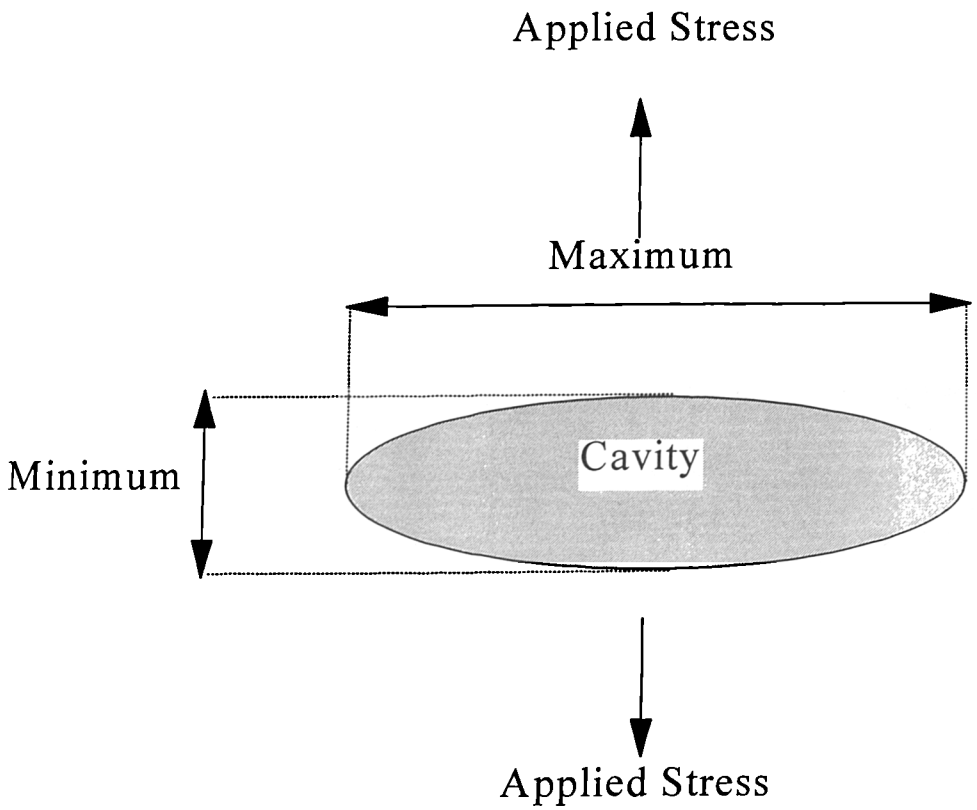

Fig 4.45 *M1 cross weld cavity aspect ratio measurements uniaxial and notch bar specimens*

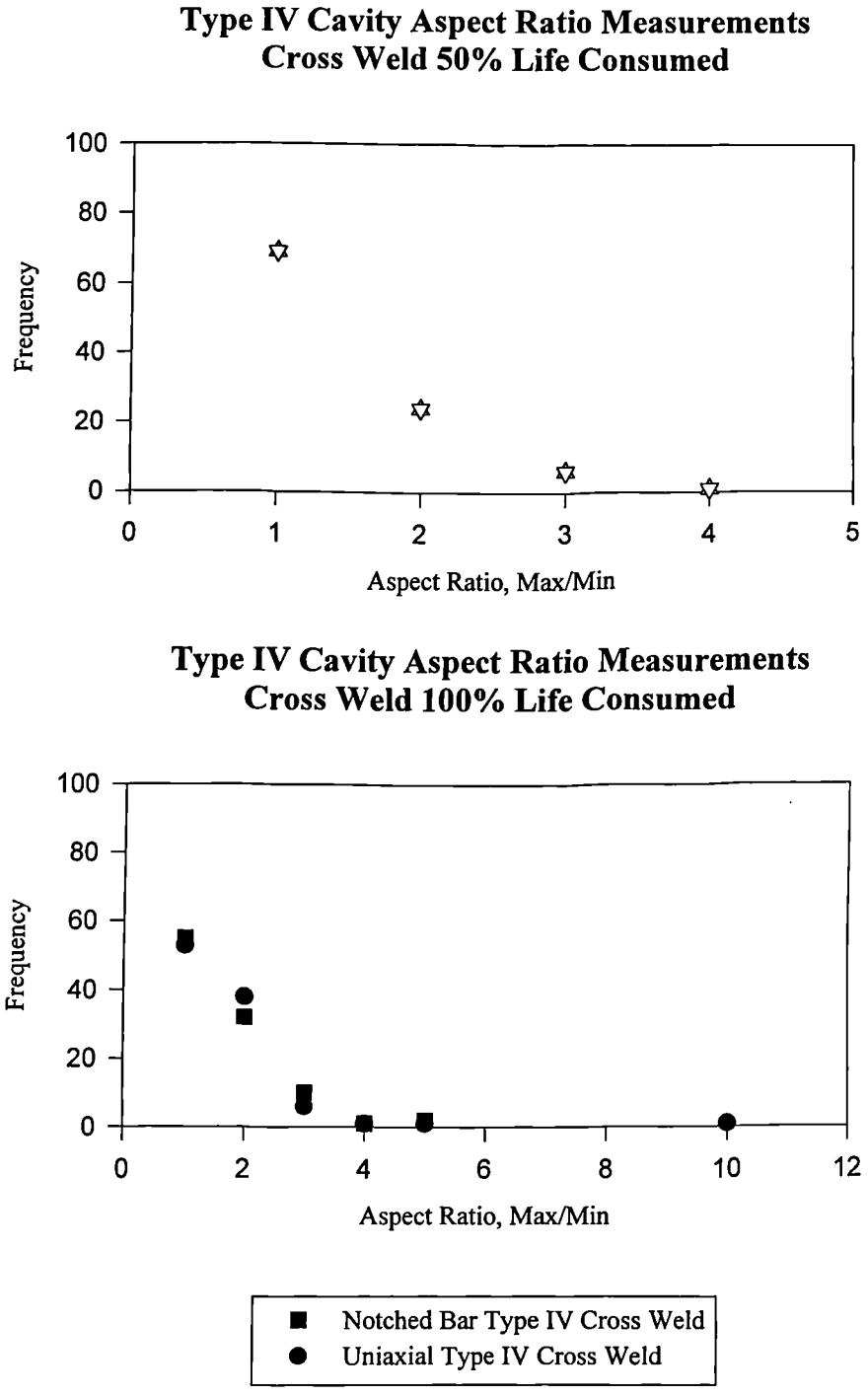

Fig 4.46 *M1 uniaxial Type IV simulated area measurements*

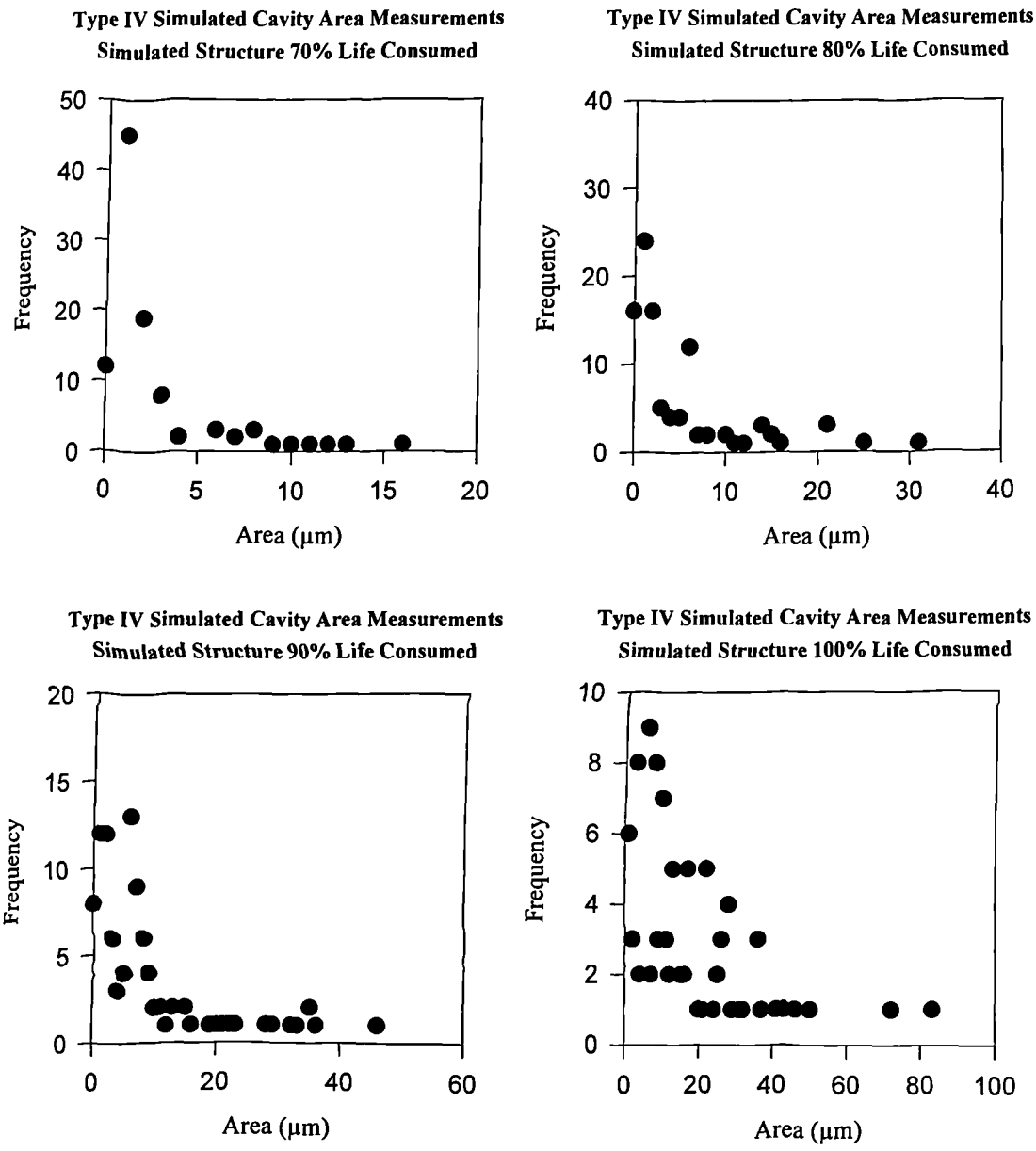

Fig 4.47 *M1 uniaxial Type IV simulated aspect ratio measurements*

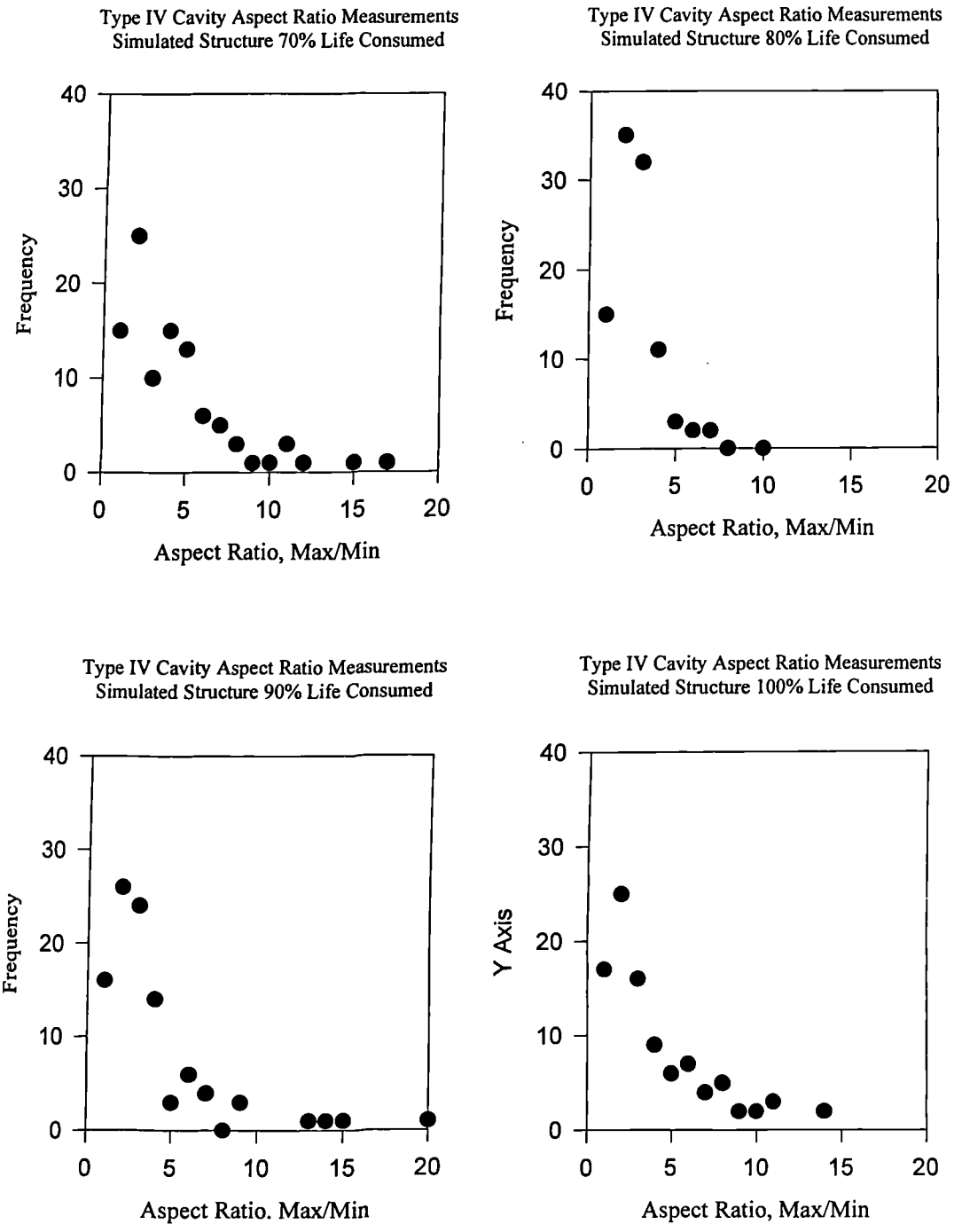

Fig 4.48 *M1 notch bar Type IV simulated area measurements*

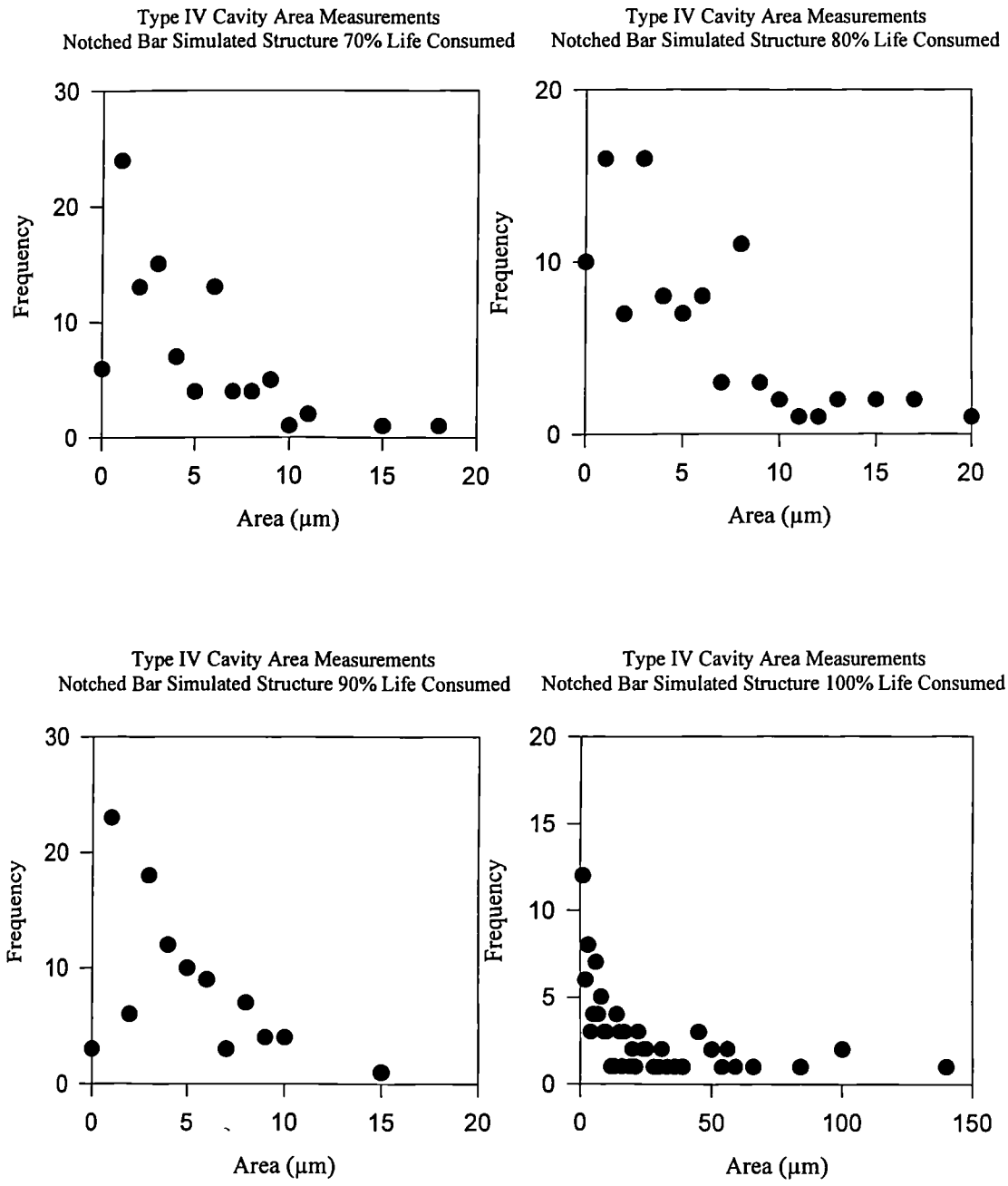

Fig 4.49 *M1 notch bar Type IV simulated aspect ratio measurements.*

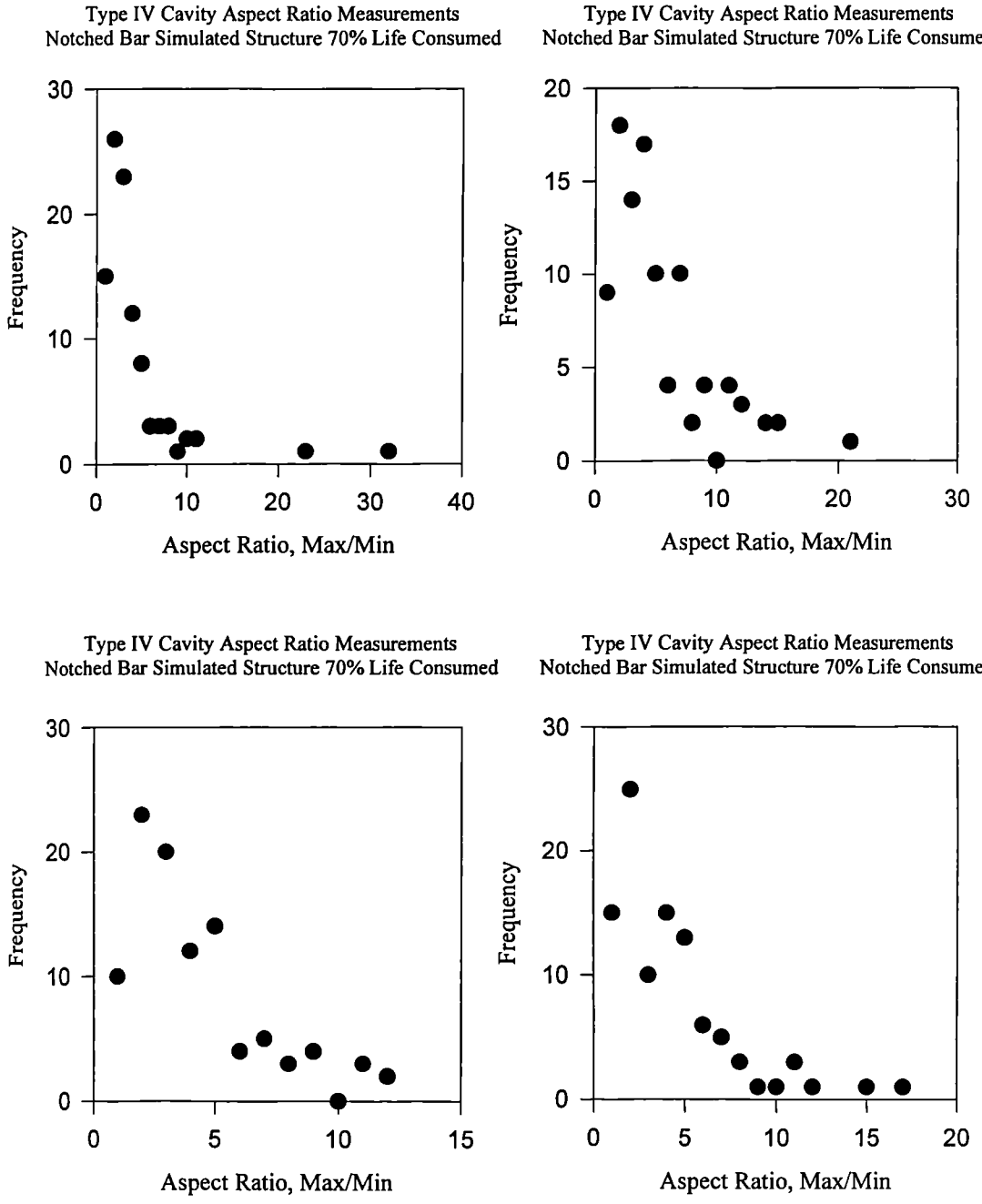

Plate 4.1. *AB parent cast, 2¼CrMo weldment. Magnification x320.*

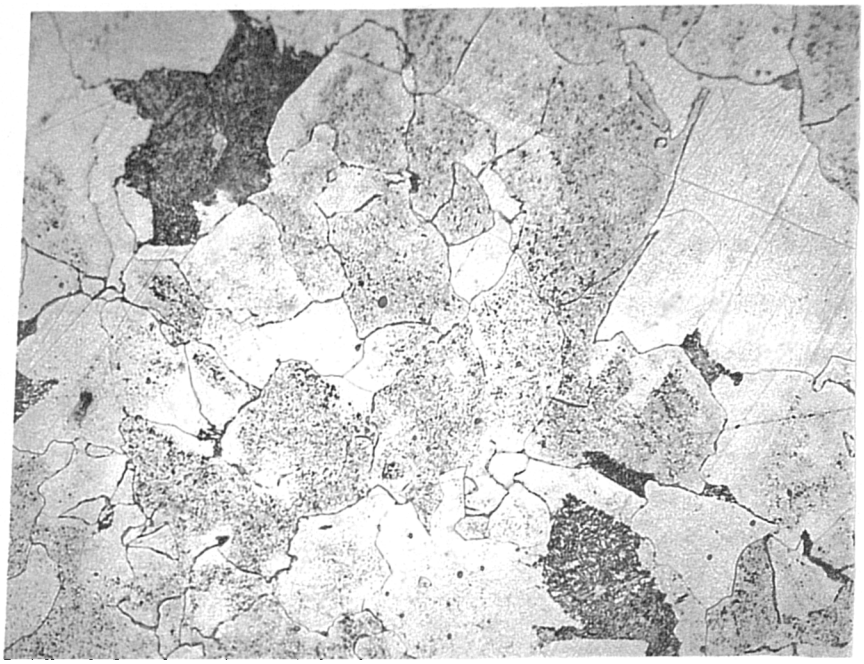

Plate 4.2. *AB parent cast, ½CrMoV weldment. Magnification x320.*

Plate 4.3. *M1 parent cast, 2¼CrMo weldment. Magnification x320.*

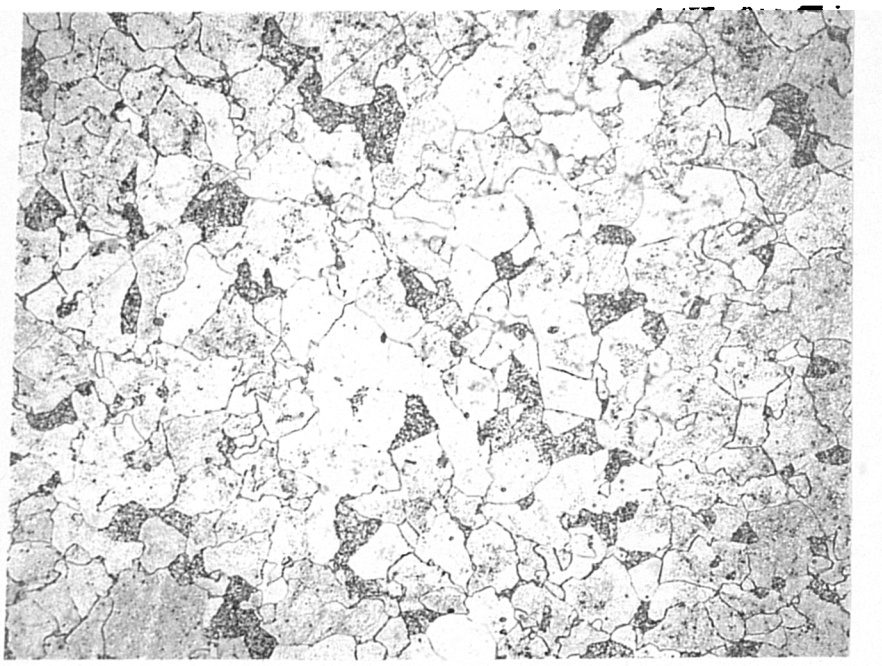

Plate 4.4. *MF parent cast, 2¼CrMo weldment. Magnification x320.*

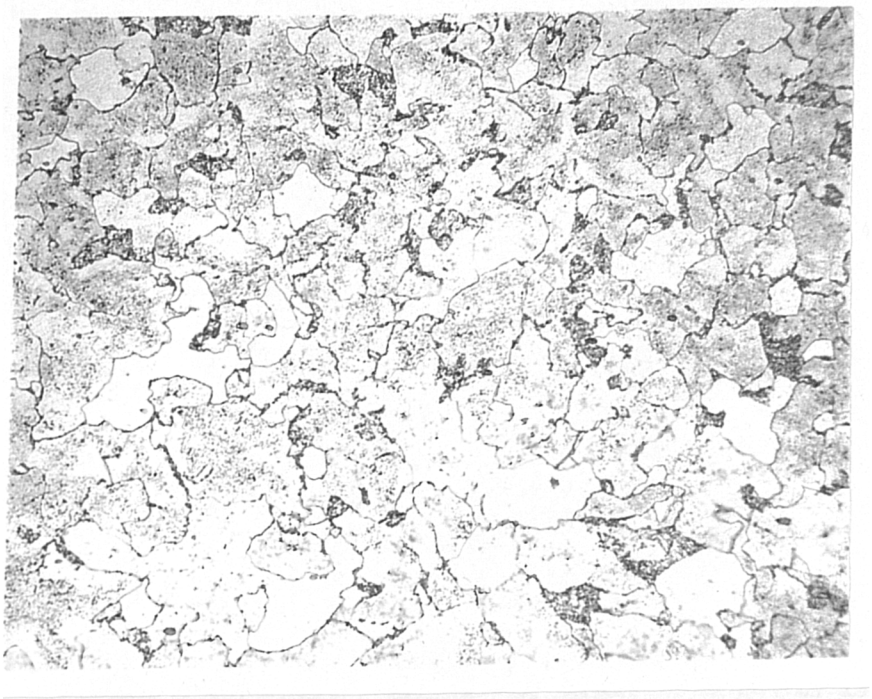

Plate 4.5. *US parent cast, 2¼CrMo Weldment. Magnification x320.*

Plate 4.6. *AB 2¼CrMo weldment. Magnification x 320.*

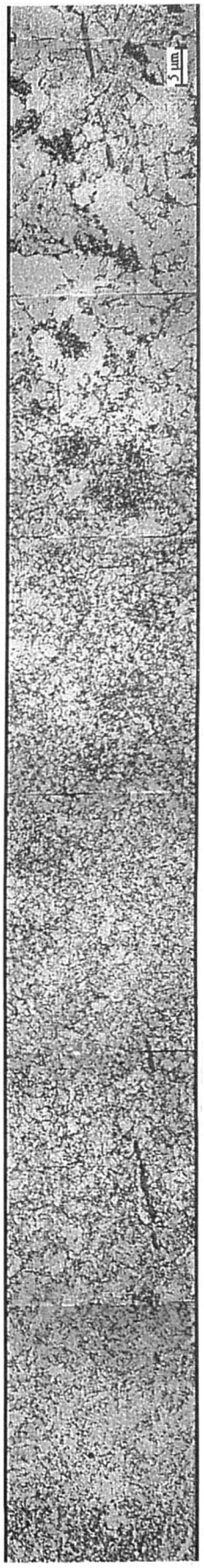

Plate 4.7. *AB ½CrMoV weldment. Magnification x 320.*

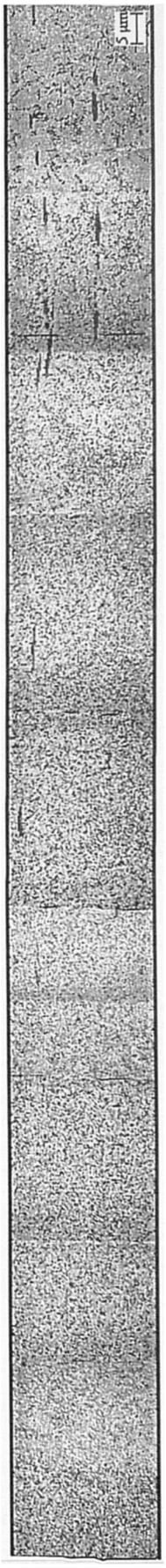

Plate 4.8. *M1 2¼CrMo weldment. Magnification x 320.*

Plate 4.9. *MF 2¼CrMo weldment. Magnification x 320.*

Plate 4.10. *US 2¼CrMo weldment. Magnification x 320.*

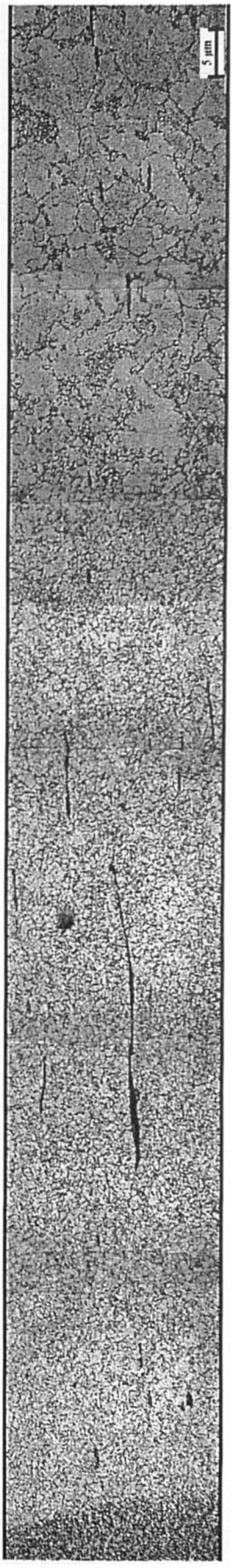

Plate 4.11. *Optical micrograph of M1 cast following heat treatment at 850°C for 10 minutes. Magnification x320*

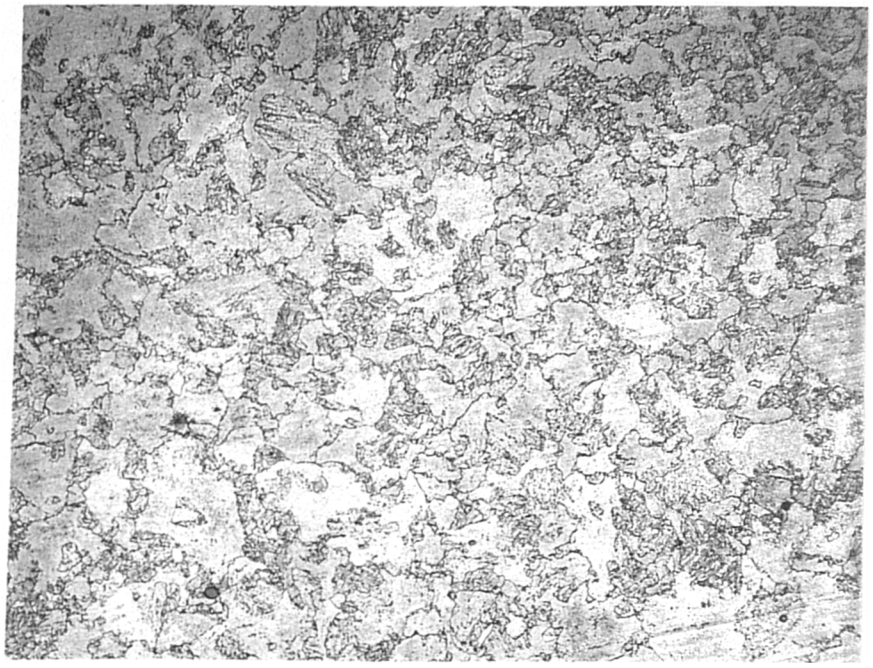

Plate 4.12. *Optical micrograph of M1 cast following heat treatment at 850°C for 20 minutes. Magnification x320*

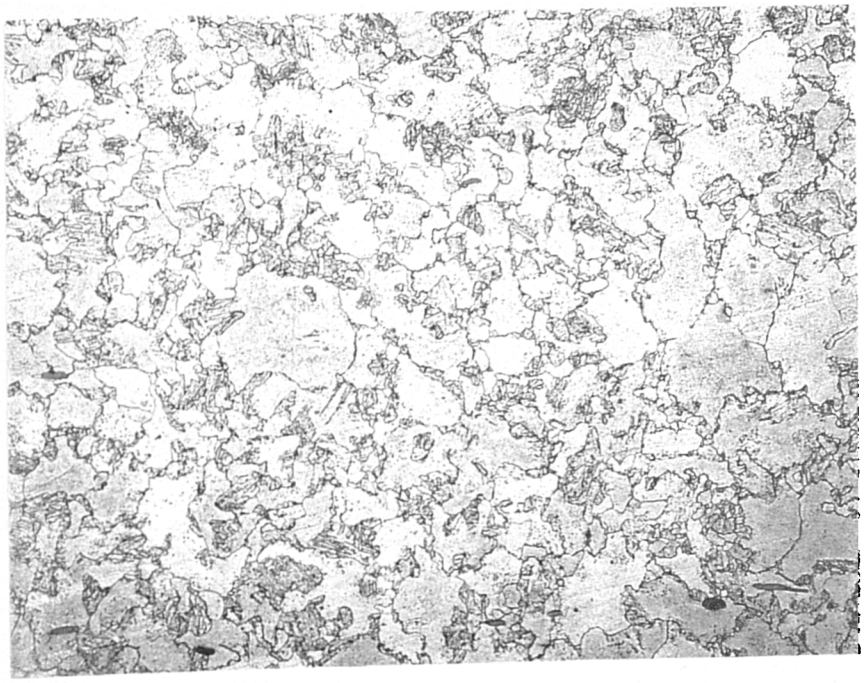

Plate 4.13. *Optical micrograph of M1 cast following heat treatment at 850°C for 30 minutes. Magnification x320*

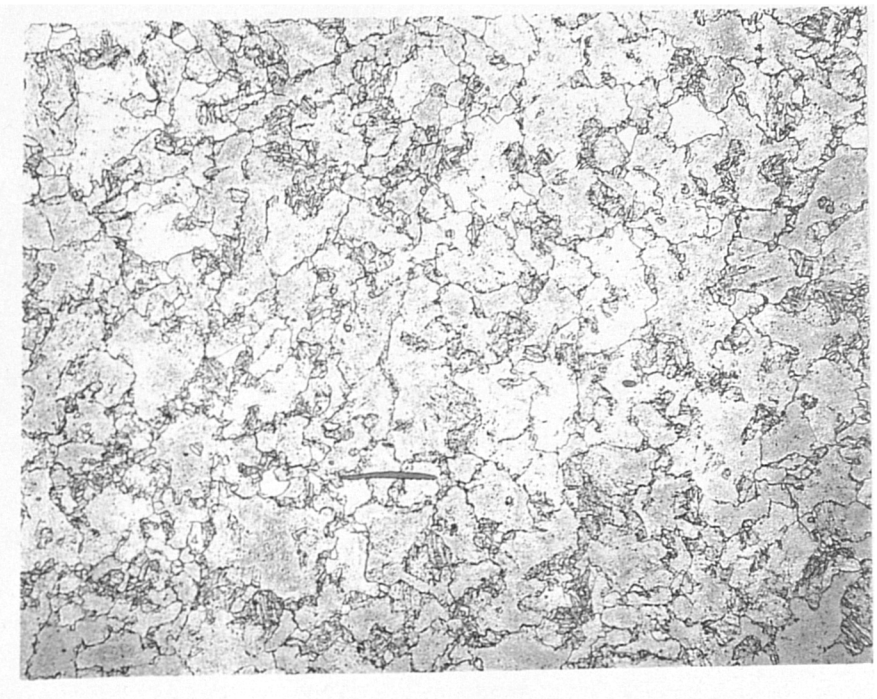

Plate 4.14. *Optical micrograph of AB cast following heat treatment at 850°C for 10 minutes. Magnification x320*

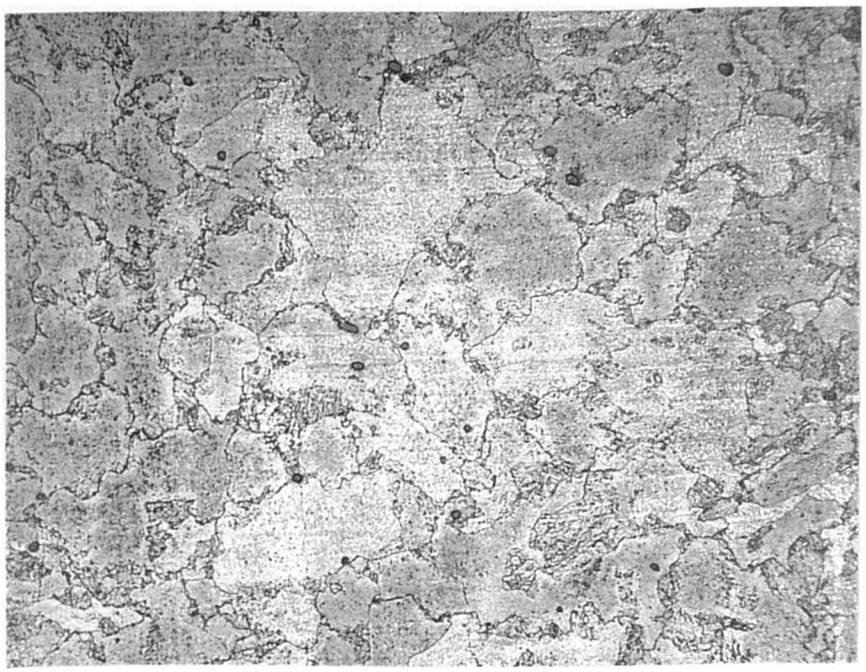

Plate 4.15. *Optical micrograph of AB cast following heat treatment at 850°C for 20 minutes. Magnification x320.*

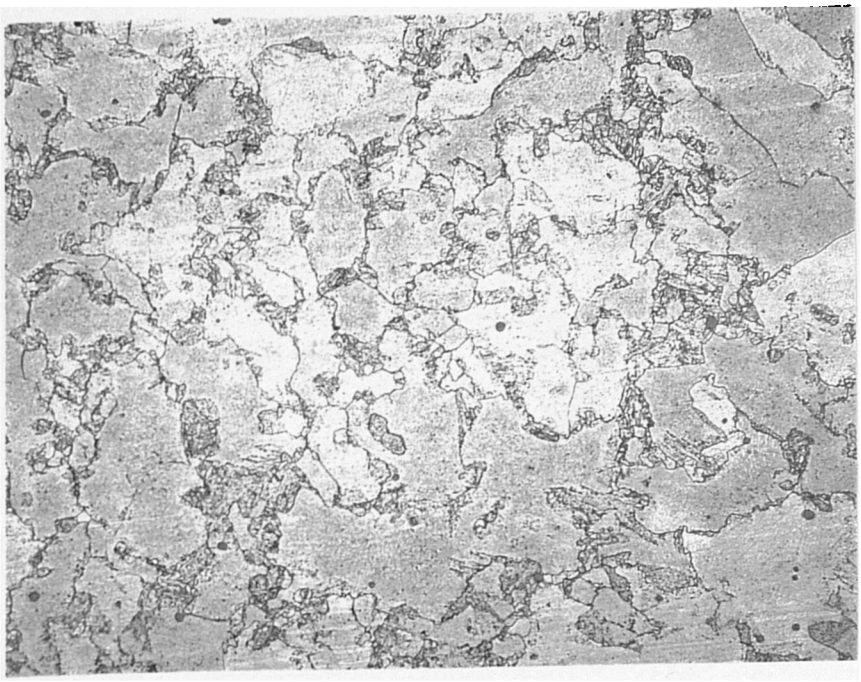

Plate 4.16. *Optical micrograph of AB cast following heat treatment at 850°C for 30 minutes. Magnification x320.*

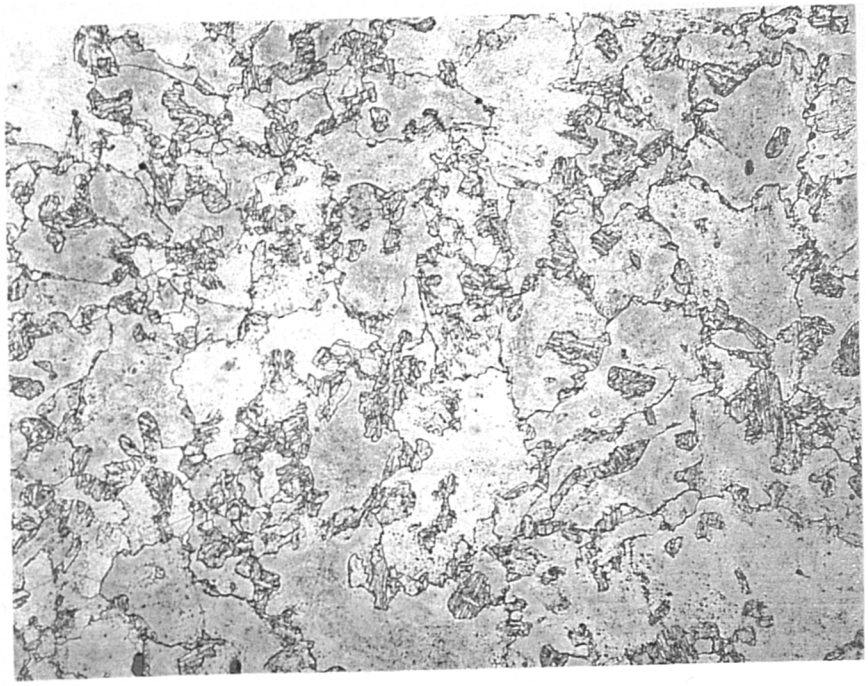

Plate 4.17. *SEM micrograph of M1 cast following heat treatment at 850°C for 30 minutes. Magnification x1000.*

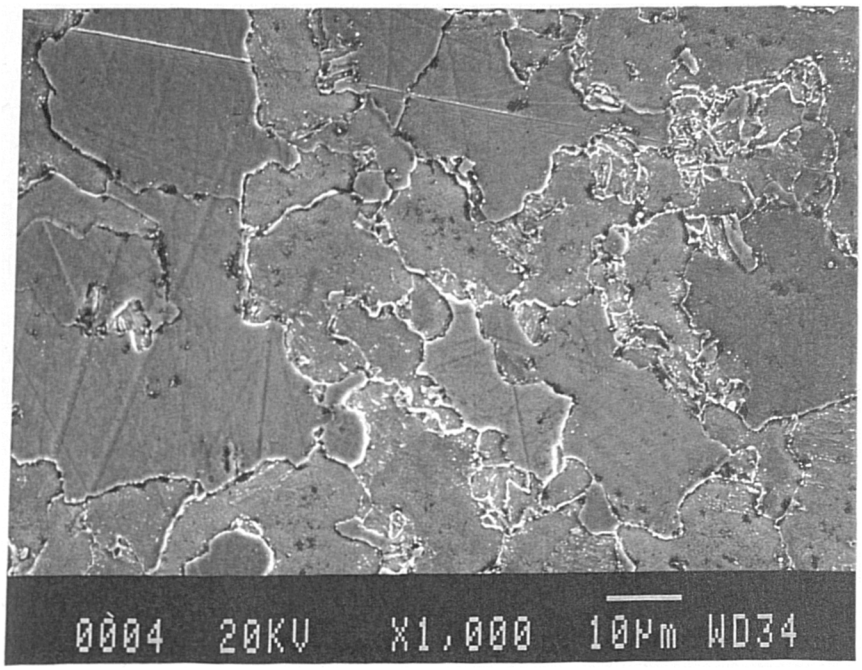

Plate 4.18. *SEM micrograph of M1 cast following heat treatment at 850°C for 30 minutes. Magnification x4300.*

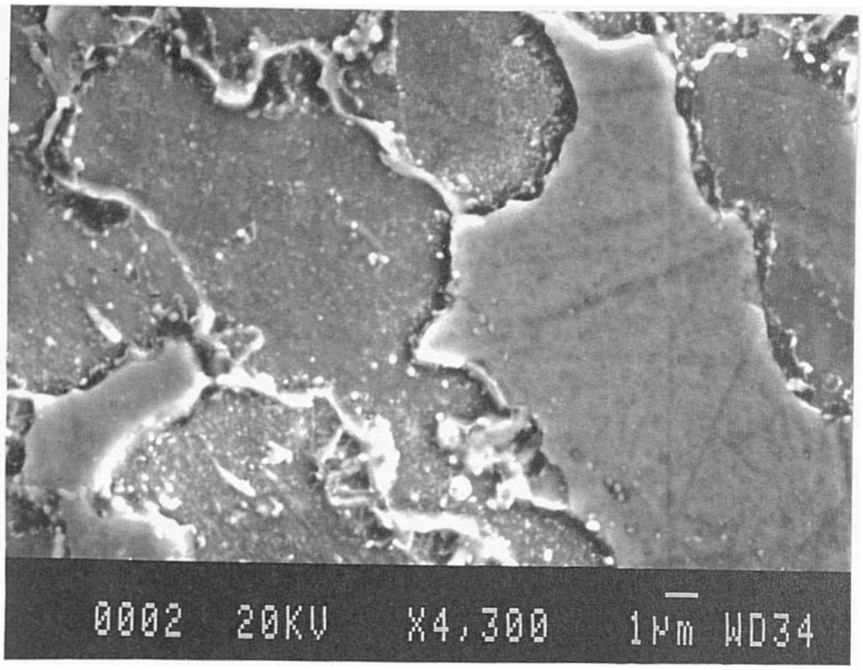

Plate 4.19. *SEM micrograph of AB cast following heat treatment at 850°C for thirty minutes. Magnification x 1000.*

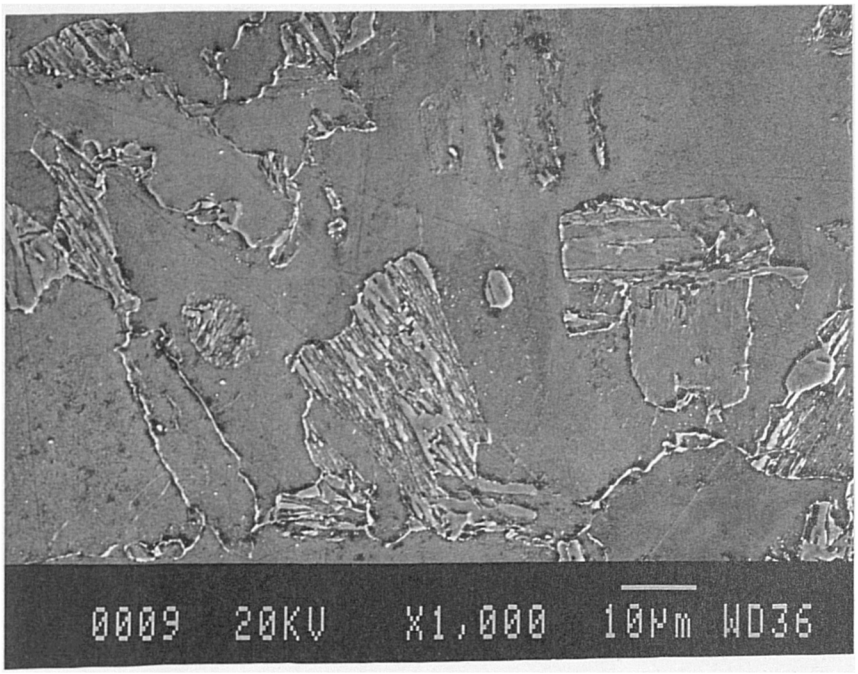

Plate 4.20. *SEM micrograph of AB cast following heat treatment at 850°C for thirty minutes. Magnification x 4300.*

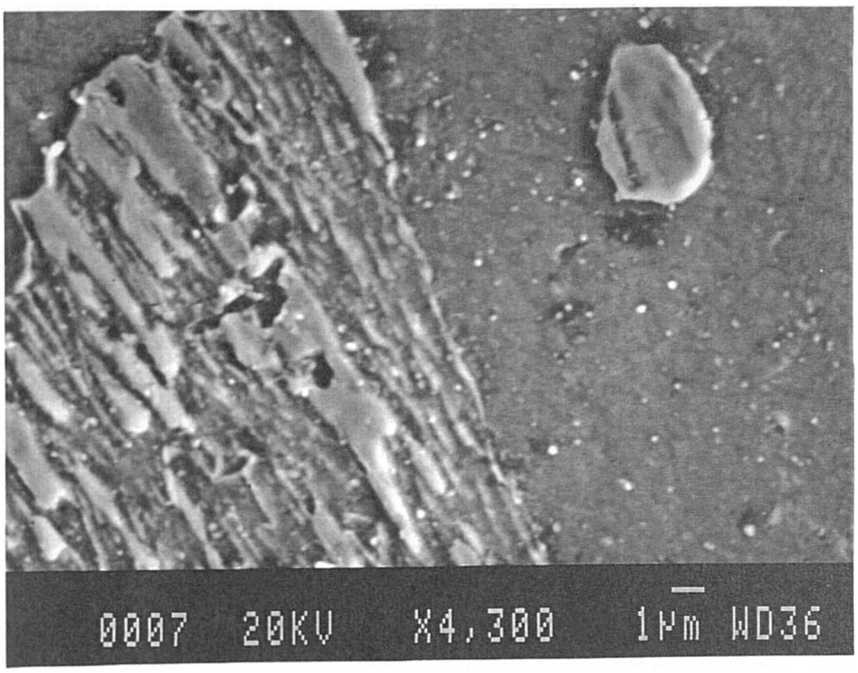

Plate 4.21. *SEM micrograph of M1 cast following heat treatment at 900°C for thirty minutes. Magnification x 1000.*

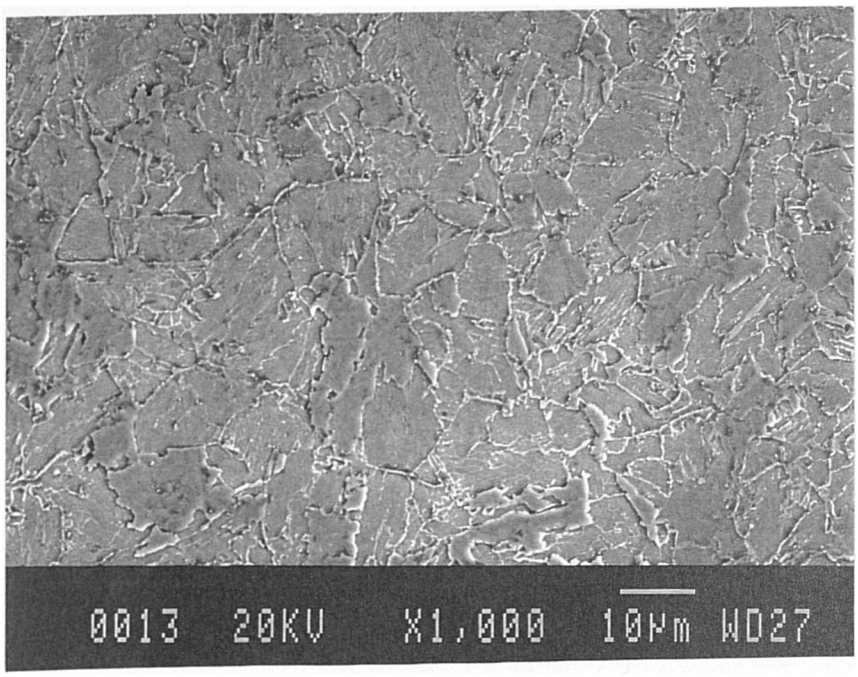

Plate 4.22. *SEM micrograph of M1 cast following heat treatment at 900°C for thirty minutes. Magnification x 4300.*

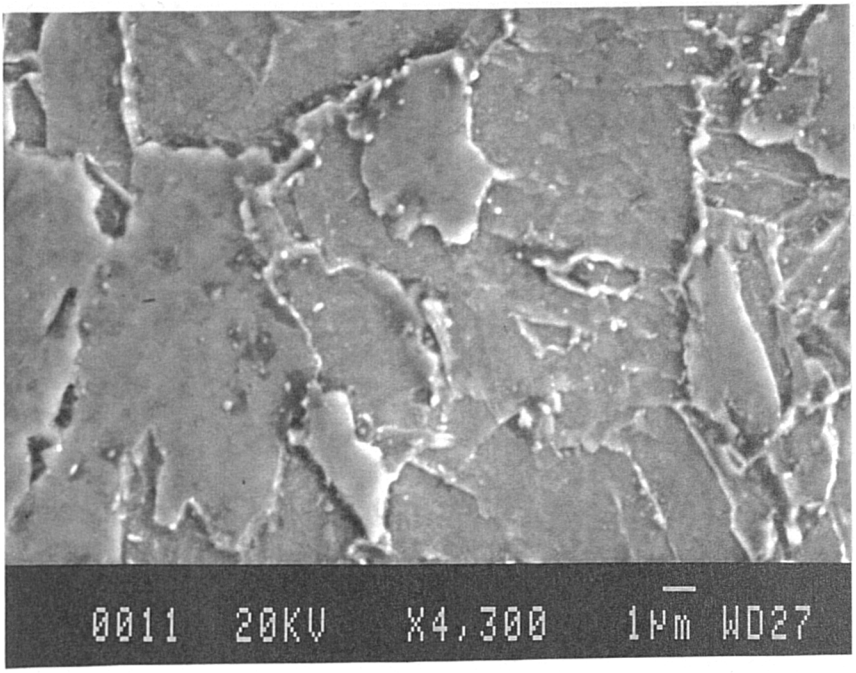

Plate 4.23. *SEM micrograph of AB cast following heat treatment at 900°C for thirty minutes. Magnification x 1000.*

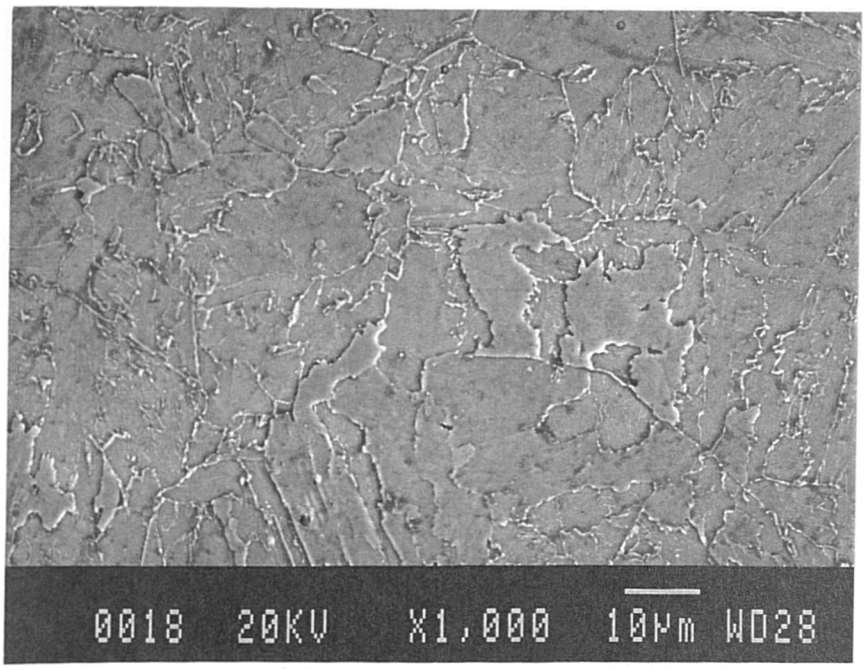

Plate 4.24. *SEM micrograph of AB cast following heat treatment at 900°C for thirty minutes. Magnification x 4300.*

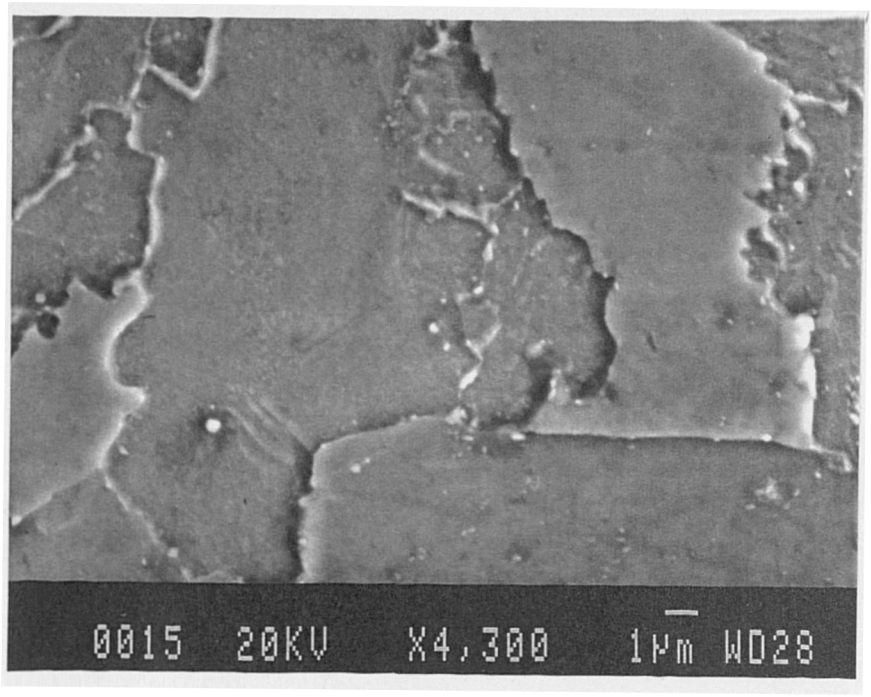

Plate 4.25. *SEM micrograph of M1 Type IV region. Magnification x1000.*

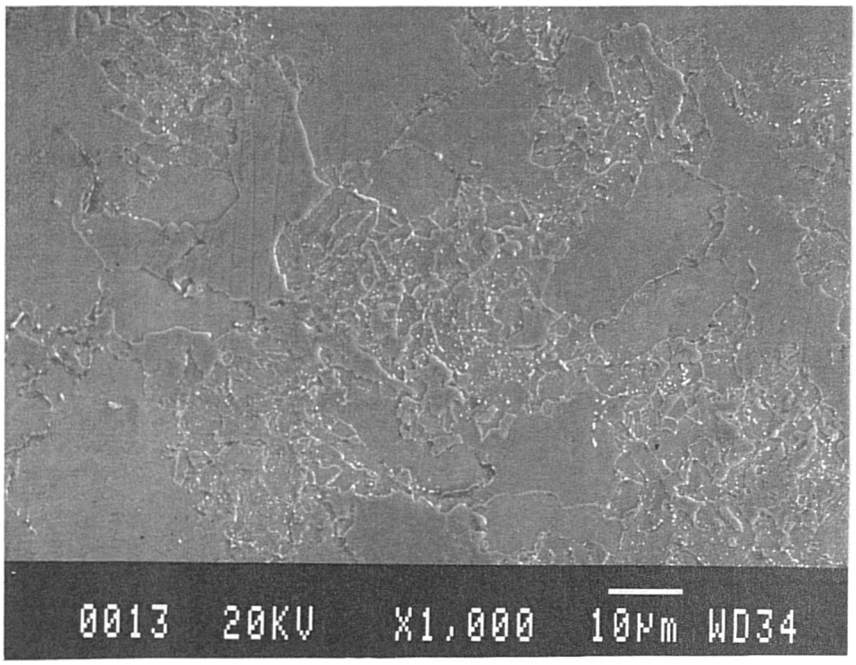

Plate 4.26. *SEM micrograph of M1 Type IV region. Magnification x 4500.*

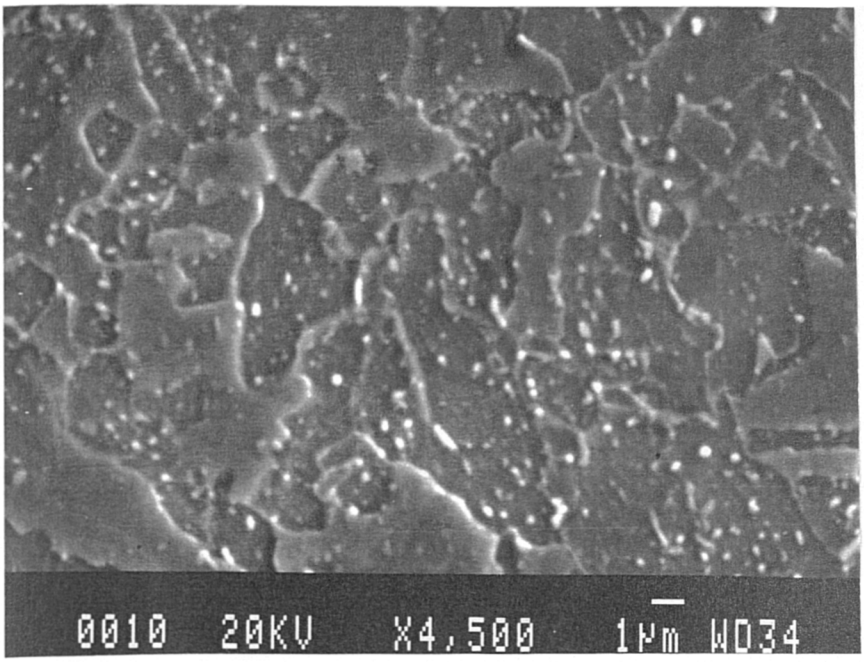

Plate 4.27. *SEM Micrograph of AB Type IV region. Magnification x1000.*

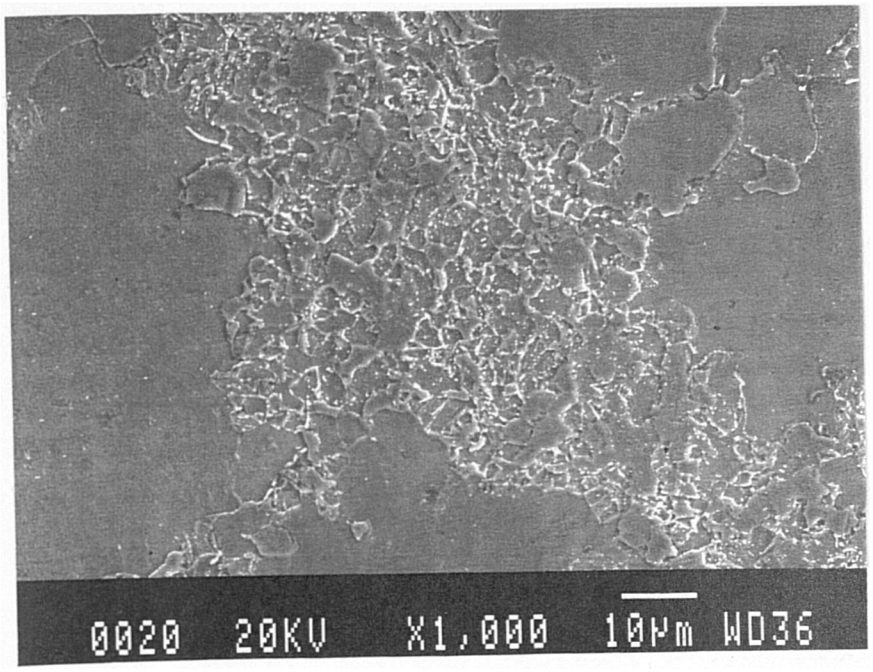

Plate 4.28. *SEM micrograph of AB Type IV region. Magnification x4500.*

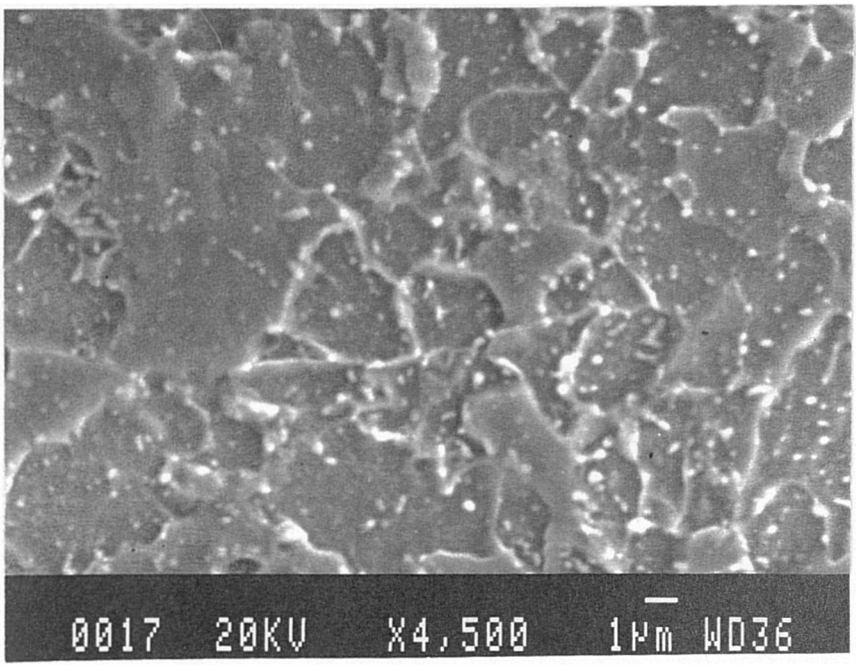

Plate 4.29. *SEM micrograph of M1 HAZ. Magnification x3500.*

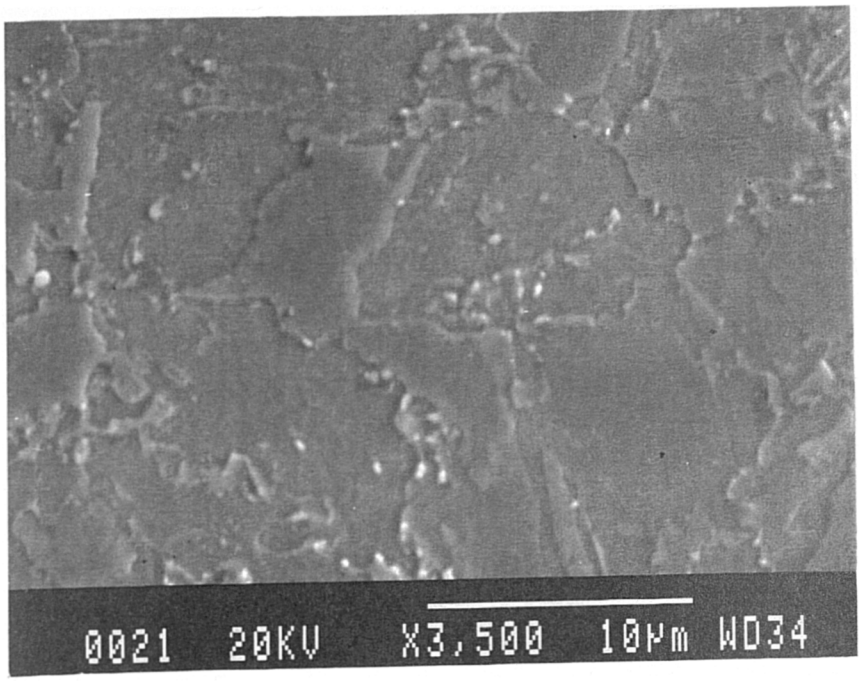

Plate 4.30. *SEM micrograph of AB HAZ. Magnification x3500.*

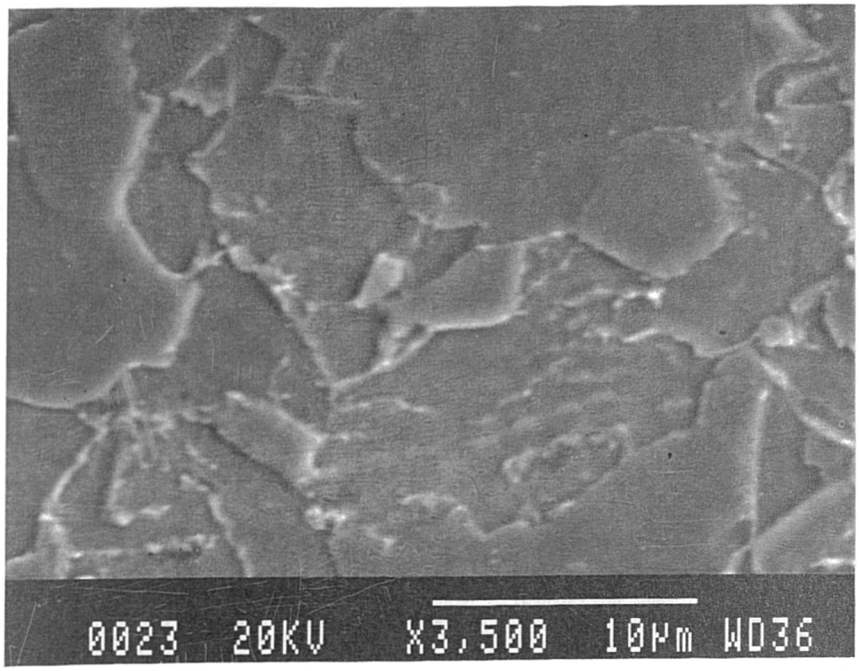

Plate 4.31. *TEM micrograph of carbides found in the aged M1 Type IV Simulated specimen.*
Magnification x14000 *Magnification x51000*

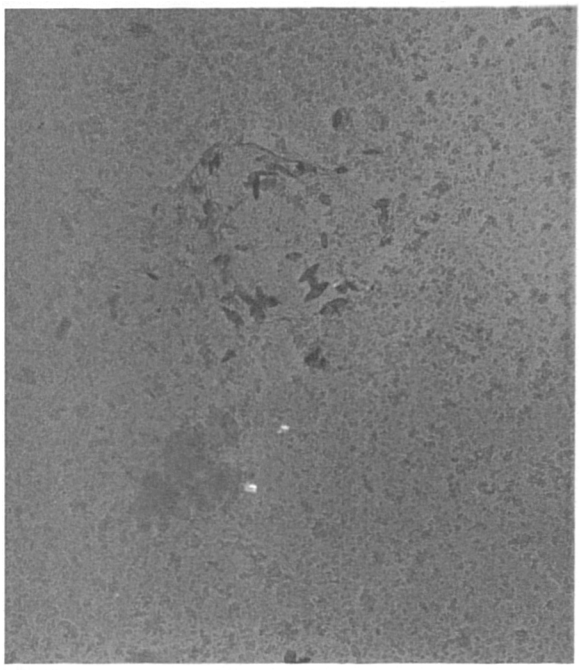

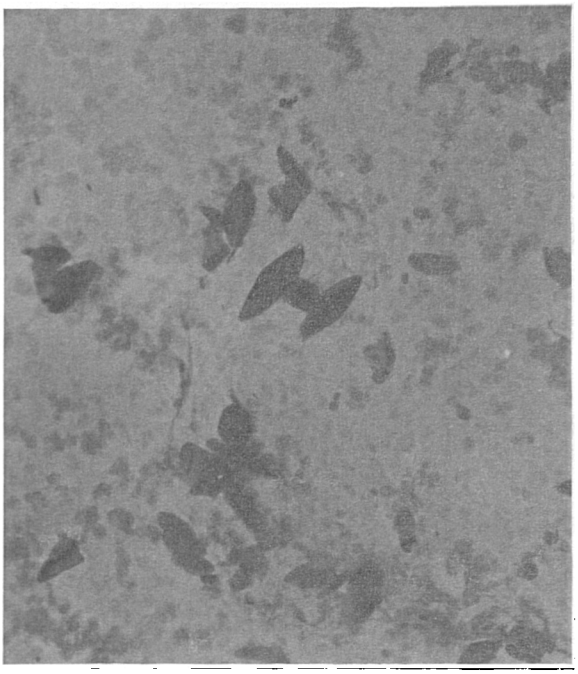

Plate 4.32. *TEM micrograph of carbides found in the aged AB Type IV simulated specimen.*
Magnification x8000 *Magnification x48000*

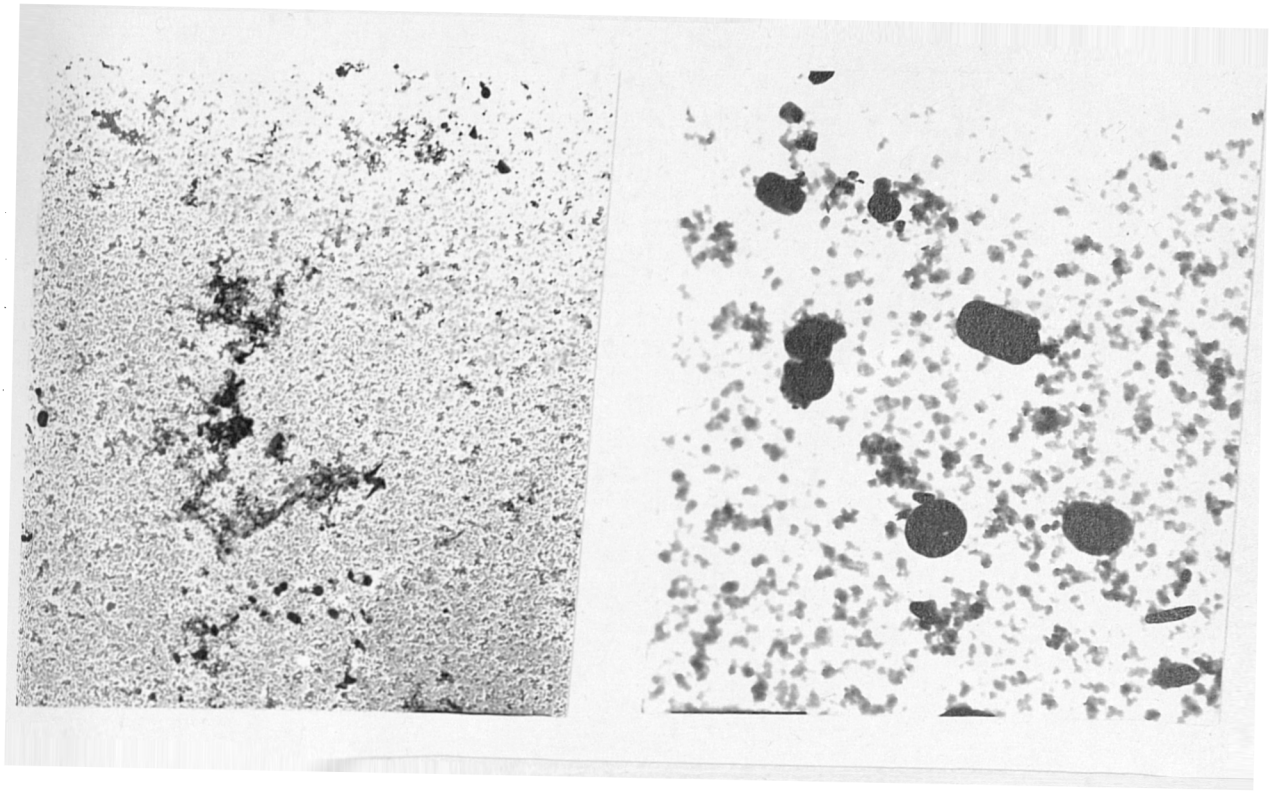

Plate 4.33. *TEM micrograph of carbides found in the as-received M1 Type IV simulated specimen.*
Magnification x8000 *Magnification x48000*

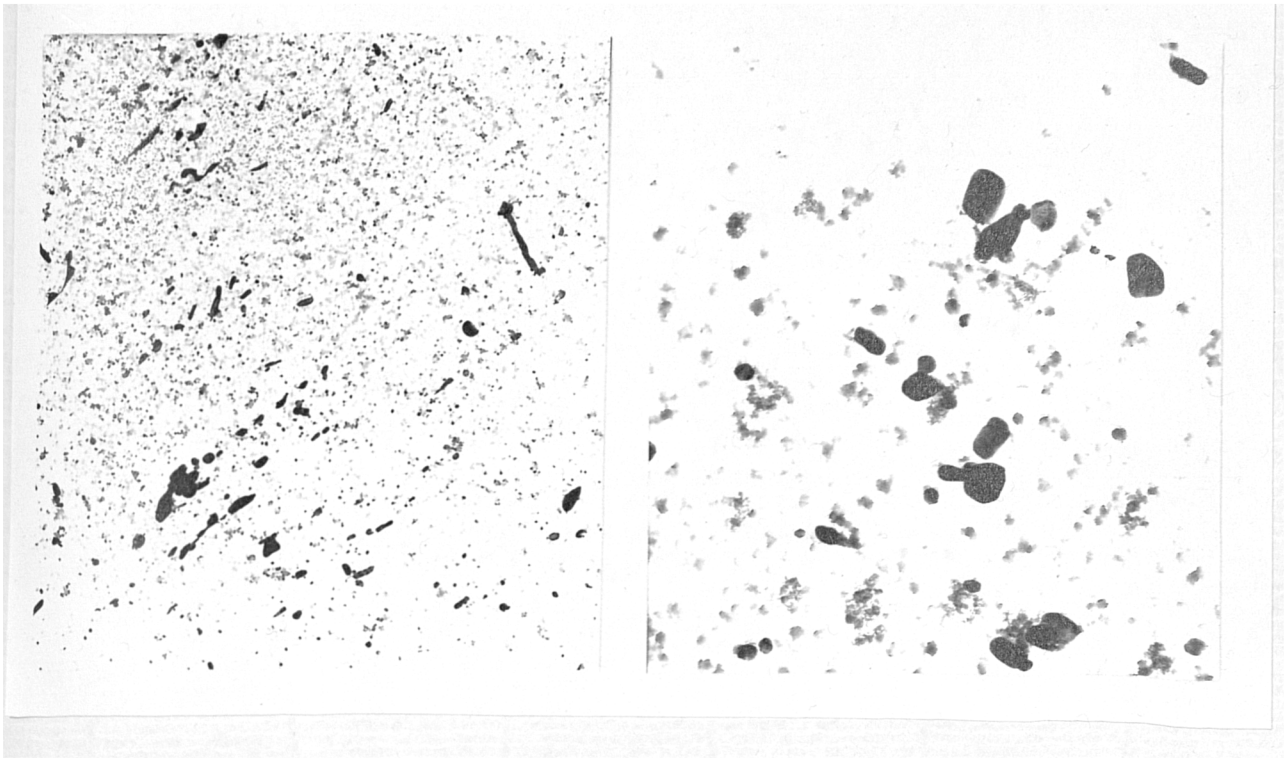

Plate 4.34. *TEM micrograph of carbides found in the as-received AB Type IV simulated specimen.*
Magnification x8000 *Magnification x48000*

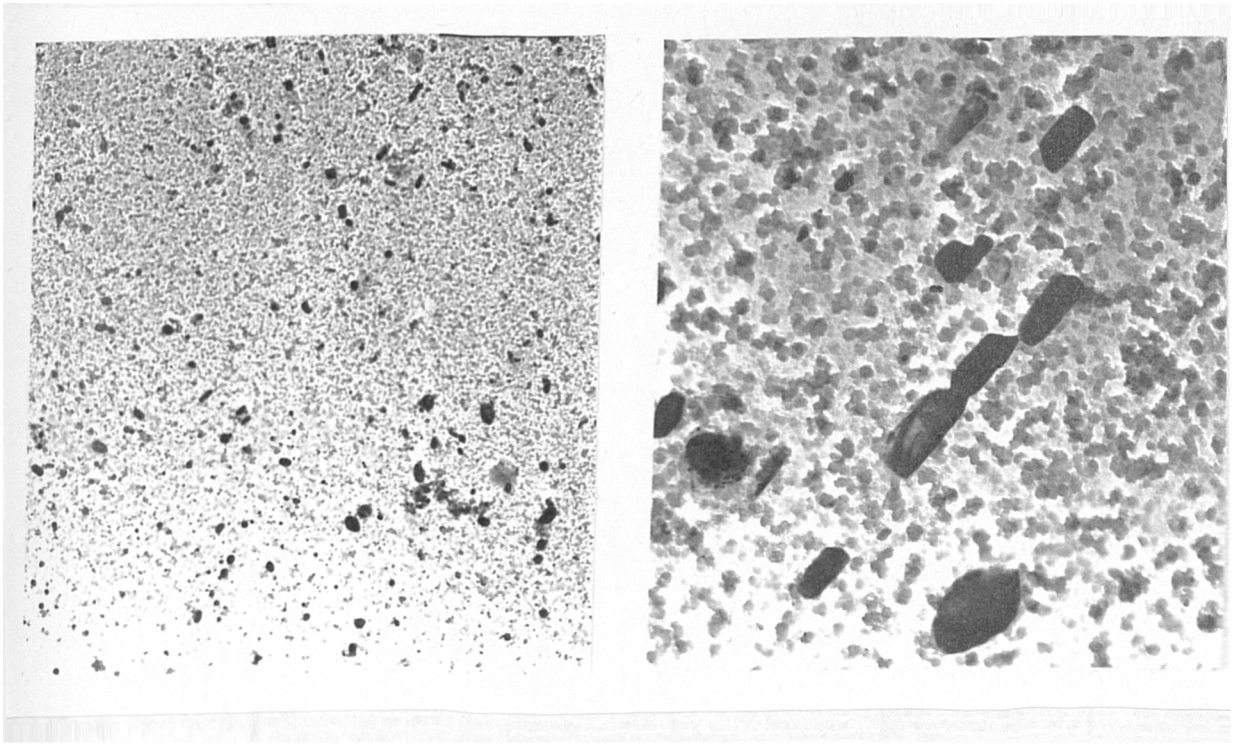

Plate 4.35. *SEM micrograph of creep cavitation in the M1 cast Type IV region. Magnification x400.*

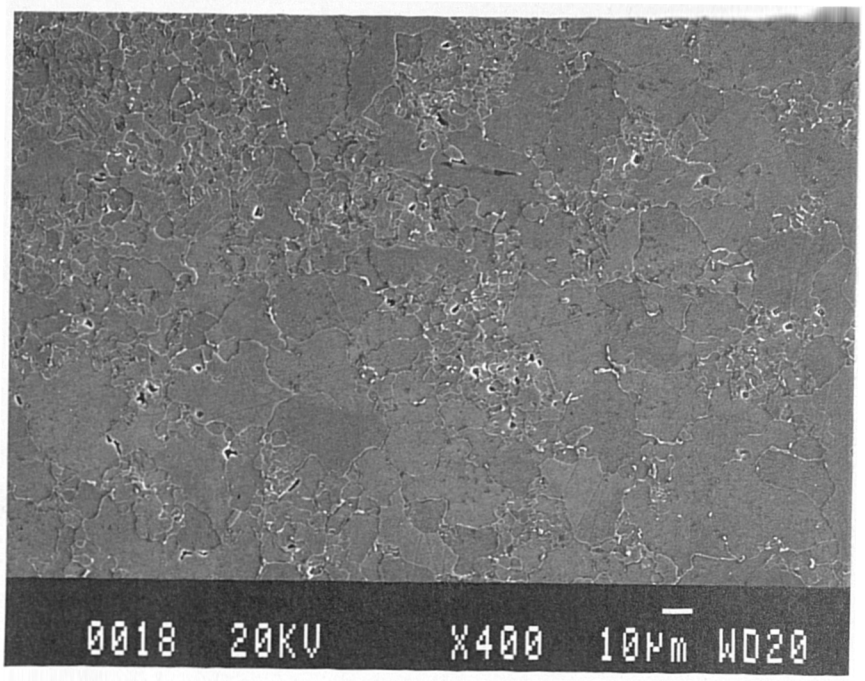

Plate 4.36. *Optical micrograph of creep cavitation in the M1 cast Type IV region. Magnification x400.*

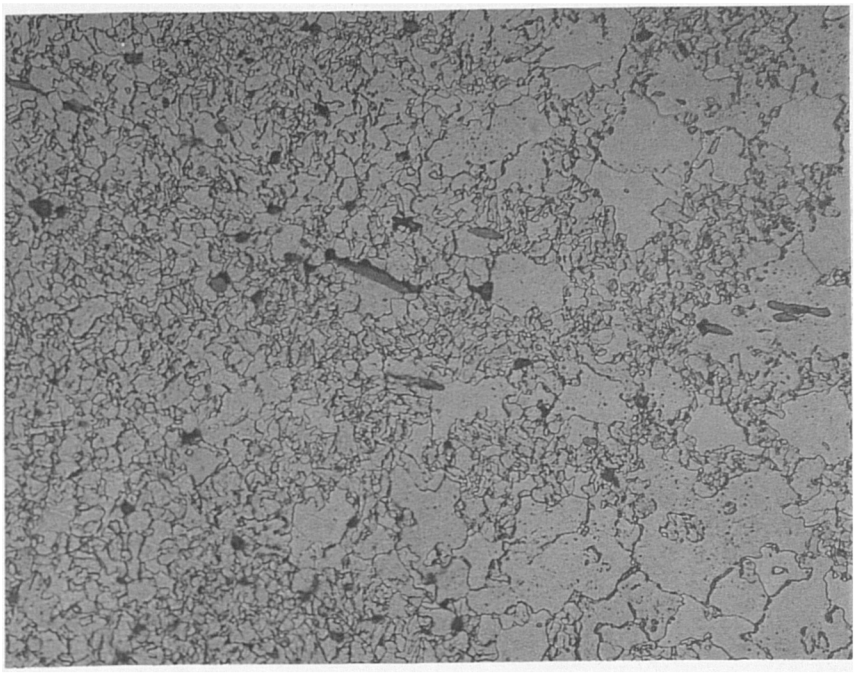

Plate 4.37. *Cavitation observed in a uniaxial M1 cast Type IV simulated structure tested at 640°C and 60 MPa. Magnification x400.*

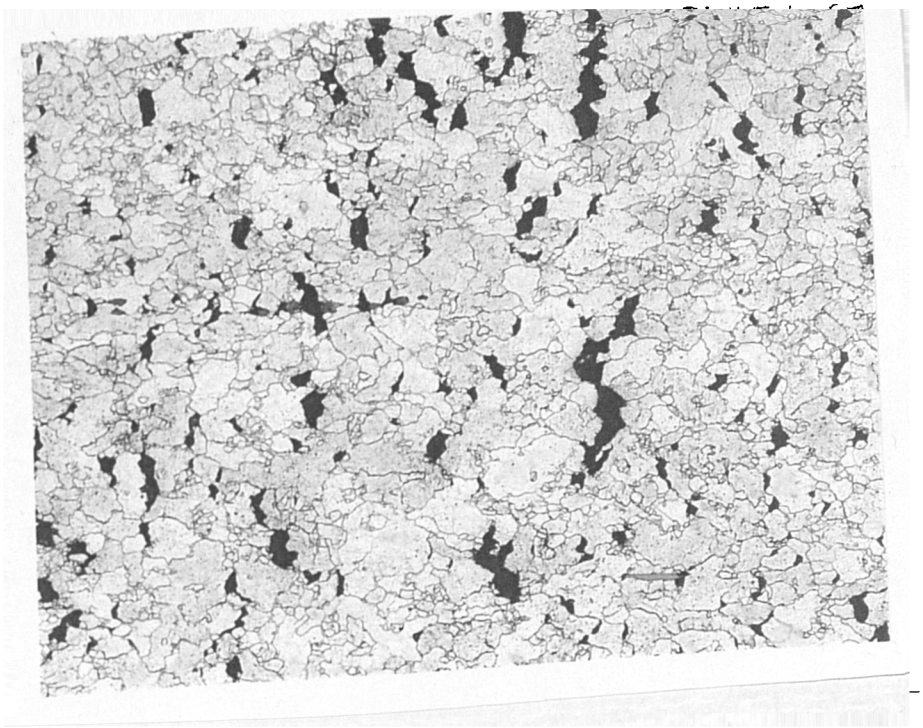

Plate 4.38. *Cavitation observed in a uniaxial M1 cast Type IV simulated structure tested at 640°C and 80 MPa. Magnification x400.*

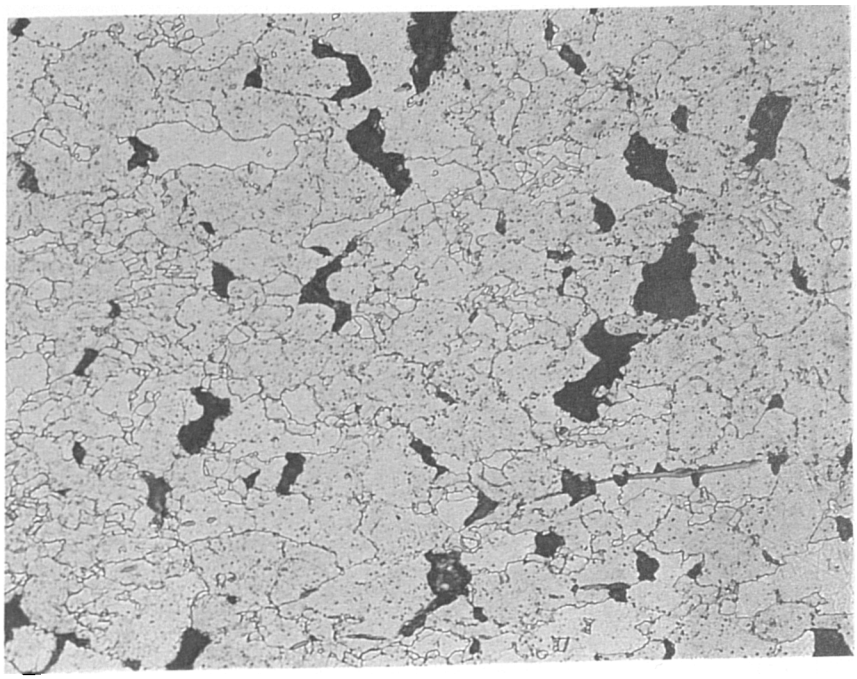

Plate 4.39. *Cavitation observed in a uniaxial M1 cast Type IV simulated structure tested at 640°C and 120 MPa. Magnification x400.*

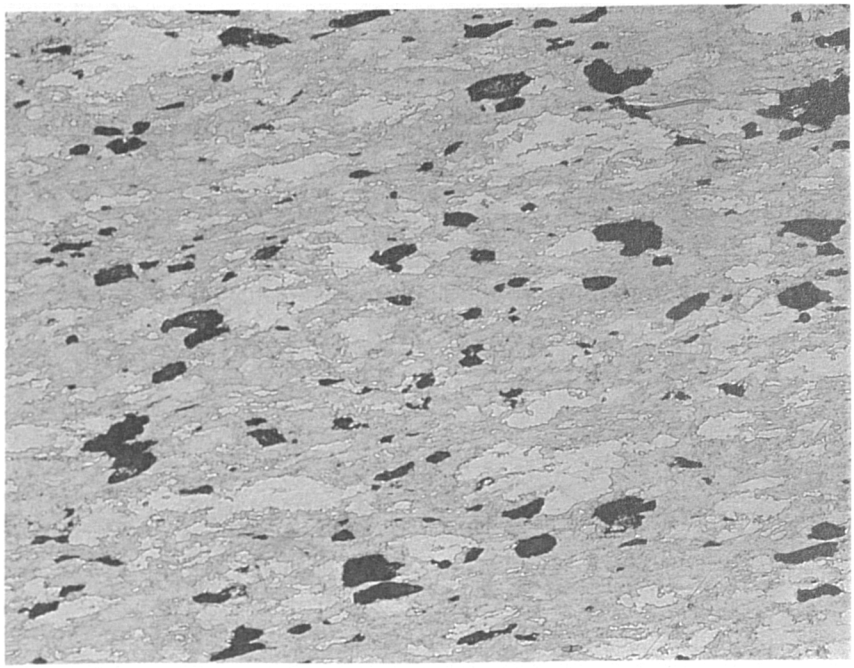

Plate 4.40. *Cavitation observed in a uniaxial M1 cast Type IV simulated structure tested at 640°C and 160 MPa. Magnification x400.*

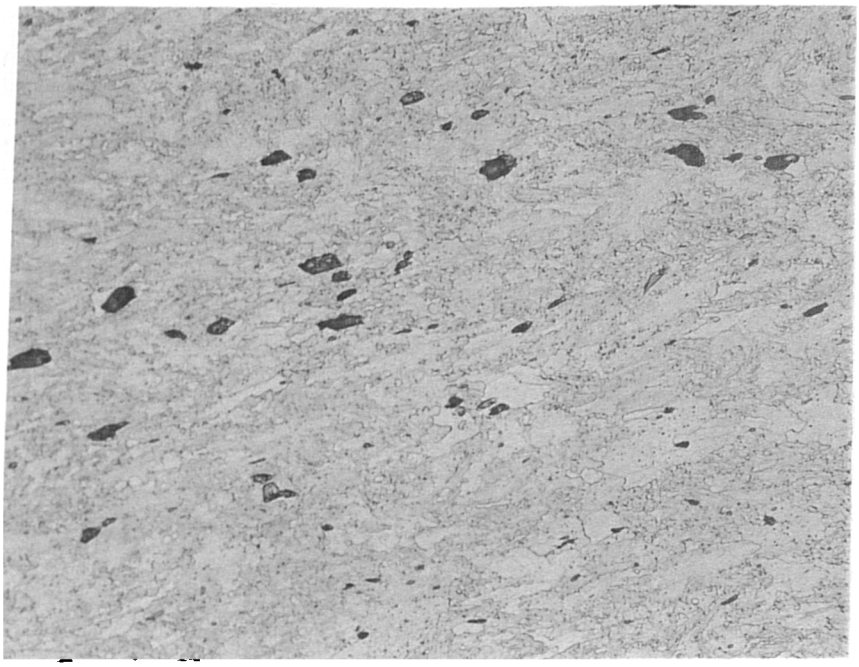

Appendix A4.

A4.1. STRESS ANALYSIS OF A BRIDGMAN (CIRCULAR) NOTCH SPECIMEN.

In Chapter 4 a circular notched specimen is used for the examination of multiaxial rupture and creep damage accumulation as a function of multiaxial stress state. The specimen design is shown in Fig. A.4.1 and is exactly the same, in terms of proportions, as the geometry discussed by Hayhurst and Webster, (**A4.1**).

An axisymmetric mesh was created as shown in Fig. A.4.2. The elements were eight-noded bi-quadratic elements. The processing was performed with ABAQUS finite element software. The creep strain rate law used, which simulates approximately the Type IV creep strength at 620°C, was;

$$\dot{\varepsilon} = 8.15x10^{-11}\sigma_{vm}^{3.5}$$

where σ_{vm} is the Von Mises equivalent stress (MPa).

The creep rate in this expression is approximately five times that of the parent material under the same loading conditions.

The stress distributions (Von Mises and the maximum principle stress) across the minimum ligament of the notch are presented in Fig. A.4.3 after 200h creep at a gross section stress of 28 MPa. The applied stress was the same as used in the circular notch tests presented in Chapter 4.

Note the non-uniform stress distribution in each case. The average maximum principle stress is the net section stress (78 MPa in this case). The average Von Mises stress is 58 MPa. The average creep strain accumulated across the minimum ligament is 2.4%. The stress distribution was found to achieve a steady state as soon as the creep strain exceeds the elastic loading strain by a factor of 2-3. The steady state stress distribution may not be accurate in the presence of more complex creep laws and when creep damage is significant (**A4.1**).

A4.2. REFERENCE.

A4.1 1986, Hayhurst, D.R. and Webster, G.A., *Techniques for Multiaxial Creep Testing,, Gooch, D.J. and How, I.M. (Eds.), Elsevier, London, pp.137-176.*

Fig A4.1 *Circumferential Bridgman Notch specimen geometry threaded bar specimen.*

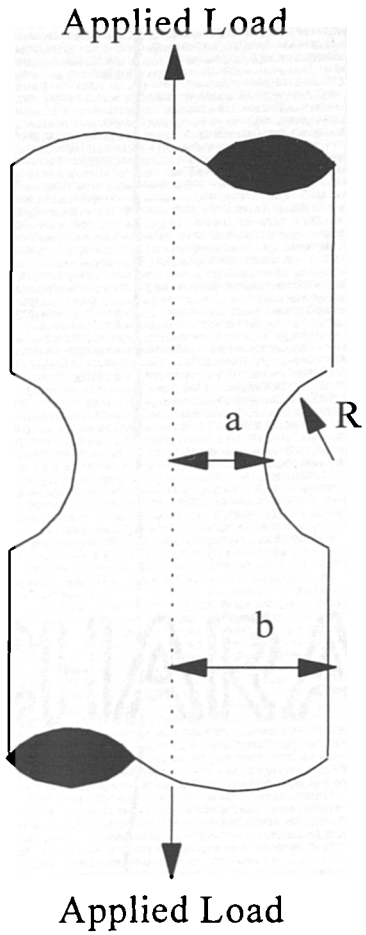

a =5.1 mm
b =8.5 mm
R = 3.4 mm

a/R= 1.5

Fig A4.2 *Axysymmetric mesh of specimen in Fig A4.1.*

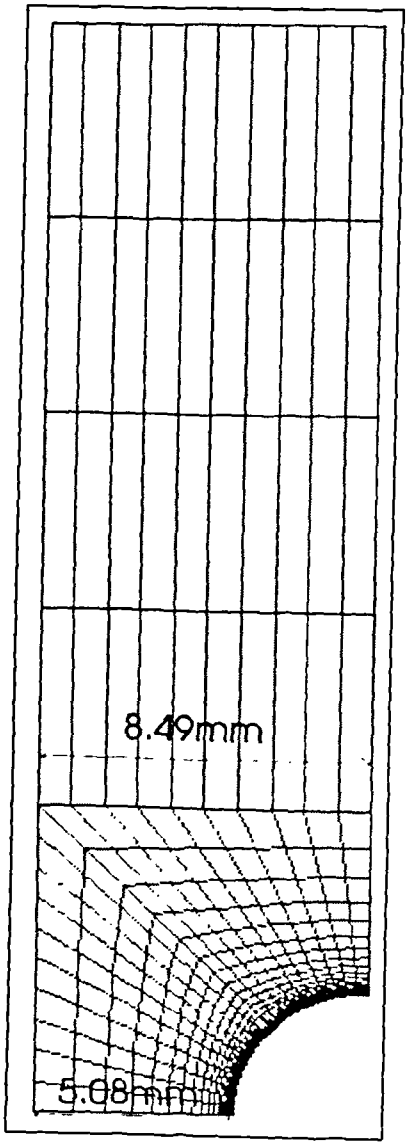

Fig A4.3 *Stress distributions across minimum ligament of circular notch specimen 5.08 mm diameter.*

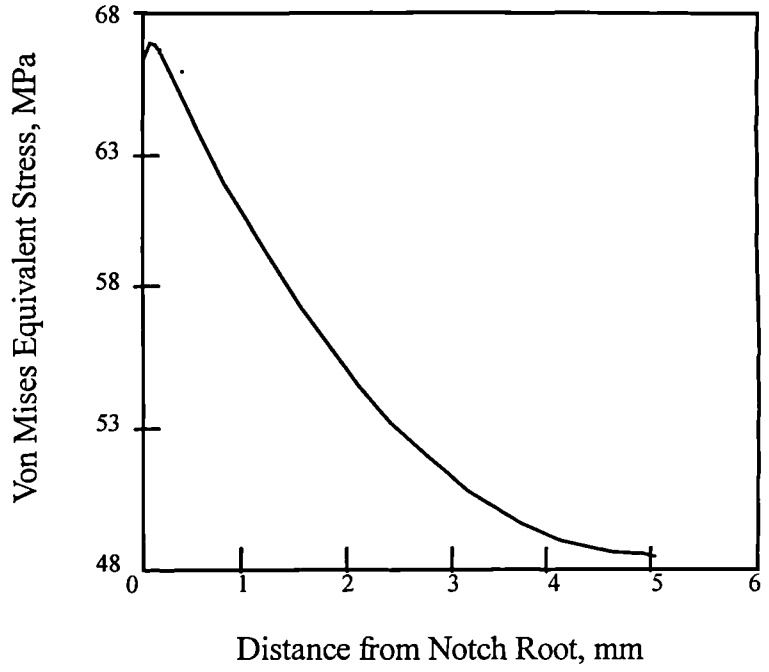

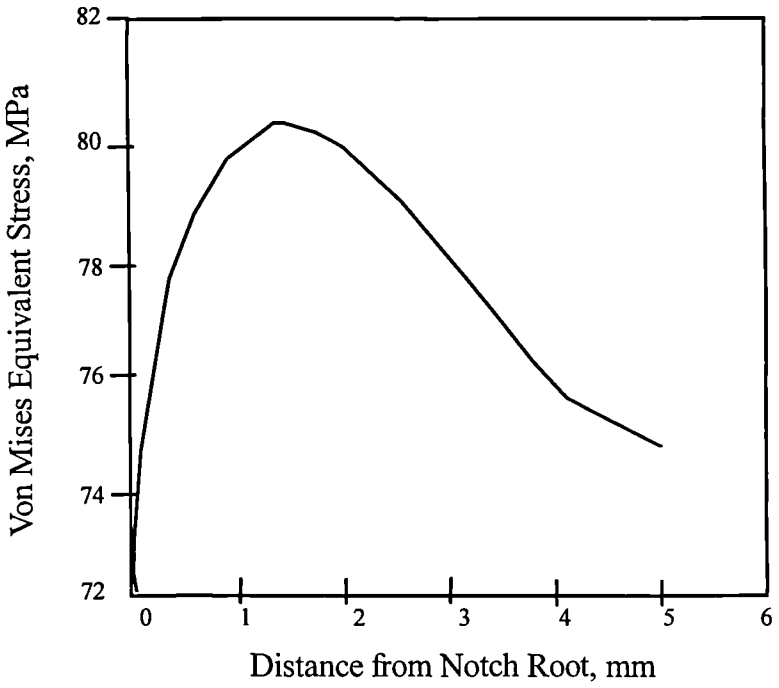

5. DISCUSSION

The aim of this discussion is to characterise the Type IV failure mode in terms of the material and weldment properties and to present the potential mechanism responsible for Type IV failure in a manner which will allow the results of this work to be used in the prediction of remaining life of welded components at high temperature.

5.1 CHARACTERISATION OF THE TYPE IV REGION

It has been found that from the two casts of ½CrMoV low alloy ferritic steels that one cast of steel designated the AB cast is resistant to Type IV failure and that the second cast designated M1 is highly susceptible to Type IV failure. The reason for the variation in the characteristics of the two casts has been investigated in some detail and the results presented. It is clear from the work carried out that there is no one factor which distinguishes the resistance of any one cast of steel to Type IV failure. However, it is clear from the work presented that there are some distinct differences between the casts AB and M1.

The primary difference between the two casts was the difference between the creep rupture properties of the two casts of steel. It was found that the ½CrMoV steels designated cast M1 and cast AB were relatively similar in terms of their creep rupture strength and that the strength of both steels was above the mean materials properties predicted by ISO. Rupture

tests did indicate that cast AB was stronger than cast M1, although both sets of rupture data fall within the ISO scatter band.

Rupture tests conducted using the homogenous Type IV simulated structures revealed that the AB Type IV simulated structure exhibited properties equivalent to the parent steel properties with little or no decrease in the rupture strength. The M1 cast in contrast indicated a complete change in material properties with a much reduced rupture strength. The results of the simulated tests was further confirmed by the cross weld tests which showed consistent results with the M1 cast weldments all failing in the Type IV region over a range of stresses and temperature, while the AB cross weld tests all failed within the weld metal.

In order to explain the variation in the rupture characteristics, the two casts were examined metallographically. In terms of the microstructure it was observed that the grain size of the M1 cast of steel was more refined than that observed in the AB cast of steel. Examination of additional casts of material used in Nuclear Electric test programmes, which have been reported to be susceptible to Type IV failure, showed a similar parent grain size. Measurement of the various grain sizes across the HAZ and into the weld metal indicated that the variation in the parent casts dominated the grain size in the Type IV region.

The parent grain size is dependent upon a number of factors including the thermal history during manufacture and during any subsequent heat treatments, but the steel characteristics are most affected by the material composition and the distribution of alloying elements and

carbides. Since the Type IV region is formed at the transition between the parent steel and the HAZ, the material properties of the Type IV region are determined by temperature. An investigation into the effects of various heat treatments on the two casts of materials revealed that the AB cast of material significantly hardened at 850°C following a heat treatment period of 30 minutes. It was noted that the M1 cast did not indicate any increase in hardness. Interestingly 850°C was found to be the temperature required to simulate the Type IV structure in order to give similar rupture strength to that found within the cross weld specimens. This was also reported by Gooch and Kimmins (**5.1**).

Micro-hardness measurements carried out on the cross weld specimens, however, did not indicate a similar trend. The results showed no sign of increased hardness in the intercritical region in the AB cast or any indication of lower hardness in the M1 cast. Laha et al (**5.2**), reported strain softening within a 2¼CrMo cross weld test, indicated by a large decrease within the Type IV region. The results obtained from the tested specimens gave no indication of this phenomenon. However, it was noted that the AB cast significantly softened as the result of thermal degeneration in the weld metal the HAZ and the parent steel. The M1 cast did not indicate as large a variation between the unaged and aged weldments.

A spectroscopic examination of the two casts of materials composition confirmed that there was little difference in the concentration of the key alloying elements. However, it was noted that the level of Aluminium contained in the AB Type IV resistant cast of material was very low in comparison with the M1 cast. This difference in the level of Aluminium

would certainly have an effect on the physical characteristics of the two casts of steel as well as the material properties of the Type IV region. In order to investigate further the differences in composition an investigation into the formation of carbides both in the parent steel and in the Type IV region was carried out. Specimens were prepared from thermally aged and unaged specimens in order to assess the effect of temperature on the carbide structure and composition. Initially the analysis was carried out using the SEM to identify any variation in the carbide location and size within the cross weld Type IV region of the AB and M1 casts. Although small variations were observed the results were inconclusive. It was therefore necessary to carry out a limited analysis of the carbides using carbon extraction replicas. The results of this analysis were compared with work presented by Westwood et al, (**5.3**).

Westwood investigated a similar situation based on a Type IV susceptible forging and a Type IV resistant cast used in the fabrication of an ex-service T piece. Using carbon replicas he reported that a number of carbides, with a similar shape and morphology to the Mo_2C carbides observed in this study, were readily observed. These carbides also included lathe like structures observed within the failed 1¼Cr½Mo low alloy steel forging. In addition, the undamaged 1¼Cr½Mo casting revealed a large density of rounded particles which are similar in morphology to the cementite found within the aged AB type IV simulated material. This suggests that the level of thermal degradation was much reduced in the casting compared with the level of degradation observed in the forging.

It is clear from the results obtained and presented in Chapter 4 that the M1 cast of steel is more susceptible to thermal degeneration as the result of the thermal cycle experienced during the welding process. The carbide structure and compositions observed indicate this degeneration and are consistent with the observation, made by Westwood, (**5.3**). The AB cast of steel shows a marked resistance to degeneration maintaining a similar carbide structure and distribution throughout the thermal cycle.

The results obtained from the carbon replicas show that the level of Molybdenum and Vanadium as well as the relative occurrence of cementite, dominate the Type IV characteristics. Further detailed investigation far beyond the scope of this work would be required to identify the exact combinations of strengthening precipitates and carbides which would make a cast of ½CrMoV steel resistant to Type IV failure and it would be unlikely that the small levels involved could be controlled adequately to produce a Type IV resistant steel. It was noted, however, that the use of a renormalising heat treatment at temperatures of 900°C would result in recrystallisation so altering the carbide structure and strengthening the material properties of the Type IV region following the welding procedure. However, this process also results in the migration of impurities and carbides towards the fusion boundary which act to reduce the material properties and has been shown to lead to Type III failure at the fusion boundary.

5.2 DEFORMATION MECHANISMS

In order to summarise the mechanical behaviour of the M1 and AB ½CrMoV casts, a mechanism map was developed and all the available cross weld and Type IV simulated

materials rupture data was plotted. Fig 5.1 shows a basic deformation map for a ½CrMoV steel based upon limited materials data published by Ashby and Frost (**5.4**) and data published by Reidel (**5.8**). Many of the materials constants were assumed to be equivalent to pure iron. Appendix 5.1 details the procedure adopted in the construction of the mechanism map. It should be noted that the construction of the map is based upon limited materials data and does not account for the change in diffusivity constants at the transformation temperature.

However, it was possible for the map to be employed as a guide to possible mechanisms which may dominate over the range of the test conditions. The three main mechanisms which are shown on the map relate to the transition from purely diffusional creep in the form of either Coble creep (**5.7**) or Nabarro-Herring creep (**5.5**) (**5.6**) to dislocation creep and thirdly plastic collapse.

As shown by the deformation map diffusional creep dominates at lower stress level and at higher temperatures. As the level of stress increases the deformation mechanisms begins to be dominated by dislocation creep. In this map dislocation creep is described by power law creep. Dislocation creep is only dependent on applied strain rate at high temperatures (above 0.3 T_m) at these temperatures a number of other mechanisms can operate. One such mechanisms which was considered important to the Type IV failure mechanism was grain boundary sliding. Finally at very high stresses, plastic flow can occur as the result of glide motion a process which neither involves dislocation annihilation or production.

A plot of all the test data generated during the test programme has been incorporated into the map both for the uniaxial Type IV simulated tests and the uniaxial M1 cross weld tests. It can be seen that the test conditions are all found within the power law creep regime. As described in Appendix 5.1 other mechanisms, dependent on strain rate, occur within the power law creep regime, one such mechanism is grain boundary sliding. Based on the results of the creep rupture data plotted on Fig 5.1 it can be seen that the majority of the test conditions occur within the regime described by the grain boundary sliding mechanism. It is demonstrated that the high stress tests are subject to a change in deformation mechanism and this was consistent with many of the findings presented. It is therefore concluded that based on the findings of the mechanisms map the dominant deformation mechanism for Type IV failure is grain boundary sliding.

5.3 CAVITATION GROWTH AND NUCLEATION

The aim of this work was to quantify the development of damage in the Type IV region by the use of cavity number density measurements and by means of cavity area measurements. The results presented in Chapter 4 show how creep cavitation damage develops as a function of temperature, stress and weld metal. The results also demonstrate the effects of multiaxiality on the development of damage within the Type IV microstructure. It is important to note that no previous measurement of cavity nucleation rates have been reported for Type IV failure in ½CrMoV steel weldments, apart from the work presented here.

5.3.1 CREEP CAVITATION DAMAGE DISTRIBUTION IN THE TYPE IV REGION

A comparison between the cavity distribution within interrupted M1 cross weld specimens tested at 640°C and 60 MPa and within an uninterrupted M1 cross weld specimen, tested under the same conditions, indicated that the level of cavity nucleation was greater in the interrupted specimen than within the uninterrupted specimen. It is suggested that the reason for the variation in the nucleation rate of cavities, despite adopting a procedure of cooling down the tests under load, arises because there was an element of recovery during the interruptions. Specimens therefore experienced a degree of primary creep during each repeated loading of the test. It is suggested that this has resulted in an enhanced nucleation rate within the interrupted specimens.

The results of the characterisation of damage within the Type IV region indicated that the development of damage was confined to a narrow region in the intercritical zone of the HAZ and the parent material observation and measurement has shown that damage was isolated and limited to the fine grains and was not associated with the parent grains. The level of damage decreases in the fine grained HAZ and is very limited in the coarse grained HAZ. There is little or no cavitation in the tempered parent steel. The distribution of damage from the surface was found to increase from very low levels at the edge to a bulk value at the centre. As a result of this observation interrupted specimens each had 0.5 mm of material removed prior to replication of the surface in order to maintain near bulk cavity damage values. Finally the development of damage through the weld was found to be relatively uniform. It is noted that Type IV failure in main steam lines often develops

subsurface, but initiates close to the outer surface and propagates inwards towards the internal surface. However, in terms of uniaxial cross weld testing it is more important to demonstrate uniform development of damage across the whole Type IV region.

5.3.2 EFFECT OF STRESS AND TEMPERATURE

The bulk of the uniaxial cross weld tests were conducted at 640°C and 60 MPa with additional tests carried out at 600°C and 620°C with stresses ranging from 45 MPa to 80 MPa. The results of the creep cavity damage assessments presented in Chapter 4 show that when the time dependency is normalised with respect to the time to failure the development of cavity damage is not dependent on the temperature within the range of temperatures tested. However the results clearly indicate that the development of cavity damage within the Type IV region of uniaxial cross weld specimens is dependent on the stress, with a greater number of cavities produced at lower stress 48 MPa than at higher stresses, 80 MPa for a given temperature of 600°C.

This result is confirmed by the test conducted using the M1 uniaxial specimens, heat treated to simulate the grain structure and strength of the Type IV region in a cross weld specimen. The results of the tests show that there is a marked decrease in the cavity number density associated with an increase in ductility at higher stresses. The results presented indicate that at a stress of approximately 70 MPa to 80 MPa there is a transition from brittle to ductile behaviour within the Type IV structure as stress increases and this is reflected by a decrease in the amount of creep cavitation damage. It has also been shown

that cavity nucleation is continuous throughout the specimen life as described by Reidel, (**5.8**), with the development of damage proportional to the accumulated creep strain.

5.3.3 EFFECT OF STRESS STATE ON CREEP CAVITATION

Creep tests carried out on notch bar specimens were used to investigate the effect of a triaxial state of stress on the development of creep cavitation within the Type IV region and within the homogeneous Type IV simulated structure used in the uniaxial test programme. Comparisons were made between the failure times and the amount of cavitation which developed as a function of time. Since triaxial stresses do not increase the number of cavities nucleated than in the corresponding uniaxial stress state it was expected that some form of notch weakening would occur, (**5.9**), (**5.10**), (**5.11**). This was confirmed by a reduction in the time to failure for the simulated notch bar specimen and the cross weld notch bar specimen. At stresses where ductility increases, failure by a necking instability, occurs leading to reduced cavitation.

It has been shown in Chapter 4 that at stresses above 60 MPa the amount of creep cavitation in the Type IV simulated and cross weld specimens begins to decrease as ductility increases. The amount of cavitation in the uniaxial plain bar simulated Type IV specimen is in fact more than double the amount of cavitation in the notch bar specimens for the same equivalent stress of 60 MPa and 640°C. This implies that the cavity number density is in fact dependent on the principal stress, similar results have been reported by Cane, (**5.12**), and Dyson and McLean, (**5.13**). Fig 5.2 shows that a good correlation exists

between the principal stress σ_1 and N_t, where N_t is the number of cavities at a constant time, t.

The results of the cavity assessment and rupture tests indicate that the Type IV region notch weakens the cross weld specimens. The results presented in Chapter 4 show that the uniaxial Type IV simulated test carried out at 640°C and 60 MPa fails in 1300 hours while the uniaxial cross weld tests conducted under the same conditions fails in a shorter time of 1065 hours. Since the levels of cavity damage are approximately equal it is assumed that the principal stress acting within the Type IV region is approximately equal to the uniaxial simulated specimen and it is the effect of triaxiality within the Type IV region which results in a reduction in the rupture strength of the Type IV material.

The difference between the notch bar Type IV simulated test and the cross weld notch bar tests demonstrates that when a triaxial stress state is superimposed upon the Type IV region the time to rupture is again reduced due to an increase in the notch weakening effect. However, the cavity number density within the cross weld notch bar specimen, although much reduced in comparison with the uniaxial specimens, is much greater than found in the Type IV simulated notch bar specimen. This would indicate that the principal stress is lower in the cross weld notch bar Type IV region than in the simulated Type IV notch bar. Hence under these conditions the Type IV region may in fact act to notch strengthen.

5.3.4 CAVITY NUCLEATION

Comparison of cavity density measurements with the relationships presented in Chapter 2 has shown that the development of cavitation within the Type IV simulated specimens is characteristic of continuous cavity nucleation. Experimental measurements show that the cavity number density is directly proportional to the creep strain accumulation to failure, Dyson (**5.14**).

More detailed cavity distribution area measurements carried out on the cross weld and Type IV simulated specimens have shown that cavity nucleation is continuous up to the time of failure. This is indicated by the distribution of cavity sizes maintaining the same shape throughout the specimen life. The measurements also showed that even at failure there was a continuous distribution of cavity sizes. It was further noted that cavity nucleation although continuous was dominated by what appeared to be a nucleation burst cycle which occurred through the life of the specimen.

5.3.5 CAVITY GROWTH

A number of cavity growth mechanisms have been discussed within Chapter 2. Two of these cavity growth mechanisms have been used to consider the results of the cavity size measurements presented in Chapter 4. The two cavity growth mechanisms considered are diffusion controlled growth and constrained diffusion controlled growth.

In diffusion controlled growth vacancies generated in the grain boundary diffuse towards and into cavities. The rate of grain boundary diffusion controls the rate of cavity growth ,

equation 2.11. Shammas, (**5.15**), presents this equation in terms of the volumetric growth of a square array of voids of radius r and separation 2c diffusional analysis predicts the growth rate $\dot{V}_D$ of each cavity to be

$$\dot{V}_D = \frac{8\pi D_{gb} w\Omega\left(\sigma - {}^{2\gamma}/_{r}\right)}{kT\left(4\ln\left({}^{c}/_{r}\right) - \left(1 - \left({}^{r}/_{c}\right)^2\left(3 - \left({}^{r}/_{c}\right)^2\right)\right)\right)}$$

equation 5.1

where:

σ	= Applied stress normal to the grain boundary
γ	= Surface energy/unit area
D_{gb}	= grain boundary diffusion coefficient
w	= Grain boundary width
Ω	= Atomic volume
k	= Boltzman constant
T	= Absolute Temperature.

Where grain boundaries are unable to accommodate the growth of a cavity, either as a result of geometric constraint inhibiting the vacancy source potential or as a result of particle inhibition, the cavity growth rate can be constrained by the adjacent material. Based on equation 2.25 the following equation relates the volumetric cavity growth rate under conditions of geometric constraint:

$$\dot{V}_C = 4c^2 d\dot{\varepsilon}$$

equation 5.2

where 'd' is the mean grain diameter.

For the purposes of applying these cavity growth mechanisms to the Type IV region and the cavity size measurements conducted during this research the following values derived from typical measurements made using the cross weld specimens and materials data for pure iron published by Reidel (**5.8**) have been used in the cavity growth rate equations.

c	$= 2\mu m$	$= 2x10^{-6}$ m
d	$= 15\mu m$	$= 0.15x10^{-4}$ m
γ	$= 1$ Nm^{-1}	
$D_{gb}w$	$= 2.26x10^{-21}$ m^{3}s^{-1} (for pure Iron)	
Ω	$= 1.17x10^{-29}$ m^3	
T	$= 913$ K	

Fig 5.3 shows the results of the analysis, including experimental measurements carried out on the M1 cross weld specimen within the Type IV region tested at 640°C and stresses ranging from 60 MPa to 160 MPa. The results of the analysis show that the growth of cavities in the Type IV region is within the limit of constraint, but at higher stresses the experimental data approaches the unconstrained limit where the cavity growth rate is much lower and is more characteristic of plastic void growth.

5.3.6 TIME TO FAILURE

The time to failure in constrained cavity growth is not dependent upon the time for cavity coalescence as is the assumption in the case of unconstrained cavity growth. In the unconstrained limit cavitating facets retain their strength and are able to support the full applied stress across the cavitated facet until the point of cavity coalescence. The final process of microcracking leading to macro cracking will only occur after cavity

coalescence and it is this factor which dominates the time to failure provided that the time from coalescence to microcracking is small.

Constrained cavity growth is dependent on the cavitated grain boundary facet off-loading the applied stress down to the level of the sintering stress, which is often assumed to be negligible. Therefore, the constrained cavitated boundary behaves like a practically traction free microcrack, although metallographically it will still appear to be structurally sound and relatively undamaged. Since the cavitated boundary no longer maintains any support to the surrounding grains it is concluded that the failure mechanism can no longer be controlled by the coalescence of the cavities, Figure 5.4 shows a schematic of a cavitated facet off loading onto a non-cavitated facet. Thus the polycrystalline constraint may retard cavity growth to coalescence but cavity coalescence is irrelevant to the final failure mechanism and therefore constrained cavity is difficult to relate directly to the failure time. Finally it is concluded by Reidel, (**5.8**), that in the constrained limit the rate controlling failure mechanism is the joining of the cavitating boundaries together with continuous nucleation of new cavities. The interaction of facets cavitating will play a central role in the process of joining failed facets producing final rupture.

5.4 CONTINUUM DAMAGE MODELS

Two continuum damage models have been discussed in Chapter 2. In this section the results presented in Chapter 4 will be assessed in terms of these models.

5.4.1 KACHANOV BASED DAMAGE MODEL

The Kachanov, (**5.16**), based model has been adapted from work initiated by Cane and Needham, (**5.17**), to relate cavity damage to remaining life. Two models were proposed one relating the 'A' parameter to time to crack initiation for large grained materials such as parent steels and coarse grained HAZ in low alloys steels and the second was developed to relate the cavity number density to time to failure for use in fine grained areas such as the Type IV region. The final relationship is still being developed to incorporate a cavity growth stress dependence, (**5.18**).

$$LF = \left[1 - \left(1 - \frac{N_A}{N_F}\right)^{\lambda}\right]^{\mu}$$

equation 5.3

where:

LF = Life Fraction consumed

N_A = Measured cavity number density, Cav/mm^2

N_F = Cavity number density at failure, Cav/mm^2

λ = Tertiary ductility ratio

μ = Primary hardening exponent.

The above approach only requires a limited amount of material properties which can be derived from creep testing or in some cases materials data books. The values for the ½CrMoV M1 cast steel have been determined as $\lambda = 3.44$, at 60 MPa and 640°C, from Fig. 5.5 while the primary hardening exponent is assumed to be unity. The cavity number

density has been derived from measurements taken from the M1 Type IV simulated and cross weld uniaxial tests at 640°C and 60 MPa which have a cavity density at failure of approximately 4000 cavities per mm^2. Using these values the Kachanov based model has been plotted against the cavitation measurements for both the cross weld Type IV region and the simulated Type IV material, Fig. 5.6.

It can be seen from the results that the model is generally conservative at predicting the level of creep cavitation damage accumulation and gives a good interpretation of the cross weld Type IV data. However, it should be noted that the model does not account for variation in the rate of cavity growth and nucleation with variation in stress, especially in modelling damage accumulation during primary creep strain at low life fractions. The error bands depicting the upper and lower bound limits of creep cavitation accumulation based on 25% of the time normalised by the time to failure clearly indicates that the lower bound estimate of damage accumulation is non conservative.

5.4.2 DYSON BASED SINH LAW

The second continuum damage model was developed by Perrin et al, (**5.19**) as part of a semi-collaborative project sponsored by Nuclear Electric modelling the results of the Bristol University uniaxial cross weld test specimens. The Sinh model has been developed from Dyson's work, (**5.20**), to interpret the creep behaviour of each of the constitutive elements of the weldment including the parent steel the weld steel and the characteristics of the HAZ and Type IV region.

(I) Parent Material

The creep behaviour of the M1 ½CrMoV steel were characterised using a set of constitutive equations developed by Perrin et al, (**5.19**). The use of physically based equations was developed to describe the various creep damage mechanisms which dominate the materials creep strength. The main elements which are found to affect the creep strength are processes such as carbide coarsening strain hardening and finally creep cavitation damage.

The strain rate is defined as follows in the uniaxial form relating creep strain rate, $\dot{\varepsilon}$, to the stress, σ:

$$\frac{d\varepsilon}{dt} = A\sinh\left[\frac{B\sigma(1-H)}{(1-\phi)(1-\varpi)}\right]$$

equation 5.4

where A, B, are material parameters used to describe the uniaxial creep behaviour.

The first state variable described by Perrin et al, (**5.19**) is the strain hardening exponent H which occurs during primary creep; initially H is equal to zero increasing with strain to a maximum value H*, where H* and h are material parameters:

$$\frac{dH}{dt} = \frac{h\dot{\varepsilon}}{\sigma}\left(1-\left(\frac{H}{H^*}\right)\right)$$

equation 5.5

The second state variable Φ describes the evolution of the spacing of the carbide precipitates.

$$\dot{\Phi} = \left(\frac{K_c}{3}\right)(1-\Phi)^4$$

equation 5.6

where Kc is a material parameter used to define the uniaxial creep behaviour.

The third and final state variable, ω, is used to express the development of creep cavitation damage. Its value ranges from zero for virgin material to 1/3 when all grain boundaries which are normal to the applied stress have cavitated and are unable to support any load. At this final value the material is deemed to have failed.

$$\frac{d\omega}{dt} = C\dot{\varepsilon}$$

equation 5.7

where C is a material parameter used to describe uniaxial behaviour.

(ii) ½CrMoV Weld Metal

Perrin et al, (**5.19**), assumed based upon tests carried out during this work that the strength of the weld metal is approximately half the strength of the parent steel. Therefore for a given stress, the lifetime of the weld metal is half that of the parent steel and the minimum creep strain rate of the weld metal is twice that of the parent material. It was further assumed, based upon limited experimental data, that the weld metal and parent steels exhibited similar ductility's and exhibit similar shapes of normalised creep strain ($\varepsilon/\varepsilon_r$) and

normalised time curves (t/t_r). Based upon these assumptions the constitutive equation for the parent steel was adopted to describe the behaviour of the matching ½CrMoV weld metal, no constitutive equations were proposed for the 2¼CrMo weld metal.

(iii) Heat Affected Zone (HAZ)

The material properties of the HAZ are normally dominated by a coarse grained structure which gives high strength with low ductility. However, the HAZ within the test weldments were found to be more refined as a result of the welding technique which was adopted during the fabrication process. This results in a higher ductility at the expense of a decrease in the creep strength. Under these microstructural conditions the HAZ has been assumed to be equivalent in materials properties to the parent steel and is described by the same constitutive equations.

(iv) Type IV Material

Analysis of the constitutive equations to describe the behaviour of the Type IV regions was based upon the M1 Type IV simulated uniaxial creep rupture tests carried out at 640°C and stresses of 60 MPa, 80 MPa, 120 MPa, and 160 MPa. Since the simulated material exhibits similar microstructural and rupture behaviour as the parent steel it was assumed by Perrin et al, (**5.19**), that the Type IV material was controlled by similar mechanisms to the parent steel. However, the relative importance of the mechanisms will be affected as a result of the thermal cycle which the material has experienced. Clearly the carbide structure in the Type IV material will be much more degenerate than within the parent

material resulting in a reduction in creep properties. However, it has also been shown by measurements of creep cavity damage that the accumulation of creep cavitation is a dominant feature of the Type IV failure mode.

Fig 5.7 shows the results of the strain measurements carried out on simulated Type IV material at 640°C at stresses of 60 MPa, 80 MPa, 120 MPa, and 160 MPa compared with the predicted strain derived from the constitutive equations.

The results of the damage accumulation are presented in Fig. 5.8 which also includes experimental cavity measurements from the M1 simulated Type IV uniaxial tests carried at 640°C and 60 MPa and the M1 cross weld cavity measurements carried out under the same conditions. For the purpose of comparison of the experimental data with the predicted damage model 'ω' the damage parameter was equated to N_a/N_f where $N_a/N_f = 1$ when 'ω' = 1/3.

It has been shown that the model gives a reasonable interpretation of the experimental results, although the results are similar to the Kachanov model the model attempts to incorporate a primary region into the description of the damage accumulation which allows a more accurate interpretation of damage accumulation at low life fractions. By using a number of damage variables the model is able to fully interpret the rate of cavity growth and nucleation with variation in stress. The error bands depicting the upper and lower bound limits of creep cavitation accumulation based on 25% of the time normalised by the

time to failure clearly indicates that the lower bound estimate of damage accumulation is more conservative than the Kachnov model.

Perrin et al (**5.19**) have combined the elements of the model to describe the interaction between the parent steel the weld HAZ and the Type IV region and have used this to model the relative rates of damage accumulation in a cross weld specimen and can be used to describe the effect of stress in an overall model of a complete weld.

5.5 STRESS STATE WITHIN THE TYPE IV REGION

If a region of creep weak material such as the Type IV region is sandwiched between two layers of much stronger material the thin layer would be subject to a high degree of constraint. The requirements for transverse strain compatibility between the two types of material would indicate a triaxial stress state which would be similar to that of a notch bar. Experimental work has shown that the mechanical properties of the Type IV region, are not directly affected by the constraint effect and that the Type IV region is decoupled from the surrounding stronger material. This is demonstrated by the similarity in failure times and cavity damage accumulation measurements in the apparently constrained cross weld specimen and the unconstrained Type IV simulated uniaxial specimens. The notch bar specimens were found to fail in a similar time , but with a lower level of cavitation which can be related to a lower principal stress level.

Grain boundary sliding has been shown by the deformation mechanism map to be the most likely dominant component of creep deformation. The mechanism allows the relaxation of

the strain compatibility at the interface between the strong and weak materials to be reduced to such a level that the constraint effect becomes negligible. Therefore, it is the ability of grains to slide which in turn reduces the requirement for strain capability which accounts for the loss of constraint within the Type IV region.

5.6 SUMMARY

It has been shown that there is evidence for two mechanisms occurring within the Type IV region. Firstly that the dominating deformation mechanism is grain boundary sliding and secondly that cavity growth occurs by constrained diffusion growth.

It has still not been proven conclusively however, whether the accumulation of creep cavitation damage within the Type IV region is dominated by the deformation failure mechanism or by the diffusion process. It is possible that the formation of voids is simply the result of the grains being unable to accommodated the stress concentration resulting from the grain boundary sliding process causing defects similar to wedge cracks at stress concentration such as triple points on grain boundaries. Alternatively, the formation of cavitation may be the result of classical nucleation followed by constrained diffusion growth of cavities. It has been shown from the cavity distribution measurements that cavity nucleation was continuous consistent with this form of classical nucleation.

However, it is equally possible that a combination of the two processes occurs with cavities nucleated by grain boundary sliding, followed by diffusion controlled growth constrained by the grain boundary sliding deformation mechanism.

To complete this section it is important to attempt to relate the results of the test programme back to the conditions experienced by high temperature components while in operation. Typically operational conditions are at lower temperatures than those which the majority of tests were conducted although the level of average test stress is of a similar order of magnitude. Therefore, it is necessary to extrapolate the results of the testing from the test temperature down to typical operation temperatures.

Using the data from tests carried out at 60 MPa at temperatures of 640°C 620°C and 600°C a regression line has been plotted and presented in Fig 5.9. Due to the limited data the results can only act as an indication of the level of cavity damage which might be expected at lower temperatures. However, at a typical operational temperature of 565°C and a mean diameter hoop stress of 60 MPa the estimated cavity number density in the Type IV region at failure would be expected to be of the order of 2200 cavities/mm^2. It should be noted that the cavity density measurements at failure may be reduced due to the effect of failure causing cavities to coalesce potentially reducing the cavity number density. Therefore, data from the same tests carried out at 60 MPa at temperatures of 640°C 620°C and 600°C using a regression line plotted through the 50% cavity number density measurements is presented alongside the cavity density measurements at failure. At a typical operational temperature of 565°C and a mean diameter hoop stress of 60 MPa the estimated cavity number density in the Type IV region at half life would be expected to be of the order of 1000 cavities/mm^2.

5.7 REFERENCES

(5.1) 1988, D.Gooch S.Kimmins
A Study Of Type IV Cracking In ½CrMoV Steel Weldments, ***CEGB Research Report, RD\L\3383\R88.***

(5.2) 1990, Laha,K., Bhanu Sankara Rao,K., And Mannan,S.L.
Creep Behavior Of Post-Weld Heat Treated 2.25Cr-1Mo Ferritic Steel Base, Weld Metal And Weldments, ***Metal Science And Engineering, A129, pp 183-195.***

(5.3) 1993, Westwood, H.J.
Quantitative microstructural studies on creep cracked main steamline weldment, ***Microstructures and Mechanical Properties of Aging Materials p155.***

(5.4) 1982, Frost, H.J., Ashby, M.F.
Deformation Mechanism Maps, Pergamon Press, Oxford.

(5.5) 1950, Herring, C.
J. Applied Physics, Vol. 21, p437.

(5.6) 1948, Nabarro, F.R.N.,
In Conference on Strength of Solids, Phys. Society London, p75.

(5.7) 1963, Coble, R.L.,
J. Appl. Phys, Vol. 34, p1679.

(5.8) 1978, Riedel,H.
Fracture At High Temperatures, ***Materials Research And Engineering, Edited By B.Ilschner, And N.J.Grant, Springer-Verlag.***

(5.9) 1979, Loveday, M.S., Dyson, B.F.,
Creep Deformation and Cavitation Damage in Nimonic 80A Under a Triaxial Tensile Stress., ***Mechanical Behavior of materials, Vol. 2, pp213-222, Ed Miller K.J., Smith, R.F.***

(5.10) 1980, Cane, B.J.,
Creep Damage Accumulation and Fracture under Multiaxial Stresses, ***ICF-5 on Advance in Fracture Research, Ed. Francois, D et al., Pergamon Press, Oxford and New York.***

(5.11) 1984, Al-Faddagh, K.D., Webster, G.A., Dyson, B.F.,
Influence of State of Stress on Creep Failure of 2¼Cr1Mo Steel., ***Mechanical Behavior of Materials IV, Vol. 2, Ed. Carlsson, Ohlson., Pergamon Press.***

(5.12) 1979, Cane, B.J.,
Creep Cavitation and Rupture in 2¼CrMo Steel Under Uniaxial and Multiaxial Stresses, ***Proc. 3rd Int. Conf. Mechanical Behavior of Materials, ICM-3, Vol. 2, p273.***

(5.13) 1977, Dyson, B.F., McLean, D.,
Creep of Nimonic 80A in Torsion and Tension, ***Metal Science, Vol. 11, p 37.***

(5.14) 1983, Dyson, B.F.
Scripta Metall., Vol. 17, pp31-37.

(5.15) 1987, Shammas, M.S.,
Remanent Life Assessment of Ferritic Weld Heat Affected Zones by a Metallographic Measurement of Cavitation Damage- The 'A' Parameter., ***CEGB Report TPRD/L/3200/R87***

(5.16) 1967, Kachanov, L.M.
The Theory of Creep, ***National Lending Library Science and Technology, Boston, Spa.***

(5.17) 1983, Needham, N.G., Cane, B.J.,
Creep Strain and Rupture Predictions by Cavitation Assessment in 2½CrMo Steel Weldments., ***ASME Int. Conf. on Advances in Life Predication Methods, Albany, New York.***

(5.18) Aplin, P Brear, J
Incorporating Primary creep into the Kachanov-Rabotnov Model - Effects on Rupture life and Ductility Prediction for ½CrMoV and 1CrMo Steels., ***ERA Technology Leatherhead.***

(5.19) 1995, Perrin, I.J., Hayhurst, D.R.,
An Interpretive Report on Data Provided by University of Bristol Involving the Characterisation of Weldment Materials Carried out by UMIST Under a Joint Programme Supported by Nuclear Electric., ***Research Report No. DMM.95.9., Private Communication.***

(5.20) 1993, Dyson, B.F., Osgerby, S.,
Modeling and Analysis of Creep Deformation and Fracture in a 1Cr½Mo Ferritic Steel., ***NPL Report DMM(A)116.***

Fig 5.1. *Deformation Mechanism Map ½CrMoV Low Alloy Ferritic Steel.*

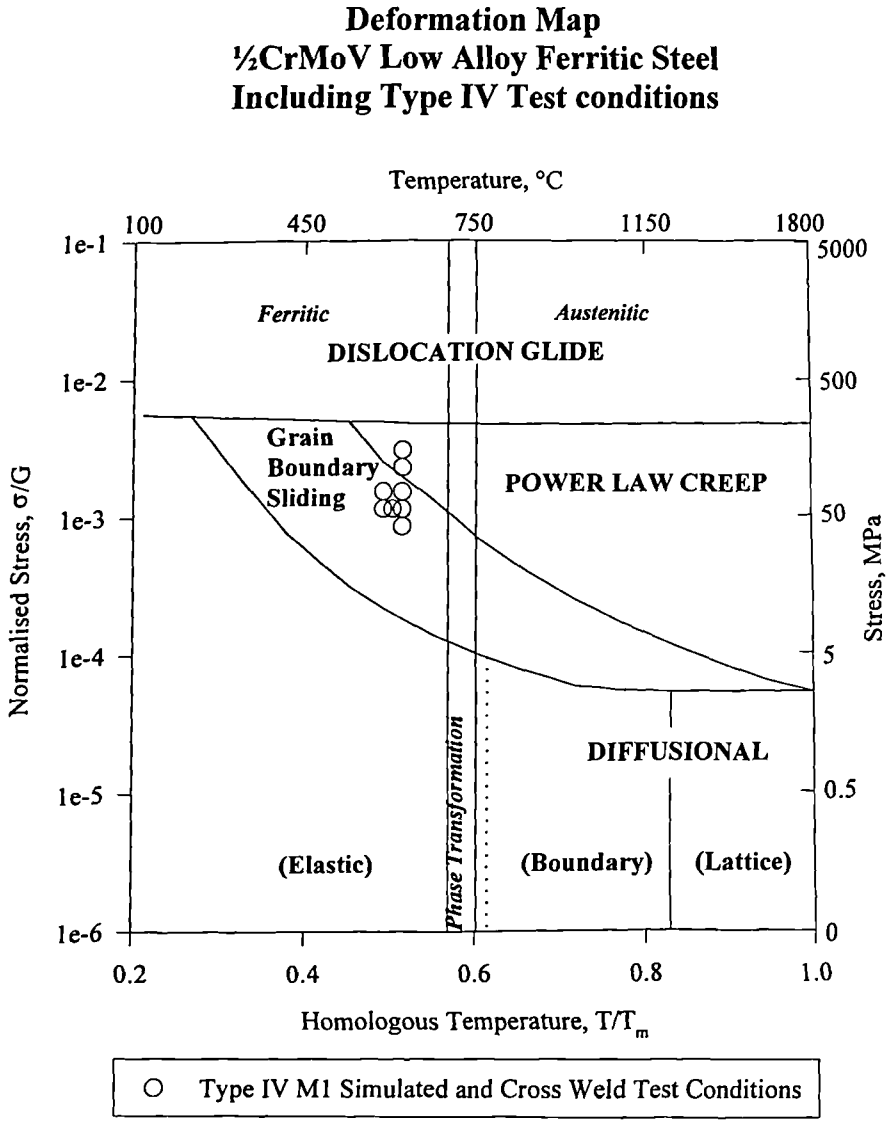

Fig 5.2. *Plot of uniaxial M1 Type IV simulated and multiaxial M1 Type IV simulated and cross weld cavity density measurements Vs the principal stress at time, t.*

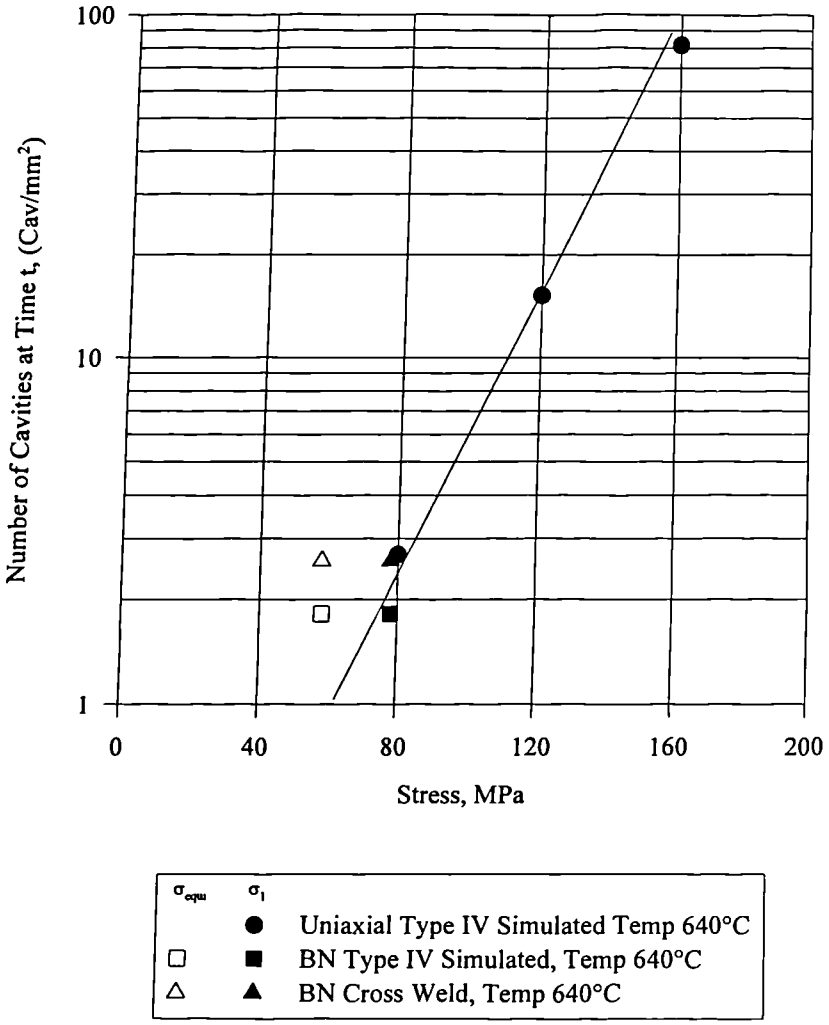

Fig 5.3. *Fracture Mechanism Map of constrained and unconstrained Diffusive cavity growth.*

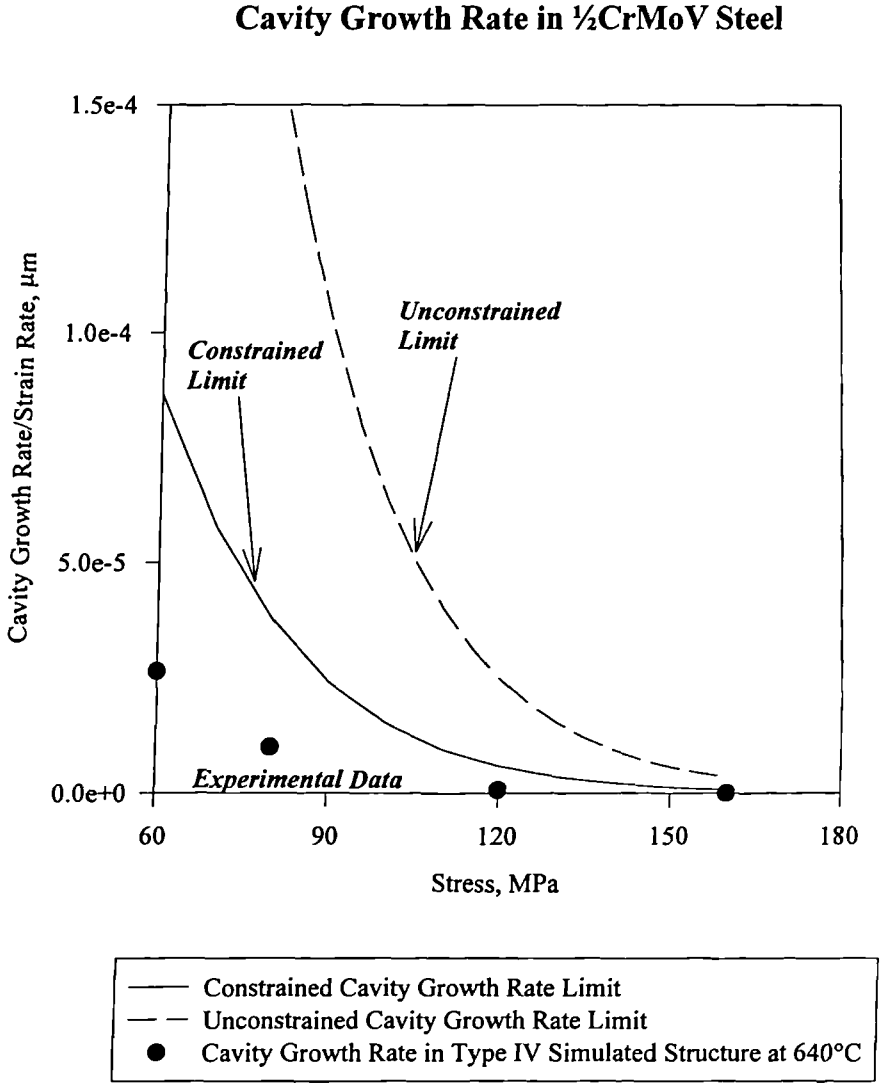

Fig 5.4. *Schematic of constrained cavitated grain boundary subjected to a stress σ, transferring load to the uncavitated grain boundary.*

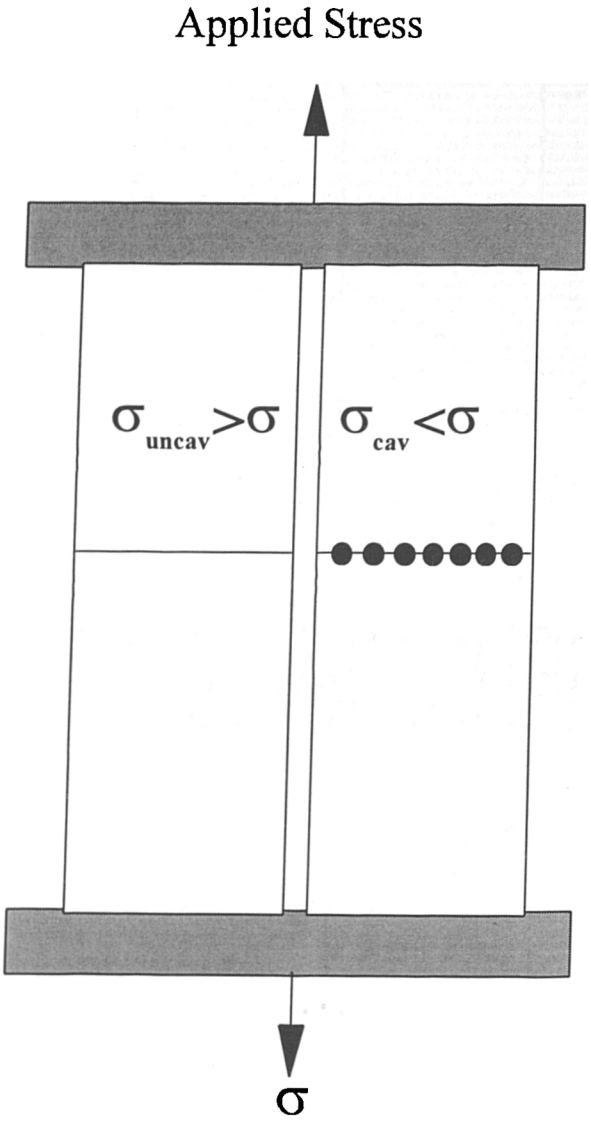

Fig 5.5. *Definition of λ using a typical creep curve.*

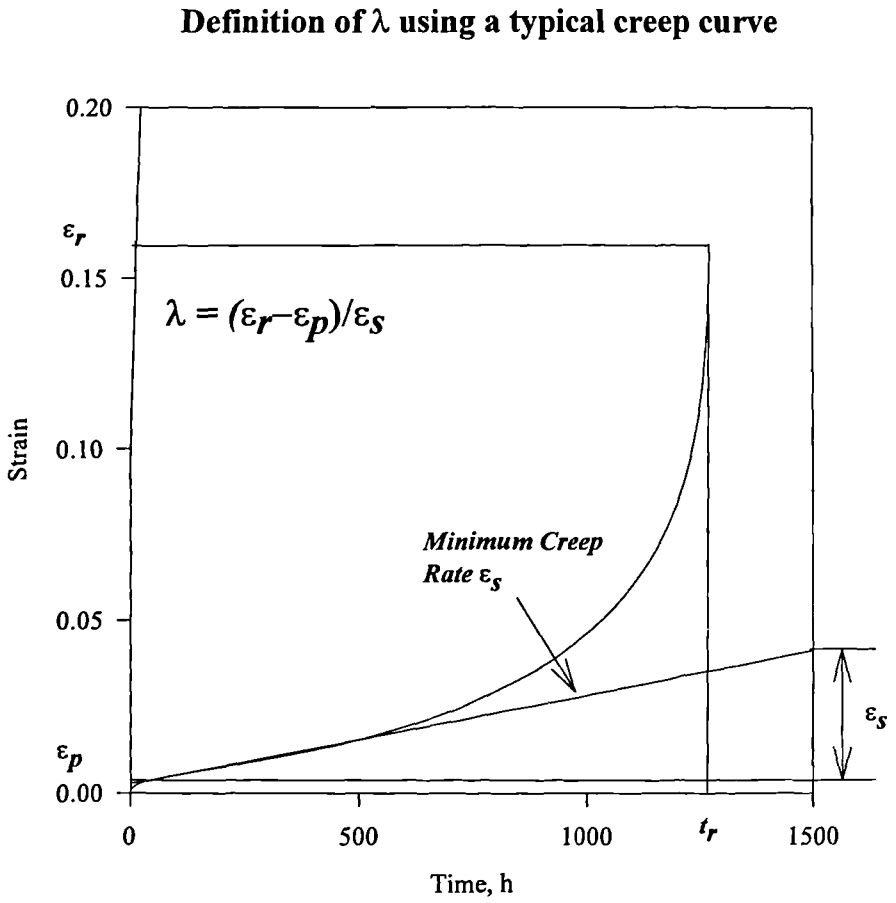

Fig 5.6. *Kachanov based damage model showing upper and lower bound limits. Interpretation of damage accumulation for Type IV simulated material and M1 ½CrMoV cross weld.*

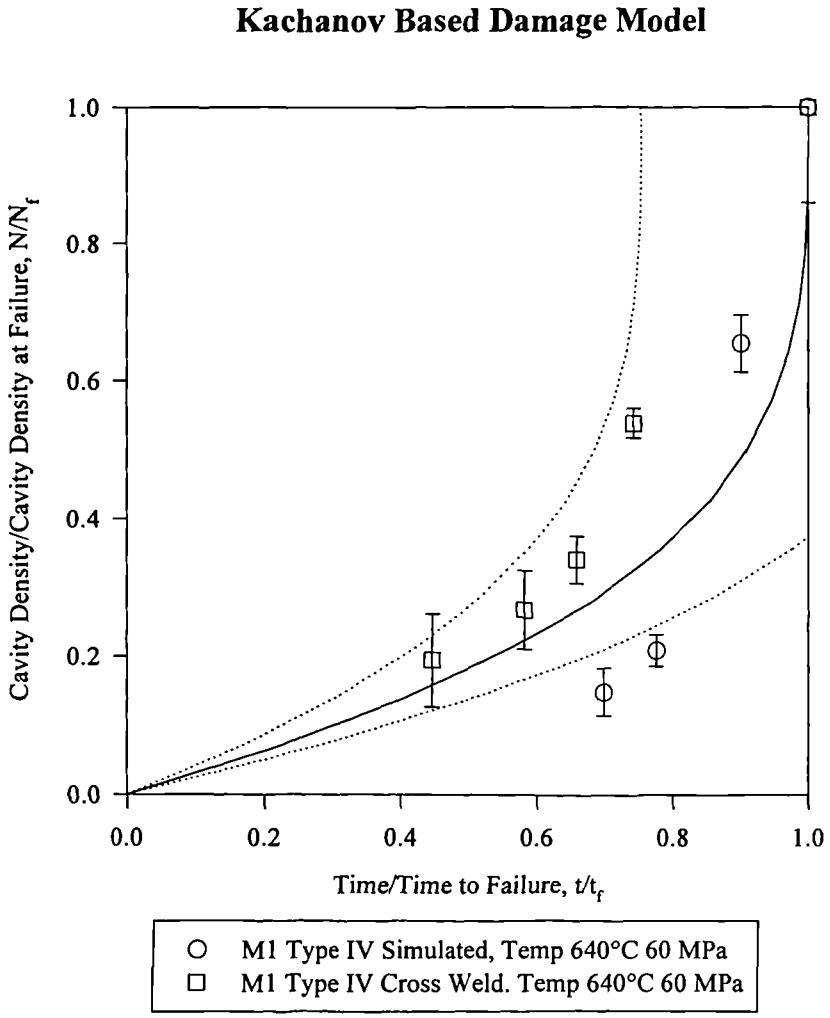

Fig 5.7. *Sinh based constitutive model developed by Perrin et al. Interpretation of creep strain curves for Type IV simulated material at 640°C.*

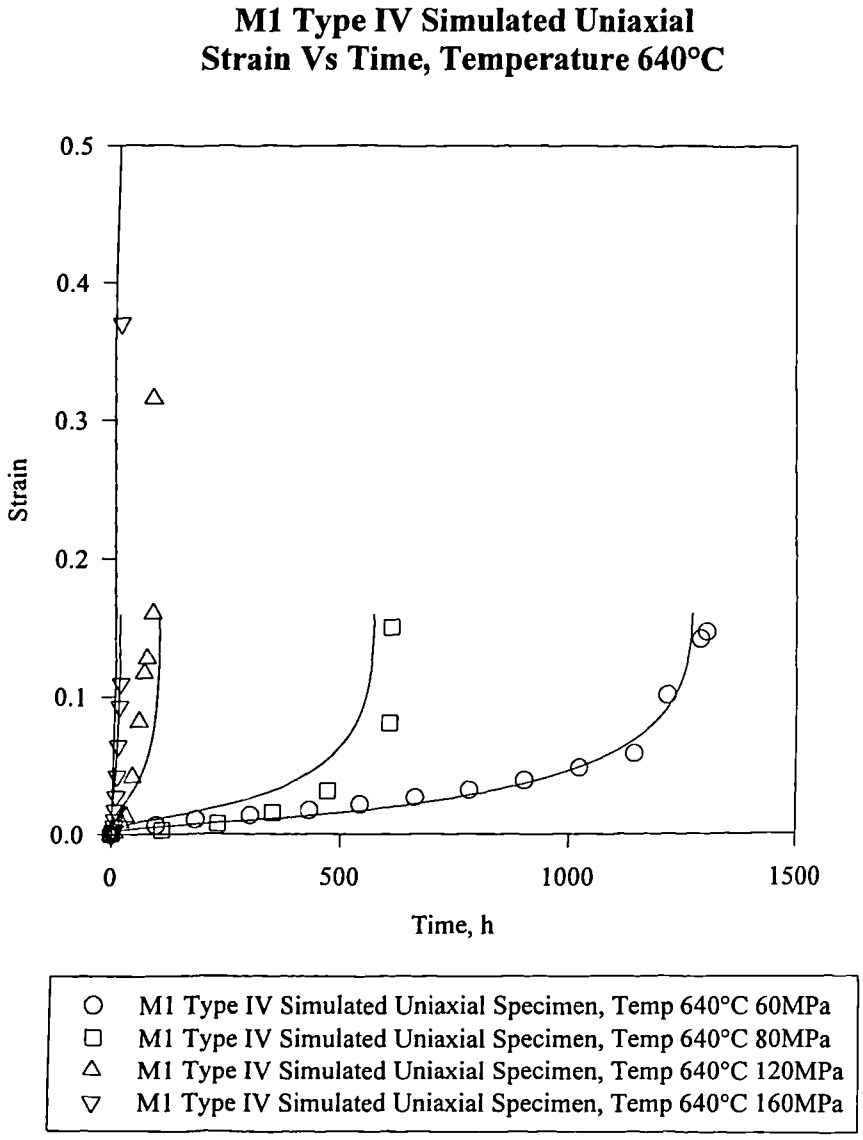

Fig 5.8. *Sinh based constitutive model developed by Perrin et al showing upper and lower bound limits. Interpretation of damage accumulation for Type IV simulated material and M1 ½CrMoV cross weld.*

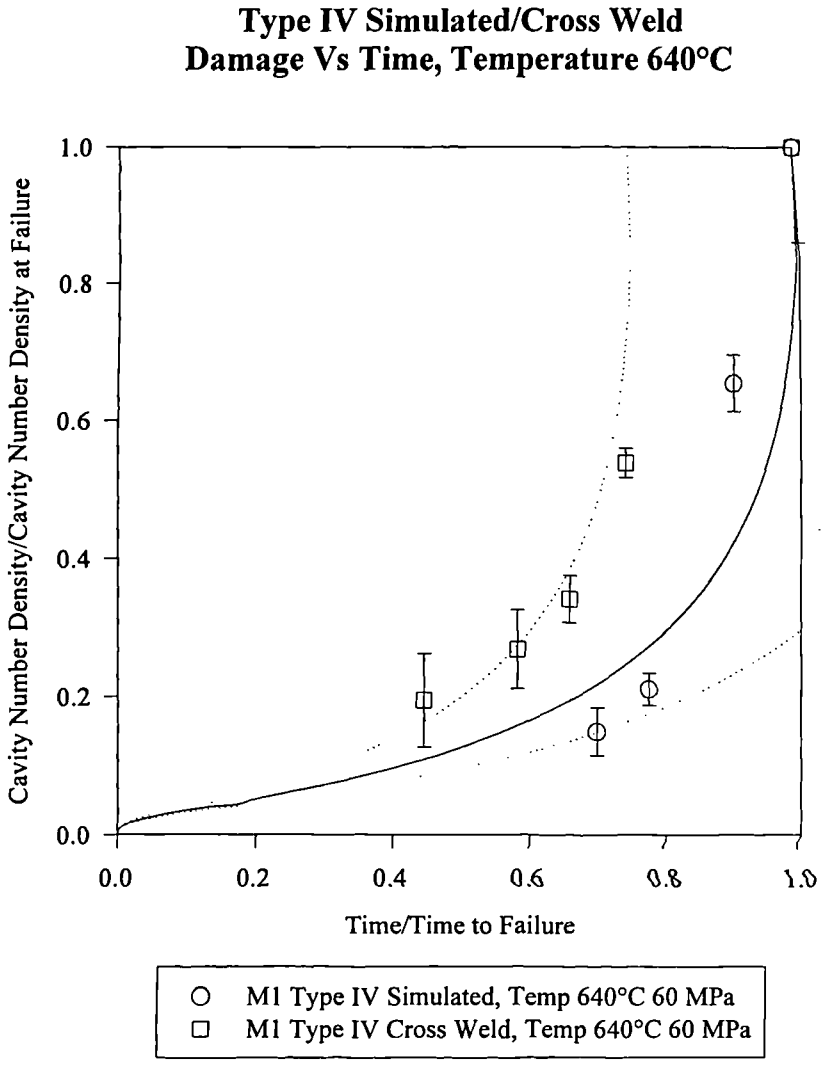

Fig 5.9. *Extrapolation of M1 cross weld cavity density experimental data at 60 MPa to service conditions.*

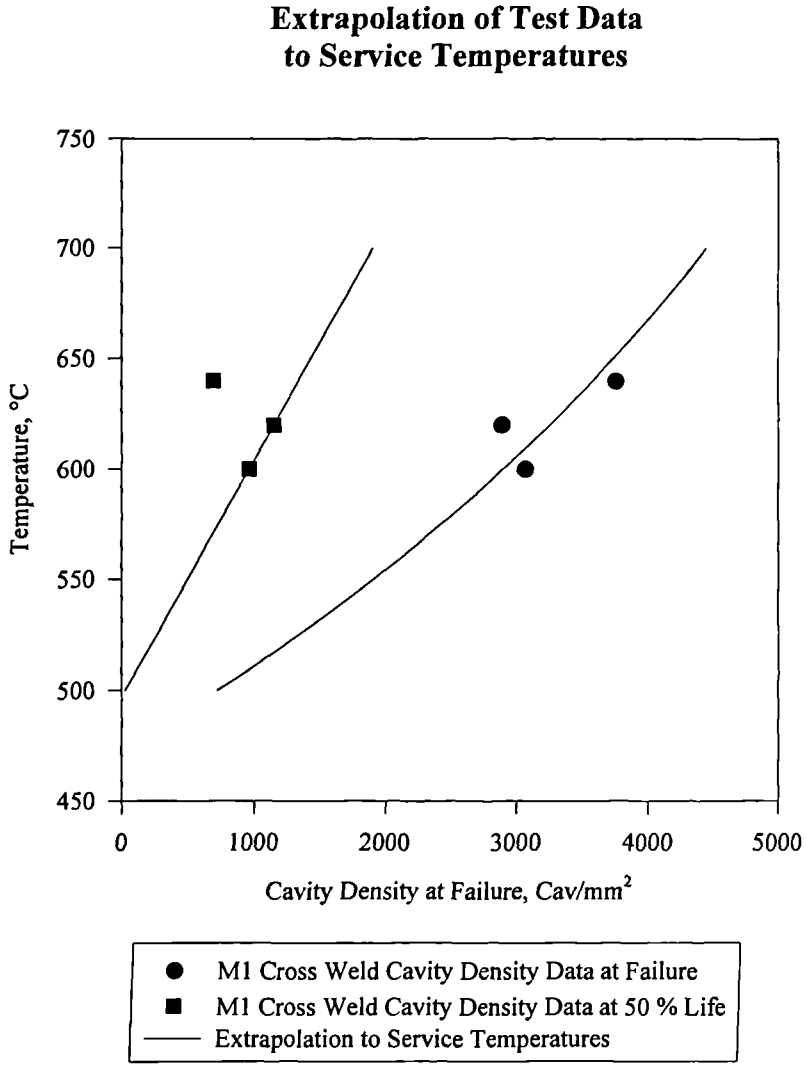

Appendix A5.

A5.1. CONSTRUCTION OF MECHANISM MAPS

A mechanism map can be used to infer the mechanisms which will operate and the potential performance of the material under various imposed conditions. The original idea of a creep diagram stems from the work of Weertman and Weertman, (**A5.1**), and deformation mechanism maps in their present form were first published by Ashby, (**A5.2**).

Maps may be plotted in various co-ordinate systems. All forms are commonly shown in some normalised stress temperature space, to which contours of creep rate , rupture life or cavity growth rate can be added. Alternatively, process rate or life can be used as one of the axes. Each map is divided into regions showing the predominant mechanism controlling behaviour in that range of conditions. Experimental data may also be displayed. It must be stressed that at present mechanism maps are indicative rather than definitive and therefore there is a limit to the degree of precision which is attached to them.

A5.1.1 CONSTRUCTION OF THE MAP

The most universal co-ordinate system is a normalised stress-temperature space. The construction of this map is based upon Langdon and Mohameds work, (**A5.3**), which proposed the use of the reciprocal of the homologous temperature Tm/T, to be used as the horizontal axis. In this form most boundaries and contours are straight and readily determined by algebraic methods. Further, this form of map is more readily related to the

stress and temperature functions which arise in most mechanistic models. Cadecs, **(A5.4)**, form of this function is followed in the construction of the map:

$$\log (\sigma/G),\ T_m/T$$

equation A5.1

A5.1.2 THE TEMPERATURE DEPENDENCE OF SHEAR MODULUS

To construct a map in such co-ordinates, it is necessary to have a model relating shear modulus to temperature. Frost and Ashby, **(A5.5)**, give various empirical forms for different alloy systems, but these are linear and unsatisfactory. Based upon classical solid state theory Mott and Jones, **(A5.6)**, Seitz, **(A5.7)**, and Brear, **(A5.8)**, have developed the following equation:

$$G_T = G_o\left[1 - 0.3\left(T_m/T\right)\exp\left(1.2\,T_m/T\right)\right]$$

equation A5.2

Thus relating the shear modulus G_T, at absolute temperature to the shear modulus at absolute zero, G_o and the reciprocal homologous temperature T_m/T.

A5.2. DEFORMATION MECHANISMS

A5.2.1 PLASTIC COLLAPSE

The ideal shear strength of a material is governed by the interatomic bond strength and represents the stress level above which elastic deformation ceases and unstable disruption

of the chemical bonding takes place. For crystalline solids, it can only be achieved in a perfect (defect free) crystal or one in which all defects are pinned or non-effective. Therefore for real materials the ideal shear strength is a purely hypothetical quantity at temperatures above absolute zero, and is given by

$$\sigma_I = \alpha_c G$$

equation A5.3

Therefore the ideal shear strength has the same temperature dependence as the shear modulus. Accepted values for the proportionality constant, αc, are 0.66 for face centred cubic (FCC) metals Tyson, (**A5.9**), and 0.1 for body centred cubic (BCC) metals Mackenzie, (**A5.10**). These values were derived from a simple static treatment of the crystal structure using an appropriate interatomic force law.

A5.2.2 DISLOCATION GLIDE

Above absolute zero, the mechanical behaviour of a crystalline solid is dominated by the defects within it. The controlling factor in flow properties are the production motion and annihilation of dislocations. At high stresses, plastic flow can occur by glide motion a process involving neither dislocation production or annihilation. Glide occurs through the crystal along preferred crystallographic planes. For macroscopic deformation to take place in a polycrystalline material, an adequate number of independent slip systems are required. Usually the process of glide is inhibited by obstacles such as immobile dislocations, solute atoms or precipitates, or in fact by the resistance of the crystal lattice to dislocation movement. The general relationship between shear stress and shear strain rate for dislocation glide Frost and Ashby, (**A5.5**) is :

$$\dot{\varepsilon}_g = \alpha_g \left(\frac{\sigma}{G}\right)^2 \nu \exp\left(\frac{-\Delta G_\sigma}{RT}\right)$$

equation A5.4

where α_g is a proportionality constant and ν is a frequency term. The activation energy ΔG_σ can be expressed as:

$$\Delta G_\sigma = \Delta G_o \left[1 - (\sigma / \tau)^p\right]$$

equation A5.5

where ΔG_0 is the activation required for the dislocation to overcome the rate limiting obstacle or lattice resistance of any applied stress, and where τ is a materials property equivalent to the stress which reduces ΔG to zero, allowing dislocation movement in the absence of thermal energy. It is thus equivalent to the flow strength at absolute zero. The value of ΔG_0 depends on the types of obstacles present and the lattice resistance. The exponents p and q depend on the distribution of the obstacles, with:

$$0 \leq p \leq 1$$

$$1 \leq q \leq 2$$

equation A5.6

whilst it is possible to calibrate equations A5.4 and A5.5 fully, there are seldom sufficient data available and it is often sufficient to take the approximation that flow by dislocation glide occurs at stresses greater than

$$\sigma_g / G_T = \tau / G_o$$

equation A5.7

A5.2.3 DISLOCATION CREEP

Whilst dislocation glide is only dependant on applied strain rate, at high temperatures (above $0.3T_m$) other mechanisms can operate and these show a strong rate dependence. This gives rise to time dependant plasticity, i.e. creep at constant applied stress or load. At these temperatures, dislocations acquire an extra degree of freedom in the form of thermally activated climb lifting dislocations out of the glide plane and therefore around obstacles when stress alone is insufficient. Under these circumstances the strain accumulated by dislocation glide between obstacles, but the rate is determined by the climb process. At the atomic level, the climb rate is determined by the diffusion of atoms and vacancies to and from the dislocation. The effective diffusion rate is governed by the path of the vacancies at higher temperatures the lattice is favoured and at lower temperatures dislocation core diffusion paths are taken.

For general purposes, power law descriptions of dislocation creep are adequate and justifiable:

$$\dot{\varepsilon}_s = A \frac{Gb}{kT} \left(\frac{\sigma}{G} \right)^n D_T$$

equation A5.8

where b is the Burgers vector , k the Boltzmanns constant and D_T the effective diffusion rate. This type of equation was first proposed by Dorn et al (**A5.11**). The proportionality constant A, can vary widely, implying that some physical quantity must be included. At higher temperatures where D_T is dominated by lattice diffusion:

$$D_T = D_L = D_{oL} \exp\left(-Q_L / RT\right)$$

equation A5.9

at lower temperatures D_T is dominated by dislocation core diffusion:

$$D_T = D_C = D_{oC} \exp\left(Q_C / RT\right)$$

equation A5.10

The stress exponent n has been attributed in many detailed models to indicate a power law dependence with n = 3, 4, 5 in the lattice diffusion regime and n = 5, 6, 7 in the core diffusion regime, the precise value in each case reflecting the relative importance of dislocation density and dislocation velocity Cadec, (**A5.4.**). Grain boundary sliding mechanisms have been shown to exhibit values of n between 5 and 6.

A5.2.4 DIFFUSION CREEP

At lower temperatures dislocation climb becomes very slow and purely diffusive mechanisms dominate the creep process. In these mechanisms, a vacancy flux acts so as to transport matter through each grain of the polycrystal, so acting to reduce the applied load if at all possible. The flux or vacancy flow may be through the lattice or along the grain boundaries.

Lattice based diffusional creep was first formalised independently by Herring, (**A5.12**) and Nabarro, (**A5.13**). The model relates the strain produced to the ratio of atomic volume to grain volume and the rate of the work done in moving one atom and finally the lattice diffusion rate, resulting in:

$$\dot{\varepsilon}_{NH} = 14\frac{\Omega}{kT}\frac{\sigma}{d^2}D_L$$

equation A5.11

where W is the atomic volume and d is the linear intercept grain size. The diffusion rate D_L is given by equation A5.9.

A similar relationship was derived by Coble, (**A5.14**), for the lower temperature grain boundary diffusion controlled process:

$$\dot{\varepsilon}_C = 44\frac{\Omega}{kT}\frac{\sigma}{d^3}\delta_B D_B$$

equation A5.12

with the grain boundary diffusion rate given by

$$D_B = D_{oB}\exp\left(-Q_B/RT\right)$$

equation A5.13

and the effective grain boundary width given by $\delta_B \cong 6b$.

A5.3. REFERENCES

(A5.1) 1965, Weertman, J., Weertman J.R.,
In Physical Metallurgy ed. Cahn, R.W. North Holland, Amsterdam, p736.

(A5.2) 1972, Ashby, M.F.
Acta Metallurgica, Vol. 20 P887

(A5.3) 1976, Langdon, R.G., Mohammed, F.A.
J.Materials Sci, Vol. 11, p317

1978, Langdon, R.G., Mohammed, F.A.
J.Materials Sci, Vol. 13, p1282.

1878, Langdon, R.G., Mohammed, F.A.
Materials Sci and Eng., Vol. 32, p103.

(A5.4) 1988, Cadek, J.
Creep in Metallic Materials, Elsevier Amsterdam.

(A5.5) 1982, Frost, H.J., Ashby, M.F.
Deformation Mechanism Maps, Pergamon Press, Oxford.

(A5.6) 1936, Mott, N.F., Jones, H.,
The Theory and Properties of Metals and Alloys
Oxford University Press.

(A5.7) 1940, Seitz, F.
The Modern Theory of Solids
Mcgraw-Hill Book Co. New York.

(A5.8) Brear, J.M.,
ERA Internal Report No 95-0987, *Private Communication.*

(A5.9) 1966, Tyson, W.R.,
Phil Mag, Vol. 14, p925.

(A5.10) 1959, Mackenzie, J.K.,
PhD Thesis University of Bristol.

(A5.11) 1969, Dorn, J.E., Mukherjee, A.K., Bird, J.E.,
Metal Trans. ASM, Vol. 62, p155.

(A5.12) 1950, Herring, C.
J. Applied Physics, Vol. 21, p437.

(A5.13) 1948, Nabarro, F.R.N.,
In Conference on Strength of Solids, Phys. Society London, p75.

(A5.14) 1963, Coble, R.L.,
J. Appl. Phys, Vol. 34, p1679.

6. CONCLUSIONS

A summary of the main conclusions regarding the results and analysis of this work along with proposals for future work are presented in this chapter.

6.1 CONCLUSIONS

6.1.1 CHARACTERISATION OF THE TYPE IV REGION

Based upon the results of the tests carried out it is concluded that Type IV failure in ½CrMoV weldments is independent of the weld metal filler, but is apparently strongly dependent upon the parent cast of steel. Analysis of grain size, structure and carbide morphology has indicated that there is a direct correlation between composition and carbide morphology and the susceptibility of a cast of steel to Type IV failure. Spctroscopic analysis of the two casts of steel M1 and AB has indicated that the AB cast of steel has a much lower concentration of Aluminium than the M1 cast. It was therefore concluded that the amount of Aluminium in the M1 cast of material has contributed to a change in the thermal response of the material to heat treatment and subsequently has produced a highly creep susceptible Type IV region in the M1 weld.

6.1.2 CREEP STRENGTH OF TYPE IV REGION

The creep rupture strength of the AB Type IV region was found to be approximately equal to the creep strength of the parent steel. From the creep rupture tests carried out it was

found that the AB simulated Type IV structure exhibited similar creep properties to the AB cross weld Type IV region. It was concluded that the AB cast of material was resistant to Type IV failure

The creep rupture strength of the M1 Type IV region was found to be approximately one third the creep strength of the parent steel. From the creep rupture tests carried out it was found that the M1 simulated Type IV structure exhibited similar creep properties to the M1 cross weld Type IV region. Based upon this finding it was concluded that the apparent constraint, which might be expected to result from the presence of a weak material bounded by two strong materials, was decoupled allowing the Type IV region to accommodate a high level of strain. The possible mechanism by which this could occur has been discussed.

6.1.3 UNIAXIAL AND MULTIAXIAL CREEP PROPERTIES

The results of the multiaxial tests, notch bar and shear pin specimens, were compared directly with uniaxial creep rupture tests. The result of the comparison indicated that the multiaxial notch bar tests failed in the same time as the uniaxial tests when the Von Mises stress was made equal to the Uniaxial test principal stress. The tests results were confirmed by a unique set of tests carried out using shear pins which were oriented such that the Type IV region was tested unconstrained by the surrounding material. Based on these results it was concluded that the time to failure mechanism of the Type IV region was dominated by the Von Mises equivalent stress.

6.1.4 DEFORMATION MECHANISMS

Evidence has been presented in the form of an unvalidated mechanism map and experimental results from cross weld and Type IV simulated rupture tests. The result combined with analysis of the stress state found within the Type IV region indicates that the deformation mechanism most dominant in Type IV failure is grain boundary sliding. It was therefore concluded that it was the ability of grains to slide past each other which enables the strain incompatibility of the Type IV region to relax which results the Type IV region being decoupled so causing the constraint effect to become negligible.

6.1.5 CAVITATION GROWTH AND NUCLEATION

Using the test data normalised with respect to the time to failure to remove any dependence of life fraction on temperature, it was concluded that the development of creep cavitation in the Type IV region was strongly dependent on the applied stress in uniaxial tests over the range of stresses tested.

It was further concluded, by use of test data normalised to take account of the influence of stress on the life fraction, that there was no apparent influence on the development of creep cavitation in the Type IV region by the temperature over the range of temperatures tested.

It was not possible to conclusively demonstrate whether the development of creep cavitation was the result of void growth related to grain boundary sliding or whether creep cavitation growth was fully dominated by constrained diffusive growth. It is possible that the true mechanism for cavity growth in the Type IV region was based upon cavity

nucleation resulting from grain boundary sliding followed constrained diffusive growth. Therefore it was concluded that the development of creep cavitation was not the true mechanism for failure but acted simply as an indicator of the grain boundary sliding mechanisms which results in final failure due to strain accumulation.

Based upon cavity growth and nucleation measurements carried out on multiaxial notch bar specimens it was concluded that the development of cavitation was dominated by the principal stress rather than by Von Mises equivalent stress which was found to dominate the creep rupture results.

6.1.6 CONTINUUM DAMAGE MODELS

The Kachnanov model presented has been shown to provide a good interpretation of the cross weld Type IV cavity damage accumulation. However, the error bands indicate that the interpretation is non conservative in the interpretation of the creep cavitation data plotted.

The Sinh law has provided a more conservative interpretation of the creep cavitation data. By incorporating a primary region into the description of the damage accumulation a more accurate description of damage accumulation at low life fractions is made possible.

The two continuum damage models presented both provide a good estimate of the remaining life capability of the Type IV region. Clearly the Sinh law is able to describe the damage mechanism in more detail than the Kachanov law, used as a result of the number of

variables used to describe the behaviour of the material. A more accurate description of the damage using the Kachanov law would require the primary hardening exponent to become stress dependent. Based upon the results obtained it can be concluded that further development of the Sinh law will provide an accurate prediction of the life capability of low alloy ferritic steel weldments at high temperature. However, each material variable would require extensive validation and an accurate and rapid methodology for physically quantifying each variable for accurate plant assessment. In these terms the Kachanov based law has already been validated and only requires limited materials information which is readily available.

6.2 FUTURE WORK

The following suggestions have been made to highlight those areas of the work presented which could be continued in future research projects.

In order to fully understand the susceptibility of materials to Type IV failure it would be necessary to undertake an extensive programme of cross weld testing and subsequent analysis using a number of casts of materials to identify the principle elements which result in a cast of steel becoming susceptible to Type IV failure.

Since Type IV failure is not limited to ½CrMoV steels an obvious development of this test programme would be to examine a number of steels and conduct quantitative metallography during creep testing. At present there is very limited data on the development of creep cavitation in fine grained HAZ and the Type IV region. It is also

true to say that most cross weld rupture data does not indicate whether the failure is in the weld metal or the Type IV region. Therefore, design codes which rely on cross weld rupture data are not completely reliable. Any testing therefore, of different materials for the purpose of publication would be of value.

One of the main areas of interest regarding the Type IV region is the complex multiaxial effects which are thought to occur. The effects of multiaxiality can be assessed in terms of three characteristics; rupture time; cavity development and ductility. The initial results of the circular notch bar test and the cross weld test indicate that a more detailed investigation into the effect of notch geometry and the resulting variation in the stress field combined with a series of shear tests based upon cavity density measurements is necessary to fully understand the damage mechanisms occurring within the Type IV region.